Dissertation
submitted to the
Combined Faculties of the Natural Sciences and Mathematics
of the Ruperto-Carola-University of Heidelberg, Germany
for the degree of
Doctor of Natural Sciences

Put forward by
David Mesterházy
born in: Berlin
Oral examination: October 30, 2013

Equilibrium and nonequilibrium scaling phenomena in strongly correlated systems

Referees :	Prof. Dr. Jürgen Berges	(first referee)
	Prof. Dr. Jens Braun	(second referee)

Abstract

In this thesis we examine universal scaling properties of strongly-correlated systems near and far from equilibrium. We discuss quantum phase transitions at vanishing temperature, multicritical and dynamic critical behavior near thermal equilibrium, and scaling properties of nonequilibrium steady states. We employ nonperturbative methods including the functional renormalization group as well as Monte Carlo simulations. A general outline of the functional renormalization group is given in the introductory chapters.

In the first part of this thesis, we investigate spinless fermions on the honeycomb lattice interacting via short-range repulsive interactions. Such a system can be seen as a simple model for suspended graphene. The short-range interactions control the ground state properties of the system that may lead to a chiral phase transition from the semimetal to the charge density wave (CDW)/Kekulé ordered state. We determine the universal scaling properties at the chiral transition, and establish the presence of large anomalous dimensions indicating the importance of strong fluctuations.

The competition of two nonvanishing order parameters and their corresponding multicritical behavior are investigated in the subsequent chapter. We characterize the bicritical and tetracritical behavior in the purely bosonic $O(N_1) \oplus O(N_2)$ symmetric model and comment on possible applications to condensed-matter and high-energy physics.

In the following chapter we discuss the long-time relaxational behavior at criticality of an order parameter with $O(N)$ symmetry coupled to an additional conserved density. We find an anomalous diffusion phase with new dynamic scaling properties. Using the functional renormalization group we determine the complete dynamic critical behavior of the model in $2 < d < 4$ dimensions and compare our results to experiments.

Finally, we investigate the scaling properties of stationary states far from equilibrium. At the example of the one-dimensional Burgers' equation we develop a novel approach to hydrodynamic turbulence using lattice Monte Carlo methods. We apply these techniques to determine the statistical properties of small-scale fluctuations in this model and identify the anomalous scaling behavior.

Zusammenfassung

Diese Dissertation befasst sich mit universellem Skalierungsverhalten in stark-korrelierten Systemen nah und fern des Gleichgewichts. Wir untersuchen Quantenphasenübergänge bei verschwindender Temperatur, multikritisches Verhalten und dynamisches kritisches Verhalten im bzw. nahe dem thermischen Gleichgewicht, sowie das Skalierungsverhalten stationärer Nichtgleichgewichtszustände mittels verschiedener nichtperturbativer Methoden, wie der funktionalen Renormierungsgruppe, sowie Monte Carlo Methoden. In den einleitenden Kapiteln dieser Arbeit geben wir einen kurzen Überblick zur funktionalen Renormierungsgruppe.

Im ersten Hauptteil dieser Arbeit, betrachten wir ein einfaches Modell für Graphen – ein System aus spinlosen Fermionen auf dem hexagonalen Gitter mit kurzreichweitigen Wechselwirkungen. Diese kontrollieren maßgeblich den Grundzustand des Systems, wobei im Falle starker Kopplung ein chiraler Phasenübergang vom Semimetall zum Ladungsdichtewelle/Kekulé-geordneten Zustand beschrieben wird. Hier bestimmen wir die kritischen Eigenschaften am chiralen Phasenübergang und beobachten insbesondere große Werte für die anomale Dimension des Ordnungsparameters und der Fermionen, welche auf eine Dominanz starker Fluktuationen hinweisen.

Die Wechselwirkung zweier nicht verschwindender Ordnungsparameter und das entsprechende kritische Verhalten nahe einem multikritischen Punkt wird im darauf folgenden Kapitel diskutiert. In einem rein bosonischen Modell mit $O(N_1) \oplus O(N_2)$-Symmetrie charakterisieren wir entsprechendes bikritisches bzw. tetrakritisches Verhalten mittels der funktionalen Renormierungsgruppe und beschreiben mögliche Anwendungen für stark-korrelierte Systeme in der Festkörper- und Hochenergiephysik.

Im folgenden Kapitel befassen wir uns mit dem Langzeit-Relaxationsverhalten eines $O(N)$-symmetrischen Ordnungsparameters nahe dem kritischen Punkt, in Anwesenheit einer zusätzlichen Erhaltungsgröße. Hier finden wir ein Regime anomaler Diffusion mit neuen dynamischen Skalierungseigenschaften. Im Rahmen der funktionalen Renormierungsgruppe bestimmen wir das vollständige dynamische Phasendiagramm des Modells in $2 < d < 4$ Dimensionen und vergleichen unsere Ergebnisse mit experimentellen Daten.

Schließlich untersuchen wir das Skalierungsverhalten in stationären Zuständen fern des Gleichgewichts. Am Beispiel der eindimensionalen Burgers-Gleichung beschreiben wir einen neuen Zugang zu hydrodynamischer Turbulenz mittels Monte Carlo Methoden. Wir bestimmen das statistische Verhalten kurzreichweitigen Fluktuationen in diesem Modell, sowie deren anomale Skalierungseigenschaften.

Publications

This thesis contains published results from the following publications and proceedings contributions that I have coauthored in the course of my thesis:

1. D. Mesterházy, J. H. Stockemer, L. F. Palhares, and J. Berges, "New Dynamic Critical Behavior for Model C," `arXiv:1307.1700 [cond-mat.stat-mech]` (submitted to *Phys. Rev. Lett.*)
2. A. Eichhorn, D. Mesterházy, and M. M. Scherer, "Multicritical behavior in models with two competing order parameters," `arXiv:1306.2952 [cond-mat.stat-mech]` (submitted to *Phys. Rev. B*)
3. D. Mesterházy, J. Berges, and L. von Smekal, "Effect of short-range interactions on the quantum critical behavior of spinless fermions on the honeycomb lattice," *Phys. Rev.* **B86** (2012) 245431, `arXiv:1207.4054 [cond-mat.str-el]`
4. J. Berges and D. Mesterházy, "Introduction to the nonequilibrium functional renormalization group," *Nucl. Phys. Proc. Suppl.* **228** (2012) 37, `arXiv:1204.1489 [hep-ph]`
5. D. Mesterházy and K. Jansen, "Anomalous scaling in the random-force-driven Burgers equation: A Monte Carlo study," *PoS* **LAT2011** (2011) 079, `arXiv:1111.2304 [nlin.CD]`
6. D. Mesterházy and K. Jansen, "Anomalous scaling in the random-force-driven Burgers equation: A Monte Carlo study," *New J. Phys.* **13** (2011) 103028, `arXiv:1104.1435 [nlin.CD]`

Declaration by author

This thesis is composed of my original work, and contains no material previously published or written by another person except where due reference has been made in the text. I have clearly stated the contribution by other authors to jointly authored works that I have included in my thesis. The content of my thesis is the result of work I have carried out since the commencement of my graduate studies at the Heidelberg Graduate School of Fundamental Physics (HGSFP), Institut für Theoretische Physik, Universität Heidelberg and does not include material that has been submitted by myself to qualify for the award of any other degree or diploma in any university or other tertiary institution.

Acknowledgments

I am deeply indebted to my advisor Jürgen Berges for his constant support and encouragement. He gave me the freedom to pursue my ideas and research and was there with advice and guidance when I needed it. His dedication and enthusiasm when it comes to physics is a source of inspiration that I will carry with me.

Also, I want to thank Jens Braun for agreeing to co-referee this thesis.

I want to express my gratitude to Karl Jansen who has always supported me in every possible way. It is hard to imagine where I would be without him.

Furthermore, I thank Luca Biferale and Raffaele Tripiccione for their kind hospitality during my visit to Rome Tor Vergata and Ferrara. I will keep in memory these great times including the interesting discussions about the Italian way of life.

It has been a great pleasure working with Jürgen Berges, Luca Biferale, Astrid Eichhorn, Karl Jansen, Leticia F. Palhares, Michael M. Scherer, Lorenz von Smekal, Jan H. Stockemer, and Raffaele Tripiccione, all of whom I want to thank for collaboration. I have greatly benefited from numerous discussions that have contributed to the research presented in this thesis.

Furthermore, I want to acknowledge useful and interesting discussions with Igor Böttcher, Jens Braun, Michael Buchhold, Léonie Canet, Shailesh Chandrasekharan, Alessandro Codello, Sebastian Diehl, Joaquin Drut, Stefan Flörchinger, Thomas Gasenzer, Holger Gies, Victor Gurarie, Martin Hasenbusch, Lukas Janssen, Anyi Li, Steven Mathey, Boris Nowak, Peter Orth, Giorgio Parisi, Jan Pawlowski, Andrea Pelissetto, Leo Radzihovsky, Daniel D. Scherer, Jörg Schmalian, Lukas Sieberer, and Nicolas Wschebor.

Special thanks go to Florian Hebenstreit, Karl Jansen, Steven Mathey, Andreas Rodigast, Michael M. Scherer, Sören Schlichting, and Jan H. Stockemer for taking their time to carefully proofread my thesis. Of course, any remaining errors or mistakes are solely due to my shortcoming.

During the last three years I have met many people with whom I shared a great time. Thanks for the great memories: Conrad Albrecht, Kirill Boguslavskii, Igor Böttcher, Pascal Büscher, Stefano Carignano, Nicolai Christiansen, Sam Edwards, Jean-Sebastien Gagnon, Daniil Gelfand, Lutz Goergen, Florian Hebenstreit, Tobias Henz, Tina Herbst, Valentin Kasper, Gerald Langhanke, Steven Mathey, Mario Mitter, Daniel Müller, Boris Nowak, Daniel Nowakowski, Sebastian Ohmer, Asier P. Orioli, Leticia F. Palhares, Andreas Rodigast, Ignacy Sawicki, David Scheffler, Michael M. Scherer, Sören Schlichting, Giulio Schober, Dénes Sexty, Jan H. Stockemer, Nils Strodthoff, Nicolas Tessore, Martin Trappe, Sebastian Wetzel, and Thorsten Zöller.

Thanks to Eric M. Foard, Mauro Sbragaglia, and Marcello Sega for making my stay at Rome Tor Vergata such a memorable experience.

Finally, I want to thank those people without whom this work would have never been possible. I want to thank my family for their continuous support. Silvia Arroyo Camejo for her constant love and encouragement. With you I am set for whatever journey may come.

Contents

1. Introduction

Phase transitions are ubiquitous in nature. They distinguish different thermodynamic phases or ground state properties of quantum many-body systems. However, there are exceptional points in the phase diagram where such a distinction becomes no longer possible. An example for such a critical point is observed in the phase diagram of carbon dioxide CO_2, where above the critical temperature T_c the liquid-gas transition ceases to exist and the system is described by a single supercritical fluid phase [1]. There are numerous other examples for such continuous phase transitions ranging from ferromagnetic and liquid-gas systems encountered in condensed-matter physics [2] to the critical endpoint in the phase diagram of quantum chromodynamics (QCD) probed by high-energy heavy-ion experiments (see Ref. [3] for a review). The single property that characterizes such points is the phenomenon of scale-invariance. As one approaches the critical point the characteristic scale of correlations ξ diverges and fluctuations become equally important on all length scales. This is beautifully illustrated by the observation of critical opalescence in light-scattering experiments of critical fluids. At the critical point where $\xi \to \infty$ the properties of the system become insensitive to the microscopic details of the inter-atomic interactions and one observes universality. Independent of the specific material properties, the critical behavior close to a continuous phase transition is characterized by a set of critical exponents, universal amplitude ratios, and scaling functions that determine the role of fluctuations for the system. Based on these quantities different systems may be grouped together in universality classes that fully characterize the properties of strongly-correlated systems in the critical state. While the concept of scale-invariance and universality seem very appealing from a theoretical point of view, one might wonder why our daily experience does not fit into this picture. Why do most systems exhibit a clear scale-dependence while at the critical point the system seems to simplify so considerably?

As naive as this question might sound, it is a very fundamental one. In fact, the same question arises in a somewhat different incarnation in quantum field theory, where back in the 1960s calculations of the fundamental properties of quantum fields in quantum electrodynamics (QED) were plagued by ultraviolet divergences (see Ref. [4] for a historical account). To obtain finite results one has to add counterterms to the theory that lead to a cancellation of divergences. However, to make contact with experiment an additional renormalization scale needs to be supplied, where the theory is fit to experimental data. Providing this information it is then possible to connect the behavior of the theory at different energy scales. Thus, quantum field theory does not explain the fundamental origin of the parameters and couplings in the theory, e.g., the $U(1)$ gauge coupling, but rather provides an explanation why these

quantities change with the energy scale at which they are measured. The scale-dependence is due to the quantum fluctuations in the vacuum state. While this procedure has led to a remarkable success of quantum field theory fitting extraordinarily well to high-precision QED experimental data (see [5] for a comprehensive review), at that time many people remained skeptical about the theoretical significance of the renormalization program. Indeed, back then the requirement of renormalizability seemed to be of a mere technical nature, necessary to yield finite results and was difficult to understand from a fundamental perspective.

In 1971 K. G. Wilson noticed the striking analogy between the scale-dependence observed in quantum field theory and the theory of phase transitions leading to the development of the renormalization group [6, 7] thereby giving a natural explanation for the seemingly *ad hoc* renormalization procedure that was developed in field theory in the decades before. The renormalization group interprets the scale-dependence of a given theory as the flow of its parameters under renormalization group transformations in an abstract space of theories. A single renormalized trajectory in this infinite-dimensional space therefore captures the behavior of a theory on a range of different scales. The significance of this idea was that the renormalization group transformations naturally lead to fixed points where the the physics is invariant under scale transformations. It is these special points in theory space that correspond to the critical phenomena that one observes at a continuous phase transition. There the behavior of the theory simplifies considerably, where the characteristics of fluctuations is captured by a finite set of quantities. Based on the huge amount of accumulated data on critical phenomena, both from experiment and numerical simulations, these ideas were simple to test which led to an immediate acceptance of the theory.

The presence of fixed points in the renormalization group flow strongly influences the possible types of behavior dividing the theory space into different attraction domains. It thus gives a clear explanation for the observation of universal scaling behavior. It relates to different renormalization group trajectories running to one and the same fixed point of the renormalization group. Thus, fixed points serve to characterize the infinite realm of possible theories into distinct universality classes fixed by just a few properties like the dimensionality or symmetries of the problem. In fact, the simplicity of the renormalization group flow at these fixed points allows for a straightforward classification and quantitative description of the critical scaling properties which yields an impressive accuracy compared to experimental data (see Ref. [8] for a comprehensive review). From the ground state properties of systems at zero temperature to systems far from equilibrium, at a fixed point of the renormalization group these theories drastically simplify. The renormalization group provides a unifying framework for our understanding of the behavior of systems at different scales.

While the underlying idea of the renormalization group is both remarkably simple and profound, in practice it might be very difficult to establish the critical properties of a particular model. Close to a critical point the fluctuations generally lead to strong correlations in the system, where perturbative techniques are only of limited use. An exception is given by the

$O(N)$ symmetric model which is super-renormalizable in three dimensions (see, e.g., [9]). This allows for a direct calculation of the critical properties in $d = 3$ Euclidean dimensions in the symmetric phase by use of sophisticated resummation techniques [10]. The ϵ-expansion developed in [11, 12] enables a computation of critical exponents around the upper or lower critical dimension but also requires some resummation procedure. Alternative nonperturbative expansion schemes, e.g., in the number of field components N [13] provide valuable information but are unable to access the physically interesting regime, where typically $N \simeq \mathcal{O}(1)$. Nonperturbative techniques that do not rely on the expansion in a small parameter are called for and in particular necessary to capture the physics at strong coupling fixed points. The functional renormalization group [14, 15] provides a nonperturbative formulation that is particularly well-suited for practical calculations (see [16–18] for an elementary introduction). It has been successfully applied to the calculation of static equilibrium critical properties [17, 19, 20], to the dynamic critical scaling for purely relaxational models [21], to field theories driven to a nonequilibrium steady state [22–24], as well as to stationary transport solutions described by nonthermal fixed points [25, 26].

In chapter 2 of this thesis, we give an account of the functional renormalization group where we derive the renormalization group flow equation that is employed extensively in this work. In the following chapters we consider different examples of fixed point solutions relating to the ground state properties of quantum many body systems, multicritical phenomena, dynamic critical behavior near equilibrium, and scaling properties far from equilibrium. In the first three chapters of this thesis, chapters 2 – 5, we apply the functional renormalization group to determine the static and dynamic critical scaling properties. In chapter 6 we employ Monte Carlo methods to determine the statistical properties of small-scale fluctuations in the stationary state far from equilibrium. In the following, we give a detailed outline of this thesis:

In chapter 3 we consider the quantum ground state properties of a system of spinless fermions on the honeycomb lattice. We discuss a particular example of a quantum critical point that describes a transition from a semimetal to a charge density wave/Kekulé-ordered state. In the semimetal phase this system features distinct points in the first Brillouin zone, so-called Dirac points, where one observes a massless linear dispersion of the quasi-particles, resembling the properties of low-energy excitations in graphene [27, 28]. The transition in the ground state properties describes a change in the spectrum of the theory, leading to the opening of a finite energy gap. Such a change can be induced either by applying an external perturbation to the system, or dynamically by strong interactions. Indeed, the vanishing density of states at the Dirac point rules out any screening of interactions and this makes the system in particular susceptible to interaction effects. Whether such a quantum phase transition is induced by the strong electron-electron interactions in suspended graphene has been a much investigated question [29–35]. The current experimental evidence does not seem to provide an indication for a finite gap however indicates the importance of interactions which lead to a strong renormalization of energy spectrum [36]. Also other experimental results indicate that graphene may be close to a quantum critical point (see, e.g., [30]). In

that case, it is important to quantify the scaling behavior at the transition since it may determine the physical response of the system [37]. Here, we determine the critical properties of the continuous quantum phase transition using a low-energy effective $U(2)$ symmetric matrix-Yukawa model in the framework of the functional renormalization group, where we find evidence for a strong dominance of fluctuations.

In chapter 4, we discuss the critical behavior in theories with two competing order parameters. For such systems, the intricate interplay of fluctuations may yield a multicritical point in the phase diagram where one observes scaling properties distinct from the respective critical lines. In fact, the system is in a different universality class and new critical exponents may occur. Such models have been applied to describe a wide variety of systems ranging from ultracold atoms to extreme states of matter in QCD (see [38] for a review). Here, we give an account of these models and investigate their critical scaling behavior with the functional renormalization group. We find different fixed point solutions that relate either to bicritical or tetracritical scaling behavior in the phase diagram and we discuss the relation of our results to available data from field-theoretic expansions, experiment, and Monte Carlo simulations.

In chapter 5 we consider the dynamic critical scaling behavior of scalar models in the long-time limit. The critical dynamics with a single relaxational order parameter has been studied previously in the context of the functional renormalization group [21]. However, the presence of conserved quantities strongly influences the dynamics [39] and it is therefore important to couple the system to additional modes related to the relevant conservation laws. Here, we provide a first analysis of such a scenario in the context of the functional renormalization group at the example of a $O(N)$ symmetric model coupled to a conserved density. This model features a complex phase diagram with different types of dynamic critical behavior. In particular, we establish the existence of an anomalous diffusion phase with new dynamic scaling properties. The existence of such a phase has been controversially discussed in the framework of the ϵ-expansion [40–43] with no clear conclusion on its existence or scaling properties. A more recent work even ruled out its existence based on the ϵ-expansion to two-loop order [43]. The functional renormalization group does not rely on such a small expansion parameter and provides an unambiguous identification of this phase.

Finally, in chapter 6 we describe a new numerical approach to determine the scaling properties of nonequilibrium steady states based on the functional integral formulation of classical-statistical dynamics [44–46] using lattice Monte Carlo simulations. Possible strategies to sample field configurations in the stationary nonequilibrium state are explored in detail explaining necessary adaptions of lattice Monte Carlo techniques to real-time dynamics. We apply these methods to a simple model for hydrodynamic turbulence – the random-force-driven Burgers' equation (see, e.g., the reviews [47, 48]). This model provides for a clear understanding of the basic mechanisms leading to the strong deviations from Gaussian behavior (intermittency) associated to the universal anomalous scaling behavior observed in various systems displaying hydrodynamic turbulence [49]. We determine the scaling spectrum of small-scale fluctuations

and find indications for a transition to a universal scaling regime.

2. Functional renormalization group

In the following, we give an account of the functional renormalization group (RG) and illustrate how critical exponents can be determined for a particular system of interest. Very good reviews exist in the literature [14, 16–20, 50–54] that give an overview over the technical details of functional renormalization, formal developments, as well as physical applications. For the interested reader (and for a more detailed account) we refer to these references. Here, we consider the $O(N)$ symmetric theory in d Euclidean dimensions as a simple example. We illustrate the construction of the functional flow equation for the scale-dependent effective action and discuss typical approximations that are used to solve the RG flow. We also comment on the inclusion of fermions and the derivation of real-time properties from the effective action.

The complete information about a theory or a physical system in general resides in correlation functions which are defined in terms of the generating functional

$$Z[J] = \int [d\varphi]\, e^{-S[\varphi]+\int d^dx\, J_a(x)\varphi_a(x)} \ . \tag{2.1}$$

The functional measure $[d\varphi] = \prod_x d\varphi(x)$ is rigorously defined in the presence of some ultraviolet cutoff Λ and (2.1) is defined in the limit, where the cutoff is removed from the theory (assuming that such a limit exists). This provides a nonperturbative definition of the theory, where the classical action $S[\varphi]$ may include arbitrary powers of the fields. However, there are few situation where the functional integral can be solved exactly. Typically, one has to rely on some approximation based on an expansion in powers of a small parameter. On the other hand, one may attempt to solve the theory using numerical lattice Monte Carlo methods (see, e.g., [55, 56] for an introduction).

Here, however, we want to consider the full generating functional to derive an exact relation that is susceptible to approximations that do not rely on a small parameter. We introduce the generating functional of connected correlation functions

$$\begin{aligned} W[J] &= \ln \int [d\varphi]\, e^{-S[\varphi]+\int d^dx\, J_a(x)\varphi_a(x)} \\ &= \sum_{n=1}^{\infty} \frac{1}{n!} \int d^dx_1 \cdots \int d^dx_n\, J_{a_1} \cdots J_{a_n} W^{(n)}_{a_1\cdots a_n}(x_1,\ldots,x_n) \ , \end{aligned} \tag{2.2}$$

which defines the moments

$$W^{(n)}_{a_1\cdots a_n}(x_1,\ldots,x_n) = \frac{\delta^n W[J]}{\delta J_{a_1}(x_1)\cdots\delta J_{a_n}(x_n)} \ , \tag{2.3}$$

that take the following form

$$W_a^{(1)}(x) = \langle\varphi_a(x)\rangle = \phi_a(x) \ , \tag{2.4}$$

$$W_{ab}^{(2)}(x,y) = \langle\varphi_a(x)\varphi_b(y)\rangle - \phi_a(x)\phi_b(y) \ , \tag{2.5}$$

to lowest order in the expansion (2.2). Note, that they are defined in the absence of external sources, i.e., $J = 0$. While the generating functional defines the correlation functions and includes all information on the theory, in practice it is more convenient to define an alternative functional that leads to a variational problem for the quantities of interest, i.e., field expectation values or higher-order correlation functions. For that purpose, we perform the Legendre-transform:

$$\Gamma[\phi] = \sup_J \left\{ \int d^dx \, J_a(x)\phi_a(x) - W[J] \right\} \ , \tag{2.6}$$

where the field-expectation value is ϕ_a is defined for nonvanishing J:

$$\phi_a(x) = \frac{\delta W[J]}{\delta J_a(x)} = \langle\varphi_a(x)\rangle_J \ , \tag{2.7}$$

and $\Gamma = \Gamma[\phi]$ defines the generating functional for one-particle-irreducible (1PI) correlation functions (see, e.g., Ref. [57] for the terminology). The functional (2.6) allows us to derive an equation of motion for the system in the presence of nonvanishing sources:

$$\frac{\delta\Gamma[\phi]}{\delta\phi_a(x)} = J_a(x) + \int d^dy \left\{ \frac{\delta J_b(y)}{\delta\phi_a(x)}\phi_b(x) - \frac{\delta W[J]}{\delta J_b(y)}\frac{\delta J_b(y)}{\delta\phi_a(x)} \right\} = J_a(x) \ . \tag{2.8}$$

A solution $\phi = \langle\varphi\rangle_J$ includes all contributions from quantum/statistical fluctuations. While eq. (2.8) certainly provides for a clear interpretation, the quantity Γ still needs to be determined. After all, we have simply made definitions without actually computing (2.1). We may obtain an expression for Γ by performing the transformation $\varphi \to \phi + \varphi$ (which leaves the functional measure invariant), whereby:

$$e^{-\Gamma[\phi]} = \int [d\varphi] \, e^{-S[\phi+\varphi] + \int d^dx \, \frac{\delta\Gamma}{\delta\phi_a(x)}\varphi_a(x)} \ . \tag{2.9}$$

Of course, this equations defines Γ in terms of a tremendously complicated equation, defining an infinite hierarchy for the derivatives of the effective action where at each order we have to solve the complete functional integral.

However, one might use an alternative definition of the theory that allows us to include fluctuations in a controlled way. For that purpose we introduce an additional term to the microscopic action

$$\Delta_k S[\varphi] = \frac{1}{2}\int \frac{d^dq}{(2\pi)^d} \, \varphi_a(-q) R_{k,ab}(q) \varphi_b(q) \ , \tag{2.10}$$

that depends on the scale-parameter k, controlling the importance of this operator. Note, that (2.10) is quadratic in the fields and plays the role of a scale-dependent mass term. The function R_k thus implements a mass-like cutoff that can be used to regulate the infrared modes of the theory. This is akin to the Kadanoff-Wilson idea of successively integrating out

momentum modes [12]. Of course, to make sure that the addition of such a term (2.10) in the functional integral does not alter the physical properties of the theory one has to formulate additional constraints that fix the possible form of the regulator function R_k. They are based on the requirements that the modified theory should reproduce the correct classical limit, as well as the full quantum/statistical correlation functions. In particular, in the limit where the scale-parameter k is removed and all modes have been taken into account we should obtain the full effective action $\Gamma_{k\to 0} = \Gamma$. On the other hand, in the opposite limit, we would like to restore the correct microscopic description of the theory. These requirements are expressed in terms of the following limiting behavior of the regulator function

$$R_k(q) \;\to\; \infty \;, \quad q^2/k^2 \ll 1 \;, \tag{2.11}$$

$$R_k(q) \;\to\; 0 \;, \quad q^2/k^2 \gg 1 \;, \tag{2.12}$$

The first constraint implements the requirement that the classical action should be restored at the ultraviolet scale

$$\lim_{k\to\Lambda} \Gamma_k = S \;. \tag{2.13}$$

while the second property describes the inclusion of all fluctuations in the limit $k \to 0$ where the scale-parameter is removed and produces the full effective action:

$$\lim_{k\to 0} \Gamma_k = \Gamma \;. \tag{2.14}$$

Apart from these conditions the regulator function may be chosen freely. By definition this freedom should not affect the physical properties of the system, both in the classical and quantum/statistical limit. It is important to point out that the implementation of the renormalization group flow in practice requires some truncation of the scale-dependent effective action that in fact, introduces a residual dependency on the regulator. However, one may employ certain optimization criteria to minimize their effect on the theory, when the limit $k \to 0$ is taken [58, 59].

The scale-parameter k can be used to to construct a flow equation for the scale-dependent effective action Γ_k. We define this quantity by introducing the scale-dependent generating functional

$$e^{W_k[J]} = \int [d\varphi]\, e^{-S[\varphi]-\Delta_k S[\varphi]+\int d^d x\, J_a(x)\varphi_a(x)} \;, \tag{2.15}$$

and considering its Legendre-transform:

$$\Gamma_k[\phi] = \sup_J \left\{ \int d^d x\, J_a(x)\phi_a(x) - W_k[J] \right\} - \Delta_k S[\phi] \;. \tag{2.16}$$

Taking the logarithmic scale derivative with respect to the quantity $t = \ln(k/\Lambda)$, where

$$\frac{\partial}{\partial t} = k\frac{\partial}{\partial k} \;, \tag{2.17}$$

we obtain

$$\begin{aligned} \frac{\partial \Gamma_k}{\partial t} &= \frac{\partial}{\partial t}\left\{-W_k[J] - \Delta_k S[\phi]\right\} \;, \\ &= \frac{1}{2}\int \frac{d^d q}{(2\pi)^d}\, \frac{\partial R_{k,ab}(q)}{\partial t} \big(W_k^{(2)}\big)_{ab}(q) \;, \end{aligned} \tag{2.18}$$

where the second functional derivative $W_k^{(2)}(q)$ (in the presence of nonvanishing sources J and R) defines the inverse regularized propagator:

$$\left(W_k^{(2)}\right)^{-1}(q) = \Gamma_k^{(2)}(q) + \Delta_k S^{(2)}(q) = \Gamma_k^{(2)}(q) + R_k(q) \ . \tag{2.19}$$

Note, that we write

$$W_{ab}^{(2)}(q) = \frac{(2\pi)^d}{\delta(0)} \frac{\delta^2 W_k[\phi]}{\delta\phi_a(-q)\delta\phi_b(q)} \ , \quad \Gamma_{k,ab}^{(2)} q) = \frac{(2\pi)^d}{\delta(0)} \frac{\delta^2 \Gamma_k[\phi]}{\delta\phi_a(-q)\delta\phi_b(q)} \ , \quad \text{etc.} \tag{2.20}$$

where the additional volume-dependency is removed from the two-point function by the formal division of $\delta(0) = \lim_{p\to 0} \delta(p)$. From these expressions, we finally derive the flow equation for the effective average action [14]:

$$\frac{\partial\Gamma}{\partial t} = \frac{1}{2}\,\mathrm{Tr} \int \frac{d^d q}{(2\pi)^d} \frac{\partial R_k(q)}{\partial t} \left(\Gamma_k^{(2)}(q) + R_k(q)\right)^{-1} \ , \tag{2.21}$$

where the trace $\mathrm{Tr}(\cdots)$ denotes a summation over field indices.

A similar derivation holds for fermionic degrees of freedom. In Euclidean dimension d the Grassmann-valued fields $\bar{\psi}$ and ψ define two independent degrees of freedom [60], and we define the regulating part of the action as:

$$\Delta_k S[\Psi] = \frac{1}{2} \int \frac{d^d q}{(2\pi)^d} \left\{\bar{\psi}_a(q) R_{F\,k,ab}(q) \psi_b(q) - \psi_a^T(q) R_{F\,k,ab}(q) \bar{\psi}_b^T(q)\right\} \ , \tag{2.22}$$

where the transposition $(\cdots)^T$ applies to the implicit Lorentz-indices of the spinors. Using the property $-R_{F\,k}(q) = R_{F\,k}(-q)$ we introduce the following field

$$\Psi(q) = \begin{pmatrix} \psi(q) \\ \bar{\psi}^T(-q) \end{pmatrix} \ , \tag{2.23}$$

which is convenient for later calculations. We see that we may write the regulator part of the action in the form

$$\Delta_k S[\Psi] = \frac{1}{2} \int \frac{d^d q}{(2\pi)^d} \, \Psi_a^T(-q) R_{k,ab}(q) \Psi_b(q) \ , \tag{2.24}$$

resembling the structure of the regulating term for the scalar degrees of freedom. Here, however, the regulator function R_k takes a block-nondiagonal form:

$$R_{k,ab}(q) = \begin{pmatrix} 0 & R_{F\,k,ab}^T(q) \\ R_{F\,k,ab}(q) & 0 \end{pmatrix} \ . \tag{2.25}$$

In fact, any additional degrees of freedom may be treated this way and we may define a formal quantity χ that incorporates the complete field content of the respective model. Note, that it does not correspond to a field, since the components transform in different representations of the Lorentz group. In the following chapters we will consider theories involving both fermionic and scalar degrees of freedom.

Until now we have not specified the form of the regulator functions, stating simply that they should satisfy certain limiting properties. To regulate the fluctuations, one typically chooses regulators of the form

$$R_{B\,k}(q) = Z_{B\,k} q^2\, r_{B\,k}(q^2) \;, \tag{2.26}$$

$$R_{F\,k}(q) = Z_{F\,k} \not{q}\, r_{F\,k}(q^2) \;, \tag{2.27}$$

where Z_B and Z_F correspond to the renormalization factors that we introduce below. They are chosen to match the momentum-structure of the propagators which is convenient to display the scaling properties at the fixed point. Eqs. (2.27) – (2.26) are fully defined in terms of the so-called shape functions r_B and r_F that describe the scheme-dependence of the renormalization group flow. For typical choices employed in this work see the Appendix B.

Before we go on to illustrate how the functional renormalization group flow equation can be solved in practice, let us comment on possible applications to real-time dynamics. Apart from our initial assumption that we restrict ourselves to d Euclidean dimension the techniques presented here are completely extendable to calculate real-time properties. For this one typically defines the field theory on a closed time path which effectively leads to a doubling of degrees of freedom (see, e.g., [26] for a review). This, simply enhances the field content of the model. However, the real issue concerns the choice of the regulator function in the presence of continuous spacetime symmetries, where the frequency/momentum-part of the propagator is not positive-definite. Such a case requires a careful choice of the regulator function (see, e.g., the discussion in Ref. [61]).

Of course, the solution of the flow equation relies on an appropriate truncation of the scale-dependent effective action. Typically, an expansion around a homogeneous field configuration $\phi = \text{const.}$ is considered, where one uses a derivative expansion [62–65]:

$$\Gamma_k[\phi] = \int d^d x \left\{ Z_k(\phi)(\partial\phi)^2 + U_k(\phi) + \mathcal{O}(\partial^2) \right\} \;, \tag{2.28}$$

$U_k(\phi)$ denotes the effective potential, which is defined by the momentum-independent contribution to the effective action. It essentially controls the phase structure of the model while the momentum-dependent part provides the contributions from fluctuations and is important to obtain a reliable estimate for the critical exponents.

One might consider an expansion in an appropriate basis of field operators $\mathcal{O}_n(\phi)$, where

$$U_k(\phi) = \sum_n \bar{g}_{n,k} \mathcal{O}_n(\phi) \;, \tag{2.29}$$

defined in terms of the bare couplings $\bar{g}_{n,k}$. Note, that the scale-dependence is indicated explicitly by an index and should not be confused with the expansion index. The bare couplings may be written in the dimensionless form $\bar{g}_n k^{-d_{\mathcal{O}_n}}$ where $d_{\mathcal{O}_n}$ corresponds to the canonical dimension of the operators $\mathcal{O}_n(\phi)$ that are included in the expansion (2.29). Together with the renormalization factor $Z_k = Z_k(\phi)$ that incorporates the effect of fluctuations, the complete

set of couplings g_n fully defines a particular truncation of the effective action to the given order in the derivative expansion. Such a truncation to $\mathcal{O}(\partial^2)$ already captures significant information about the critical properties at a fixed point. In particular, applied together with the field expansion (2.29) it provides a reliable way to compute leading and subleading critical exponents [62, 64–70]. We should note however, that the quality of the truncation largely depends on the expected critical behavior of the model under investigation. While a continuous phase transition is well-described by an expansion in powers of field operators, a first-order may only be poorly resolved [71, 72].

We derive the renormalization group equations for the dimensionless renormalized couplings which provides an appropriate parametrization of the RG flow to identify fixed points solutions. Indeed, at the fixed point the physics is scale-independent and is characterized by constant values of the parameters and couplings of the model, $g_n = g_{n,*}$. The renormalization group flow equations for the couplings g_n (β-functions) decompose into a dimensional part which comes from the canonical dimension of the corresponding operator $\mathcal{O}_n(\phi)$ and an additional contribution from (2.21)

$$\beta_{g_n} = \frac{\partial g_n}{\partial t} = (-d_{\mathcal{O}_n} + c_n\eta)g_n + \cdots \ . \tag{2.30}$$

The dimensional part of the flow receives additional corrections $\sim c_n\eta$ from the field renormalization, which is encoded in the anomalous dimension

$$\eta(\phi) = -\frac{\partial \ln Z_k(\phi)}{\partial t} \ , \tag{2.31}$$

evaluated at the minimum of the effective action. We will write $\beta_n \equiv \beta_{g_n}$ in the following. A fixed point corresponds to a special point theory space, where the β-functions vanish, i.e., $\beta_n(g_*) = 0$ for all n, and g_* denotes the fixed point values. Such a point controls the overall topology of the renormalization group flow and divides the theory space into distinct attraction domains. It is thus important to ask about the properties of the flow in their vicinity to understand the possible behavior of the theory. For that purpose, we consider the linearized β-functions at the fixed point, taking the form:

$$\beta_n = \sum_m \frac{\partial \beta_n(g_*)}{\partial g_m}(g_m - g_{m,*}) + \mathcal{O}(g^2) \ . \tag{2.32}$$

This enables us to ask about the stability properties under the successive inclusion of fluctuations, where the fixed point will feature relevant and irrelevant directions, defined in terms of the behavior of linear perturbations

$$g_n - g_* = \sum_I c_I v_n^I \, (k/\Lambda)^{-\theta_I} \ . \tag{2.33}$$

They are written in terms of the eigenbasis v^I of the stability matrix $(\partial\beta_n/\partial g_m)$, where c_I correspond to expansion coefficients, independent of the scale-parameter k, and Λ is the ultraviolet scale in the system. The exponents θ_I define to the eigenvalues of the stability matrix, where

$$\frac{\partial \beta_n(g_*)}{\partial g_m} v_m^I = -\theta_I v_n^I \ . \tag{2.34}$$

Note, that in general the eigenvalues θ_I may be complex. However, only the real part Re θ_I determines the stability properties at the fixed point. In particular, considering the infrared properties of the theory, we inspect the $k \to 0$ behavior of perturbations. We may distinguish the following cases: If Re $\theta_I > 0$, the corresponding eigendirection v^I describes a relevant perturbation at the fixed point. In this case, the corresponding term (2.33) will grow when approaching the limit $k \to 0$, while Re $\theta_I < 0$ characterizes an irrelevant perturbation that eventually dies out in the infrared limit. In the special case, where Re $\theta_I = 0$ the corresponding operator is called marginal.

The scaling spectrum $\{\theta_I\}$ together with the anomalous dimension η characterizes the scaling behavior in the vicinity of the critical point. Typically, however, not all critical exponents will be independent of each other. Scaling relations might hold that relate their values to each other. In the following chapters we will frequently encounter such relations. For an overview on these relations we refer to [8].

This concludes our overview on the functional renormalization group. In the successive chapters we will indicate the necessary adaptions, i.e., special choices of regulator functions or alternative truncations explicitly.

3. Quantum phase transition for low-dimensional chiral fermions

Since the experimental realization of graphene [27, 28] there has been a tremendous activity leading to new intriguing phenomena in condensed matter physics [73]. The characteristic feature of graphene is the presence of the so-called Dirac points at the corners of the first Brillouin zone. At these special points, a linear dispersion for the low-energy excitations occurs [74], closely resembling that of massless relativistic fermions. The massless relativistic dispersion leads to remarkable electronic properties. A prominent example is the observation of the anomalous quantum Hall effect corresponding to a pseudospin–$\frac{1}{2}$ Berry phase [27, 75]. Moreover, graphene may serve as a simple toy model for studying long sought-after quantum relativistic effects [73] as, e.g., Klein tunneling [76, 77] and Zitterbewegung [78]. These phenomena can be understood in the framework of noninteracting relativistic Dirac fermions which are realized in monolayer graphene on a substrate. However, for suspended graphene [79–81] the situation is different and the system is strongly influenced by the large unscreened Coulomb interactions [82]. In what way the dynamics modifies the low-energy behavior of the excitations in graphene is an important open question. This parallels the situation in strongly interacting quantum field theories, as e.g., quantum chromodynamics (QCD) where the interaction at low energies leads to the spontaneous breaking of chiral symmetry [83]. In that sense, graphene can be seen as a laboratory for strongly interacting fermions. For suspended graphene the essential question is whether the Coulomb interactions are strong enough to drive the system close to an interacting fixed point. In the vicinity of a fixed point the system is governed only by the low-energy modes. The details of the underlying lattice theory are no longer relevant, and the theory drastically simplifies. There it often occurs that one has additional symmetries that are not present in the lattice theory [84]. Striking examples being the effective relativistic dispersion and the effective chiral symmetry for the low-energy theory.

Here, we consider the situation where the low-energy theory is defined in the vicinity of an interacting fixed point and we inquire specifically about its critical properties. In fact, suspended graphene may be expected to be close to a nontrivial quantum critical point if the coupling is sufficiently strong [29]. While in the perturbative regime short-range interactions are irrelevant for the dynamics, at strong coupling this is not necessarily so. Local four fermion interactions can be generated dynamically and may play an important role even for the long-range correlated system [35, 85–87]. In the past, the role of the short-range repulsive

interactions has been studied in the framework of the tight-binding model on the honeycomb lattice where, depending on the strength of the interactions, a competition between the staggered density and nontrivial topological phases was found [88]. Although both types of order are conceivable, for the case of suspended graphene, one expects a semimetal-Mott insulator phase transition [31, 32, 34, 35, 86, 87, 89–91], where the chiral symmetry is broken spontaneously by a nonzero vacuum expectation value of the chiral condensate. This corresponds to a type of staggered density phase [90–92] that alternates on the two sublattices of the bipartite honeycomb lattice.

We specifically address the critical properties for this chiral phase transition using the nonperturbative functional renormalization group [14, 19]. In particular, we neglect the influence of the long-range Coulomb interactions and characterize the properties of the short-range repulsive quantum critical point. Our approach circumvents the problems of a purely perturbative approach close to criticality, and for the first time, allows us to follow the flow of this model into the broken phase. Introducing composite degrees of freedom for the order parameters, we show that our model has a continuous phase transition in the universality class of a three-dimensional matrix Yukawa model with $U(2)$ symmetry.

Here, we formulate the low-energy effective theory for spinless fermions on the honeycomb lattice interacting via a short-range repulsive interaction. In particular, such a model may be used to study the dynamics of strongly-interacting fermions in graphene. We discuss the symmetry properties of the effective model and consider the physical significance of different fermion bilinears in the microscopic lattice description. In the framework of the functional renormalization group we derive the flow equations for the partially bosonized model and determine the critical exponents at the continuous chiral phase transition. We find new critical exponents that determine a universality class distinct from the Gross-Neveu model typically considered for these models.

3.1. Low-energy theory

On a substrate the low-energy theory of graphene is described by the free Lagrangian

$$\mathcal{L} = i\bar{\psi}^a \gamma_\mu \partial_\mu \psi^a \ , \tag{3.1}$$

with the linear dispersion of Dirac quasiparticles. The flavor index takes the values $a = 1, \ldots, N_f$ and characterizes the physical spin of the quasiparticles. For a single layer of graphene, the number of Dirac fermions is $N_f = 2$. Here, we take $N_f = 1$, which corresponds to a system of spinless fermions on the honeycomb lattice whose band structure can also be modeled by photonic crystals [93–98]. In the following, we will leave the value N_f unspecified as long as not stated otherwise. The low-energy excitations on the honeycomb lattice in two space dimensions are described in terms a Lagrangian in $d = 3$ Euclidean space-time dimensions, with the index $\mu = 0, 1, 2$. That is, throughout this chapter we assume full

Euclidean rotational invariance. For the 2+1-dimensional relativistic theory, this translates to the statement that the dynamical critical exponent is assumed to be $z = 1$ and that the Fermi velocity v_F is noncritical. In fact, it has been argued that close to the semimetal-insulator critical point Lorentz-symmetry breaking perturbations are irrelevant and that a description in terms of a Euclidean-invariant low-energy theory is viable [87, 91, 99]. In Euclidean space-time[1] the Lagrangian (3.1) satisfies Osterwalder-Schrader reflection positivity [100], and the spinors $\psi^\dagger \equiv i\bar{\psi}\gamma_0$ are not conjugate to ψ, but instead define independent degrees of freedom. Furthermore, we use a reducible chiral representation for the fermions where the gamma matrices satisfy the Dirac algebra

$$\{\gamma_\mu, \gamma_\nu\} = 2\delta_{\mu\nu} \ , \quad \mu, \nu = 0, 1, 2 \ , \tag{3.2}$$

and are given explicitly by

$$\gamma_0 = \begin{pmatrix} 0 & -i\sigma_3 \\ i\sigma_3 & 0 \end{pmatrix} \ , \quad \gamma_k = \begin{pmatrix} 0 & -i\sigma_k \\ i\sigma_k & 0 \end{pmatrix} \ , \quad k = 1, 2 \ , \tag{3.3}$$

where σ_k, $k = 1, 2, 3$ denote the 2×2 Pauli matrices. Apart from these matrices the Dirac algebra consists of the two matrices

$$\gamma_3 = \begin{pmatrix} 0 & \mathbb{1} \\ \mathbb{1} & 0 \end{pmatrix} \ , \qquad \gamma_5 = \begin{pmatrix} \mathbb{1} & 0 \\ 0 & -\mathbb{1} \end{pmatrix} \ , \tag{3.4}$$

that anticommute with all γ_μ, $\mu = 0, 1, 2$, and with each other, as well as their combination $\gamma_{35} = (i/2)[\gamma_3, \gamma_5]$. Note, that these matrices do not appear in the Lagrangian (3.1) which gives rise to a certain freedom to define the discrete symmetries [101] (see Sec. 3.2).

In the chiral representation the states with definite chirality

$$\gamma_5 \psi_\pm = \pm \psi_\pm \ , \tag{3.5}$$

are taken to define the excitations around the two distinct Dirac points $\vec{K}_+$ and $\vec{K}_- = -\vec{K}_+$ at opposite corners of the first Brillouin zone. It is exactly at these two points where the one-particle spectrum becomes linear and can be modeled by a theory of relativistic Dirac fermions (3.1). The remaining components of the chiral left- and right-handed fermions essentially characterize the excitations on the two triangular sublattices A and B of the bipartite honeycomb lattice. To make this mapping explicit we give the connection to the one-particle fermion operators that describe the hopping of electrons on the honeycomb lattice. The free tight-binding Hamiltonian

$$H_0 = -t \sum_{\langle i,j \rangle} \left(u^{\dagger a}(\vec{r}_i) v^a(\vec{r}_j) + \text{H. c.} \right) \ , \tag{3.6}$$

defines the dynamics, where a summation over the spin (flavor) indices $a = 1, \ldots, N_f$ is implied (recall that the flavor index relates to the physical spin of the particles on the honeycomb

[1] For our Euclidean conventions see, e.g., [60].

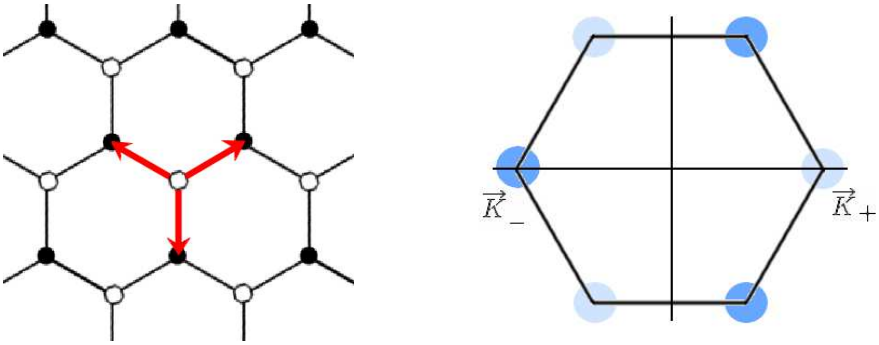

Figure 3.1.: (**Left**) The bipartite hexagonal lattice with the two sublattices A and B indicated by full and open dots. The red arrows denote the nearest neighbor hopping in the tight-binding Hamiltonian (3.6). (**Right**) The two inequivalent Dirac points $\vec{K}_+$ and $\vec{K}_-$ at opposite corners of the first Brillouin zone.

lattice). Here, t is the hopping parameter and the sum is taken over all nearest neighbor sites on the honeycomb lattice. The operators $u^a(\vec{r}_i)$ and $v^a(\vec{r}_j)$ anticommute and define the fermionic excitations on the two sublattices A and B. In the low-energy limit, where we consider only the linear excitations around the two Dirac points, this model reproduces the free Dirac Lagrangian (3.1) (in units where $v_F = ta\sqrt{3}/2 = 1$, with a being the lattice spacing). It is this limit that provides the connection between the microscopic degrees of freedom that enter the dynamics (3.6) and the low-energy excitations of the continuum theory (3.1). Following this correspondence, the Dirac spinor ψ has a direct representation in terms of the single-particle fermionic operators $u^a_\pm$ and $v^a_\pm$, defined at the two Dirac points $\vec{K}_\pm$, respectively. It is given by

$$\psi \;=\; \begin{pmatrix} u_+ \\ iv_+ \\ iv_- \\ u_- \end{pmatrix} \;, \quad \bar{\psi} = -\left(iv_-^\dagger,\, u_-^\dagger,\, u_+^\dagger,\, iv_+^\dagger\right) \;, \tag{3.7}$$

up to a global phase factor, where we have dropped the flavor indices for simplicity, and we will write them explicitly when needed. The relative phases follow from the chosen representation of the Dirac algebra (3.3). It immediately follows that the two-component chiral left- and right-handed fermions can be identified as

$$\psi_+ = \begin{pmatrix} u_+ \\ iv_+ \end{pmatrix} \;, \quad \psi_- = \begin{pmatrix} iv_- \\ u_- \end{pmatrix} \;. \tag{3.8}$$

Note that this identification of the spinor degrees of freedom in the chiral representation is equivalent to the one given, e.g., in [30]. Both the decomposition of the honeycomb lattice into the two sublattices, and the two inequivalent Dirac points in the first Brillouin zone are illustrated in Fig. 3.1.

The low-energy theory of Dirac fermions (3.1) has a continuous $U(2)$ chiral symmetry which is not apparent on the level of the microscopic tight-binding model (3.6). It is generated by

the matrices $\mathbb{1}$, γ_3, γ_5, and γ_{35} with following transformation properties

$$U_{\mathbb{1}}(1): \quad \psi \to e^{i\theta}\psi \ , \qquad \bar{\psi} \to \bar{\psi}e^{-i\theta} \ , \tag{3.9}$$

$$U_{\gamma_3}(1): \quad \psi \to e^{i\gamma_3\theta}\psi \ , \qquad \bar{\psi} \to \bar{\psi}e^{i\gamma_3\theta} \ , \tag{3.10}$$

$$U_{\gamma_5}(1): \quad \psi \to e^{i\gamma_5\theta}\psi \ , \qquad \bar{\psi} \to \bar{\psi}e^{i\gamma_5\theta} \ , \tag{3.11}$$

$$U_{\gamma_{35}}(1): \quad \psi \to e^{i\gamma_{35}\theta}\psi \ , \qquad \bar{\psi} \to \bar{\psi}e^{-i\gamma_{35}\theta} \ , \tag{3.12}$$

where θ is a real parameter. In fact, this $U(2)$ chiral symmetry leads to a global $U(2N_f)$ symmetry which plays an important role for the dynamics, as it constrains the possible interactions for the low-energy theory close to the critical point. Specifically, for the local four fermion interactions it is possible to define a complete set of operators that respect the $U(2N_f)$ flavor symmetry [90, 91, 102]. The corresponding operators are quasi-local in the microscopic lattice description (i.e., next neighbor and next-to-nearest neighbor). We have four such interactions, two of which are of flavor-singlet type, with the vector Thirring-like interaction

$$(\bar{\psi}^a\gamma_\mu\psi^a)^2 \ , \tag{3.13}$$

and the scalar Gross-Neveu-like interaction

$$(\bar{\psi}^a\gamma_{35}\psi^a)^2 \ . \tag{3.14}$$

Furthermore, there is a flavor-nondiagonal generalized Nambu-Jona-Lasinio interaction

$$(\bar{\psi}^a\psi^b)^2 - (\bar{\psi}^a\gamma_3\psi^b)^2 - (\bar{\psi}^a\gamma_5\psi^b)^2 + (\bar{\psi}^a\gamma_{35}\psi^b)^2 \ , \tag{3.15}$$

and another flavor-nondiagonal interaction of vector-type

$$(\bar{\psi}^a\gamma_\mu\psi^b)^2 + \left(\bar{\psi}^a\frac{\sigma_{\mu\nu}}{\sqrt{2}}\psi^b\right)^2 - (\bar{\psi}^a i\gamma_\mu\gamma_3\psi^b)^2 - (\bar{\psi}^a i\gamma_\mu\gamma_5\psi^b)^2 \ , \tag{3.16}$$

where $\sigma_{\mu\nu} = \frac{i}{2}[\gamma_\mu, \gamma_\nu]$ and $(\bar{\psi}^a\Gamma^{(j)}\psi^b)^2 \equiv \bar{\psi}^a\Gamma^{(j)}\psi^b\bar{\psi}^b\Gamma^{(j)}\psi^a$, with $\Gamma^{(j)}$ some element of the Dirac algebra. This defines all interactions invariant under the global $U(2N_f)$ symmetry [90, 91, 102]. However, this set of operators is over-complete. By Fierz transformations it is possible to show that only two of the above operators are linearly independent. Thus, we may choose to write any $U(2N_f)$-complete theory in terms of only the scalar and vector flavor-singlet interactions

$$\mathcal{L} = i\bar{\psi}^a\gamma_\mu\partial_\mu\psi^a + \frac{\bar{g}_V}{2N_f}\left(\bar{\psi}^a\gamma_\mu\psi^a\right)^2 + \frac{\bar{g}_S}{2N_f}\left(\bar{\psi}^a\gamma_{35}\psi^a\right)^2 \ , \tag{3.17}$$

which fully parametrize the short-range interactions. This theory is invariant also under the discrete parity, charge, and time reversal operations.

3.2. Symmetry properties

A possible instability triggered by the local four fermion interactions can lead to very different patterns of spontaneous symmetry breaking. Such an instability essentially leads to a non-vanishing vacuum expectation value of some fermion bilinear $\langle\bar{\psi}\Gamma^{(j)}\psi\rangle$, with $\Gamma^{(j)}$ an element

of the Dirac algebra. To identify the physical role of the order parameters in the low-energy theory we review the properties of generic fermion bilinears under discrete symmetry transformations. This enables us to map the order parameters in the low-energy theory onto the corresponding quantities in the microscopic lattice model. Such an identification is necessary, as different representations of the Dirac algebra may lead to very different interpretations for the order parameters and for the fermion masses that are generated dynamically by the interactions. It is this mapping that allows us to understand the properties of the possible phases and their relevance for graphene.

3.2.1. Discrete symmetries

Here, we take the parity transformation to reverse both spatial coordinates. This choice reflects the direct mapping to the tight-binding model where the parity operation is defined with respect to the center of the first Brillouin zone (see, e.g., the discussion in [30]). It is important to emphasize that reversing both spatial coordinates does not necessarily correspond to a rotation in the two-dimensional plane, since the generators for both transformations in spinor space do not have to coincide.

For the fermions parity acts in the following way

$$\mathrm{P}\psi(x)\mathrm{P}^{-1} = P\psi(\tilde{x}) \ , \qquad \tilde{x} = (x_0, -x_1, -x_2) \ , \tag{3.18}$$

with the unitary matrix P acting on the spinor components. Parity transformations should leave the kinetic term invariant, and we see that any operator of the form

$$P \in \{\gamma_0, i\gamma_1\gamma_2, i\gamma_0\gamma_3, i\gamma_0\gamma_5\} \ , \tag{3.19}$$

will do the trick. However, each of these possibilities can lead to very different transformation properties for the fermion bilinears $\bar{\psi}\Gamma^{(j)}\psi$. E.g., in principle we could obtain a mass term $i\bar{\psi}\psi$ that is parity-odd. This is in contrast to the usual situation in three-dimensional relativistic field theories where one doubles the degrees of freedom to define a parity-even mass term for the fermions [101, 103]. Here, we want to find those order parameters that correspond to the physical excitations on the honeycomb lattice. Therefore, we define the discrete symmetry operations in such a way that they are consistent with the identification of the spinor components with the one-particle fermion operators on the honeycomb lattice. It is clear that an inversion about the center of the first Brillouin zone should exchange both, the Dirac points and the sublattices. Since, in the chiral representation, the states with definite chirality correspond to the excitations around the two inequivalent Dirac points $\vec{K}_+$ and $\vec{K}_- = -\vec{K}_+$, this leaves only two possibilities for the operator P, namely those that exchange states with opposite chirality: γ_0 and $i\gamma_0\gamma_5$. In principle, we could choose any one of the two. We define $P = \gamma_0$ which yields the same transformation properties for the fermion bilinears $\bar{\psi}\Gamma^{(j)}\psi$ as in [30] so that the mass term $i\bar{\psi}\psi$ and $i\bar{\psi}\gamma_{35}\psi$ are parity-even, whereas $\bar{\psi}\gamma_3\psi$ and $\bar{\psi}\gamma_5\psi$ are

parity-odd.[2] The components of the Dirac spinor (3.7) transform under parity according to

$$\begin{pmatrix} u_+ \\ iv_+ \\ iv_- \\ u_- \end{pmatrix} \xrightarrow[\mathrm{P}]{} \begin{pmatrix} v_- \\ iu_- \\ iu_+ \\ v_+ \end{pmatrix} , \tag{3.20}$$

where it is understood that the transformed spinor has reversed spatial coordinates.

Charge conjugation is defined as

$$\mathrm{C}\psi\,\mathrm{C}^{-1} = (\bar{\psi}C)^T . \tag{3.21}$$

with the unitary operator C being any one of the following possibilities

$$C \in \{\gamma_2, i\gamma_0\gamma_1, i\gamma_2\gamma_3, i\gamma_2\gamma_5\} . \tag{3.22}$$

This follows from the requirement that under charge conjugation $i\bar{\psi}\gamma_\mu\psi \to -i\bar{\psi}\gamma_\mu\psi$ should hold. Again, the question is how to constrain this set of operators. It is clear that charge conjugation should leave the two Dirac points invariant. However, it exchanges the sublattices A and B as it transforms particles into antiparticles. We are left with two possibilities for the operator C: γ_2 and $i\gamma_2\gamma_5$. Here, we define $C = i\gamma_2\gamma_5$ where the fermion bilinears $i\bar{\psi}\psi$, $\bar{\psi}\gamma_3\psi$, and $i\bar{\psi}\gamma_{35}\psi$ are even under charge conjugation, and $\bar{\psi}\gamma_5\psi$ is odd. For the components of the Dirac spinor charge conjugation acts as

$$\begin{pmatrix} u_+ \\ iv_+ \\ iv_- \\ u_- \end{pmatrix} \xrightarrow[\mathrm{C}]{} \begin{pmatrix} -v_+^\dagger \\ -iu_+^\dagger \\ iu_-^\dagger \\ v_-^\dagger \end{pmatrix} . \tag{3.23}$$

Notice, that the chiral left- and right-handed components transform with a relative phase factor.

We are left with the antiunitary time reversal[3]

$$\mathrm{T}\psi\mathrm{T}^{-1} = T\psi , \tag{3.24}$$

where the unitary matrix T is given by

$$T \in \{i\gamma_2, \gamma_0\gamma_1, \gamma_2\gamma_3, \gamma_2\gamma_5\} . \tag{3.25}$$

Time reversal changes both the momentum and spin of the quasiparticles where we neglect the part of the operator that acts on the physical spin, given by some nondiagonal matrix in

[2] Note, that the generator for parity transformations $P = \gamma_0$ does not correspond to the generator of rotations $\frac{1}{4}[\gamma_1, \gamma_2]$ in the two-dimensional plane, even though in both cases the sign of both spatial coordinates is flipped.

[3] Note, that in Euclidean space time reversal simply complex conjugates c-numbers without changing the sign of spatial momentum components or Euclidean time.

	P	C	T
$i\bar{\psi}\psi$	$+$	$+$	$+$
$\bar{\psi}\gamma_3\psi$	$-$	$+$	$+$
$\bar{\psi}\gamma_5\psi$	$-$	$-$	$+$
$i\bar{\psi}\gamma_{35}\psi$	$+$	$+$	$-$
$i\bar{\psi}\gamma_\mu\psi$	$i\bar{\psi}\tilde{\gamma}_\mu\psi$	$-i\bar{\psi}\gamma_\mu\psi$	$i\bar{\psi}\gamma_\mu\psi$

Table 3.1.: Transformation properties of fermion bilinears under P, C, and T where $\tilde{\gamma}_\mu = (\gamma_0, -\gamma_1, -\gamma_2)$.

flavor space). As it reverses the momentum it should exchange the two inequivalent Dirac points at opposing corners of the first Brillouin zone $\vec{K}_+$ and $\vec{K}_- = -\vec{K}_+$. Thus, it appears that we again have two possibilities: $i\gamma_2$ and $\gamma_2\gamma_5$. We take $T = i\gamma_2$ for which the bilinears $i\bar{\psi}\psi$, $\bar{\psi}\gamma_3\psi$, and $\bar{\psi}\gamma_5\psi$ are even, and $i\bar{\psi}\gamma_{35}\psi$ is odd under time reversal. The action of the transformation (3.24) on the components of the Dirac spinor is then given by

$$\begin{pmatrix} u_+ \\ iv_+ \\ iv_- \\ u_- \end{pmatrix} \xrightarrow[\mathrm{T}]{} -i \begin{pmatrix} u_- \\ iv_- \\ iv_+ \\ u_+ \end{pmatrix} . \tag{3.26}$$

However, it should be kept in mind that for simplicity we neglect the transformation that acts on the true spin (i.e. flavor) indices.

From these considerations it follows that in the chiral representation the mass term $i\bar{\psi}\psi$ is invariant separately under P, C, and T. All other mass terms break at least one of the discrete symmetries. The properties of the various fermion bilinears are summarized in Tab. 3.1.

Apart from the antiunitary time reversal symmetry

$$[\mathcal{D}, i\gamma_2 K] = 0 , \tag{3.27}$$

that was defined in the previous section, the Euclidean Dirac operator with a possible mass term $\mathcal{D} = \gamma_\mu\partial_\mu + m$ has another antiunitary symmetry $\mathrm{S} = -i\gamma_0\gamma_1 K$ which is written as

$$[\mathcal{D}, -i\gamma_0\gamma_1 K] = 0 . \tag{3.28}$$

Here, the operator K denotes complex conjugation. In terms of the Dirac spinor components the symmetry (3.28) exchanges the excitations on the two sublattices A and B, and also the physical spin of the quasiparticles (as for the time reversal symmetry, we will neglect the part acting on the spin components in the following). In contrast to the time reversal (3.24) however, it does not exchange the two Dirac points. That is, it reverses the momentum of the chiral left- and right-handed excitations independently, and in that sense eq. (3.28) can be seen as a time reversal acting separately at the two inequivalent Dirac points [77]. While the time reversal symmetry satisfies $(i\gamma_2 K)^2 = 1$, and therefore defines an orthogonal symmetry

here (an additional minus sign arises when including the true spin components), we have $(-i\gamma_0\gamma_1 K)^2 = -1$ for the antiunitary operator (3.28), which corresponds to a symplectic symmetry (in the spinless case). These two different antiunitary symmetries are essentially due to the fact that one has an even number of two-component Weyl fermions in the low-energy theory.

The commutator of both antiunitary operators T and S vanishes, and therefore their product

$$\mathrm{TS} = i\gamma_{35} \ , \tag{3.29}$$

gives a well-defined unitary operator, exchanging both the two Dirac points and sublattices A and B. Clearly, if both T and S are symmetries of the theory then the discrete chiral transformation TS also defines a symmetry operation. In Tab. 3.2 we have collected the transformation properties of the fermion bilinears under the antiunitary and discrete chiral transformations.

Let us comment on the importance of the antiunitary symmetries. Typically, in QCD-like theories the antiunitary symmetry of the Dirac operator is related to the (pseudo)reality of the fermion color representation. Though three-color QCD with quarks in the fundamental representation does not fall into this class, examples are two-color QCD, adjoint QCD, or the G_2 gauge theory [104–106]. In these theories the antiunitary symmetry is responsible for an enlargement of the $SU(N_f) \times SU(N_f) \times U(1)$ chiral and baryon number symmetries to a global $SU(2N_f)$ extended flavor symmetry when the fermions are massless. Furthermore, it determines the dynamics of the low-energy excitations giving rise to different patterns of spontaneous symmetry breaking [104–106]. Considering the low-energy theory of free massless fermions (3.1) with the antiunitary symmetries (3.27) and (3.28) and the global $SU(2N_f)$ flavor symmetry, one is very much reminded of the situation in QCD-like theories with real or pseudoreal fermion color representations. Here, however, the extended flavor symmetry is a simple consequence of the reducible four-dimensional representation for the fermions in three space-time dimensions. As far as the the antiunitary symmetries of the Dirac operator are concerned, one has to ask whether they are relevant for the low-energy dynamics in presence of interactions or disorder [107–111]. In fact, when the fermions are charged and couple to an abelian $U(1)$ gauge field, the Dirac operator in the gauge-field background does not have the antiunitary symmetries (3.27) and (3.28). Such a 2+1 dimensional QED dynamics can be modeled in the context of Random Matrix Theory by a chiral Gaussian Unitary ensemble (chGUE), that belongs to the class AIII after Cartan's classification of symmetric spaces [112–116]. The spontaneous breaking of the antiunitary symmetries is then ruled out. Of course, in the instantaneous approximation, the Coulomb field alone would not break the time-reversal invariance. However, close to the charge neutral point this approximation breaks down when the Fermi velocity increases due to the strong electron-electron interaction [36, 117]. Therefore, in the following we are interested especially in the chiral symmetry breaking mass term which leaves the antiunitary symmetries unchanged.

	T	S	TS
$i\bar{\psi}\psi$	+	+	+
$\bar{\psi}\gamma_3\psi$	+	−	−
$\bar{\psi}\gamma_5\psi$	+	−	−
$i\bar{\psi}\gamma_{35}\psi$	−	−	+
$i\bar{\psi}\gamma_\mu\psi$	+	+	+

Table 3.2.: Transformation properties of fermion bilinears under the antiunitary and discrete chiral transformations.

3.2.2. Order parameters

From the above discussion it follows that the expectation value $i\langle\bar{\psi}\psi\rangle$ is invariant under P, C, and T whereas both $\langle\bar{\psi}\gamma_3\psi\rangle$ and $\langle\bar{\psi}\gamma_5\psi\rangle$ are parity-odd (compare Tab. 3.1). All three order parameters break the extended $U(2N_f)$ flavor symmetry, generating a dynamical mass for the fermions. The symmetry breaking pattern is given by [118–120]

$$U(2N_f) \to U(N_f) \times U(N_f) \ . \tag{3.30}$$

It is clear how to identify these order parameters with the excitations in the underlying lattice model. They can be mapped onto the staggered density phase where one has an alternating density on the two different sublattices A and B [90–92, 121], and a bond ordered phase that corresponds to a hopping texture on the nearest-neighbor links in the language of the tight-binding model [122]. Indeed, a nonvanishing staggered density on the two sublattices breaks parity and we may associate the order parameter $\langle\bar{\psi}\gamma_3\psi\rangle$ with such a phase. The corresponding bilinear measures the imbalance in the local densities of the two sublattices and therefore does not mix the chiral modes. This is immediately apparent when we write the bilinear directly in terms of the one-particle fermion operators on the honeycomb lattice:

$$\langle\bar{\psi}\gamma_3\psi\rangle \to \langle v_+^\dagger v_+\rangle + \langle v_-^\dagger v_-\rangle - \langle u_+^\dagger u_+\rangle - \langle u_-^\dagger u_-\rangle \ . \tag{3.31}$$

The order parameter for the bond ordered phase however, should couple excitations both at the two inequivalent Dirac points $\vec{K}_+$ and $\vec{K}_-$ and on the two sublattices A and B [30, 122], which is accomplished by the bilinear $i\langle\bar{\psi}(\cos\alpha + \gamma_5 \sin\alpha)\psi\rangle$. The parameter α controls the hopping texture, and depending on its value, one obtains either a parity-conserving, or a parity-breaking type of order (see Tab. 3.1). Again, switching to the language of the single-particle excitations on the honeycomb lattice this corresponds to the bilinear

$$\begin{aligned} i\langle\bar{\psi}(\cos\alpha + \gamma_5 \sin\alpha)\psi\rangle \quad \to \quad & (\cos\alpha + \sin\alpha)\left(\langle v_-^\dagger u_+\rangle + \langle u_-^\dagger v_+\rangle\right) \\ & + \ (\cos\alpha - \sin\alpha)\left(\langle u_+^\dagger v_-\rangle + \langle v_+^\dagger u_-\rangle\right) . \end{aligned} \tag{3.32}$$

The condensate $i\langle\bar{\psi}\gamma_{35}\psi\rangle$ is in a sense special, as it leaves the chiral symmetry intact. However, it does break the time reversal symmetry. This corresponds to a topologically nontrivial phase

that relates to counter-propagating currents on the two different types of sublattices [123, 124]. In terms of the one-particle fermion operators it is written as

$$i\langle\bar{\psi}\gamma_{35}\psi\rangle \to -\langle v_+^\dagger v_+\rangle + \langle v_-^\dagger v_-\rangle + \langle u_+^\dagger u_+\rangle - \langle u_-^\dagger u_-\rangle \ . \tag{3.33}$$

The identification of the order parameters given here is equivalent to the one proposed in [30] where a chiral representation for the Dirac algebra was used also. A complete classification of all possible bilinears is given in [125, 126].

3.3. A simple model: Spinless fermions on the honeycomb lattice

Here, we focus on the case of a single flavor Dirac Lagrangian with a local four fermion interaction. This essentially corresponds to a low-energy theory of spinless fermions on the honeycomb lattice with a nearest neighbor and next-to-nearest neighbor coupling [88]. In the purely fermionic description, one may expect that above some critical value for the coupling, the short-range repulsive interactions give rise to an instability. Here, we go beyond a mean field approach by introducing a set of composite fields that allows us to follow the system into the ordered phase. Even for this simple model there is a complex phase diagram with different types of order: Depending on the strength of the interactions there is a competition between a staggered density phase and a topologically nontrivial phase [88]. The global symmetry group for this model is $U(2)$ and the symmetry breaking pattern for the chiral transition is given by $SU(2) \to U(1)$ while the topological phase transition leaves the $U(2)$ symmetry intact but breaks time reversal invariance.

For this simple model the relevant dynamics of the $SU(2) \to U(1)$ chiral phase transition is adequately described by taking into account only the fluctuations in a generalized Nambu-Jona-Lasinio-type channel (3.15). To illustrate this point we make a Fierz-transformation to write the flavor-singlet four fermion interactions in terms of a vector- and a NJL-type interaction:

$$\begin{aligned}&\frac{\bar{g}_V}{2N_f}(\bar{\psi}^a\gamma_\mu\psi^a)^2 + \frac{\bar{g}_S}{2N_f}(\bar{\psi}^a\gamma_{35}\psi^a)^2 \\ &= \frac{\bar{g}_V - \bar{g}_S}{2N_f}(\bar{\psi}^a\gamma_\mu\gamma^a)^2 - \frac{\bar{g}_S}{2N_f}\left\{(\bar{\psi}^a\psi^b)^2 - (\bar{\psi}^a\gamma_3\psi^b)^2 - (\bar{\psi}^a\gamma_5\psi^b)^2 + (\bar{\psi}^a\gamma_{35}\psi^b)^2\right\} \ .\end{aligned} \tag{3.34}$$

One may recognize that line defined by $\bar{g}_V - \bar{g}_S = 0$ in the $(\bar{g}_V, \bar{g}_S)$-coupling plane defines a theory where the vector-like interaction $(\bar{\psi}^a\gamma_\mu\psi^a)^2$ becomes irrelevant and the flavor-nondiagonal NJL-type interaction dominates. In fact, this scenario is realized for small numbers of fermion flavors N_f close to a non-Gaussian fixed point as has been demonstrated in a functional renormalization group investigation of the generalized Thirring model (3.17) in three dimensions

[102]. Thus, we expect that the critical properties of spinless fermions on the honeycomb lattice in the vicinity of the chiral critical point are well-described by a generalized NJL-model. Of course, strictly speaking, this model may not be in the same universality class as the full $U(2)$-symmetric single flavor model (3.17) which is characterized by three different interacting fixed points that describe very different types of critical behavior. The continuous chiral phase transition, however, corresponds to a Thirring-like fixed point which is very close to being the pure NJL-type interaction with $\bar{g}_V = \bar{g}_S$ for $N_f = 1$, but which moves towards the Thirring axis $\bar{g}_S = 0$ for $N_f \to \infty$ [102].

To see how the repulsive interactions drive the system into the broken phase we integrate out the flavor nondiagonal NJL-type interaction via a Hubbard-Stratonovich transformation. In this way we obtain a matrix Yukawa model with a $U(N)$ symmetry for $N = 2$ species of massless, two-component Weyl fermions ψ^a and $\bar{\psi}^a$, $a = 1, \ldots, N$. For the spinless fermions on the honeycomb lattice $N = 2$, which corresponds to a single Dirac fermion $N_f = 1$ in the reducible representation as, e.g., modeled in microwave photonic crystals [97, 98]. The Weyl fermions couple to a Hermitian matrix field Φ_{ab} and the action of this model is given by

$$S[\Phi, \bar{\psi}, \psi] = \int d^d x \left\{ \bar{\psi}^a i\partial\!\!\!/ \psi^a + \bar{h}\, \bar{\psi}^a i \Phi_{ab} \psi^b + \frac{1}{2} \bar{m}^2 \,\mathrm{tr}\, \Phi^2 \right\} , \tag{3.35}$$

where the trace $\mathrm{tr}(\cdots)$ acts on the indices of the matrix field. Here, and in the following, we define $\partial\!\!\!/ \equiv \sigma_\mu \partial_\mu$ which belongs to the irreducible representation $\gamma_0 = \sigma_3$, and $\gamma_k = \sigma_k$, $k = 1, 2$. Eq. (3.35) constitutes the starting point for our investigation in the framework of the functional renormalization group.

3.4. Functional renormalization group

The full information about the quantum dynamics of a theory is given by the quantum effective action Γ, which is the generating functional for one-particle irreducible correlation functions. The functional renormalization group is a nonperturbative approach to determine the quantum effective action, taking into account all quantum fluctuations. Implementing Wilson's renormalization group idea [6, 12], the fluctuations are included successively by integrating out the higher modes. Thereby, one obtains the scale-dependent effective action Γ_k with all the fluctuations included above the characteristic momentum scale k. The scale-dependence is implemented by an infrared regulator R_k to suppress the fluctuations of the low-momentum modes in the theory. In the limit $k \to 0$, when all quantum fluctuations are included, the functional renormalization group yields the full effective action Γ.

The flow equation for the scale-dependent effective action is given by [14, 16–20, 50–54]

$$\frac{\partial \Gamma_k[\chi]}{\partial t} = \frac{1}{2} \,\mathrm{STr} \left\{ \frac{\partial R_k}{\partial t} \left(\Gamma_k^{(1,1)}[\chi] + R_k \right)^{-1} \right\} , \tag{3.36}$$

where $t = \ln k/\Lambda$ defines the scale parameter, and Λ is some appropriate ultraviolet scale where we impose the microscopic dynamics. The supertrace STr in (3.36) denotes a summation over

fields and possible internal indices, as well as an integration over momentum, while it provides a minus sign in the fermionic sector. The second functional derivatives of the scale-dependent effective action $\Gamma_k^{(1,1)}$ define the fluctuation matrix. In the momentum representation, we have

$$\left(\Gamma_k^{(1,1)}[\chi]\right)_{IJ}(p,q) \equiv \frac{\overrightarrow{\delta}}{\delta\chi_I^T(-p)}\,\Gamma_k[\chi]\,\frac{\overleftarrow{\delta}}{\delta\chi_J(q)}\ , \tag{3.37}$$

where the indices I, J label the different components of the auxiliary field χ that contains the complete field content of our model: the matrix field Φ_{ab} and N species of Weyl fermions ψ^a and $\bar{\psi}^a$, i.e., [4]

$$\chi^T(-p) \equiv \left(\Phi^T(-p)\,,\,\psi^T(-p)\,,\,\bar{\psi}(p)\right)\ , \tag{3.38}$$

and

$$\chi(q) \equiv \begin{pmatrix} \Phi(q) \\ \psi(q) \\ \bar{\psi}^T(-q) \end{pmatrix}\ , \tag{3.39}$$

where we have suppressed the flavor indices. Together with the infrared regulator R_k it represents the full regularized inverse propagator $\left(\Gamma_k^{(1,1)} + R_k\right)$ at the scale k.

The regulator function R_k takes the following form

$$R_k(p) = \begin{pmatrix} R_{B,k}(p) & 0 & 0 \\ 0 & 0 & R_{F,k}^T(p) \\ 0 & R_{F,k}(p) & 0 \end{pmatrix}\ , \tag{3.40}$$

where in the bosonic and fermionic sector, we have

$$R_{B,k}(p) = Z_{B,k}p^2 r_{B,k}(p^2)\ , \tag{3.41}$$

$$R_{F,k}(p) = Z_{F,k}\not{p}\, r_{F,k}(p^2)\ . \tag{3.42}$$

Both are fully described by the regulator shape functions $r_{B,k}$ and $r_{F,k}$ that characterize the scheme-dependence of the renormalization procedure. Since they depend only on the dimensionless ratio $y = p^2/k^2$ we will drop the index k in the following. The fermion regulator shape function r_F is taken to satisfy the constraint $p^2(1 + r_B) = p^2(1 + r_F)^2$ and thus, is completely determined by the choice of r_B.

In practice, to solve (3.36) one is bound to rely on approximations for the scale-dependent effective action Γ_k where one truncates the set of possible operators following an expansion scheme, e.g., in powers of derivatives [62, 65, 66]. However, such an approximation also induces a spurious dependence on the regulator for the full quantum effective action when the scale k is sent to zero [58, 59, 127]. Here, we therefore employ two different types of infrared regulators to test the regulator scheme-dependence of our results in the physical limit. We consider the optimized regulator [58, 59]

$$r_B(y) = \left(\frac{1}{y} - 1\right)\theta(1-y)\ , \tag{3.43}$$

[4] Since the matrix-valued field Φ is Hermitian, Φ and Φ^* are not independent degrees of freedom.

and also an exponential-type regulator

$$r_B(y) = (\exp(y) - 1)^{-1} \ . \tag{3.44}$$

3.4.1. Scale-dependent effective action

Our *ansatz* for the scale-dependent effective action is given by

$$\Gamma_k[\Phi, \bar{\psi}, \psi] = \int d^d x \Big\{ Z_{F,k}\, \bar{\psi}^a i\partial\!\!\!/ \psi^a + \frac{1}{2} Z_{B,k}\, \mathrm{tr}\, (\partial_\mu \Phi)^2 + \bar{h}_k\, \bar{\psi}^a i \Phi_{ab} \psi^b + U_k(\Phi) \Big\} \ . \tag{3.45}$$

In contrast to the microscopic model, we have a kinetic term for the composite field and a scale-dependent wavefunction renormalization both for the fermions and the bosons. Thus, we include the bosonic fluctuations that give a nontrivial momentum structure for the fermion interactions [83, 128]. Clearly, our *ansatz* (3.45) goes far beyond a simple mean-field approximation where one neglects the fluctuations from the composite degrees of freedom.

For the $U(N)$ matrix-model the effective average potential $U_k(\Phi)$ is a function of the invariants of the $U(N)$ symmetry group. For system of $N = 2$ Weyl fermions there are exactly two invariants both of which are quadratic, i.e., $\bar{\sigma}_k = (\mathrm{tr}\, \Phi)^2/2$ and $\bar{\rho}_k = \mathrm{tr}\, \Phi^2/2$ in the fields. A nonvanishing vacuum expectation value for the composite field Φ_{ab} signals the dynamical generation of a mass for the fermions. Depending on the flavor structure of the matrix field we have different types of order: The chirally broken phase corresponds to a vacuum configuration which is either nondiagonal, or diagonal nonuniform (so that the trace vanishes, i.e., $\mathrm{tr}\, \Phi = 0$). On the other hand, $\Phi_{ab} \sim \delta_{ab}$, breaking the discrete Z_2 symmetry, in the nontrivial topological phase which we will not consider here. Close to the phase transition only those fluctuations of the Φ-field will play a significant role that give a contribution to the quadratic invariant $\bar{\rho}_k$ – the $\bar{\sigma}_k$-field is irrelevant there. Thus, to investigate the nature of the chiral phase transition we may neglect the fluctuations of the $\bar{\sigma}_k$-field. However, we want to emphasize that this approximation is no way essential for the following calculations.

We expand the effective average potential in powers of $\bar{\rho}_k$ around the minimum $\bar{\rho}_{0,k}$, given by the scale-dependent vacuum expectation value:

$$U_k(\bar{\rho}_k) = \bar{m}_k^2 (\bar{\rho}_k - \bar{\rho}_{0,k}) + \sum_{n=2}^{n_{\max}} \frac{\bar{\lambda}_{n,k}}{n!} (\bar{\rho}_k - \bar{\rho}_{0,k})^n \ . \tag{3.46}$$

This approximation captures all the relevant fluctuation at the chiral phase transition. In the symmetric regime the vacuum expectation value $\bar{\rho}_{0,k}$ is zero whereas in the chirally broken phase $\bar{\rho}_{0,k} \neq 0$ and the mass $\bar{m}_k^2$ becomes zero. In our *ansatz* we include the first set of irrelevant operators according to a naive power counting with respect to the canonical mass dimension.

3.4.2. Flow equation for the effective average potential

To extract the flow equations for the parameters and couplings in the scale-dependent effective action (3.45) one has to project the functional flow given by the r. h. s. of (3.36) onto the corresponding operators. For the couplings that appear in the effective average potential this is done by evaluating the second functional derivative $\Gamma_k^{(1,1)}$ in a constant background configuration of the matrix field Φ_{ab}.

The flow equation for the effective average potential receives contributions both from the boson and fermion degrees of freedom

$$\frac{\partial U_k(\Phi)}{\partial t} = \frac{\partial U_{B,k}(\Phi)}{\partial t} + \frac{\partial U_{F,k}(\Phi)}{\partial t} \ . \tag{3.47}$$

To keep the notation clear, we will drop the k-index in the following. Where necessary, we will revert to our original notation.

From (3.36) we obtain the boson contribution to the effective average potential

$$\frac{\partial U_B}{\partial t} = \frac{1}{2}\int \frac{d^dq}{(2\pi)^d}\,\frac{\partial R_B}{\partial t}\sum_i G_B(\bar{M}_{Bi}) \ , \tag{3.48}$$

where the full regularized boson propagator G_B is given in the Appendix A. We sum over all mass eigenvalues $\bar{M}_{Bi}^2$ of the mass matrix as given by the second derivatives of the potential

$$\bar{M}_B^2(\Phi)_{\,ab,cd} = \frac{\partial^2}{\partial\Phi^{T\,ab}\Phi^{cd}}U_k(\Phi) \tag{3.49}$$

The mass matrix in the nondiagonal constant background configuration $\Phi_{ab} = \Phi_0\Sigma_{ab}$ is given by:

$$\bar{M}_B^2(\Phi)_{\,ab,cd}(p,q) = \left[\frac{\partial U_k}{\partial\bar{\rho}}\delta_{ac}\delta_{bd} + \Phi_0^2\frac{\partial^2 U_k}{\partial\bar{\rho}^2}\Sigma_{ab}\Sigma_{cd}^T\right]\delta(p,q) \ , \tag{3.50}$$

where the eigenvalues are

$$\bar{M}_{B,0}^2 = \frac{\partial U_k}{\partial\bar{\rho}} \ , \quad \bar{M}_{B,R}^2 = \frac{\partial U_k}{\partial\bar{\rho}} + N\Phi_0^2\frac{\partial^2 U_k}{\partial\bar{\rho}^2} \ , \tag{3.51}$$

corresponding to the masses of the Goldstone and radial modes.

For illustrational purposes we perform the derivation of the flow equation in the fermion sector explicitly by integrating out the fermions in the action. To evaluate the fermion contribution to the effective average potential it is useful to write the action in terms of the four-component spinors

$$\Psi(q) = \begin{pmatrix}\psi(q)\\ \bar{\psi}^T(-q)\end{pmatrix} \ , \tag{3.52}$$

which is constructed from the two independent degrees of freedom ψ and $\bar{\psi}$. In that case, the fermion bilinear part of the action takes the form

$$\Gamma_{k,\Psi\Psi} = \int_{(q_0>0)}\frac{d^dq}{(2\pi)^d}\Psi^{T\,a}(-q)\mathcal{D}_{ab}(q)\Psi^b(q) \ , \tag{3.53}$$

in momentum space. Note, that the domain of integration is restricted to positive frequencies $q_0 > 0$ to counteract the doubling of degrees of freedom that comes from switching to the four-component spinors (3.52). In this basis, the inverse regularized fermion propagator is given by

$$\mathcal{D}_{ab}(q) = Z_F(1+r_F)\begin{pmatrix} & \not{q}^T \\ \not{q} & \end{pmatrix}\delta_{ab} + i\bar{h}(q)\begin{pmatrix} & -\Phi_{ab}^T \\ \Phi_{ab} & \end{pmatrix} , \tag{3.54}$$

where $\bar{h}(q) \equiv \bar{h}(-q,q)$ denotes the momentum-dependent Yukawa coupling.[5] As for the boson contribution, we evaluate the inverse propagator $\mathcal{D}_{ab}(q)$ in a constant background field Φ_{ab}. Performing the integration over the Grassmann fields, the fermion contribution to the potential takes the form

$$U_F = -\int_{(q_0>0)} \frac{d^dq}{(2\pi)^d}\, \ln\det \mathcal{D}(q) , \tag{3.55}$$

where the determinant acts on the flavor and spinor indices. To evaluate this expression we put $\mathcal{D}_{ab}(q)$ in standard diagonal form. That is, by a unitary transformation we diagonalize $\Phi_{ab} = \Phi_a\delta_{ab}$, so that $\mathcal{D}_{ab}(q) = \mathcal{D}_a(q)\delta_{ab}$, and the determinant in (3.55) can be written as

$$\det \mathcal{D}_a = \left(Z_F^2(1+r_F)^2q^2 + \bar{h}(q)^2\Phi_a^2\right)^2 . \tag{3.56}$$

With this result, the fermion contribution to the flow equation (3.47) becomes

$$\frac{\partial U_F}{\partial t} = -2\int \frac{d^dq}{(2\pi)^d}\, q^2\, Z_F(1+r_F)\,\frac{\partial}{\partial t}\big(Z_F r_F\big)\,\sum_a \widetilde{G}_F(\bar{M}_{Fa}) , \tag{3.57}$$

where $\widetilde{G}_F(\bar{M}_{Fa}) = (\det\mathcal{D}_a)^{-\frac{1}{2}}$. One may easily verify that this is just the result that is obtained when the supertrace in (3.36) is computed directly, using the definition of the full regularized propagators (see Appendix A), and the regulator R_F. Here, the masses $\bar{M}_{Fa}$ denote the N eigenvalues of the $N\times N$ matrix $\bar{h}(q)\Phi$.

Eq. (3.48) and (3.57) together give the full contribution to the effective average potential. To investigate the critical properties at the phase transition, however, it is convenient to bring the flow equations to a form where one may easily identify possible fixed point solutions. For that purpose, we switch to dimensionless renormalized quantities $\rho = k^{2-d}Z_B\bar{\rho}$ and $u(\rho) = k^{-d}U_k(\rho)$. Then, the flow equation for the potential is given by

$$\frac{\partial u}{\partial t} = -du + k^{-d}\frac{\partial U_k}{\partial t}\bigg|_{\bar{\rho}} + (d-2+\eta_B)\rho k^{-d}\frac{\partial U_k}{\partial \rho}\bigg|_t , \tag{3.58}$$

where we have introduced the scalar anomalous dimension $\eta_B \equiv -\partial\ln Z_B/\partial t$. Substituting our previous result this finally gives

$$\begin{aligned}\frac{\partial u}{\partial t} &= -du + (d-2+\eta_B)\rho u' \\ &\quad + 2v_d\Big\{(N^2-2)l_0^{(B)}(u';\eta_B) + l_0^{(B)}(u'+2\rho u'';\eta_B) \\ &\quad - 2Nl_0^{(F)}\left(\frac{2}{N}\rho h^2;\eta_F\right)\Big\} ,\end{aligned} \tag{3.59}$$

[5] For the momentum dependent Yukawa coupling $\bar{h}(-p,q)$ the momenta p and q denote the incoming fermion momenta at the Yukawa vertex.

where the prime $u' \equiv \partial u/\partial\rho|_t$ denotes differentiation with respect to the dimensionless renormalized field ρ, and $v_d = \left(2^{d+1}\pi^{d/2}\Gamma\left(d/2\right)\right)^{-1}$. Furthermore, $\eta_F \equiv -\partial \ln Z_F/\partial t$ and $h^2 = k^{d-4}Z_F^{-2}Z_B^{-1}\bar{h}^2$ is the dimensionless renormalized Yukawa coupling. Here, we have introduced the threshold functions $l_0^{(B)}$ and $l_0^{(F)}$ that parametrize the boson and fermion one-loop integrals contributing to the effective average potential. They are defined in Appendix B where their form is given explicitly for the optimized regulator (3.43). The corresponding expressions for the exponential regulator (3.44) can be found in, e.g., [19, 83]. The threshold functions carry the full scheme-dependence of the renormalization group equations. In that sense, the flow equations are universal – only the dimensionality and symmetries determine the flow and the regulator-dependence resides solely in the threshold functions.

In the symmetric regime, we may derive the flow equations for the dimensionless renormalized couplings $\epsilon = k^{-2}Z_B^{-1}\bar{m}^2$ and $\lambda_n = k^{(n-1)d-2n}Z_B^{-n}\bar{\lambda}_n$, $n = 2, \ldots, n_{\max}$, from (3.59) simply by differentiating with respect to field ρ, that is, we have $\epsilon = u'$ for the mass parameter and $\lambda_n = u^{(n)}$ for the couplings. The derivatives of the threshold functions are evaluated as

$$\frac{\partial}{\partial w} l_n^{(B)}(w;\eta_B) = -\left(n + \delta_{n,0}\right) l_{n+1}^{(B)}(w;\eta_B) \;, \tag{3.60}$$

and equivalently for $l_n^{(F)}(w;\eta_F)$. Here, we give the flow equations for the mass parameter ϵ, and the couplings λ_2, and λ_3 in the symmetric phase:

$$\begin{aligned}
\frac{\partial\epsilon}{\partial t} &= (-2+\eta_B)\epsilon - 2v_d\left\{\left(N^2+1\right)\lambda_2\, l_1^{(B)}\left(\epsilon;\eta_B\right) - 4h^2\, l_1^{(F)}\left(0;\eta_F\right)\right\} \;, && (3.61)\\
\frac{\partial\lambda_2}{\partial t} &= (d-4+2\eta_B)\lambda_2 + 2v_d\left\{\left(N^2+7\right)\lambda_2^2\, l_2^{(B)}\left(\epsilon;\eta_B\right) - \left(N^2+3\right)\lambda_3\, l_1^{(B)}\left(\epsilon;\eta_B\right)\right.\\
&\quad \left. - \frac{8}{N}h^4\, l_2^{(F)}\left(0;\eta_F\right)\right\} \;, && (3.62)\\
\frac{\partial\lambda_3}{\partial t} &= (2d-6+3\eta_B)\lambda_3 - 2v_d\left\{2\left(N^2+25\right)\lambda_2^3\, l_3^{(B)}\left(\epsilon;\eta_B\right)\right.\\
&\quad - 3\left(N^2+13\right)\lambda_2\lambda_3\, l_2^{(B)}\left(\epsilon;\eta_B\right) + \left(N^2+5\right)\lambda_4\, l_1^{(B)}\left(\epsilon;\eta_B\right)\\
&\quad \left. - \frac{32}{N^2}h^6\, l_3^{(F)}\left(0;\eta_F\right)\right\} \;. && (3.63)
\end{aligned}$$

The flow equations for the higher order couplings can be obtained by a simple differentiation with respect to the field, and are not given here explicitly.

As the system goes over into the broken phase, the scale-dependent mass parameter ϵ goes to zero, and the field assumes a nonvanishing expectation value $\rho_0 \neq 0$, defined by $u'(\rho_0) = 0$. Due to the scale-dependence of ρ_0, which is given by

$$\frac{\partial\rho_0}{\partial t} = -\frac{1}{\lambda_2}\frac{\partial u'(\rho_0)}{\partial t} \;, \tag{3.64}$$

we get an additional contribution to the flow (3.59) in the broken phase:

$$\frac{\partial\lambda_n}{\partial t} = \left.\frac{\partial\lambda_n}{\partial t}\right|_{\rho_0} + \lambda_{n+1}\frac{\partial\rho_0}{\partial t} \;. \tag{3.65}$$

There, the flow equations for ρ_0, and the couplings λ_2, and λ_3 are given by

$$\begin{aligned}
\frac{\partial \rho_0}{\partial t} &= (2-d-\eta_B)\rho_0 + 2v_d\Big\{\left(N^2-2\right) l_1^{(B)}\left(0;\eta_B\right) + \left(3+\frac{2\rho_0\lambda_3}{\lambda_2}\right) l_1^{(B)}\left(2\rho_0\lambda_2;\eta_B\right) \\
&\quad - \frac{4}{\lambda_2}h^2\, l_1^{(F)}\left(\frac{2}{N}\rho_0 h^2;\eta_F\right)\Big\}, \qquad (3.66)\\
\frac{\partial \lambda_2}{\partial t} &= (d-4+2\eta_B)\lambda_2 + 2v_d\Big\{\left(N^2-2\right)\lambda_2^2\, l_2^{(B)}\left(0;\eta_B\right) + \left(3\lambda_2+2\rho_0\lambda_3\right)^2 l_2^{(B)}\left(2\rho_0\lambda_2;\eta_B\right) \\
&\quad - \left(2\lambda_3+2\rho_0\lambda_4-\frac{2\rho_0\lambda_3^2}{\lambda_2}\right) l_1^{(B)}\left(2\rho_0\lambda_2;\eta_B\right) \\
&\quad - \frac{8}{N}h^4\, l_2^{(F)}\left(\frac{2}{N}\rho_0 h^2;\eta_F\right) - 4\frac{\lambda_3}{\lambda_2}h^2\, l_1^{(F)}\left(\frac{2}{N}\rho_0 h^2;\eta_F\right)\Big\}, \qquad (3.67)\\
\frac{\partial \lambda_3}{\partial t} &= (2d-6+3\eta_B)\lambda_3 - 2v_d\Big\{\left(N^2-2\right)\left(2\lambda_2^3\, l_3^{(B)}\left(0;\eta_B\right) - 3\lambda_2\lambda_3\, l_2^{(B)}\left(0;\eta_B\right)\right) \\
&\quad + 2\left(3\lambda_2+2\rho_0\lambda_3\right)^3 l_3^{(B)}\left(2\rho_0\lambda_2;\eta_B\right) \\
&\quad - 3\left(3\lambda_2+2\rho_0\lambda_3\right)\left(5\lambda_3+2\rho_0\lambda_4\right) l_2^{(B)}\left(2\rho_0\lambda_2;\eta_B\right) \\
&\quad + \left(4\lambda_4+2\rho_0\lambda_5-\frac{2\rho_0\lambda_3\lambda_4}{\lambda_2}\right) l_1^{(B)}\left(2\rho_0\lambda_2;\eta_B\right) \\
&\quad - \frac{32}{N^2}h^6\, l_3^{(F)}\left(\frac{2}{N}\rho_0 h^2;\eta_F\right) + 4\frac{\lambda_4}{\lambda_2}h^2\, l_1^{(F)}\left(\frac{2}{N}\rho_0 h^2;\eta_F\right)\Big\}. \qquad (3.68)
\end{aligned}$$

The flow equations for the higher order couplings can easily be obtained via (3.65).

Recall that the relevant symmetry breaking pattern for the simple model (Sec. 3.3) is given by $SU(2) \to U(1)$. This is in direct correspondence to the $O(3) \to O(2)$ transition in the three-component vector model [15, 129]. Building on our previous remark concerning the universality of the renormalization group flow, we observe that in the bosonic sector (neglecting the fermion contributions) the flow equations for the effective potential are identical to the flow equations for the three-dimensional $O(3)$ vector model [129]. We want to emphasize that this is a simplification that occurs only for the special case where $N = 2$. In the general case, the flow equations for the effective potential correspond to the matrix Yukawa model with $U(N)$ symmetry.

3.4.3. Boson anomalous dimension

For the computation of the boson anomalous dimension $\eta_B = -\partial \ln Z_B/\partial t$ we first evaluate the flow equation (3.36) in a spatially varying field configuration $\Phi(x)$. This is necessary for the projection onto the kinetic term and the wavefunction renormalization Z_B. In particular, we consider a distortion around the nondiagonal vacuum configuration $\Phi_{ab} = \Phi_0\Sigma_{ab}$ characterized by a nonvanishing momentum Q, i.e.

$$\Phi_{ab}(x) = \Phi_0\Sigma_{ab} + \underbrace{\left(\delta\Phi e^{-iQx} + \text{c.c.}\right)}_{\equiv\Delta(x)}\Lambda_{ab}\ , \qquad (3.69)$$

where the Hermitian matrices Σ and Λ satisfy the properties $\Sigma^T = -\Sigma$ and $\Lambda^T = \Lambda$. Clearly, the fluctuations in the Λ-direction are orthogonal to the ground state orientation. Though

we take only one of the possible orthogonal directions for the fluctuations into account this still yields a complete description of those contributions coming from the Goldstone modes. Of course, in the broken phase, we also have fluctuations $\sim \Delta'(x)\Sigma_{ab}$ from the radial mode that give additional contributions to the boson anomalous dimension.

In momentum space the configuration (3.69) reads

$$\Phi_{ab}(p) = \Phi_0 \delta(p,0)\Sigma_{ab} + \Delta(p,Q)\Lambda_{ab} \ , \tag{3.70}$$

where we define $\delta(p,q) \equiv (2\pi)^d \delta^{(d)}(p-q)$, and the amplitude is given by

$$\Delta(p,Q) = \left(\delta\Phi\delta(p,Q) + \delta\Phi^*\delta(-p,Q)\right) \ . \tag{3.71}$$

Taking the *ansatz* (3.69) one may easily verify that

$$\frac{\partial Z_B}{\partial t} \equiv \frac{1}{N} \lim_{Q\to 0} \frac{\partial}{\partial Q^2} \left[\lim_{\delta\Phi\to 0} \frac{\partial}{\partial(\delta\Phi\delta\Phi^*)} \frac{\partial \Gamma_k}{\partial t} \right] \ , \tag{3.72}$$

gives us the flow equation for the momentum-independent part of the wavefunction renormalization Z_B. Here, we neglect all momentum-dependence of the wavefunction renormalization. Eq. (3.72) defines a projection of the flow equation (3.36) onto the flow of the wavefunction renormalization, i.e., $\partial\Gamma_k/\partial t\,|_{Z_B} \equiv \partial Z_B/\partial t$. In the following, we will use this notation frequently.

To evaluate (3.72) we make use of a series expansion of the flow equation. Using the decomposition of the full inverse regularized propagator

$$\Gamma_k^{(1,1)} + R_k = G_k^{-1} + F_k \ , \tag{3.73}$$

which is written in terms of F_k containing all field-dependent fluctuations around the background field configuration, and the inverse background field propagator G_k^{-1} that carries the explicit regulator dependence, we may write the flow equation (3.36) as a series expansion in powers of the fields:

$$\frac{\partial \Gamma_k}{\partial t} = \frac{1}{2}\,\mathrm{STr}\,\frac{\partial R_k}{\partial t}\,G_k + \frac{1}{2}\,\mathrm{STr}\,\widehat{\frac{\partial}{\partial t}}\left(G_k F_k\right) - \frac{1}{4}\,\mathrm{STr}\,\widehat{\frac{\partial}{\partial t}}\left(G_k F_k\right)^2 + \mathcal{O}(F_k^3) \ . \tag{3.74}$$

Here we have defined the formal derivative operator

$$\widehat{\frac{\partial}{\partial t}} \equiv \frac{\partial R_k}{\partial t} \frac{\partial}{\partial\left(G_k^{-1}\right)} \ , \tag{3.75}$$

that acts on the inverse regularized matrix propagator G_k^{-1} (see Appendix A). In terms of (3.69) the leading contribution to the fluctuation is $F_k^n \sim \mathcal{O}(\Delta^n)$ and for the calculation of the anomalous dimension only the second order term $\delta^{(2)}\Gamma_k$ in the fluctuation F_k is important. Clearly, the lowest order term will not contribute, as it is independent of $\delta\Phi$ and $\delta\Phi^*$ and thus yields a vanishing contribution to (3.72). The $\delta^{(1)}\Gamma_k$ term does include combinations of the type $\sim \delta\Phi\delta\Phi^*$, however, they are independent of momentum Q^2. Thus, the lowest order

term relevant in (3.72) is the second order term $\delta^{(2)}\Gamma_k$ in the series expansion, and specifically, we will need those terms in F_k that are of linear order in the amplitude Δ. Apart from the bosonic background Φ_{ab} we need to specify the fermionic background configuration, where we take

$$\psi = \bar{\psi} = 0 \ . \tag{3.76}$$

Then, the matrix of second functional derivatives $\Gamma_k^{(1,1)}$ becomes block-diagonal in the boson and fermion subspaces and we may treat the boson and fermion contributions to (3.72) separately.

We start with the bosonic sector. For matrix-valued fields, it is convenient to work in the nondiagonal basis for the propagators and the fluctuations [130, 131]. We follow the outline given above, and evaluate the second order term $\delta^{(2)}\Gamma_B = -\frac{1}{4}\,\mathrm{STr}\,\hat{\partial}_t\,(G_B F_B)^2$ in the series expansion where the index B denotes the corresponding quantities in the bosonic sector where we have dropped the k-index for clarity, i.e., $\Gamma_{B,k} \equiv \Gamma_B$, $G_{B,k} \equiv G_B$, etc. For that we need the boson propagator in the constant background configuration $\Phi_{ab} = \Phi_0 \Sigma_{ab}$ which takes the following form

$$(G_B)_{ab,cd}\,(p) = \frac{1}{A(p)}\left(\delta_{ac}\delta_{bd} - \frac{B}{A(p)+NB}\Sigma_{ab}\Sigma^T_{cd}\right) \ , \tag{3.77}$$

where we have introduced the quantities

$$A(p) = Z_B(1+r_B)p^2 + \frac{\partial U_k}{\partial \bar{\rho}} \ , \quad B = \Phi_0^2\,\frac{\partial^2 U_k}{\partial \bar{\rho}^2} \ . \tag{3.78}$$

Furthermore, we need the contribution from the fluctuations to linear order in Δ, which is given by

$$(F_B)_{ab,cd}(p,q) = \Delta(p-q,Q)\,\Phi_0 \frac{\partial^2 U_k}{\partial \bar{\rho}^2}\left(\Sigma_{ab}\Lambda^T_{cd} + \Lambda_{ab}\Sigma^T_{cd}\right) + \mathcal{O}(\Delta^2) \ . \tag{3.79}$$

With these results we can immediately compute the trace in $\delta^{(2)}\Gamma_B$ and evaluate the projection onto the kinetic term:

$$\delta^{(2)}\Gamma_B\Big|_{Z_B} = -N\Phi_0^2\left(\frac{\partial^2 U_k}{\partial \bar{\rho}^2}\right)^2 \lim_{Q\to 0}\frac{\partial}{\partial Q^2}\int \frac{d^dp}{(2\pi)^d}\,\widehat{\frac{\partial}{\partial t}}\Big\{G_{B,0}(p)G_{B,R}(p+Q)\Big\} \ . \tag{3.80}$$

The indices on the propagators G_B refer to the corresponding eigenvalues of the mass matrix $\bar{M}_B^2$, i.e., $G_{B,0} \equiv G_B(\bar{M}_{B,0})$ etc. that are given by:

$$\bar{M}^2_{B,0} = \frac{\partial U_k}{\partial \bar{\rho}} \ , \quad \bar{M}^2_{B,R} = \frac{\partial U_k}{\partial \bar{\rho}} + N\Phi_0^2\,\frac{\partial^2 U_k}{\partial \bar{\rho}^2} \ . \tag{3.81}$$

These propagators $G_{B,0}$ and $G_{B,R}$ belong to the Goldstone modes and radial mode, respectively. We want to emphasize that the derivative operator $\widehat{\partial/\partial t}$ appearing in (3.80) is different from the one defined in (3.75). That is, we slightly abuse the notation and take

$$\widehat{\frac{\partial}{\partial t}} \ \equiv \ \partial_t R_B \frac{\partial}{\partial\left(G_B^{-1}\right)} + \frac{2}{Z_F}\frac{\widetilde{G}_F^{-1}(0)}{1+r_F}\partial_t\left(Z_F r_F\right)\frac{\partial}{\partial\big(\widetilde{G}_F^{-1}\big)} \ , \tag{3.82}$$

from now on, where it is understood that $\widetilde{G}_F^{-1}(0)$ is simply the kinetic part of $\widetilde{G}_F^{-1}$ (evaluated at zero mass). Since (3.75) is a matrix operator there is no risk of confusion. Notice, that (3.80) is proportional to the vacuum amplitude Φ_0 and thus, the boson contribution to the wavefunction renormalization vanishes in the symmetric regime.

We evaluate the contribution to the flow equivalently in the fermion subspace. For the nondiagonal background configuration (3.69) the fermion propagator is given by

$$G_F = \begin{pmatrix} 0 & G_F^{(+)} \\ G_F^{(-)\,T} & 0 \end{pmatrix} , \tag{3.83}$$

where the components $G_F^{(\pm)}$ are take the form

$$\left(G_F^{(\pm)}\right)_{ab}(p) = \widetilde{G}_F(p)\left(Z_F(1+r_F)\not{p}\,\delta_{ab} \mp i\bar{h}(p)\Phi_0\Sigma_{ab}\right) , \tag{3.84}$$

and

$$\widetilde{G}_F(p) = \left(Z_F^2(1+r_F)^2p^2 + \bar{h}(p)^2\Phi_0^2\right)^{-1} . \tag{3.85}$$

In the fermion subspace the fluctuations are given by

$$\left(F_F\right)_{ab}(p,q) = i\bar{h}(-p,q)\Delta(p-q,Q)\begin{pmatrix} 0 & -\Lambda_{ab}^T \\ \Lambda_{ab} & 0 \end{pmatrix} + \mathcal{O}(\Delta^2) . \tag{3.86}$$

Going through the same steps as above, that is, computing the trace in $\delta^{(2)}\Gamma_F$, and evaluating the projection (3.72) we obtain

$$\begin{aligned} \delta^{(2)}\Gamma_F\Big|_{Z_B} \;=\; & -2\lim_{Q\to 0}\frac{\partial}{\partial Q^2}\int\frac{d^dp}{(2\pi)^d}\left[\bar{h}(-p,p+Q)\right]^2 \\ & \times\widehat{\frac{\partial}{\partial t}}\Big\{Z_F(p)(1+r_F(p))\widetilde{G}_F(p) \\ & \quad\times Z_F(p+Q)\left(1+r_F(p+Q)\right)\widetilde{G}_F(p+Q) \\ & \quad+\Phi_0^2\,\bar{h}(p)\bar{h}(p+Q)\widetilde{G}_F(p)\widetilde{G}_F(p+Q)\Big\} , \end{aligned} \tag{3.87}$$

where $\left[\bar{h}(-p,p+Q)\right]^2 \equiv \bar{h}(-p,p+Q)\bar{h}(-p-Q,p)$. Putting both results (3.80) and (3.87) together $\partial_t Z_B = \delta^{(2)}\Gamma_B\big|_{Z_B} + \delta^{(2)}\Gamma_F\big|_{Z_B}$ and using the definition $\eta_B = -\partial_t \ln Z_B$ we obtain the evolution equation for the boson anomalous dimension:

$$\begin{aligned} \eta_B \;=\; & 16\frac{v_d}{d}\Big\{\rho_0\,\lambda_2^2\,m_{2,2}^{(B)}(\epsilon,\epsilon+2\rho_0\lambda_2;\eta_B) + h^2\,m_4^{(F)}\left(\frac{2}{N}\rho_0h^2;\eta_F\right) \\ & +\frac{2}{N}\rho_0h^4\,m_2^{(F)}\left(\frac{2}{N}\rho_0h^2;\eta_F\right)\Big\} . \end{aligned} \tag{3.88}$$

Here we have introduced the threshold functions $m_{2,2}^{(B)}$, $m_2^{(F)}$ and $m_4^{(F)}$ that define the one-loop contribution appearing in the calculation of the wavefunction renormalization. They are given explicitly in Appendix B.

In the broken phase the wavefunction renormalization will get additional contributions from the radial mode [15, 129]. In principle, these terms should be taken into account, however, since most of the running takes place in the symmetric regime, we do not expect them to play any major role.

3.4.4. Fermion anomalous dimension and Yukawa coupling

The derivation of the flow equation for the fermion anomalous dimension $\eta_F \equiv -\partial_t \ln Z_F$ and the Yukawa coupling h^2 proceeds in the same way as explained in Sec. 3.4.3. Here, the only difference is, that we need to choose a nonhomogeneous configuration for the fermion fields, where in the momentum-representation we have

$$\psi(q) = \psi\delta(q,Q) \;, \qquad \bar{\psi}(q) = \bar{\psi}\delta(q,Q) \;. \tag{3.89}$$

The matrix field is evaluated in the constant background configuration $\Phi_{ab} = \Phi_0\Sigma_{ab}$, where the boson and fermion propagators are given by (3.77) and (3.84), respectively.

Starting from the *ansatz* for the fermions (3.89) we evaluate the fluctuation matrix

$$F_k(p,q) = \begin{pmatrix} 0 & i\bar{h}(p-q,q)\,\bar{\psi}_b(q-p)\delta_{ac'} & -i\bar{h}(q,-q+p)\,\psi_a^T(-q+p)\delta_{bc'} \\ -i\bar{h}(-q+p,-p)\,\bar{\psi}_{a'}^T(q-p)\delta_{b'c} & 0 & 0 \\ i\bar{h}(-p,p-q)\,\psi_{b'}(-q+p)\delta_{a'c} & 0 & 0 \end{pmatrix} , \tag{3.90}$$

where we indicate the flavor indices on the right-hand side explicitly. Recall, that the fluctuation is defined as the field-dependent part of the second functional derivative of the scale-dependent effective action. The functional derivative from the left is taken with respect to the fields $\left(\Phi_{ab}^T, \psi_c^T, \bar{\psi}_c\right)$ which defines the row indices. The primed column indices are defined equivalently via the right-hand functional derivative. Together with the background field propagator G_k (see Appendix A) we evaluate the second order contribution $\delta\Gamma_k^{(2)} = -(1/4)\,\mathrm{STr}\,\widehat{\partial/\partial t}\,(G_kF_k)^2$ in the series expansion. A short calculation yields

$$\begin{aligned} \delta\Gamma_k^{(2)} \;=\; & \frac{1}{2}\int\frac{d^dq}{(2\pi)^d}\frac{d^dp}{(2\pi)^d}\widehat{\frac{\partial}{\partial t}}\Big\{ \left[\bar{h}(p-q,q)\right]^2 (G_B)_{ab,cd}\,(p)\bar{\psi}_d(q-p)\big(G_F^{(+)}\big)_{ca}(q)\psi_b(q-p) \\ & + \left[\bar{h}(q,p-q)\right]^2 (G_B)_{ab,dc}\,(p)\psi_d^T(-q+p)\big(G_F^{(-)}\big)_{cb}^T(q)\bar{\psi}_a^T(p-q)\Big\} \;. \end{aligned} \tag{3.91}$$

Inserting the expressions the boson and fermion propagators (3.77) and (3.84) this can be written in the form:

$$\begin{aligned} \delta\Gamma_k^{(2)} \;=\; & \frac{1}{N}\int\frac{d^dp}{(2\pi)^d}\widehat{\frac{\partial}{\partial t}}\Big\{ \left[\bar{h}(Q,p)\right]^2 \widetilde{G}_F(p)\Big[Z_F\,(1+r_F) \\ & \times \bar{\psi}^a \not{p}\big\{\left(N^2-2\right)G_{B,0}(p-Q) + G_{B,R}(p-Q)\big\}\psi^a \\ & + i\bar{h}(Q)\,\bar{\psi}^a\,\Phi_0\Sigma_{ab}\left\{2G_{B,0}(p-Q) - G_{B,R}(p-Q)\right\}\psi^b\Big]\Big\} \;. \end{aligned} \tag{3.92}$$

Projecting this equation onto the corresponding operators in the *ansatz* for the scale-dependent effective action we obtain the evolution equation for the fermion anomalous dimension

$$\eta_F = \frac{8}{N}\frac{v_d}{d}h^2\left\{(N^2-2)m_{1,2}^{(FB)}\left(\frac{2}{N}\rho_0h^2,\epsilon;\eta_F,\eta_B\right) + m_{1,2}^{(FB)}\left(\frac{2}{N}\rho_0h^2,\epsilon+2\rho_0\lambda_2;\eta_F,\eta_B\right)\right\} , \tag{3.93}$$

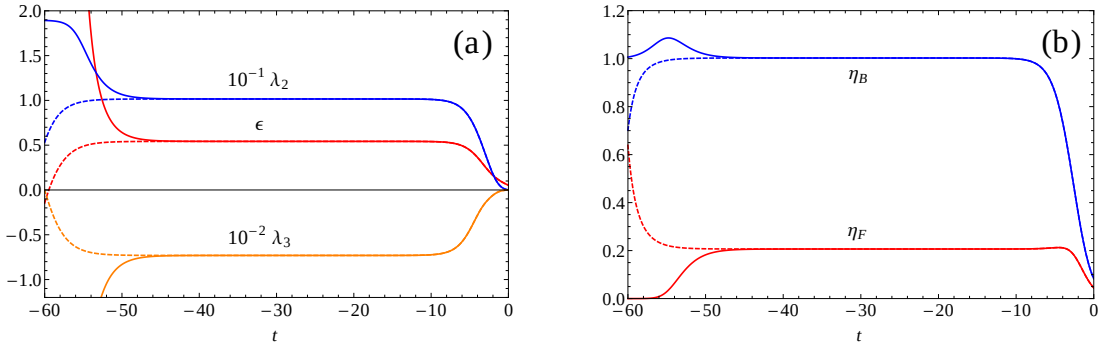

Figure 3.2.: Renormalization group flow (a) for the dimensionless renormalized parameter ϵ, the (rescaled) dimensionless renormalized couplings $10^{-1}\lambda_2$, and $10^{-2}\lambda_3$, and (b) for the boson and fermion anomalous dimensions η_B and η_F as a function of the scale parameter $t = \ln(k/\Lambda)$ close to the critical trajectory. The full and dashed curves refer to initial conditions just above and below the critical parameter $\epsilon_{\Lambda,(cr)}$, respectively.

and the flow equation for the momentum-independent part of the Yukawa coupling

$$\begin{aligned}\frac{\partial h^2}{\partial t} &= (d-4+2\eta_F+\eta_B)h^2 - \frac{8}{N}h^4 v_d \left\{ 2\, l_{1,1}^{(FB)}\left(\frac{2}{N}\rho_0 h^2, \epsilon; \eta_F, \eta_B\right)\right. \\ &\quad \left. - l_{1,1}^{(FB)}\left(\frac{2}{N}\rho_0 h^2, \epsilon + 2\rho_0\lambda_2; \eta_F, \eta_B\right)\right\} \\ &\quad + \frac{16}{N}\rho_0 h^4 v_d \left\{ 2\lambda_2\, l_{1,2}^{(FB)}\left(\frac{2}{N}\rho_0 h^2, \epsilon; \eta_F, \eta_B\right)\right. \\ &\quad \left. - (2\lambda_2 + 2\rho_0\lambda_3)\, l_{1,2}^{(FB)}\left(\frac{2}{N}\rho_0 h^2, \epsilon + 2\rho_0\lambda_2; \eta_F, \eta_B\right)\right\} \\ &\quad + \frac{32}{N^2}\rho_0 h^6 v_d \left\{ 2\, l_{2,1}^{(FB)}\left(\frac{2}{N}\rho_0 h^2, \epsilon; \eta_F, \eta_B\right) - l_{2,1}^{(FB)}\left(\frac{2}{N}\rho_0 h^2, \epsilon + 2\rho_0\lambda_2; \eta_F, \eta_B\right)\right\} . \end{aligned} \tag{3.94}$$

Here, we have defined the threshold functions $m_{1,2}^{(FB)}$, $l_{1,1}^{(FB)}$, $l_{1,2}^{(FB)}$, and $l_{2,1}^{(FB)}$ that are given explicitly in Appendix B. Together with the flow equations for the parameters and couplings of the effective average potential and the anomalous dimension for the bosons they constitute a closed set of differential equations that can be solved numerically.

3.5. Critical properties of the quantum phase transition

We evolve the flow equations starting from an appropriate ultraviolet scale Λ to the physical limit $k \to 0$. The following results have been obtained for the set of initial conditions: $Z_{B,\Lambda} = 10^{-10}$, $Z_{F,\Lambda} = 1$, $\bar{h}_\Lambda^2 = \Lambda$, where the mass at the ultraviolet scale $\bar{m}_\Lambda^2$ is taken as a free parameter, and all higher order couplings are set to zero, i.e., $\bar{\lambda}_{n,\Lambda} = 0$, $n = 2, \ldots, n_{\max}$. By varying the dimensionless mass ϵ_Λ at the ultraviolet scale we may tune the

system across a quantum phase transition. Here, $\delta\epsilon = |\epsilon_\Lambda - \epsilon_{\Lambda,(cr)}|$ measures the deviation of the parameter ϵ_Λ from its critical value $\epsilon_{\Lambda,(cr)}$. Close to $\epsilon_{\Lambda,(cr)}$ we find a fixed point solution for the dimensionless renormalized parameters and couplings. That is, the parameters and couplings stay nearly constant over a wide range of scales as illustrated in Fig. 3.2. This is a clear indication for the presence of a continuous phase transition where the system displays a universal scaling behavior. For $\delta\epsilon > 0$, where the mass parameter ϵ_Λ is above the critical value $\epsilon_{\Lambda,(cr)}$, the solution stays in the symmetric regime. However, starting just below $\epsilon_{\Lambda,(cr)}$ the scale-dependent mass eventually becomes negative which signals the transition into the broken phase. This result does not depend on the special choice of initial conditions, that is, we have checked the stability of our results for different initial values of $Z_{B,\Lambda}$, $\bar{h}^2_\Lambda$, and $\bar{\lambda}_{n,\Lambda}$. Furthermore, the fixed point solution exists for all considered truncations of the effective average potential (see Tab. 3.4), where we have taken the Taylor series expansion of the effective potential up to the tenth order in the field Φ. The independence of the scaling solution both on the initial conditions and higher order operators in the effective potential is a manifestation of universality near a continuous phase transition.

In the symmetric phase both the wavefunction renormalization Z_B and the renormalized mass $m^2_R = Z_B^{-1}\bar{m}^2$ at the scale k receive large contributions from the massless fermions. That is $\eta_B \to 1$ for $k \to 0$ even far from the phase transition which can be clearly seen in Fig. 3.2(b) where the boson anomalous dimension assumes a value close to one in the symmetric phase. To compute the critical scaling we introduce the renormalized mass $\tilde{m}^2_R$ at a fixed scale k_c:

$$\tilde{m}^2_R(k_c, \delta\epsilon) = k_c^2 \left(u'_{k_c}(0) - u'_{k_c,(cr)}(0) \right) \ . \tag{3.95}$$

It is given in terms of the first derivatives of the effective average potential in the symmetric phase, where the scale $k_c = r_c \tilde{m}_R$ is defined via the parameter r_c in a standard way [132, 133].

The critical exponent ν characterizes the divergence of the correlation length at the critical point. Here, the correlation length is identified with the inverse renormalized mass [19, 129] as given in (3.95) and the critical exponent ν is defined as [132, 133]

$$\nu = \frac{1}{2} \lim_{\delta\epsilon \to 0} \frac{\partial \ln \tilde{m}^2_R(k_c, \delta\epsilon)}{\partial \ln \delta\epsilon} = \lim_{\delta\epsilon \to 0} \left(\hat{\nu}(k_c, \delta\epsilon) + \tilde{\nu}(k_c, \delta\epsilon)\nu \right) , \tag{3.96}$$

where

$$\hat{\nu}(k, \delta\epsilon) = \frac{1}{2} \left. \frac{\partial \ln \tilde{m}^2_R(k, \delta\epsilon)}{\partial \ln \delta\epsilon} \right|_t , \tag{3.97}$$

$$\tilde{\nu}(k, \delta\epsilon) = \frac{1}{2} \left. \frac{\partial \ln \tilde{m}^2_R(k, \delta\epsilon)}{\partial t} \right|_{\delta\epsilon} . \tag{3.98}$$

The value for the critical exponent ν is independent of the parameter r_c, as long as $r_c \lesssim 1$. This essentially corresponds to the requirement that the scale k_c is sufficiently close to the limiting value $k \to 0$. In our calculations we have taken $r_c \simeq 0.01$.

The critical exponent γ determines the divergence of the susceptibility which is encoded in the nonrenormalized mass $\bar{m}^2 = Z_B m^2_R$ [19, 129]. Although it is evaluated in the symmetric

	4th order	6th order	8th order	10th order
η_B	0.989	0.999	1.003	1.000
η_F	0.223	0.211	0.207	0.210
ν	1.922	1.936	1.791	1.874
γ	1.942	1.939	1.786	1.875
$\nu(2-\eta_B)$	1.942	1.939	1.786	1.875
β	1.911	1.935	1.793	1.874
$\frac{1}{2}\nu(d-2+\eta_B)$	1.911	1.935	1.793	1.874

Table 3.3.: $N = 2$ critical exponents for different orders in the local potential approximation (LPA). For comparison the exponents γ and β are also determined from the scaling relations $\gamma = \nu(2-\eta_B)$ and $\beta = \nu(d-2+\eta_B)/2$.

phase, it is not affected by the fluctuations of the fermions. We have

$$\gamma = \lim_{\delta\epsilon\to 0} \frac{\partial \ln \bar{m}^2(\delta\epsilon)}{\partial \ln \delta\epsilon} \ . \tag{3.99}$$

Finally, the critical exponent β measures the fluctuations of the renormalized order parameter $\rho_{0,k}$ and is defined in the broken phase:

$$\beta = \frac{1}{2} \lim_{\delta\epsilon\to 0} \frac{\partial \ln \rho_0^2}{\partial \ln \delta\epsilon} \ . \tag{3.100}$$

We extract the anomalous dimensions η_B and η_F the same way as the critical couplings. Close to the critical parameter $\epsilon_{\Lambda,(cr)}$ the renormalization group flow approaches the fixed point solution where the system is scale-invariant. That is, the solutions to the flow equation stay constant over a wide range of scales where we may extract the corresponding quantities. The values of the anomalous dimensions η_B and η_F are defined at the critical point in the window where we have a plateau (see Fig. 3.2). Our results are summarized in Tab. 5.1 where we show the values of the critical exponents. They are given for different orders of the series expansion for the effective average potential and were obtained using the optimized regulator (3.43). We have also calculated the critical exponents for the exponential regulator. For that calculation, however, we neglect the dependence on the anomalous dimensions in the threshold functions. Since the anomalous dimensions are of order one, this gives a very rough estimate of the systematic error for our results. We find an agreement of the critical exponents on the 10% level. The scaling relations $\gamma = \nu\,(2-\eta_B)$ and $\beta = \nu\,(d-2+\eta_B)\,/2$ for the critical exponents provide a consistency check of our calculations and are also given in Tab. 5.1. We see that our results show a reasonable convergence in the series expansion.

In Tab. 3.4 we give the values of the critical parameters and couplings, where the asterisk denotes the fixed point values, i.e., $\epsilon_* \equiv u'_*$, $\lambda_{2,*} \equiv u_*^{(2)}$ etc. These quantities are not universal and depend on the particular renormalization group scheme. It is important to comment on their behavior in the series expansion of the effective average potential. Taking into

	4th order	6th order	8th order	10th order
ϵ_*	0.4842	0.5242	0.5424	0.5288
$\lambda_{2,*}$	10.7678	10.3744	10.1573	10.3210
$\lambda_{3,*}$		-48.5405	-73.0962	-54.6552
$\lambda_{4,*}$			-1956.82	-485.084
$\lambda_{5,*}$				219713
h_*^2	12.8622	12.9203	12.9438	12.9264

Table 3.4.: $N = 2$ fixed point values for different orders in the local potential approximation (LPA).

account only the relevant operators, that is, expanding the potential to fourth order, yields a reasonably good result for the scaling exponents. This can also be seen directly in Tab. 3.4 where the inclusion of higher order irrelevant operators does not significantly alter the values for the relevant critical couplings, in contrast to the higher order couplings, that vary strongly for different orders of the expansion. The relevant couplings are completely stable and show that the important physical information is captured already in the lowest truncation with all relevant operators included.

3.6. Summary

We have calculated the critical exponents at the quantum critical point for the three-dimensional matrix Yukawa type model with $U(2)$ symmetry, which describes $N = 2$ species of Weyl fermions. This theory captures the relevant fluctuations close to the chiral phase transition for a low-energy effective model of spinless fermions on the honeycomb lattice. We have shown that the calculated critical exponents at the continuous quantum critical point define a new universality class distinct from Gross-Neveu or Neveu-Yukawa type models. In particular this system is special in the sense that it is characterized by large values of the anomalous dimensions. Similar results have been obtained in a single Dirac cone model where the semimetal-superfluid transition was investigated using functional renormalization group techniques [134, 135]. There, also a second order phase transition was found with large values for the anomalous dimensions, both for the anomalous dimensions of composite and fermion fields. In the context of compact three-dimensional QED one also observes a large value for the anomalous dimension of the gauge field $\eta_A = 1$, where the result holds exactly due to gauge invariance [136, 137]. Whether these nontrivial properties can be found in suspended graphene is still an important open question. To see if these results are indeed relevant for graphene requires us to include the long-range Coulomb interactions. In that case one has to ask whether the instantaneous interaction is relevant for the critical dynamics, or if one has an effective restoration of Euclidean rotational symmetry. Although, there are indications for such a behavior in the critical region of a Gross-Neveu-Yukawa fixed point for the

semimetal-insulator transition [87, 91] until now this is an open issue.

4. Multicritical behavior of two competing order parameters

Competing order parameters arise generically in a wide variety of systems ranging from ultracold atoms to extreme states of matter in QCD. Typically, their interaction give rise to a rich phase structure with first or second order phase transitions separating the different phases, as well as special points in the phase diagram where one observes multicritical behavior. Such multicritical points are encountered when critical lines meet or intersect and are characterized by additional relevant operators. While the values of critical exponents are independent of the position along a critical line, this is no longer true at its endpoints. There, the system belongs to a different universality class and new critical exponents may occur. Due to the interplay of different order parameters the physics at a multicritical point can be quite intricate with a complex phase structure in its neighborhood. It is therefore useful to consider simple examples that provide an understanding of the phase structure and the possible types of scaling encountered at such points.

One example is given by the tricritical point which separates a line of critical points from a first order line (see, e.g., [138] for a review). It was noticed early on, that such a situation is naturally encountered when a line of three-phase coexistence ends in an extended parameter space of the system [139, 140]. According to this scenario, three critical lines meet at the tricritical point, hence the terminology. The upper critical dimension of a tricritical point is $d = 3$ where the scaling properties are completely described in terms of mean-field exponents (up to logarithmic corrections [141–143]). Tricritical points have been discussed in the literature in the context of, e.g., the two-fluid ^{3}He – ^{4}He mixing point [139, 144], transitions in ordinary fluid mixtures [145, 146], and the chiral phase transition in QCD with two massless quarks [147–151]. While a tricritical point can be modeled by theories with a single order parameter and a nonordering field, we encounter more interesting examples if different competing fields simultaneously become critical.

Examples for multicritical points that result from the competition of two distinct types of order are the bicritical and related tetracritical point [152–155]. See Fig. 4.1 for an illustration of the associated phase diagrams. A bicritical point marks the endpoint of a first order line of two-phase coexistence. At this point, two critical lines meet, separating the two ordered phases from a disordered phase. At a tetracritical point the first order transition is replaced by a mixed phase which is bounded by two distinct critical lines. Both the bicritical

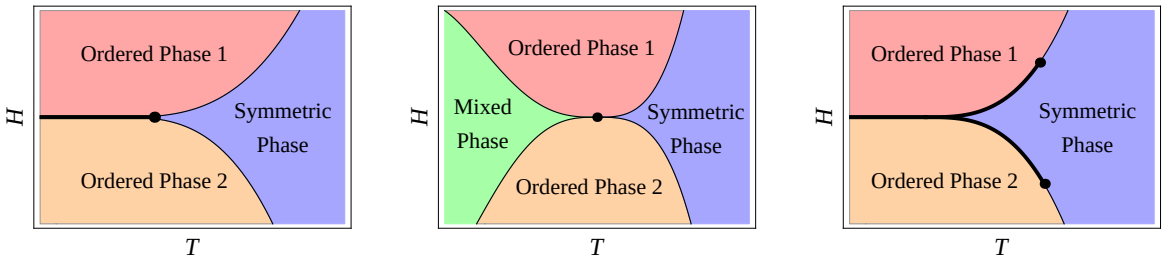

Figure 4.1.: Illustration of possible phase diagrams in the vicinity of a multicritical point as a function of two relevant parameters, e.g., temperature T and external magnetic field H. Thick lines represent a first order phase transition. (**Left**) A first order line ends at a bicritical point, where two critical lines separate the ordered phases from the symmetric phase. (**Middle**) A tetracritical point appears where four critical lines merge at a single point. In contrast to the bicritical point an additional mixed phase appears where both order parameters are nonvanishing. (**Right**) First order transition at the multicritical point. The two distinct first-order lines, separating the disordered from the respective ordered phase, end at a tricritical point where a critical line continues.

and tetracritical point allow for nontrivial scaling behavior in three dimensions, in contrast to the tricritical point. This makes them particularly interesting from a theoretical perspective. Experimentally, the spin-flop transition for anisotropic antiferromagnets in a uniform external magnetic field provides a prominent example for such a multicritical behavior [152–154, 156]. Furthermore, bicritical or tetracritical points may also be relevant for models of high-temperature superconductivity [157–161] as well as the competition between supersolid and superfluid order in ^{4}He [162].

Certainly, more complicated situations are conceivable if the parameter space of the system is enlarged. However, in the following we will focus only on the simplest case of two competing types of order. Their interaction exhibits a wide range of possibilities for the phase structure of the considered models, including the above mentioned multicritical points. A class of theories that features such multicritical behavior is given by the $O(N_1)\oplus O(N_2)$ symmetric models [38, 163], composed of two real-valued vector fields ϕ_{1a}, $a = 1, \ldots, N_1$ and ϕ_{2b}, $b = 1, \ldots, N_2$ in the irreducible representation of the $O(N_1)$ and $O(N_2)$ symmetry group, respectively. Depending on the values of N_1 and N_2, these theories may realize different scenarios for the phase diagram in the vicinity of a multicritical point, characterized by different fixed points of the renormalization group [152–154]. The stability of such a fixed point, as well as its physical accessibility determine the type of critical behavior that one observes for a given model. If no stable fixed point exists, or if the microscopic model lies outside its domain of attraction, one finds a first order phase transition in the system. However, the influence of further symmetry-breaking fields may change the situation, possibly even restoring a continuous transition [164]. In the case where both fields have a Z_2 Ising symmetry, the isotropic Heisenberg-like fixed

point is expected to be the stable one [163]. It generally features an enhanced $O(N_1 + N_2)$ symmetry and describes either a bicritical or a tetracritical point. The fact, that the isotropic fixed point can describe two distinct scenarios for the phase diagram is due to the presence of a dangerously irrelevant operator [165, 166]. Further fixed points exist that are expected to be stable for some combination of values N_1 and N_2. In particular, beyond some critical value of $N = N_1 + N_2$ one always expects a tetracritical point which is either described by a biconal or decoupled fixed point. To determine the phase structure of the model, it is important to understand which of these fixed points eventually determines the critical scaling. While a lot of work has already been done [38, 152–154, 163, 167, 168], certain aspects of these theories are still under debate. This is partly due to the fact that available data on the phase diagram of specific microscopic models [169, 170] is challenging to interpret, where the presence of small crossover exponents and intricate interplay of nonuniversal behavior complicate the analysis of experimental and Monte Carlo data [171]. Clearly, a nonperturbative method that is able to access both the scaling properties, as well as the nonuniversal physics is of advantage.

Here, we apply the nonperturbative functional renormalization group to theories with two competing order parameters and determine their possible scaling solutions and respective stability properties. The functional renormalization group avoids subtle issues in the resummation of high-order perturbative series for fixed dimension $d = 3$, and expansions in $\epsilon = 4 - d$ (see e.g., [172–174]) that are required to calculate critical exponents. Furthermore, unlike numerical Monte Carlo techniques, it is free from finite-size effects and discretization artifacts. In that sense, the functional renormalization group complements these methods. Taken together, they provide us with the possibility to understand physical systems in great qualitative as well as quantitative detail.

Of course, the $O(N_1) \oplus O(N_2)$ symmetric theories constitute only one example for theories that feature multicritical phenomena. In fact, a wide class of matrix models can be reduced to a coupled theory of two distinct order parameters in a certain range of their parameter space. We have already seen in the previous chapter that the unitary matrix models naturally lead to different order parameters in the bosonic sector with the possibility of multicritical behavior, if the relevant parameters are appropriately tuned. In particular, for spinless fermions on the honeycomb lattice we found a competition between a charge-density wave and a topological insulator state [175] that might lead to a decoupled tetracritical point for the phase diagram (see also the discussion of a $Z_2 \times O(2)$ symmetric biconal fixed point in a related model [99]). In the following, we will consider only the bosonic sector, where we discuss the mapping from the unitary matrix models to the $O(N_1) \oplus O(N_2)$ symmetric theories and point out their relevance for low-energy effective theories considered in the context of QCD.

4.1. Low-energy effective theory

To determine the low-energy properties of the $O(N_1) \oplus O(N_2)$ symmetric models, we use the following *ansatz* for the scale-dependent effective action

$$\Gamma_k = \int d^d x \left\{ \frac{1}{2} Z_{1,k} \left(\partial \phi_1\right)^2 + \frac{1}{2} Z_{2,k} \left(\partial \phi_2\right)^2 + U_k(\phi_1, \phi_2) \right\} , \tag{4.1}$$

where U_k is the scale-dependent effective potential and $Z_{1,k}$ and $Z_{2,k}$ denote the renormalization factors. The theory is defined in d Euclidean dimensions, where the dimension is kept as a free parameter in the following. However, in the evaluation of the flow equations we will be particularly interested in the case where $d = 3$. Here, we employ two different approximations of the effective action (4.1). First, we consider the case of scale-independent renormalization factors $\partial Z_{1,k}/\partial k = 0$ and $\partial Z_{2,k}/\partial k = 0$, i.e., $Z_{1,k} = Z_{2,k} = 1$, in the local potential approximation (LPA). This defines the lowest order contribution of a systematic expansion in derivatives which yields a good approximation to the phase structure of the model, while critical indices are only poorly resolved. Going beyond the leading order, we allow for scale-dependent renormalization factors but neglect their field-dependence. This provides a first reasonable approximation to determine the critical scaling properties. We derive the flow equations for the renormalization factors using a correspondence from the unitary matrix models. This is described in detail in Sec. 4.5.

For the potential we use a series expansion in a suitable basis of field operators $\mathcal{O}_m(\phi_1)$ and $\mathcal{O}_n(\phi_2)$, given by

$$U = \sum_{m,n} \bar{g}_{m,n} \mathcal{O}_m(\phi_1) \mathcal{O}_n(\phi_2) , \tag{4.2}$$

where the quantities $\bar{g}_{m,n}$ denote the generalized bare couplings, evaluated at the potential minimum (we will drop the k index for all scale-dependent quantities in the following sections). Such an approximation is justified near a continuous phase transition where the potential minimum continuously evolves from the high-momentum scale to the infrared. However, theories with two competing order parameters exhibit a rich critical behavior which allows both for first order and second order phase transitions [176, 177]. First order phase transitions, where the field-expectation value evolves into a metastable state in the course of the renormalization group flow, are difficult to capture by this approach. Instead one needs to resolve the full field dependence of the potential [71, 72, 178, 179]. It is thus important to understand when a truncated series expansion for the potential is applicable, giving controlled results for the critical behavior near the transition. We will come back to this issue in detail when we discuss possible scaling solutions to the flow equations (see Sec. 4.6).

4.2. Fluctuation matrix and mass spectrum

Here, we derive the field-dependent propagator and the related mass spectrum of the theory. Both enter the exact flow equation for the scale-dependent effective action and thereby de-

termine the RG flow equations for the one-particle irreducible n-point functions $\Gamma^{(n)}$. The propagator is defined in terms of the inverse two-point function, which is given by

$$\left(\Gamma^{(2)}_{IJ}\right)_{ab}(p) = Z_I p^2 \delta_{IJ}\delta_{ab} + \left(\bar{M}^2_{IJ}\right)_{ab} \ , \tag{4.3}$$

and characterizes the fluctuations around the expansion point of the effective action (4.1). The indices $I, J = 1, 2$ refer to the two sectors of the theory and we use the short-hand notation where index pairs (I, a), (J, b), etc., denote the field components ϕ_{Ia} and ϕ_{Jb}, respectively. The zero-momentum part of the two-point function defines the mass matrix $\bar{M}^2 = \Gamma^{(2)}(0)$, and its eigenvalues determine the spectrum of the theory. We emphasize, that these quantities are defined to be field-dependent. Only after deriving the flow equations for higher n-point functions, we set the fields to the appropriate minimum configuration.

To determine the mass spectrum, it is convenient to parametrize the field-dependence in terms of invariants of the $O(N_1) \oplus O(N_2)$ symmetry group, e.g., $\bar{\rho}_1 = \phi_1^2/2$ and $\bar{\rho}_2 = \phi_2^2/2$. Also, we rotate both fields such that they point in the 1-direction, $\phi_{Ia} = \|\phi_I\| \, \delta_{a1}$, $a = 1, \ldots, N_I$, where $\|\phi_I\| = \sqrt{\phi_{Ia}\phi_{Ia}}$ defines the norm of the N_I-component vector. With this choice for the field configuration, the zero-momentum part of the two-point function takes the following form

$$\left(\bar{M}^2_{IJ}\right)_{ab} = \frac{\partial U}{\partial \bar{\rho}_I}\delta_{IJ}\delta_{ab} + 2\left\{\bar{\rho}_I \frac{\partial^2 U}{\partial \bar{\rho}_I^2}\delta_{IJ} + \sqrt{\bar{\rho}_I \bar{\rho}_J}\,\frac{\partial^2 U}{\partial \bar{\rho}_I \partial \bar{\rho}_J}\left(\delta_{I1}\delta_{J2} + \delta_{I2}\delta_{J1}\right)\right\}\delta_{a1}\delta_{b1} \ . \tag{4.4}$$

We find $N_1 - 1$ degenerate eigenvalues $\bar{M}_1^2 = \partial U/\partial \bar{\rho}_1$, $N_2 - 1$ eigenvalues $\bar{M}_2^2 = \partial U/\partial \bar{\rho}_2$, and two modes with masses

$$\bar{M}^2_{\pm} = \frac{1}{2}\left(\bar{M}^2_{R,1} + \bar{M}^2_{R,2} \pm \sqrt{\left(\bar{M}^2_{R,1} - \bar{M}^2_{R,2}\right)^2 + 4\bar{\delta}}\right) \ , \tag{4.5}$$

where $\bar{M}^2_{R,I} = \partial U/\partial \bar{\rho}_I + 2\bar{\rho}_I \partial^2 U/\partial \bar{\rho}_I^2$, $I = 1, 2$, and the quantity $\bar{\delta} = 4\bar{\rho}_1\bar{\rho}_2\left(\partial^2 U/(\partial\bar{\rho}_1\partial\bar{\rho}_2)\right)^2$ parametrizes the coupling between the two sectors. In the RG flow equations these quantities are evaluated for a specific field configuration which defines the expansion point for the effective action (4.1). Depending on the regime that one is interested in, different expansions of the effective action may be appropriate. In fact, within our truncation the complete field dependence of the model is carried by the effective potential and the question in particular concerns which basis of field operators should be used for the expansion of the potential. Here, we expand the fields around their expectation values $\phi_{1,0}$ and $\phi_{2,0}$, defined by the scale-dependent minimum of the effective potential. Thus, we may distinguish the following cases:

- In the symmetric phase, both $\phi_{1,0}$ and $\phi_{2,0}$ are zero, and we use an expansion for the potential of the form

$$U = \bar{m}_1^2\bar{\rho}_1 + \bar{m}_2^2\bar{\rho}_2 + \sum_{m+n\geq 2}\frac{\bar{\lambda}_{m,n}}{m!\,n!}\bar{\rho}_1^m\,\bar{\rho}_2^n \ . \tag{4.6}$$

  In this case, the physical masses of the theory are

$$\bar{M}_1^2 = \bar{M}_+^2 = \bar{m}_1^2 \ , \quad \bar{M}_2^2 = \bar{M}_-^2 = \bar{m}_2^2 \ . \tag{4.7}$$

- If we assume that only one of the expectation values vanishes, say $\phi_{2,0} = 0$ and $\phi_{1,0} \neq 0$, then

$$U = \bar{m}_2^2 \bar{\rho}_2 + \sum_{m+n\geq 2} \frac{\bar{\lambda}_{m,n}}{m!\, n!} (\bar{\rho}_1 - \bar{\rho}_{1,0})^m \bar{\rho}_2^n \ , \tag{4.8}$$

  and the corresponding masses

$$\bar{M}_1^2 = 0 \ , \ \bar{M}_+^2 = 2\bar{\rho}_{1,0}\bar{\lambda}_{2,0} \ , \quad \bar{M}_2^2 = \bar{M}_-^2 = \bar{m}_2^2 \ . \tag{4.9}$$

  Of course, a similar case applies if the sectors are interchanged.

- Finally, for both $\phi_{1,0} \neq 0$ and $\phi_{2,0} \neq 0$, we use the following expansion

$$U = \sum_{m+n\geq 2} \frac{\bar{\lambda}_{m,n}}{m!\, n!} (\bar{\rho}_1 - \bar{\rho}_{1,0})^m (\bar{\rho}_2 - \bar{\rho}_{2,0})^n \ , \tag{4.10}$$

  where the physical masses are given by

$$\bar{M}_1^2 = \bar{M}_2^2 = 0 \ , \quad \bar{M}_\pm^2 = \bar{\rho}_{1,0}\bar{\lambda}_{2,0} + \bar{\rho}_{2,0}\bar{\lambda}_{0,2} \pm \sqrt{\left(\bar{\rho}_{1,0}\bar{\lambda}_{2,0} - \bar{\rho}_{2,0}\bar{\lambda}_{0,2}\right) + 4\bar{\rho}_{1,0}\bar{\rho}_{2,0}\bar{\lambda}_{1,1}^2} \ . \tag{4.11}$$

This concludes our discussion of the mass spectrum.

4.3. RG flow of the effective potential

We derive the renormalization group flow equation for the effective potential from the exact flow equation

$$\frac{\partial \Gamma}{\partial t} = \frac{1}{2} \operatorname{Tr} \int \frac{d^d q}{(2\pi)^d} \frac{\partial R(q)}{\partial t} \left(\Gamma^{(2)}(q) + R(q) \right)^{-1} \ , \tag{4.12}$$

where, as usual, $t = \ln k/\Lambda$ denotes the scale parameter (defined with respect to some UV scale Λ), and the trace $\operatorname{Tr} \cdots$ goes over the index pairs (I, a) etc. The theory is regularized by a mass-like regulator function, which we choose such that it acts separately in the two sectors, i.e., $(R_{IJ})_{ab}(p) = R_I(p)\delta_{IJ}\delta_{ab}$, $I, J = 1, 2$, while its momentum-dependence is determined by the function $R_I(p) = Z_I(k^2 - p^2)\theta(k^2 - p^2)$. Other choices for the regulator are possible, e.g., where the two sectors are regularized independently. However, the above form is the simplest choice that is compatible with the symmetries of the effective action (4.1). The chosen regulator satisfies an optimization criterion [58, 59] which allows us to derive fully analytic expressions for the nonperturbative β-functions.

Computing the trace over all diagonal contributions of the regularized propagator, we obtain

the flow equation for the effective potential:

$$\begin{aligned}\frac{\partial U}{\partial t} &= \frac{1}{2}\int\frac{d^dq}{(2\pi)^d}\left\{\frac{\partial R_1(q)}{\partial t}\left[\frac{N_1-1}{Z_1q^2+R_1(q)+\bar{M}_1^2}\right.\right.\\ &\quad\left.+\frac{Z_1q^2+R_1(q)+\bar{M}_{R,2}^2}{\left(Z_1q^2+R_1(q)+\bar{M}_{R,1}^2\right)\left(Z_2q^2+R_2(q)+\bar{M}_{R,2}^2\right)-\bar{\delta}}\right]\\ &\quad+\frac{\partial R_2(q)}{\partial t}\left[\frac{N_2-1}{Z_2q^2+R_2(q)+\bar{M}_2^2}\right.\\ &\quad\left.\left.+\frac{Z_2q^2+R_2(q)+\bar{M}_{R,1}^2}{\left(Z_1q^2+R_1(q)+\bar{M}_{R,1}^2\right)\left(Z_2q^2+R_2(q)+\bar{M}_{R,2}^2\right)-\bar{\delta}}\right]\right\}\ . \end{aligned}\tag{4.13}$$

Taking derivatives with respect to the fields and afterwards setting the fields to their minimum values, we obtain the flow equations for higher n-point functions $\Gamma^{(n)}$. Here, we consider only local interactions and thus, the RG flow of n-point correlation functions is reduced the to a set of flow equations for the couplings that parametrize the higher order operators in an expansion of the effective potential. The flow equation (4.13) therefore defines an infinite hierarchy for the derivatives of the potential $U^{(m,n)}=\partial^{m+n}U/(\partial\bar{\rho}_1^m\partial\bar{\rho}_2^n)$, $m,n\geq 1$, that are evaluated at the minimum of the potential. Their flow equations are given by

$$\frac{\partial}{\partial t}U^{(m,n)}=\frac{\partial}{\partial t}U^{(m,n)}\big|_{\bar{\rho}_{1,0},\bar{\rho}_{2,0}}+U^{(m+1,n)}\big|_t\frac{\partial\bar{\rho}_{1,0}}{\partial t}+U^{(m,n+1)}\big|_t\frac{\partial\bar{\rho}_{2,0}}{\partial t}\ ,\tag{4.14}$$

and include the contributions both from the explicit scale-dependence of the potential and the field expectation values (written in terms of the quadratic invariants $\bar{\rho}_{1,0}=\phi_{1,0}^2/2$ and $\bar{\rho}_{2,0}=\phi_{2,0}^2/2$). Here, $\cdots|_{\bar{\rho}_{1,0},\bar{\rho}_{2,0}}$ means that the respective quantity should be evaluated for fixed $\bar{\rho}_{1,0}$ and $\bar{\rho}_{2,0}$, and equivalently $\cdots|_t$ for a fixed scale parameter t.

The hierarchy (4.14) is closed by a truncated series expansion of the effective potential up to some finite order in the fields

$$U=\bar{m}_1^2\left(\bar{\rho}_1-\bar{\rho}_{1,0}\right)+\bar{m}_2^2\left(\bar{\rho}_2-\bar{\rho}_{2,0}\right)+\sum_{m+n\geq 2}^{n_{max}}\frac{\bar{\lambda}_{m,n}}{m!\,n!}\left(\bar{\rho}_1-\bar{\rho}_{1,0}\right)^m\left(\bar{\rho}_2-\bar{\rho}_{2,0}\right)^n\ ,\tag{4.15}$$

where we use an expansion that is adapted the case where both fields simultaneously become critical. That is, we evaluate (4.15) in the symmetry broken phase where both masses are zero, $\bar{m}_1^2=\bar{m}_2^2=0$, while the fields assume a nonvanishing expectation value. In that case, we need to determine the RG flow equations for $\bar{\rho}_{1,0}$ and $\bar{\rho}_{2,0}$. They are derived from the requirement that both masses are fixed to zero and do not flow, i.e., $\partial U^{(1,0)}/\partial t=\partial U^{(0,1)}/\partial t=0$ at the minimum of the potential. From (4.14) we derive the set of linear equations

$$\frac{\partial}{\partial t}U^{(1,0)}\big|_{\bar{\rho}_{1,0},\bar{\rho}_{2,0}} = -U^{(2,0)}\big|_t\frac{\partial\bar{\rho}_{1,0}}{\partial t}-U^{(1,1)}\big|_t\frac{\partial\bar{\rho}_{2,0}}{\partial t}\ ,\tag{4.16}$$

$$\frac{\partial}{\partial t}U^{(0,1)}\big|_{\bar{\rho}_{1,0},\bar{\rho}_{2,0}} = -U^{(1,1)}\big|_t\frac{\partial\bar{\rho}_{1,0}}{\partial t}-U^{(0,2)}\big|_t\frac{\partial\bar{\rho}_{2,0}}{\partial t}\ .\tag{4.17}$$

which we may solve in the nonsingular case, that is, when the quantity

$$\bar{\Delta}=\det\left(\frac{\partial^2U}{\partial\bar{\rho}_I\partial\bar{\rho}_J}\right)=U^{(2,0)}|_tU^{(0,2)}|_t-\left(U^{(1,1)}|_t\right)^2\ ,\tag{4.18}$$

is nonvanishing. We obtain

$$\frac{\partial\bar{\rho}_{1,0}}{\partial t} = \bar{\Delta}^{-1}\left(-U^{(0,2)}\big|_t\frac{\partial}{\partial t}U^{(1,0)}\big|_{\bar{\rho}_{1,0},\bar{\rho}_{2,0}} + U^{(1,1)}\big|_t\frac{\partial}{\partial t}U^{(0,1)}\big|_{\bar{\rho}_{1,0},\bar{\rho}_{2,0}}\right) , \tag{4.19}$$

$$\frac{\partial\bar{\rho}_{2,0}}{\partial t} = \bar{\Delta}^{-1}\left(U^{(1,1)}\big|_t\frac{\partial}{\partial t}U^{(1,0)}\big|_{\bar{\rho}_{1,0},\bar{\rho}_{2,0}} - U^{(2,0)}\big|_t\frac{\partial}{\partial t}U^{(0,1)}\big|_{\bar{\rho}_{1,0},\bar{\rho}_{2,0}}\right) . \tag{4.20}$$

If $\bar{\Delta} = 0$, this solution does not apply, and we need to find an alternative strategy to derive the flow equations. For that purpose, we solve the algebraic equation $\bar{\Delta} = 0$ and substitute one of the solutions, e.g., $U^{(1,1)}|_t = \sqrt{U^{(2,0)}|_t\, U^{(0,2)}|_t}$, into eqs. (4.16) and (4.17). This yields a flow equation for a *single* radial excitation:

$$\frac{\partial}{\partial t}\left(\sqrt{U^{(2,0)}|_t}\,\bar{\rho}_{1,0} + \sqrt{U^{(0,2)}|_t}\,\bar{\rho}_{2,0}\right) = -\frac{1}{2}\left(\frac{1}{\sqrt{U^{(2,0)}|_t}}\frac{\partial}{\partial t}U^{(1,0)}\big|_{\bar{\rho}_{1,0},\bar{\rho}_{2,0}} + \frac{1}{\sqrt{U^{(0,2)}|_t}}\frac{\partial}{\partial t}U^{(0,1)}\big|_{\bar{\rho}_{1,0},\bar{\rho}_{2,0}}\right) . \tag{4.21}$$

In fact, this explains why we encountered the singular scenario in the first place. If $\bar{\Delta} = 0$, we see that the mass spectrum for the case of two nonvanishing fields $\bar{\rho}_{1,0} \neq 0$ and $\bar{\rho}_{2,0} \neq 0$, reduces to $\bar{M}_1^2 = \bar{M}_2^2 = \bar{M}_-^2 = 0$, $\bar{M}_+^2 = 2\left(\bar{\rho}_{1,0}\bar{\lambda}_{2,0} + \bar{\rho}_{2,0}\bar{\lambda}_{0,2}\right)$. The theory then features an enhanced continuous $O(N_1 + N_2)$ rotational symmetry which is broken down to the $O(N_1 + N_2 - 1)$ symmetry group. The breaking of this symmetry gives rise to only one independent nonvanishing expectation value, where the scale-dependence follows from the requirement $\partial U^{(1,0)}/\partial t + \partial U^{(0,1)}/\partial t = 0$. Note, that this implies that only one of the masses is fixed to zero, since $\partial U^{(1,0)}/\partial t - \partial U^{(0,1)}/\partial t$ is not fixed by the $\bar{\Delta} = 0$ constraint. Thus, for the symmetry enhanced case it is necessary to use a different expansion for the potential which is adopted to this situation. In particular, we will use an expansion where only one of the field expectation values is nonzero. We will come back to this phenomenon of symmetry enhancement when we discuss scaling solutions to the flow equations (see Sec. 4.6).

Eqs. (4.13) – (4.21) define the complete set of flow equations to leading order in the derivative expansion for the $O(N_1) \oplus O(N_2)$ model. However, going beyond this approximation, including the effect of scale-dependent anomalous dimensions, we furthermore need to provide the flow equations for the renormalization factors Z_1 and Z_2. Their flow equations are given in Sec. 4.5.

4.4. Scaling form of the RG flow equations

To identify possible fixed point solutions where the theory is scale-independent we write the flow equations in terms of dimensionless renormalized quantities, i.e., we introduce the associated invariants $\rho_1 = Z_1 k^{2-d}\bar{\rho}_1$ and $\rho_2 = Z_1 k^{2-d}\bar{\rho}_2$, as well as the dimensionless effective potential $u = k^{-d}U$. The order parameters in the two sectors are defined only in the $k \to 0$ limit: $\lim_{k\to 0} Z_I^{-1} k^{d-2}\rho_I$, $I = 1, 2$, when all fluctuations have been taken into account.

The scaling form of the RG equation (4.13) reads

$$\begin{aligned}\frac{\partial u}{\partial t} &= -du + (d-2+\eta_1)\rho_1\frac{\partial u}{\partial \rho_1} + (d-2+\eta_2)\rho_1\frac{\partial u}{\partial \rho_2} \\ &\quad + 2v_d\Big\{(N_1-1)l_0(\epsilon_1;\eta_1) + \tilde{l}_0(\epsilon_{R,1},\epsilon_{R,2},\delta;\eta_1) \\ &\quad + (N_2-1)l_0(\epsilon_2;\eta_2) + \tilde{l}_0(\epsilon_{R,2},\epsilon_{R,1},\delta;\eta_2)\Big\}\ , \end{aligned} \tag{4.22}$$

where $\epsilon_{R,1} = Z_1^{-1}k^{-2}\bar{m}_{R,1}^2$ and $\epsilon_{R,2} = Z_2^{-1}k^{-2}\bar{m}_{R,2}^2$ denote the dimensionless renormalized mass eigenvalues, and the coupling parameter $\delta = Z_1^{-1}Z_2^{-1}k^{4-d}\bar{\delta}$. The anomalous dimensions $\eta_1 = -\partial \ln Z_1/\partial t$ and $\eta_2 = -\partial \ln Z_2/\partial t$ define the scaling contributions to the renormalization factors and are given in Sec. 4.5.

Using the optimized regulator function, the threshold functions l_0 and $\tilde{l}_0$ take the following form:

$$l_0(w;\eta) = \frac{2}{d}\left(1-\frac{\eta}{d+2}\right)\frac{1}{1+w}\ , \tag{4.23}$$

$$\tilde{l}_0(w_1,w_2,w_3;\eta) = \frac{2}{d}\left(1-\frac{\eta}{d+2}\right)\frac{1+w_2}{(1+w_1)(1+w_2)-w_3}\ . \tag{4.24}$$

We have already defined the class of threshold functions $\partial l_n(w;\eta)/\partial w = -(n+\delta_{n0})\,l_{n+1}(w;\eta)$, $n \geq 0$, by successive differentiations of l_0. The function $\tilde{l}_0(w_1,w_2,w_3;\eta)$ is of a similar type and reduces to the l_0 function in certain limits: $\lim_{w_3\to 0}\tilde{l}_0(w_1,w_2,w_3;\eta) = l_0(w_1;\eta)$, and $\lim_{w_2\to 0}\tilde{l}_0(w_1,w_2,w_3;\eta) = l_0(w_1-w_3;\eta)$. These two properties of the threshold function essentially describe the decoupling of the two sectors, as well as the vanishing of either one of the field expectation values.

The effective potential is given by

$$u(\rho_1,\rho_2) = \epsilon_1(\rho_1-\rho_{1,0}) + \epsilon_2(\rho_2-\rho_{2,0}) + \sum_{m+n\geq 2}^{n_{max}}\frac{\lambda_{m,n}}{m!\,n!}(\rho_1-\rho_{1,0})^m(\rho_2-\rho_{2,0})^n\ , \tag{4.25}$$

where $\epsilon_1 = Z_1^{-1}k^{-2}\bar{m}_1^2$, $\epsilon_2 = Z_2^{-1}k^{-2}\bar{m}_2^2$, and $\lambda_{m,n} = Z_1^{-m}Z_2^{-n}k^{(m+n)(d-2)-d}\bar{\lambda}_{m,n}$ denote the renormalized dimensionless masses and couplings in the given representation of the potential. Here, we use truncations up to 12th order in the fields $n_{max} = 2,\ldots,6$, which is sufficient to establish the convergence of critical exponents [63, 68, 69, 180, 181].

To determine the fixed point structure of the theory and their respective scaling properties, we need to define an appropriate expansion point for the effective potential (4.25). Which one is appropriate, is determined by the fixed point that one is interested in. Let us consider first the case, where the potential is expanded around two simultaneously nonvanishing field expectation values, $\rho_{1,0} \neq 0$ and $\rho_{2,0} \neq 0$. In that case, the dimensionless, renormalized masses ϵ_1 and ϵ_2 are zero, and the RG flow equations for $\rho_{1,0}$ and $\rho_{2,0}$ take the following form

$$\frac{\partial \rho_{1,0}}{\partial t} = \Delta^{-1}\left(-\lambda_{0,2}\frac{\partial}{\partial t}u^{(1,0)}\big|_{\rho_{1,0},\rho_{2,0}} + \lambda_{1,1}\frac{\partial}{\partial t}u^{(0,1)}\big|_{\rho_{1,0},\rho_{2,0}}\right)\ , \tag{4.26}$$

$$\frac{\partial \rho_{2,0}}{\partial t} = \Delta^{-1}\left(\lambda_{1,1}\frac{\partial}{\partial t}u^{(1,0)}\big|_{\rho_{1,0},\rho_{2,0}} - \lambda_{2,0}\frac{\partial}{\partial t}u^{(0,1)}\big|_{\rho_{1,0},\rho_{2,0}}\right)\ , \tag{4.27}$$

where $\Delta = \lambda_{2,0}\lambda_{0,2} - \lambda_{1,1}^2$. As explained in the previous section, this set of equations applies only if $\Delta \neq 0$. When $\Delta = 0$, we should expand around a field configuration where only one of the expectation values is nonvanishing, e.g., $\rho_{1,0} \neq 0$ and $\rho_{2,0} = 0$, while the masses $\epsilon_1 = 0$ and $\epsilon_2 \neq 0$. The corresponding flow equation is given by

$$\frac{\partial \rho_{1,0}}{\partial t} = -\frac{1}{\lambda_{2,0}} \frac{\partial}{\partial t} u^{(1,0)}\big|_{\rho_{1,0}} \ . \tag{4.28}$$

Of course, due to the enhanced rotational symmetry, the choice of the sector where the vacuum expectation value is nonvanishing is completely arbitrary.

Let us comment briefly on the validity of a truncation of the type (4.25) where the potential is expanded in some basis of field operators. Typically, such a series expansion provides a good approximation to the critical properties of the theory if we expand around the global minimum of the effective potential. However, depending on the values of the couplings $\lambda_{m,n}$ different possibilities may appear, that are distinguished by the discriminant

$$\Delta = \lambda_{2,0}\lambda_{0,2} - \lambda_{1,1}^2 \ . \tag{4.29}$$

Here, the couplings have been evaluated at the expansion point of the potential. Eq. (4.29) defines the determinant of the Hessian $\partial^2 u/(\partial\rho_I \partial\rho_J)$ that determines the behavior of the potential in the vicinity of the expansion point. If $\Delta > 0$, it defines a minimum of the potential (assuming both eigenvalues of the Hessian are nonnegative), $\Delta = 0$ corresponds to a degeneracy point, whereas $\Delta < 0$ describes a saddle-point solution. Clearly, fixed point solutions can be discarded if the couplings satisfy $\Delta < 0$. In that case, the potential is simply not expanded around the minimum and the series expansion will capture the properties at the transition only poorly. To properly resolve the full potential flow one should resort to grid methods instead (see, e.g., [178]). Not only does the quantity (4.29) characterize the type of extrema and the convergence properties of the truncation at the fixed point, it also plays an important role for the stability and convergence properties of the RG flow. This is due to the fact, that the sign of Δ is a renormalization group invariant – it does not change in the course of the RG flow. This is true, as long as the regulator function respects the possible symmetries of the model. The invariance of Δ has an important implication for the analysis of scaling solutions: If a stable fixed point exists in a region of the parameter/coupling space characterized by $\Delta \geq 0$ we may follow the renormalization group flow of the ground state from the microscopic theory to the low-energy effective theory within a series expansion of the effective potential. For such a situation we observe a convergence of the critical exponents. In contrast, in the region where $\Delta < 0$, one might encounter a first order transition. Thus, if one wants to solve for the complete RG flow, it depends on the particular microscopic model which truncation one should use for the effective potential.

4.5. Relation to matrix models

Before we move on to determine the fixed point solutions to the RG flow equations, let us comment on an interesting relation between the coupled scalar theories and matrix models. The class of $O(N_1) \oplus O(N_2)$-models appears naturally in theories where the order parameter is matrix-valued. Generally, matrix models can be phrased in terms of invariants of the reducible tensor representation of a given symmetry group which essentially describe the competing fields of the theory. Their identification relies on the decomposition of the tensor representation into irreducible representations that determine the possible types of symmetry breaking. This identification makes it possible to establish a correspondence to the $O(N_1) \oplus O(N_2)$-models simply by considering the dynamics in the two sectors of the theory that feature the required symmetry. However, we point out that this does not mean that the matrix model will necessarily show the same multicritical behavior in the phase diagram. The presence of further ordering or nonordering fields might drastically change the nature of the transition that one eventually observes for these models. Thus, a complete analysis of the phase diagrams for such matrix models is typically quite intricate.

As an example, we consider the $U(2)$ matrix model written in terms of a Hermitian 2×2 matrix Φ, where the decomposition of the tensor representation $\overline{\mathbf{2}} \otimes \mathbf{2} = \mathbf{3} \oplus \mathbf{1}$ yields a coupled theory of two scalar fields with $O(3) \oplus Z_2$ symmetry. The corresponding order parameters define the two invariants of the $U(2)$ matrix model that are written in terms of the trace in the defining representation $\bar{\sigma}_1 = (\mathrm{tr}\,\Phi)^2/2$ and $\bar{\sigma}_2 = \mathrm{tr}\,\Phi^2/2$. While the invariant $\bar{\sigma}_1$ captures the breaking of the Z_2 center symmetry of the $O(3) \simeq SU(2)$ subgroup, a nonvanishing vacuum expectation value for the order parameter $\bar{\sigma}_2$ leads to a breaking of the $SO(3)$ symmetry.[1] The effective potential for such a matrix model can be written solely in terms of these two invariants, i.e., $U(\Phi) = U(\bar{\sigma}_1, \bar{\sigma}_2)$, where higher order operators Φ^n can be expressed completely in terms of linear combinations of $\bar{\sigma}_1$ and $\bar{\sigma}_2$ to some given power. Note that both invariants define field monomials of degree two and thus lead to a similar competition for the two order parameters, as discussed at the example of the $O(N_1) \oplus O(N_2)$ models. Let us examine the expansion of the potential in terms of these invariants

$$U(\Phi) = \sum_{m+n \geq 2} \frac{\bar{\lambda}_{m,n}}{m!\,n!} \left(\bar{\sigma}_1 - \bar{\sigma}_{1,0}\right)^m \left(\bar{\sigma}_2 - \bar{\sigma}_{2,0}\right)^n \ , \tag{4.30}$$

where $\bar{\sigma}_{1,0}$ and $\bar{\sigma}_{2,0}$ denote the corresponding expectation values in the symmetry broken phase. The mass spectrum for this theory is identical to the coupled $O(3) \oplus Z_2$ model. In particular, it follows that the purely bosonic $U(2)$ matrix model allows for a similar scenario where the symmetry of the theory enhanced to a $O(4)$ rotational symmetry. This is an explicit example of universality – the flow equations are completely independent of the field representations as long as the underlying symmetry and dimensionality of the problem are the same.

[1] The global $U(1)$ symmetry typically corresponds to charge conservation and is not broken by interactions.

Let us use a different physical context to elucidate a subtlety in such matrix models: Another prominent example featuring the $U(2)$ symmetry group appears in the context of low-energy effective models for QCD, e.g., the quark-meson model with two light quark flavors [130, 182, 183]. It features a similar $SU(2)_L \times SU(2)_R \times U(1)_A$ symmetry which is written in terms of a generic complex matrix in the $\overline{\mathbf{2}} \otimes \mathbf{2}$ representation. If we consider only the bosonic sector, such a theory can be written in terms of four invariants $\bar{\sigma}_i = \mathrm{tr}\left(\Phi^\dagger \Phi\right)^i$, $i = 1, \ldots, 4$, of the symmetry group. Similar to the discussion above, examining a polynomial expansion of the effective potential one could expect an enhanced $O(8)$ symmetry at the multicritical point. However, it turns out that the competing order parameters do not enter with the same canonical mass dimension which leads to different dynamics compared to the Hermitian $U(2)$ matrix model. In particular, there are no competing operators of degree two (the only mass-like invariant being $\mathrm{Tr}\,\Phi^\dagger\Phi$). The situation is different however, in the case without the $U(1)_A$ axial symmetry, where an additional order parameter is allowed that violates this symmetry. It can be expressed in terms of a linear combination of operators $\det\Phi$ and $\det\Phi^\dagger$ which are quadratic in the fields.

For our purposes it is useful to focus on the $U(N)$ symmetric matrix models. Here, we demonstrate a mapping to the $O(N_1) \oplus O(N_2)$ theory, where we use a truncation for the scale-dependent action of the form

$$\Gamma = \int d^d x \left\{ \frac{1}{2} Z_\Phi \,\mathrm{tr}\,(\partial\Phi)^2 + U(\Phi) \right\} . \tag{4.31}$$

The trace $\mathrm{tr}\cdots$ goes over the diagonal components of the matrix Φ_{ab}, $a, b = 1, \ldots, N$, in the given representation and we introduce a scale-dependent renormalization factor Z_Φ, neglecting its possible field-dependence. This *ansatz* extends the discussion of the $U(2)$ model (see the previous chapter 3) to the general case of N components. The representation Φ_{ab} can be decomposed in the following way $\overline{\boldsymbol{N}} \otimes \boldsymbol{N} = (\boldsymbol{N}^2 - \mathbf{1}) \oplus \mathbf{1}$, where we associate the two invariants $\bar{\sigma}_1 = (\mathrm{tr}\,\Phi)^2/2$ and $\bar{\sigma}_2 = \mathrm{tr}\,\Phi^2/2$ to the Z_2 and $O(N^2-1)$ order parameter, respectively. In the following, we neglect all higher order operators, and expand the potential only in $\bar{\sigma}_1$ and $\bar{\sigma}_2$, i.e., $U(\Phi) \sim U(\bar{\sigma}_1, \bar{\sigma}_2)$. In that case, it is possible to exploit universality to map the flow equations onto the class of $O(N^2-1) \oplus Z_2$ symmetric theories.

For the given truncation (4.31), we use the results from the previous chapter leaving the dimension of the matrix representation N as a free parameter. Only after deriving the flow equations, we specify N (and set it to possibly noninteger values). In particular, we use the scaling contribution to the renormalization factor, i.e., $\eta_\Phi = -\partial \ln Z_\Phi / \partial t$ derived in the previous chapter, to obtain an estimate of the critical exponents in the two-coupled vector models. We emphasize at this point that the derivation of η_Φ takes into account only the contributions from the massless Goldstone modes, which in the $O(N^2-1) \oplus Z_2$ decomposition are seen to originate from the sector with the continuous $O(N^2-1)$ symmetry. Thus, the truncation (4.31) is equivalent to an *ansatz* (4.1) where the renormalization factors are chosen such that $Z_1 = 0$ and $Z_2 = Z_\Phi$. This gives a reasonable approximation to the multicritical scaling behavior for the class of $O(N) \oplus Z_2$ models, while the general case $O(N_1) \oplus$

$O(N_2)$ with $N_1 \neq 1$ and $N_2 \neq 1$ is not accessible by such an identification. The anomalous dimension η_Φ for the $O(N) \oplus Z_2$ symmetric theories is thus given by

$$\eta_\Phi = 8\frac{v_d}{d}\rho_{2,0}\lambda_{0,2}^2\Big\{ m_{2,2}\left(0,\epsilon_+;\eta_\Phi\right) + m_{2,2}\left(0,\epsilon_-;\eta_\Phi\right) \\ - \Big(m_{2,2}\left(0,\epsilon_+;\eta_\Phi\right) - m_{2,2}\left(0,\epsilon_-;\eta_\Phi\right)\Big)\frac{\rho_{1,0}\lambda_{2,0} - \rho_{2,0}\lambda_{0,2} - 4\rho_{1,0}\rho_{2,0}\lambda_{1,1}^2/(2\rho_{2,0}\lambda_{0,2})}{\sqrt{\left(\rho_{1,0}\lambda_{2,0} - \rho_{2,0}\lambda_{0,2}\right)^2 + 4\rho_{2,0}\rho_{0,2}\lambda_{1,1}^2}}\Big\} \ . \tag{4.32}$$

where we have adopted the notation from the two-coupled field theories, and the threshold function $m_{2,2}(w_1,w_2;\eta) = (1+w_1)^{-2}(1+w_2)^{-2}$. We explicitly check that the parametrization of the scaling contribution to the renormalization factor Z_Φ captures the enhanced symmetry scenario. Indeed, in the limit where $\lambda_{1,1} = \sqrt{\lambda_{2,0}\lambda_{0,2}}$, we obtain

$$\eta_\Phi = 16\frac{v_d}{d}\rho_{2,0}\lambda_{0,2}^2 m_{2,2}\left(0, 2\left(\rho_{1,0}\lambda_{2,0} + \rho_{2,0}\lambda_{0,2}\right); \eta_\Phi\right) \ , \tag{4.33}$$

which is identical with the corresponding result for $O(N)$ vector models at the degeneracy point, where $\lambda_{2,0} = \lambda_{0,2} = \lambda$ and $\rho_{1,0} + \rho_{2,0} = \rho_0$:

$$\eta_\Phi = 16\frac{v_d}{d}\rho_0\lambda^2 m_{2,2}\left(0, 2\rho_0\lambda; \eta_\Phi\right) \ , \tag{4.34}$$

in the limit $\rho_{1,0} \to 0$. We will keep the index "Φ" for the anomalous dimension to emphasize that the the obtained results use the given correspondence from the reduced $U(N)$ models. With these results we may now ask for scaling solutions of the functional RG and investigate their critical properties.

4.6. Fixed points from the functional RG

Scale-invariant solutions of the renormalization group are classified according to their symmetry. The presence of these symmetries divides the theory space, spanned by the parameters and couplings of the model, into distinct subspaces that are closed under renormalization group transformations. If a fixed point exists in such a closed subspace, it defines a scale-invariant solution that inherits the symmetry from the subspace it is embedded in. Thus, it is reasonable to ask about the possible symmetries of the $O(N_1) \oplus O(N_2)$ symmetric theories by discussing the properties of the vacuum manifold.

As a simple example, let us consider the coupled $Z_2 \oplus Z_2$ theory, where both sectors feature a discrete Z_2 Ising symmetry. To illustrate the symmetry properties of the theory, we consider a series expansion for the effective potential to 4th order in the fields

$$u(\rho_1,\rho_2) = \frac{1}{2}\lambda_{2,0}\left(\rho_1 - \rho_{1,0}\right)^2 + \frac{1}{2}\lambda_{0,2}\left(\rho_2 - \rho_{2,0}\right)^2 + \lambda_{1,1}\left(\rho_1 - \rho_{1,0}\right)\left(\rho_2 - \rho_{2,0}\right) \ . \tag{4.35}$$

where both field expectation values are nonvanishing, $\rho_{1,0} \neq 0$ and $\rho_{2,0} \neq 0$. Depending on the values of the parameters and couplings, we may distinguish the following scenarios:

- All couplings are zero – the theory is noninteracting. This defines a singular point in theory space.

- If one of the sectors is trivial, either $\lambda_{2,0}$ or $\lambda_{0,2}$ is zero, and the coupling $\lambda_{1,1}$ vanishes. In this case, the theory is invariant under the discrete Z_2 Ising symmetry. Thus, we obtain two distinct Z_2-invariant subspaces in the space of $Z_2 \oplus Z_2$ models.

- Both the sectors are interacting, $\lambda_{2,0} \neq 0$ and $\lambda_{0,2} \neq 0$. Here, it is instructive to consider a reparametrization of the fields, where $\tilde{\rho}_1 = \sqrt{\lambda_{2,0}}\,\rho_{1,0}$ and $\tilde{\rho}_2 = \sqrt{\lambda_{0,2}}\,\rho_{2,0}$ (we assume that both $\lambda_{2,0}$ and $\lambda_{0,2}$ are positive). Then, the reparametrized potential takes the form

$$u(\tilde{\rho}_1, \tilde{\rho}_2) = \frac{1}{2}\left(\tilde{\rho}_1 - \tilde{\rho}_{1,0}\right)^2 + \frac{1}{2}\left(\tilde{\rho}_2 - \tilde{\rho}_{2,0}\right)^2 + \frac{\lambda_{1,1}}{\sqrt{\lambda_{2,0}\lambda_{0,2}}}\left(\tilde{\rho}_1 - \tilde{\rho}_{1,0}\right)\left(\tilde{\rho}_2 - \tilde{\rho}_{2,0}\right) \ , \quad (4.36)$$

  where the parameter $\xi = \lambda_{1,1}/\sqrt{\lambda_{2,0}\lambda_{0,2}}$ determines the symmetry properties of the theory. For values in the range $0 < \xi < 1$, the theory in general displays a discrete $Z_2 \times Z_2$ symmetry. However, the points $\xi = 0$ and $\xi = 1$ are special, and the symmetry of theory is enhanced.[2]

  Discrete $Z_2 \times Z_4$ symmetry: Let us first consider the situation when $\xi = 0$, where the two sectors are decoupled. We define the complexified invariant $\tilde{\rho} = (\tilde{\rho}_1 + i\tilde{\rho}_2)/\sqrt{2}$ and write the potential as: $u(\tilde{\rho}, \tilde{\rho}^*) = |\tilde{\rho} - \tilde{\rho}_0|^2$. In this case the theory allows for an additional discrete Z_2 symmetry, where $\tilde{\rho} \leftrightarrow \tilde{\rho}^*$. In fact, for the two-scalar model this symmetry is identical to a mirror symmetry that relates the two sectors in the case when the expectation values satisfy $\rho_{1,0} = \rho_{2,0}$, i.e., $\phi_1 \leftrightarrow \phi_2$. The value $\xi = 0$ defines a closed subspace in theory space that is invariant under $Z_2 \times Z_4$ symmetry.

  Continuous $O(2)$ symmetry: When $\xi = 1$ the couplings satisfy, $\lambda_{1,1} = \sqrt{\lambda_{2,0}\lambda_{0,2}}$. In that case, we may write the rescaled potential in terms of the quadratic invariant $\tilde{\rho} = \tilde{\rho}_1 + \tilde{\rho}_2$: $u(\tilde{\rho}) = (\tilde{\rho} - \tilde{\rho}_0)^2/2$. Clearly, in this form the potential exhibits an enhanced continuous $O(2)$ symmetry. This symmetry defines an invariant subspace given by requirement that $\Delta = 0$, where different points on the hypersurface are equivalent up to a reparametrization of the fields.

The discussed scenarios are summarized in Fig. 4.2. They divide the theory space in distinct invariant subspaces and give a complete characterization of the symmetry properties of the model (as well as possible fixed points of the RG). Of course, this discussion generalizes to more elaborate truncations of the effective potential, where the classification of symmetries is more complicated due to the presence of additional couplings. Also, these results similarly apply to the class of $O(N_1) \oplus O(N_2)$ models, where the illustration of the possible symmetries is more difficult. We find that possible fixed points of the theory are distinguished by the $O(N_1 + N_2)$, $Z_2 \times O(N_1) \times O(N_2)$, and $O(N_2) \times O(N_2)$ symmetries.

[2] Let us point out that in principle, given the requirement of stability $\Delta \geq 0$, a negative coupling $-\sqrt{\lambda_{2,0}\lambda_{0,2}} \leq \lambda_{1,1} < 0$ is also permissible. Thus we might consider the extended region $-1 \leq \xi \leq 1$. In that case, we find another enhanced $O(1,1)$ symmetry ($\xi = -1$) which, however, is not compatible with the positivity of the renormalization factors Z_1 and Z_2.

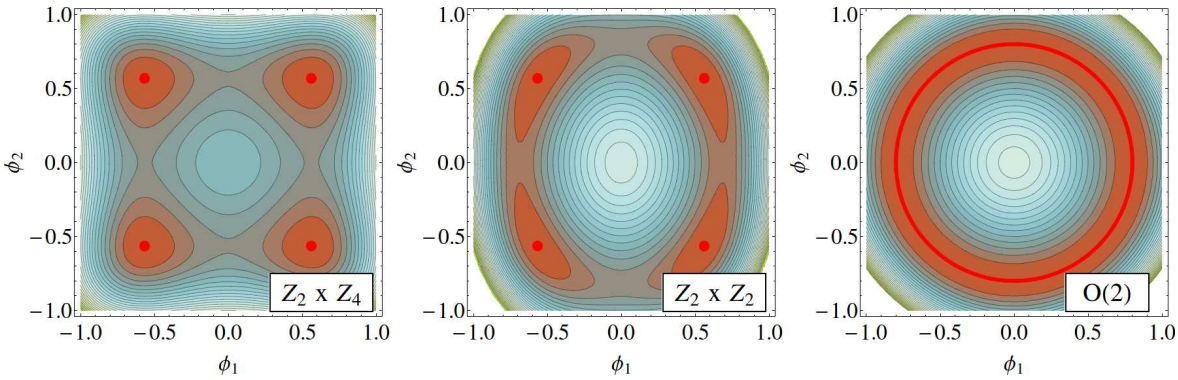

Figure 4.2.: Effective potential $u(\phi_1, \phi_2)$ for the $Z_2 \oplus Z_2$ scalar theory, expanded to 4th order in the fields. We find several possible scenarios for the ground state manifold if both field expectation values are nonvanishing: Two with a discrete symmetry $Z_2 \times Z_4$ and $Z_2 \times Z_2$, and one with a continuous $O(2)$ symmetry.

While the above symmetry considerations help to classify possible fixed point solutions, their existence and stability properties are yet to be determined. The stability of scaling solutions is given by the number of relevant parameters that require tuning to reach the continuous transition. At a multicritical point typically several parameters have to be adjusted, and the fixed point with the least number of relevant parameters is the stable one. The critical indices for the noninteracting fixed points can be inferred completely from dimensional analysis. The Gaussian fixed point (GFP) has five relevant directions and is never stable. The partially interacting, decoupled Gaussian fixed points (DGFP) featuring either $O(N_1)$ or $O(N_2)$ symmetry have at least two relevant directions that we may infer from the noninteracting sector. Furthermore, one relevant direction is added from the knowledge of the Wilson-Fisher fixed point. Similarly for the interacting models, we deduce the existence of the $Z_2 \times O(N_1) \times O(N_2)$ symmetric decoupled fixed point (DFP) with at least two relevant directions, as well as the isotropic Heisenberg-like fixed point (IFP) with $O(N_1 + N_2)$ symmetry and at least one relevant eigendirection. The remaining critical indices may receive sizable corrections from fluctuations and are determined from the eigenvalues of the stability matrix $\partial\beta/\partial g = (\partial\beta_{i,j}/\partial g_{m,n})$ at the respective fixed point which is determined by numerically solving the RG flow equations (4.22) – (4.28).

The stability matrix is defined by the derivatives of the nonperturbative β-functions $\beta_{i,j} = \partial g_{i,j}/\partial t$ with respect to the dimensionless, renormalized generalized couplings $g_{m,n}$. We linearize the β-functions at the fixed point defined by the couplings $g_{m,n\,*}$:

$$\beta_{i,j} = \sum_{m,n} \frac{\partial \beta_{i,j}}{\partial g_{m,n}} \left(g_{m,n} - g_{m,n\,*}\right) + \mathcal{O}(g^2) \ . \tag{4.37}$$

The solution is written in the form

$$g_{m,n} = g_{m,n\,*} + \sum_I c_I \, v^I_{m,n} (k/\Lambda)^{-\theta_I} \ , \tag{4.38}$$

N	$\theta_1 = y_{2,2}$	$\theta_2 = y_{2,0}$	$\theta_3 = y_{4,4}$	$\theta_4 = y_{4,2}$	$\theta_5 = y_{4,0}$	ϕ_T
2	1.756	*1.453*	-0.042	-0.446	*-0.743*	1.209
3	1.790	*1.362*	0.086	-0.380	*-0.756*	1.314
4	1.818	*1.292*	0.196	-0.324	*-0.775*	1.407
5	1.842	*1.240*	0.289	-0.283	*-0.797*	1.485
10	1.908	*1.116*	0.568	-0.154	*-0.879*	1.710
100	1.990	*1.010*	0.951	-0.015	*-0.988*	1.970
∞	2	*1*	1	0	*-1*	2

Table 4.1.: Critical indices for the isotropic fixed point (IFP) to 12th order LPA including a scale-dependent anomalous dimension η_Φ. The leading and subleading $O(N)$ exponents are highlighted in italics. The critical indices can be related to the scaling dimensions $y_{i,j}$ from Ref. [163]. The crossover exponent is given by $\phi_T = y_{2,2}\nu$ where $\nu = 1/\theta_2$ is the correlation length exponent.

where θ_I and v^I define the eigenvalues and corresponding eigendirections of the stability matrix at the fixed point:

$$\frac{\partial\beta(g_*)}{\partial g}\, v^I = -\theta_I v^I \ . \tag{4.39}$$

If Re $\theta_I > 0$ the corresponding eigendirection v^I is relevant in the IR limit $k \to 0$, while Re $\theta_I < 0$ characterize irrelevant eigendirections. If Re $\theta_I = 0$ the eigendirection is marginal. We want to point out that in general the eigenvalues may assume complex values. However, since only their real part matters for the discussion of stability properties, we take θ_I to refer to the real part only. Furthermore, we define the ordering for the eigenvalues: $\theta_1 > \theta_2 > \ldots$

This concludes our discussion of possible scaling solutions and their respective stability properties. In the following, we determine the fixed point solutions from the functional RG in $d = 3$ Euclidean dimensions.

4.6.1. Isotropic Heisenberg-like fixed point

The invariant subspaces of the $O(N_1) \oplus O(N_2)$ theory allow us to deduce both the existence of fixed points as well as their critical exponents. In the previous section we have argued that an isotropic Heisenberg-like fixed point should exist in the $O(N_1 + N_2)$ symmetric subspace from the knowledge of the Wilson-Fisher fixed point. It defines a special point on the $\Delta = 0$ hypersurface in theory space. The IFP features two critical indices θ_1 and θ_2 that are positive for all values of $N = N_1 + N_2$. Only one of these exponents, namely $\theta_2 = 1/\nu$, relates to the correlation length exponent ν for the related $O(N)$ model. Together with the subleading exponent $\theta_5 = -\omega$ the known $O(N)$ exponents are highlighted in italics in Tab. 4.1. The remaining critical indices are determined from a 12th order LPA truncation including η_Φ, where $\rho_{1,0} \neq 0$ and $\rho_{2,0} = 0$, adapted to the enhanced symmetry at the fixed point.

n	4	6	8	10	12
LPA	4.51	2.05	2.165	2.225	2.225
LPA+η_Φ	4.71	2.335	2.235	2.305	2.315

Table 4.2.: Stability transition of the $O(N)$ symmetric IFP for different truncations of the effective potential. Results are shown for truncations up to 12th order LPA including the anomalous dimension η_Φ. Beyond the 10th order truncation one expects a convergence of the results for the transition, where at 12th order we obtain the value $N \simeq 2.23$ (LPA) and $N \simeq 2.32$ (LPA+η_Φ).

In Tab. 4.1 we show only the five largest critical indices, that we compare to available data for the scaling behavior at the IFP. High-temperature series expansions currently give the best estimates of critical exponents: $y_{2,2} = 1.7639(11)$ for $N = 2$, $y_{2,2} = 1.7906(3)$ for $N = 3$ and $y_{2,2} = 1.8145(5)$ for $N = 4$ [171]. The RG scaling dimension $y_{2,2}$ is associated to the relevant quadratic tensor operator in the enhanced $O(N)$ symmetric theory (see, e.g., [163]) and corresponds to the largest exponent θ_1 in our functional RG calculations. We find very good agreement at the given level of the truncation. The combination of the two largest exponents θ_1 and θ_2 defines the crossover exponent $\phi_T = \theta_1/\theta_2 = y_{2,2}\nu$. Here, we compare our result $\phi_T = 1.314$ for $N = 3$ with $\phi_T = 1.260$ from the five-loop ϵ-expansion [163] and $\phi_T = 1.275$ from the two-loop $\epsilon = 4 - d$ expansion [167]. A similar quality of agreement is found also for other values of N. The third-largest exponent θ_3 relates to the scaling dimension $y_{4,4}$ of the cubic-symmetry perturbation [163]. For the case of $y_{4,4}$, the Monte Carlo data from Ref. [171] gives $y_{4,4} = -0.108(6)$ for $N = 2$, $y_{4,4} = 0.013(4)$ for $N = 3$ and $y_{4,4} = 0.125(5)$ for $N = 4$. Here, our values are larger, and we expect to obtain better precision at higher orders in the truncation. From our results to 12th order LPA+η_Φ we observe that the exponent θ_3 is negative for small N and changes its sign between $2 < N < 3$. Since the larger eigenvalues θ_1 and θ_2 are positive for all values of N, it is θ_3 that decides about the stability of the IFP. We determine the value of N, where θ_3 changes its sign, to be $N \simeq 2.32$ in the given 12th order LPA+η_Φ truncation (cf. Tab. 4.2). We may compare this results to the value $N = 2.89(4)$ obtained in six-loop calculation in fixed dimension [184] and $N \simeq 2.6$ from a two-loop ϵ-expansion [167] as well the $\mathcal{O}(\epsilon^5)$ result $N \simeq 2.87(5)$ from [184]. While the largest critical exponents θ_1 and θ_2 already show good quantitative precision, the values for the subleading exponents θ_3, θ_4, and θ_5 are less accurate. Higher precision is expected to be achieved by a extending the truncation to higher orders in the derivative expansion as, e.g., shown at the example of the Ising model in Refs. [67, 70]. For instance, the seven-loop result for the critical exponent of the correlation length, $\nu = 0.6304(13)$ [185] compares well to the functional RG estimate in fourth order of the derivative expansion $\nu = 0.632$ [67].

To study the effect of terms beyond our truncation, we vary the numerical value for η_Φ by hand and test the variation the stability transition. Although this is not a self-consistent solution to the set of flow-equations, it can provide a measure for the sensitivity of results

on terms beyond the truncation. Assuming that the variation of the anomalous dimension negligible, i.e., $\partial\eta_\Phi(\{g_*\})/\partial g_{m,n} \ll 1$, we obtain a variation of $\Delta N \simeq 0.25$ when varying η_Φ of order $\mathcal{O}(0.1)$.

The presence of only two positive exponents θ_1 and θ_2 below $N = 3$, implies that two parameters need to be tuned to reach the IFP in the case of the $Z_2 \oplus Z_2$ model. This is illustrated in Fig. 4.3 where the two relevant couplings are fixed to their respective critical values. The IFP is IR attractive in this case and will dominate the RG flow as long as the initial couplings lie inside its domain of attraction. The RG trajectories diverge if this condition is not fulfilled. In this case one expects a first order transition for the phase diagram. Of course, the situation changes for $N \geq 3$ where the IFP becomes unstable and one needs to tune an additional parameter to reach the fixed point. However, for a given model a third tunable parameter may simply not be accessible. We may therefore expect that the IFP is physically relevant only for two Z_2 Ising-like critical lines meet.

The nature of the transition described by the IFP sensitively depends on the quantity Δ [165, 166], which is a dangerously irrelevant operator at the fixed point (see, e.g., [186]). For $\Delta < 0$ one expects a bicritical point and for $\Delta > 0$ the transition should be tetracritical. However, the IFP defines a special point on the $\Delta = 0$ hypersurface, where RG trajectories may approach the fixed point from both sides, i.e., either from the $\Delta > 0$ or the $\Delta < 0$ region. Therefore, depending on the initial microscopic model one will either observe a bicritical or tetracritical behavior for the phase diagram (provided that it lies within the domain of attraction of the IFP). To pin down the structure of the phase diagram in the vicinity of the IFP requires a calculation of the scaling function of the free energy.

Finally, let us remark on previous application of the functional RG to a related N-vector model with cubic anisotropy. There, the critical value for N for the stability transition was determined to be $N \simeq 3.1$ [187]. In contrast to our calculations, an exponential instead of an optimized regulator was used. Furthermore, a truncation up to 8th in the fields was considered, and including derivative terms up to second order in momenta and 4th order in the fields. In our calculations, we see a shift of roughly $\mathcal{O}(0.1)$ to larger values in the stability transition N when going from 8th order LPA to 12th order (see Tab. 4.2). The same applies if one asks about the η_Φ-dependence of our results, where a shift of similar magnitude to higher values is observed. Thus, our results favor a transition $N \lesssim 3$ which is also found in high-order perturbative field-theory expansions [184, 188–194]. One should wonder about the reason for this discrepancy. Clearly, it gives an indication to go beyond the simple LPA truncation, including also higher derivative terms, to investigate systematic errors of the truncation.

4.6.2. Decoupled fixed point

Apart from the isotropic fixed point, the decoupled fixed point (DFP) also features an enhanced symmetry, where the theory is invariant under $Z_2 \times O(N_1) \times O(N_2)$. As for the IFP,

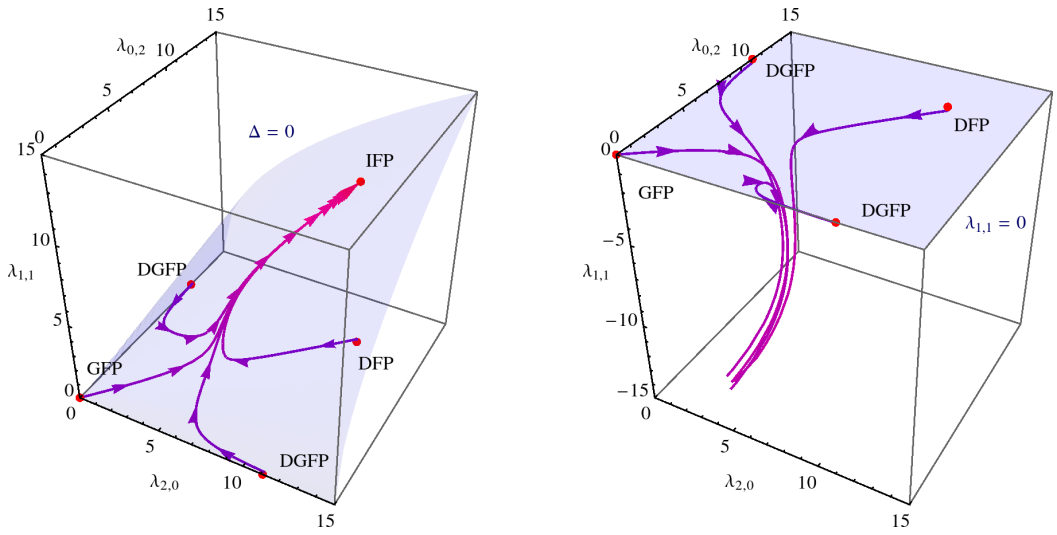

Figure 4.3.: RG flow of the quartic couplings to 4th order LPA for the $Z_2 \oplus Z_2$ scalar model. The relevant parameters are fixed to their respective critical values at the isotropic fixed point (IFP). The RG trajectories converge to the stable IFP in the infrared if the initial values are chosen within the domain of attraction (**left**). Otherwise the flow diverges (**right**) in which case one expects a first order transition. Both the $\Delta = 0$ and $\lambda_{1,1} = 0$ surfaces (highlighted in blue) define invariant subspaces of the RG flow that are protected by symmetry.

symmetry constraints simplify our discussion of its stability properties. In fact, from the fixed point potential, we see that it is the quartic perturbation $g_w \phi_1^2 \phi_2^2$ that determines the stability at the DFP. It scales as two composite energy-like operators with scaling dimensions, $(1-\alpha_1)/\nu_1$ and $(1-\alpha_2)/\nu_2$, where α_1 and α_2 correspond to the specific heat exponents in the two sectors, and ν_1, ν_2 denote the corresponding correlation length exponents.[3] From the scaling relation $\alpha_I = 2 - \nu_I d$ we obtain an exact expression for the RG scaling dimension of the quartic perturbation [196–198]:

$$y_w = \frac{\alpha_1}{2\nu_1} + \frac{\alpha_2}{2\nu_2} = \frac{1}{\nu_1} + \frac{1}{\nu_2} - d \; . \tag{4.40}$$

Thus, the stability properties of the DFP are completely determined from the critical exponents in the decoupled $O(N_1)$ and $O(N_2)$ sectors. Recall, that the two largest eigenvalues $\theta_1 = 1/\nu_1$ and $\theta_2 = 1/\nu_2$ are positive for all values of N, while the subleading exponents $\theta_4 = -\omega_1$ and $\theta_5 = -\omega_2$ are associated to the Wegner's exponents in the two separate sectors and are always negative. It is thus the third largest exponent θ_3 which decides about the stability of the DFP and we may identify $\theta_3 = y_w$ for this fixed point.

Here, we determine the five largest critical indices using the scaling relation and the $O(N)$ critical exponents from a 12th order LPA analysis including the anomalous dimension η (cf. Tab. 4.3). Our results are summarized in Tab. 4.4. They are in accordance with data cited

[3]Note, that the composite operators scale as $\langle \phi_I^2(k) \phi_I^2(-k) \rangle \sim k^{-\alpha_I/\nu_I}$ at the critical point. They correspond to the relevant part of the energy density (see, e.g., [195]).

N	ν_{fRG}	ν_{MC}	η_{fRG}	η_{MC}
1	0.637	0.63002(10)	0.044	0.03627(10)
2	0.685	0.6717(1)	0.044	0.0381(2)
3	0.731	0.7112(5)	0.041	0.0375(5)
4	0.772	0.750(2)	0.037	0.0360(3)

Table 4.3.: Critical exponents for $O(N)$-models in three dimensions in a derivative expansion to second order $\mathcal{O}(\partial^2)$ and an expansion of the effective potential to 12th order in the fields in comparison to the Monte Carlo results in Ref. [199] for $N = 1$, Ref. [200] for $N = 2$, Ref. [201] for $N = 3$ and Ref. [171]. These are values obtained by the same truncation/regularization scheme presented in this work and are employed to produce estimates for the critical exponent θ_3 which decides about the stability of the decoupled fixed point (DFP).

in [163, 167]. In particular, keeping the value $N_1 = 1$ fixed we obtain the value $N_2 \simeq 2.31$ for the stability transition, to be compared with, e.g., to $N_2 \simeq 2.17$ from Ref. [167]. For $N \gtrsim 4$ this fixed point is always stable, and we conclude that this applies also for the case $N_1 = 2$, $N_2 = 3$, relevant for high-temperature superconductors. Since the coupling between the sectors vanishes at the DFP we expect that $\Delta > 0$ (due to stability requirements). Thus, in its domain of stability we may associate a tetracritical behavior to this fixed point. The relevant stability regions for the DFP and IFP are summarized in Fig. 4.4.

We may check the quality of our truncation by computing the exponent θ_3 directly from the diagonalization of the stability matrix at the DFP and comparing the obtained value with the result from the exact scaling relation. We observe a discrepancy, yielding a shift of the stability transition of the DFP in the (N_1, N_2)-plane to a slightly smaller values, roughly of order $\mathcal{O}(0.01)$. In fact, the reason for this disagreement is clear – the scaling relation (4.40) relates critical exponents of leading order to those that are subleading, which are typically not well-resolved to lowest order $\mathcal{O}(\partial^0)$ in the derivative expansion. Thus, it is expected that going to higher orders in the derivative expansion this deviation will disappear.

4.6.3. Biconal fixed point

Apart from the fixed points that feature an enhanced symmetry we find another interacting fixed point with $O(N_1) \times O(N_2)$ symmetry as suggested by the symmetry considerations (see Sec. 4.6). In the literature this solutions is known as the biconal fixed point (BFP). It has first been discussed in Ref. [152] and was further studied in Refs. [163, 167]. To find this fixed point a truncation to 8th order LPA was used without anomalous dimensions, i.e., $\eta_1 = \eta_2 = 0$. The previous analysis of the IFP and DFP solutions was simplified due to the presence of the enhanced symmetry, or by exploiting exact scaling relations. Here, in the absence of such constraints, we need to solve for the complete set of parameters and couplings, which makes

N	N_1	N_2	$\theta_1 = 1/\nu_1$	$\theta_2 = 1/\nu_2$	$\theta_3 = y_w$	$\theta_4 = -\omega_1$	$\theta_5 = -\omega_2$
3	1	2	1.571	1.459	0.030	-0.728	-0.735
4	1	3	1.571	1.367	-0.062	-0.728	-0.748
4	2	2	1.459	1.459	-0.082	-0.735	-0.735
5	1	4	1.571	1.296	-0.133	-0.728	-0.768
5	2	3	1.459	1.367	-0.174	-0.735	-0.748

Table 4.4.: Critical exponents at the decoupled fixed point (DFP) as a function of field components N_1 and N_2 to 12th order LPA. The anomalous dimension η_1 and η_2 are included from the knowledge of the properties of the $O(N)$ vector model (data taken from Tab. 4.3), and using the exact scaling relation (4.40).

the search for fixed point solutions more demanding. The BFP is notoriously difficult to find. This is partly due to its restricted domain of stability (see Fig. 4.4). In particular, from the thin lines in Fig. 4.4 we see that this fixed point should exist and be stable only in the region $1.17 \lesssim N_2 \lesssim 1.50$, $N_1 = 1$, at the given order of the truncation. On the other hand, we see that by varying the number of field components, this fixed point traverses different regions in theory space (cf. Fig. 4.4). While for small $N_2 < 1.17$, $N_1 = 1$ it is situated in the $\Delta < 0$ region, at the stability transition $N \simeq 2.17$ (8th order LPA) it collides with the IFP and continues into the $\Delta > 0$ region. At $N_2 \simeq 1.5$, $N_1 = 1$, it merges with the DFP, which, in this order of the approximation, is the stable fixed point beyond this value. Note, that the position of the stability transition for the DFP is determined here without employing the scaling relation (4.40), by directly competing the critical indices. This yields the consistent result, that for each point in the (N_1, N_2)-plane, there is only one stable fixed point. Using the scaling relation (4.40), will typically induce a shift of the stability transition to smaller values of N_2.

In the stability region (see Fig. 4.4) the couplings at the BFP satisfy $\Delta > 0$ and – similar to the DFP – we might expect a tetracritical behavior for the phase diagram of the respective model. It is thus important to distinguish the critical scaling properties properly to compare the results for the stability regions in Fig. 4.4 with experiment or Monte Carlo simulations. Since we have used only a 8th LPA truncation without anomalous dimensions to establish the existence of this fixed point, it is necessary to extend this analysis to obtain also the scaling exponents. This is left for future work.

4.6.4. Stability regions

Let us summarize the stability properties of the fixed point solutions for the $O(N_1) \oplus O(N_2)$ model and comment on the quality of the different truncations used in our work. The stability regions are illustrated in Fig. 4.4 as a function of the field components (N_1, N_2). We observe that the stability region of the BFP is significantly enhanced when we include a nonvanishing

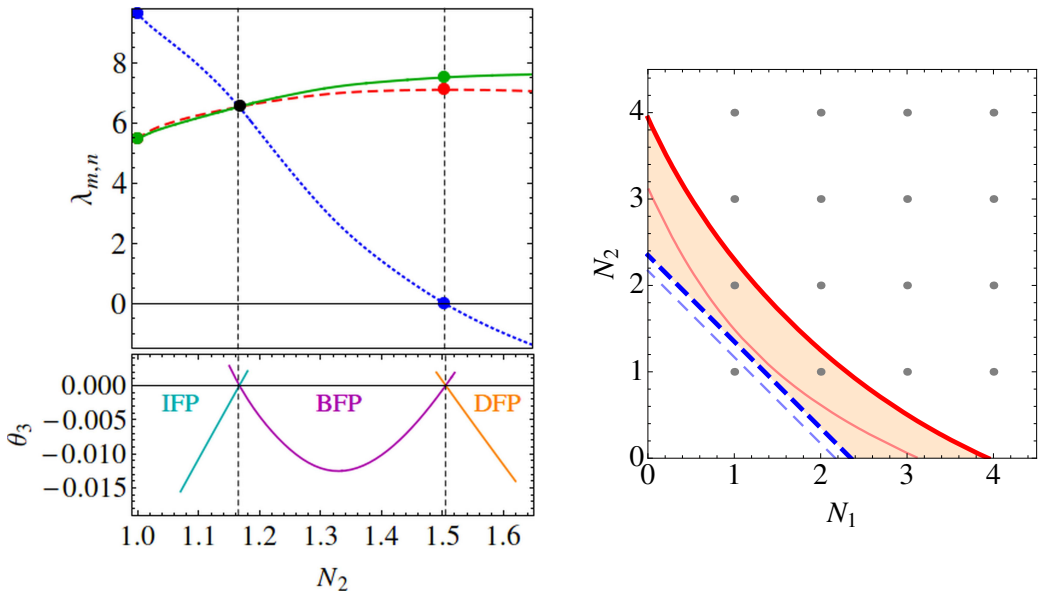

Figure 4.4.: (**Left**) Fixed point values of the quartic couplings $\lambda_{2,0}$ (green, solid line), $\lambda_{0,2}$ (red, dashed line), and $\lambda_{1,1}$ (blue, dotted line) at the biconal fixed point (BFP) as a function of field components N_2, while $N_1 = 1$. The subleading exponent θ_3 indicates the stability of the respective fixed point solutions. It is negative for the BFP in the region $1.17 \lesssim N_2 \lesssim 1.5$ indicating its stability, whereas for $N_2 \lesssim 1.17$ the isotropic fixed point (IFP) and for $N_2 \gtrsim 1.5$ the decoupled fixed point (DFP) are stable. (**Right**) Stability regions for the $O(N_1) \oplus O(N_2)$ symmetric theory. Thin lines correspond to the results from an 8th order LPA analysis, while thick lines include the effect of a scale-dependent anomalous dimension η_Φ to 12th order in LPA. The intermediate region (marked in red) indicates the stability region of the BFP. For larger values of (N_1, N_2) the DFP is always stable, while for $N \lesssim 2.32$ the IFP is the stable fixed point.

anomalous dimension η_Φ as compared to the lowest order $\mathcal{O}(\partial^0)$ LPA result. In particular, we want to emphasize that a nonvanishing anomalous dimension in fact extends the stability region in such a way that the $N = 3$ models (where a XY and Ising critical line meet) are included in this region, which is especially relevant for the discussion of anisotropic antiferromagnets in an external field [152–154]. Of course, it is clear why such a large shift occurs when we include a scale-dependent anomalous dimension in our truncation – the stability transition lines in the (N_1, N_2)-plane sensitively depend on the position where the subleading exponent θ_3 changes sign. To accurately capture the stability properties of the competing fixed points it is therefore necessary to go to higher orders in the derivative expansion to obtain quantitative results also for subleading exponents [66, 67, 69, 70].

While it is important to properly resolve the stability regions of the interacting fixed points, let us point out that the critical scaling exponents of the interacting fixed points in the $O(N_1) \oplus O(N_2)$ are very similar. Compare, e.g., the critical indices of the IFP in Tab. 4.1

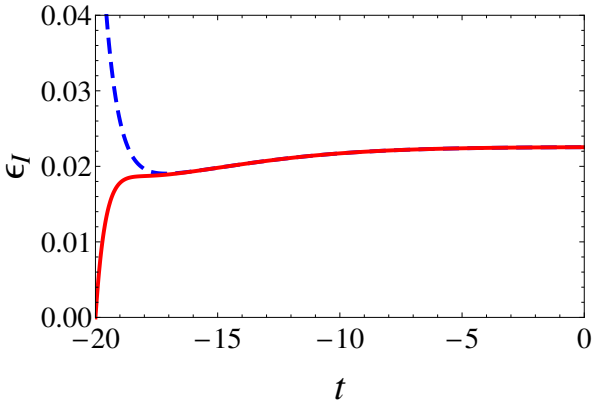

Figure 4.5.: Two dimensionless mass eigenvalues in the $Z_2 \oplus Z_2$ model as a function of scale parameter $t = \ln k/\Lambda$, on a trajectory connecting the DFP in the UV (high t) with the IFP in the IR (low t).

with those of the DFP in Tab. 4.4. Similarly, the critical exponents of the BFP are very close to those of the Heisenberg-like IFP with a difference of roughly $\mathcal{O}(0.001)$ in ν [163]. Thus, it might be very difficult in practice to associate given Monte Carlo data, or data from experiments to a particular fixed point. In light of these difficulties, it is worthwhile to look also for alternative quantities, e.g., universal amplitude ratios that might allow to distinguish the different fixed points more reliably [163].

4.7. Applications

The class of $O(N_1) \oplus O(N_2)$ models and their respective fixed point solutions have been discussed at length in the past, in particular in the context of condensed matter systems. For anisotropic antiferromagnets in a uniform magnetic field where two critical lines in the XY and Ising universality class meet ($N = 3$), our results from the LPA truncation including anomalous dimensions favor the multicritical BFP. According to the sign of $\Delta > 0$ at the fixed point, we conclude that the transition should describe a tetracritical point in the phase diagram. This is in accordance with results from high-order perturbative expansions [163] and [167, 169] and Monte Carlo simulations [171]. However, Monte Carlo data presented in Ref. [170] indicate a bicritical point which is in accordance with experimental results [202, 203]. This discrepancy is probably due to the fact that the relevant microscopic model lies outside the attraction domain of the stable BFP. However, due to the similar values of critical exponents at the biconal FP and the isotropic Heisenberg-like FP it is very hard to distinguish the two fixed points from experimental or Monte Carlo data [171].

Another model that has featured prominently, is the effective $O(5)$ symmetric theory for high-temperature superconductivity, where one has an $O(3)$ antiferromagnetic and a competing $U(1) \simeq SO(2)$ order parameter associated with the d-wave superconducting state [157, 160]. Here, our results suggest that the IFP with the enhanced $O(5)$ symmetry is not

stable, and one should rather expect that the DFP is the relevant fixed point for the model, describing a tetracritical point in the phase diagram. However, the effect of fermions seems to exclude a mixed phase as indicated by calculations of the $t-t'$ Hubbard model [204]. Typically, the investigation of these systems is quite involved, where one also needs to consider effects of doping and random impurities. A detailed discussion of these systems and their scaling properties may be found, e.g., in [163]. Finally, let us remark that the multicritical DFP is also expected to describe the critical behavior in liquid crystals with two XY order parameters ($N = 4$), at the nematic–smectic–A–smectic–C multicritical point [197].

In the previous sections, we have already commented on the possible relevance of the $O(N_1)\oplus O(N_2)$ models in the context of the low-energy properties of QCD (see Sec. 4.5). Here, we want to mention another interesting scenario for the coupled $Z_2 \oplus Z_2$ model where both fields feature a discrete Z_2 Ising-like symmetry [205]. While the emergence of massless modes from symmetry breaking is only expected from continuous symmetries this is obviously not the case by inspecting the flow of the renormalized masses in the $Z_2 \oplus Z_2$ theory, see Fig. 4.5. Here, we show a particular RG trajectory that connects the DFP in the UV with the IFP in the IR ($d = 3$). Of course, at the IFP the discrete symmetry of the model is enhanced to a continuous $O(2)$ rotational symmetry, where its breaking leads to the generation of a single massless mode, in accordance with Goldstone's theorem. A similar scenario applies to the extended class of $Z_2 \oplus Z_2 \oplus \cdots$ models where multiple Ising-like order parameters are coupled. However, the fixed point structure of these models and their RG flow can in general be very complex.

In principle such a mechanism might be invoked to generate a mass hierarchy in a system where the microscopic Lagrangian contains equal masses. If the system allows for an enhancement of the symmetry, then a spontaneous breaking of this additional symmetry in the infrared must produce a massless Goldstone mode. Small explicit symmetry breaking terms can then give a small mass to this pseudo-Goldstone mode. Compared to the other masses in the theory the pseudo-Goldstone boson mass could then remain rather small, thus producing a hierarchy.

4.8. Discussion and outlook

Here, we have presented a first analysis of the $O(N_1) \oplus O(N_2)$ symmetric models within LPA-type truncations of the functional renormalization group including anomalous dimensions. We have discussed the possible fixed points of these theories as well as their scaling properties. The largest critical exponents compare nicely with high-order field theoretic expansion at fixed dimension $d = 3$ or in $\epsilon = 4 - d$ or Monte Carlo data [163, 171, 184, 188–193, 206]. However, to capture the subleading behavior requires more sophisticated truncations where we expect in particular a change in the stability regions of the respective fixed point solutions in the (N_1, N_2) phase diagram (see Fig. 4.4). Taking into account also the field-dependence of the

renormalization factors, or going to higher orders in the derivative expansion might eventually lead to a transition from the IFP to the BFP around $N \simeq 3$ in accordance with [187]. This would be interesting, as it might explain data from experiments [202, 203] and Monte Carlo simulations [170] that has been challenging to interpret. Let us emphasize however, that to investigate physical systems of interest and to establish their phase diagram, it is necessary to solve for the complete RG flow where one should apply grid methods to capture also the nonuniversal physics.

Let us comment on possible extensions of this work. The multicritical points considered here only take into account bosonic fluctuations of the order parameters. Close to a quantum critical point also fermionic fluctuations become important. Thus, it would be interesting to consider the possible scenarios that appear when fermions are included. We have already discussed the RG flow equations for the case of spinless fermions on the honeycomb lattice in the previous chapter. In that context, the presence of fermionic fluctuations may lead to new multicritical fixed points with different scaling properties.

Finally, let us point out that the coupled scalar models considered here are typically applied to describe the multicritical behavior of low-dimensional condensed matter systems [152–156], or might be relevant to the discussion of low-energy models of QCD [207] where the presence of a nonvanishing temperature leads to dimensional reduction and a decoupling of fermionic degrees of freedom. However, it is important to remark that at $T = 0$ one may expect more complicated behavior, where the fluctuations at the multicritical point are no longer described by the two distinct order parameters. In that case, this may lead to a single continuous transition between the two distinct ordered phases [208, 209] instead of a first order transition as encountered in the context of the $O(N_1) \oplus O(N_2)$ models.

5. Critical dynamics for relaxational models close to thermal equilibrium

Dynamic properties such as transport coefficients or relaxation rates play a crucial role for a wide variety of physical systems, ranging from dynamics of ultracold atoms at nanokelvin temperatures to heavy-ion collisions at relativistic energies. Irrespective of the details of the underlying microscopic dynamics, the systems can be grouped into different dynamic universality classes close to a critical point. This classification extends the known static universality classes that are essentially determined by the dimensionality and symmetries of the system to include the presence of additional conservation laws. The corresponding conserved quantities lead to a strong slowing down of the system and influence the type of dynamics that one may expect following a small initial perturbation of the system in the equilibrium state.

The simplest scenario for such a situation is the direct relaxation from an initially prepared state towards equilibrium described phenomenologically by a stochastic Langevin equation. Such an approach corresponds to a mesoscopic description of the dynamics where the noise term models the thermal fluctuations close to equilibrium. Following the standard classification scheme [39] the universality class of Model A is characterized by the purely relaxational dynamics of a nonconserved N-component order parameter. This model has been much studied in the literature [41, 210, 211] where it was first applied to describe the anomalous attenuation of sound in ^{4}He near the λ-point [39, 212] and is usually considered to describe the critical dynamics of uniaxial magnetic systems [40, 210], e.g., the homogeneous Ising antiferromagnet FeF_2 [213] with sufficient nonconservation of magnetization. The presence of strong fluctuations at the critical point leads to the phenomenon of critical slowing down, with the critical dispersion $\omega \sim k^z$, characterized by the dynamic scaling exponent $z = 2 + c\eta$ in the case of Model A [39, 210]. The dynamic exponent expressed in terms of the anomalous dimension η, and an additional coefficient c which depends both on the spatial dimension d and the number of field components N of the model [214] and bears no relation to static exponents. In that respect, Model A is quite different compared to the other dynamic universality classes that usually exhibit an exact scaling relation between the dynamic and static scaling exponents.[1]

[1] The other notable exception being Model H [39, 215] at the gas-liquid critical point, where the dynamics of the nonconserved order parameter couples to the heat and momentum current.

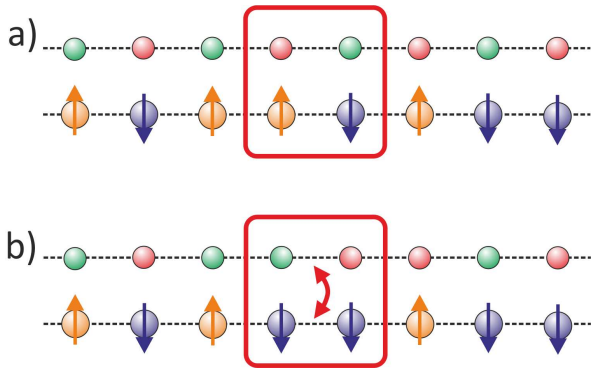

Figure 5.1.: Illustration of dynamics in the kinetic Ising model with an additional coupling to a conserved density. (**a**) The spins (different orientations, orange/purple) couple to a conserved density (occupied or vacant lattice sites, red/green) via the mode-coupling. (**b**) The magnetization is not conserved and single spin-flips are allowed by the dynamics, while the conserved density is continuously distributed on the lattice.

Typically, the presence of conservation laws strongly affects the dynamic critical scaling properties, further slowing down the system at criticality where excitations cannot be removed by a local dissipation process but are transported over a wide range of scales [216, 217]. In fact, the presence of slow modes coupling to the order parameter may lead to quite complex dynamics where the system persists in a nonequilibrium state even asymptotically for large times [218, 219]. One example of such a system in the family of the relaxational models is Model C [39]. It is characterized in terms of an N-component order parameter that exhibits relaxational dynamics and is coupled to a conserved density. In contrast to Model A, the dynamic critical behavior features a strong scaling region in the (N, d) phase diagram, where the dynamic critical exponent $z = 2 + \alpha/\nu$ is completely determined in terms of the specific heat exponent α and correlation length exponent ν [40, 220, 221]. Thus, there exists an intimate relation between the dynamic and static scaling properties which appears quite generically for systems with conservation laws. Typically, this model is discussed in the context of ferromagnetic systems in the presence of large anisotropy [222] where an appropriate microscopic description is given by the kinetic Ising model ($N = 1$) that couples the spins to an additional conserved density. In this model the Z_2 spins follow Glauber kinetics where a single-spin flip is allowed for a given time step, while the conserved charge can only be distributed on the lattice (Fig. 5.1). The importance of this model is based on the observation that the critical dynamics is described by strong scaling, i.e., $z = 2+\alpha/\nu$. Model C has a wide range of application. It has been considered to describe critical dynamics of mobile impurities [223, 224], structural phase transitions [225–227], long-wavelength fluctuations near the QCD critical point [228, 229], and also in the context of out-of-equilibrium dynamics [218, 230].

Despite its importance and a long history of discussions [40, 42, 43, 46, 220, 221, 231], parts of the phase diagram for the dynamic critical behavior of Model C are still controversial. The

reason for this uncertainty is that the physics is nonperturbative and only few theoretical approaches apply. Previous calculations have mainly relied on the ϵ-expansion in $d = 4 - \epsilon$ dimensions, while direct numerical simulations [232] still represent an exception. The existence of the so-called weak, strong, and decoupled scaling regions is undebated. However, there have been conflicting claims on quantitative properties and even on the possible existence of another distinctive region in the phase diagram of Model C. Earlier results [40, 42, 46, 220, 221] found evidence for such a region, however, due to a multiplicative logarithmic correction it was unclear whether the calculated dynamic scaling persists to higher orders in the ϵ-expansion. Other results to second order showed that the field-theoretic β-function for the ratio of kinetic coefficients exhibits an essential singularity in this region [42]. It was speculated that this property might even restore critical behavior with a dynamic scaling exponent identical to the strong scaling $z = 2 + \alpha/\nu$. However, in more recent work [43, 231] this peculiar region was discarded as an artifact of the ϵ-expansion, which was argued to break down in the region where $2 < N < 4$ for dimensions close to $d = 4$.

Here, we compute the (N, d) phase diagram for the dynamic critical behavior of Model C using the functional renormalization group. We establish an anomalous diffusion phase with new scaling properties: It satisfies weak scaling for $2 < N < 4$ close to $d = 4$, however, the conserved density diffuses only on asymptotic times. We compute the scaling exponents characterizing the different phases as well as subleading exponents to determine their stability properties. This presents the first determination of the dynamic critical properties of relaxational models in the framework of the functional RG including the dynamics of conserved quantities. Such an analysis can be extended to investigate also other dynamic universality classes, or even to connect the dynamic low-energy properties with the microscopic physics of relativistic theories such as QCD.

5.1. Mesoscopic dynamics

The effective dynamics for Model C is governed by the set of Langevin-type stochastic equations

$$\frac{\partial}{\partial t}\varphi_a(x,t) = -\Omega \frac{\delta \mathcal{H}[\varphi,\varepsilon]}{\delta \varphi_a(x,t)} + \eta_a(x,t) \,, \tag{5.1}$$

$$\frac{\partial}{\partial t}\varepsilon(x,t) = \Omega_\varepsilon \nabla^2 \frac{\delta \mathcal{H}[\varphi,\varepsilon]}{\delta \varepsilon(x,t)} + \zeta(x,t) \,, \tag{5.2}$$

where $a = 1, \ldots, N$ labels the field components of the order parameter field φ_a, and ε corresponds to the conserved density which satisfies an equation of diffusion-type. The kinetic coefficients Ω and Ω_ε denote the relaxation rate and diffusion rate, respectively. The functional $\mathcal{H}$ that essentially defines the dynamics depends both on the order parameter as well as on the conserved density, and is given by

$$\mathcal{H} = \int d^d x \left\{ \frac{1}{2} (\nabla\varphi)^2 + \frac{1}{2}\bar{m}^2\varphi^2 + 3\frac{\bar{\lambda}}{4!}\left(\varphi^2\right)^2 + \frac{1}{2}\varepsilon^2 + \frac{1}{2}\bar{\gamma}\varepsilon\varphi^2 \right\} . \tag{5.3}$$

It couples the conserved density to the composite operator φ^2 and defines the stationary state configuration for the dynamics. The stochastic driving terms η_a and ζ are assumed to be centered and Gaussian

$$\begin{aligned} \big\langle \eta_a(x,t)\eta_b(x',t')\big\rangle &= 2\Omega k_B T\, \delta_{ab}\delta(x-x')\delta(t-t')\ , & (5.4)\\ \big\langle \zeta(x,t)\zeta(x',t')\big\rangle &= -2\Omega_\varepsilon k_B T\nabla^2\delta(x-x')\delta(t-t')\ , & (5.5)\end{aligned}$$

where the temperature sets the scale for the amplitude of the stochastic noise. Thus, it satisfies a fluctuation-dissipation theorem (where we will set $k_BT = 1$ in the following), see Sec. 5.1.1.

To investigate this class of systems we construct the generating functional for static and dynamic correlation functions in terms of a functional integral formalism for stochastic dynamics [44–46, 233, 234]. We illustrate the construction of the field-theoretical classical action for Model C, as it will serve as the appropriate starting point to construct low-energy effective models. Also, we discuss some of the subtleties that may arise in the functional approach to classical statistical dynamics.

We introduce the partition function

$$Z \sim \int [d\varphi]\,[d\varepsilon]\,[d\eta]\,[d\zeta]\ \delta[\varphi-\varphi_\eta]\,\delta[\varepsilon-\varepsilon_\eta]\ \exp\left\{-\frac{1}{4}\int_{[t_0,\infty)} d^dx\,dt\ \left(\frac{1}{\Omega}\eta^2+\frac{1}{\Omega_\varepsilon}\zeta(-\nabla^{-2})\zeta\right)\right\}\ , \tag{5.6}$$

which is given by the trace over all possible states of the system, i.e., all field-force configurations for some given set of initial conditions. Here, φ_η and ε_ζ denote field-configurations that define solutions to the mesoscopic dynamics introduced above, while the information about the initial conditions is taken to reside in the functional measure:

$$\int [d\varphi]\,[d\varepsilon] = \left(\int \prod_{x,t\in[t_0,\infty)} d\varphi(x,t)\,d\varepsilon(x,t)\right)\ P_\varphi\big[\varphi(x,t_0)-\varphi_0\big]\,P_\varepsilon\big[\varepsilon(x,t_0)-\varepsilon_0\big]\ , \tag{5.7}$$

where an averaging over initial conditions is applied with the respective probability distribution functionals $P_{\varphi/\varepsilon}[\cdots]$. The δ-functionals in (5.6) impose the dynamics, while the integration over the noise generates small perturbations around the classical dynamics. To integrate out the noise, we perform the change of variables

$$\delta[\varphi-\varphi_\eta] = \delta\left[\frac{\partial}{\partial t}\varphi+\Omega\frac{\delta\mathcal{H}}{\delta\varphi}-\eta\right]\det\left[\frac{\delta\eta}{\delta\varphi}\right]\ , \tag{5.8}$$

where $\det[\delta\eta/\delta\varphi]$ is the Jacobian from the change of variables $\eta\to\phi$. Let us forget about the functional determinant for a moment, and consider what happens to the transformed δ-functional. We may use the formal decomposition

$$\delta\left[\frac{\partial}{\partial t}\varphi+\Omega\frac{\delta\mathcal{H}}{\delta\varphi}-\eta\right]\ \sim\ \int[d\tilde\varphi]\ \exp\left\{-\int_{[t_0,\infty)} d^dx\,dt\,\tilde\varphi_a\left(\frac{\partial}{\partial t}\varphi_a+\Omega\frac{\delta\mathcal{H}}{\delta\varphi_a}-\eta_a\right)\right\}\ , \tag{5.9}$$

where we have introduced the Martin-Siggia-Rose (MSR) response field $\tilde\varphi$ [44], with an appropriate measure $\int[d\tilde\varphi]$. We may proceed similarly with the conserved density and introduce a

Figure 5.2.: Tadpole diagrams contributing at one-loop in perturbation theory.

conjugate $\tilde{\varepsilon}$-field. Then, after performing the integration over the stochastic noise, we obtain the Martin-Siggia-Rose/Janssen-de Dominicis functional integral [44–46]:

$$Z \sim \int [d\tilde{\varphi}]\,[d\varphi]\,[d\tilde{\varepsilon}]\,[d\varepsilon]\,e^{-S}\ , \tag{5.10}$$

where, after an appropriate rescaling of the fields $\tilde{\varphi} \to \Omega^{-1}\tilde{\varphi}$ and $\tilde{\varepsilon} \to \Omega_{\varepsilon}^{-1}\tilde{\varepsilon}$, we obtain the field-theoretical classical action for Model C:

$$S = \int_{[t_0,\infty)} d^dx\,dt \left\{ \tilde{\varphi}_a \left(\Omega^{-1}\frac{\partial}{\partial t}\varphi_a + \frac{\delta \mathcal{H}}{\delta \varphi_a} \right) - \Omega^{-1}\,\tilde{\varphi}^2 + \tilde{\varepsilon} \left(\Omega_{\varepsilon}^{-1}\frac{\partial}{\partial t}\varepsilon - \nabla^2 \frac{\delta \mathcal{H}}{\delta \varepsilon} \right) + \Omega_{\varepsilon}^{-1}\,\tilde{\varepsilon}\nabla^2\tilde{\varepsilon} \right\}\ . \tag{5.11}$$

Note, that we use a slightly different convention for the conjugate fields $\tilde{\varphi}$ and $\tilde{\varepsilon}$, where one usually considers the Wick-rotated fields on the imaginary axis, i.e., $\tilde{\varphi} \to i\tilde{\varphi}$ and $\tilde{\varepsilon} \to i\tilde{\varepsilon}$.

Let us now comment on the role of the functional determinant that we have neglected so far. In fact, it plays a subtle role and controls the contributions from tadpole diagrams that are in principle allowed by the dynamics of the vertices in the microscopic action (corresponding perturbative one-loop diagrams of the microscopic action are shown in Fig. 5.2). The propagators in the closed loops corresponds to the retarded/advanced propagators in the fields $\tilde{\varphi}$ and φ. We, see that a nonvanishing contribution from these diagrams would lead to additional terms in the effective potential that are not present in the classical action (5.11). In fact, if we simply neglect the functional determinant such diagrams must be taken into account explicitly in perturbation theory, or in the *ansatz* for the scale-dependent effective action for dynamic correlation functions. However, writing the determinant in the following form

$$\det\left[\left(\frac{\partial}{\partial t} + \frac{\delta^2 \mathcal{H}}{\delta\varphi_a(t)\varphi_b(t')}\right)\delta(t-t')\right] \ \sim\ \exp\left\{\theta(0)\int_{[t_0,\infty)} d^dx\,dt\,\frac{\delta^2\mathcal{H}}{\delta\varphi_a(t,x)\varphi_b(t,x)}\delta_{ab}\right\}\ , \tag{5.12}$$

we see that it defines an additional contribution to the classical action that is proportional to the quantity $\theta(0)$. The same type of contributions appear if the one-loop tadpole diagrams in Fig. 5.2 are evaluated. In fact, the functional determinant (5.12) exactly cancels the tadpole diagrams that are obtained from the interaction terms in the original action [235].

Let us point out another interpretation of this problem. It relates to the coefficient $\theta(0)$ in (5.12). The fact that such a coefficient must appear comes from the definition of the causal propagation forward in time, where the free propagator $\partial G^{(0)}(t-t')/\partial t = \delta(t-t')$ is chosen as $G^{(0)}(t-t') = \theta(t-t')$, and from the evaluation of the trace in the functional determinant, which yields $\sim \theta(0)$. As it stands it is an ill-defined quantity. Only a given discretization

for the action (5.11), provides an unambiguous definition of dynamics, where $\theta(0)$ is fixed to a specified value [236, 237]. For the Itō backward-time prescription $\theta(0)$ is exactly zero [235, 238]. In that case of course, we do not have to worry about additional contributions from the diagrams shown in Fig. 5.2. In fact, we will drop the functional determinant in the following, thereby implicitly assuming the Itō description holds for the discretized dynamics. This is also reflected in the RG flow equations that are given in Sec. 5.4. No closed loops with a single retarded or advanced propagator appear. We want to emphasize that this problem generically appears for first-order differential equations and is absent for relativistic dynamics, where the time-ordered propagator describes both a forward and backward-propagation in time.

5.1.1. Fluctuation dissipation theorem and time-reversal symmetry

The coupled set of stochastic equations of motion (5.1) and (5.2) describe the relaxation from some initial state which one has to specify to completely define the dynamics. However, one might expect that the system generally relaxes to the equilibrium state at asymptotic times, where it loses memory of the initial conditions. Formally, this may be achieved by sending the initial time to $t_0 \to -\infty$ and assuming the existence of a fluctuation-dissipation relation (FDR). Thus, on the level of the microscopic action, we extend the time integration to infinity, while the FDR is imposed directly by the choice of the coefficients for quadratic contributions in the auxiliary fields, i.e., $\Omega^{-1}\tilde{\varphi}^2$ and $\Omega_\varepsilon^{-1}\tilde{\varepsilon}\nabla^2\tilde{\varepsilon}$. The quadratic operators characterize the type of fluctuations around the saddle-point solution defined by the classical dynamics and the scale of these fluctuations is set by the temperature. In fact, we see that on the level of the action this is related to the presence of an additional time-reversal symmetry (TRS), i.e., $t \to -t$, where $\varphi_a \to \varphi_a$ and $\varepsilon \to \varepsilon$, while the auxiliary fields transform as [239]:

$$\tilde{\varphi}_a \to \tilde{\varphi}_a - \frac{\partial}{\partial t}\varphi_a \ , \quad \tilde{\varepsilon} \to \tilde{\varepsilon} + \nabla^{-2}\frac{\partial}{\partial t}\varepsilon \ . \tag{5.13}$$

We may check that this leads to a fluctuation-dissipation relation by examining the transformation properties of the connected two-point correlation functions under this symmetry:

$$\left\langle \varphi_a(t)\tilde{\varphi}_b(t')\right\rangle \to \left\langle \varphi_a(t')\tilde{\varphi}_b(t)\right\rangle - \frac{\partial}{\partial t}\left\langle \varphi_a(t')\varphi_b(t)\right\rangle \ . \tag{5.14}$$

Thus, using the property $\langle\varphi(t)\tilde{\varphi}(t')\rangle \sim \theta(t-t')$, the response function can be written in terms of the time-derivative of the statistical correlation functions of the φ-field

$$\left\langle \varphi_a(t)\tilde{\varphi}_b(t')\right\rangle = -\theta(t-t')\frac{\partial}{\partial t}\left\langle \varphi_a(t)\varphi_b(t')\right\rangle \ . \tag{5.15}$$

This also makes the role of the auxiliary field clear – it models the infinitesimal fluctuations that are put into the system by the stochastic noise.

A similar relation hold for the response function of ε-field, as well as for the mixed two-point

functions:

$$\left\langle \varepsilon(t)\tilde{\varepsilon}(t')\right\rangle = \nabla^{-2}\theta(t-t')\frac{\partial}{\partial t}\left\langle \varepsilon(t)\varepsilon(t')\right\rangle \ , \tag{5.16}$$

$$\left\langle \varepsilon(t)\tilde{\varphi}_a(t')\right\rangle = -\theta(t-t')\frac{\partial}{\partial t}\left\langle \varepsilon(t)\varphi_a(t')\right\rangle \ , \tag{5.17}$$

$$\left\langle \varphi_a(t)\tilde{\varepsilon}(t')\right\rangle = \nabla^{-2}\theta(t-t')\frac{\partial}{\partial t}\left\langle \varphi_a(t)\varepsilon(t')\right\rangle \ , \tag{5.18}$$

Time-reversal symmetry provides a strong constraint for the dynamics – it reduces the number of independent correlation functions. Breaking this symmetry, e.g., by evolving the system from a generic initial state at finite time may, in the presence of slow modes, keep the system in a nonequilibrium state for asymptotic times [218, 219, 240]. Here, we will keep this symmetry and ask about the dynamic critical properties of the system close to equilibrium.

5.2. Low-energy effective dynamics

To investigate the low-energy effective dynamics we use the following truncation for the scale-dependent effective action

$$\begin{aligned}\Gamma_k = \int d^dx\, dt \Big\{ &\tilde{\phi}_a\left(\Omega_k^{-1}\frac{\partial}{\partial t} - Z_k\nabla^2\right)\phi_a + \tilde{\phi}_a\frac{\partial U_k}{\partial \phi_a} - \Omega_k^{-1}\tilde{\phi}^2 \\ &+ \tilde{\mathcal{E}}\left(\Omega_{\mathcal{E},k}^{-1}\frac{\partial}{\partial t} - Z_{\mathcal{E},k}\nabla^2\right)\mathcal{E} - \tilde{\mathcal{E}}\nabla^2\frac{\partial U_k}{\partial \mathcal{E}} + \Omega_{\mathcal{E},k}^{-1}\tilde{\mathcal{E}}\nabla^2\tilde{\mathcal{E}}\Big\} \ ,\end{aligned} \tag{5.19}$$

which defines the generating functional of one-particle irreducible static and dynamic correlation functions, and depends on the field expectation values $\phi_a = \langle\varphi_a\rangle$, $\mathcal{E} = \langle\varepsilon\rangle$, as well as their corresponding response fields. At the scale k the theory is characterized in terms of the kinetic coefficients Ω_k and $\Omega_{\mathcal{E},k}$, the renormalization functions Z_k and $Z_{\mathcal{E},k}$, and the derivatives of the effective potential $U_k(\phi,\mathcal{E})$. Eq. (5.19) provides a truncation to leading order in the derivative expansion, where we take the renormalization coefficients to be scale-dependent but neglect their field-dependence, i.e., $\partial Z_k/\partial k \neq 0$ and $\partial\Omega_k/\partial k \neq 0$, and similarly in the $\mathcal{E}$-sector. This provides a first approximation to derive the dynamic critical scaling properties of the $O(N)$ model coupled to a conserved density. Of course, the quality of this truncation is largely determined by the type of field expansion that is used for the effective potential. Thus, let us comment on the type of truncations that we will consider in the following.

Here, we use a series expansion in an appropriate basis of field operators $\mathcal{O}_m(\phi)$ and $\mathcal{O}_n(\mathcal{E})$, given by

$$U(\phi,\mathcal{E}) = \sum \bar{g}_{m,n}\mathcal{O}_m(\phi)\mathcal{O}_n(\mathcal{E}) \ , \tag{5.20}$$

where $\bar{g}_{m,n}$ denote the generalized bare couplings, defined at the expansion point of the effective action. We drop the k-index in the following to ease the notation. The conserved density $\mathcal{E}$ couples to the composite operator ϕ^2 and we assume a linear coupling $\sim \bar{\gamma}\mathcal{E}\phi^2/2$. Such an *ansatz* yields a momentum-independent interaction of the two sectors in Eq. (5.19) via $\tilde{\phi}_a\partial U/\partial\phi_a = \bar{\gamma}\mathcal{E}\tilde{\phi}_a\phi_a$, as well as a mixing term $\tilde{\mathcal{E}}\nabla^2\partial U/\partial\mathcal{E} = \bar{\gamma}\tilde{\mathcal{E}}\nabla^2\phi^2/2$ which carries a

momentum-dependence. The same coupling $\bar{\gamma}$ parametrizes two different types of interactions and this strongly constrains the dynamics for this model as we will see in the following. We expect that such a truncated series expansion will provide a reasonable approximation to establish the static and dynamic critical scaling properties of Model C.

5.3. Propagators and mass spectrum

The dynamics of the theory at the expansion point of the scale-dependent effective action is characterized in terms of the second functional derivatives of the effective action as well as higher n-point functions $\Gamma^{(n)}$. From the *ansatz* (5.19) we obtain:

$$\left(\Gamma^{(2)}_{\tilde{\phi}\phi}\right)_{ab}(q,\omega) = \left(-i\Omega^{-1}\omega + Zq^2\right)\delta_{ab} + \frac{\partial^2 U}{\partial\phi_a\partial\phi_b} \ , \tag{5.21}$$

$$\Gamma^{(2)}_{\tilde{\mathcal{E}}\mathcal{E}}(q,\omega) = -i\Omega^{-1}_{\mathcal{E}}\omega + Z_{\mathcal{E}}q^2 \ , \tag{5.22}$$

$$\left(\Gamma^{(2)}_{\phi\tilde{\mathcal{E}}}\right)_{a}(q,\omega) = q^2\frac{\partial^2 U}{\partial\phi_a\partial\mathcal{E}} \ , \tag{5.23}$$

$$\left(\Gamma^{(2)}_{\mathcal{E}\tilde{\phi}}\right)_{a}(q,\omega) = \frac{\partial^2 U}{\partial\phi_a\partial\mathcal{E}} \ , \tag{5.24}$$

$$\left(\Gamma^{(2)}_{\tilde{\phi}\tilde{\phi}}\right)_{ab}(q,\omega) = -2\Omega^{-1}\delta_{ab} \ , \tag{5.25}$$

$$\Gamma^{(2)}_{\tilde{\mathcal{E}}\tilde{\mathcal{E}}}(q,\omega) = -2\Omega^{-1}_{\mathcal{E}}q^2 \ , \tag{5.26}$$

while the remaining two-point functions vanish identically, i.e., $\Gamma^{(2)}_{\phi\phi} = \Gamma^{(2)}_{\mathcal{E}\mathcal{E}} = \Gamma^{(2)}_{\mathcal{E}\phi} = \Gamma^{(2)}_{\phi\mathcal{E}} = \Gamma^{(2)}_{\tilde{\mathcal{E}}\tilde{\phi}} = \Gamma^{(2)}_{\tilde{\phi}\tilde{\mathcal{E}}} = 0$. Note, that the two-point functions with the two derivatives interchanged are related to each other by complex conjugation, e.g., $\Gamma^{(2)}_{\phi\tilde{\phi}} = \left(\Gamma^{(2)}_{\tilde{\phi}\phi}\right)^*$.

All information about the spectrum of the theory resides solely in the ϕ-sector. Therefore, we define the mass matrix as the momentum-independent part of the two-point function $\Gamma^{(2)}_{\phi\tilde{\phi}}$ in the ϕ-sector only, i.e. $(\bar{M}^2)_{ab} = \partial^2 U/(\partial\phi_a\partial\phi_b)$. To evaluate its form, we write the potential in terms of the quadratic invariant $\bar{\rho} = \phi^2/2$, and consider a field configuration that is rotated in the one-directions, i.e., $\phi_a = \|\phi\|\delta_{a1}$, exploiting the $O(N)$ rotational symmetry of the theory. We obtain:

$$\left(\bar{M}^2\right)_{ab} = \frac{\partial U}{\partial\bar{\rho}}\delta_{ab} + 2\bar{\rho}\frac{\partial^2 U}{\partial\bar{\rho}^2}\delta_{a1}\delta_{b1} \ . \tag{5.27}$$

Its eigenvalues are easily determined, and we have $N-1$ degenerate masses $\bar{M}^2_0 = \partial U/\partial\bar{\rho}$ and one eigenvalue $\bar{M}^2_R = \partial U/\partial\bar{\rho} + 2\bar{\rho}\partial^2 U/\partial\bar{\rho}^2$. We emphasize that the mass matrix is defined to carry a field dependence. Only, after deriving the full set of flow equations for the n-point functions $\Gamma^{(n)}$, do we evaluate the masses at the physical point, defined by the field configuration minimizing the effective potential.

In principle, we could consider similar models with competing order as in the previous section, where both field expectation values are nonvanishing [168, 241, 242]. However, here we are interested in the dynamic critical properties at the Wilson-Fisher fixed point and

we consider the theory in the symmetry broken phase, where only the scale-dependent field expectation value $\bar{\rho}_0 \neq 0$ is nonvanishing and $\mathcal{E} = 0$. For that purpose, we use an expansion of the potential to 4th order in the fields:

$$U(\phi, \mathcal{E}) = \frac{\bar{\lambda}}{2} \left(\bar{\rho} - \bar{\rho}_0\right)^2 + \bar{\gamma}\mathcal{E} \left(\bar{\rho} - \bar{\rho}_0\right) \ , \tag{5.28}$$

where the physical masses are evaluated to:

$$\bar{M}_0^2 = \bar{m}_0^2 = 0 \ , \qquad \bar{M}_R^2 = \bar{m}_R^2 = 2\bar{\rho}_0\bar{\lambda} \ . \tag{5.29}$$

Together with the second functional derivatives of the effective action, the mass spectrum defines the propagators of the theory. Here, we give the propagators and vertices for the theory (5.19) that we use later on to evaluate the diagrams that contribute to the RG flow. In particular, we discuss the two different scenarios, where the coupling between the sectors is zero, and where it is nonvanishing:

- Let us first consider the case where the coupling $\bar{\gamma}$ is zero. The regularized retarded propagator in the ϕ-sector is given by

$$G_{\phi\tilde{\phi}}(q, \omega) = \left(-i\Omega^{-1}\omega + Zq^2 + R_\phi(q, \omega) + \bar{M}^2\right)^{-1} \ , \tag{5.30}$$

  where the mass matrix is defined in (5.27) and for now the regulator function $R_\phi(q, \omega)$ is completely arbitrary, assuming only a frequency and momentum dependence. Later, when we derive the renormalization group equations we will specify its form. In the $\mathcal{E}$-sector the retarded propagator is evaluated to

$$G_{\mathcal{E}\tilde{\mathcal{E}}}(q, \omega) = \left(-i\Omega_{\mathcal{E}}^{-1}\omega + Z_{\mathcal{E}}q^2 + R_{\mathcal{E}}(q, \omega)\right)^{-1} \ , \tag{5.31}$$

  where $R_{\mathcal{E}}(q, \omega)$ defines the corresponding regulator function. The advanced propagators have a similar form and are obtained by simple complex conjugation, e.g., $G_{\tilde{\phi}\phi} = \left(G_{\phi\tilde{\phi}}\right)^*$, while the statistical correlation functions are defined by the fluctuation-dissipation relation ($k_B T = 1$):[2]

$$G_{\phi\phi}(q, \omega) = \frac{2}{\omega} \operatorname{Im} G_{\phi\tilde{\phi}}(q, \omega) \ , \tag{5.33}$$

$$G_{\mathcal{E}\mathcal{E}}(q, \omega) = \frac{2}{\omega} q^2 \operatorname{Im} G_{\mathcal{E}\tilde{\mathcal{E}}}(q, \omega) \ . \tag{5.34}$$

  Eqs. (5.30) – (5.34) are the only nonvanishing propagators in the decoupled case. In particular, there are no nondiagonal entries in the matrix propagator that mix the two sectors.

[2] In fact, this follows immediately from (5.15), where by $G_{\phi\phi}(t-t') = \langle\varphi(t)\varphi(t')\rangle$ and $G_{\phi\tilde{\phi}}(t-t') = \langle\varphi(t)\tilde{\varphi}(t')\rangle$, we obtain:

$$2i \operatorname{Im} G_{\phi\tilde{\phi}}(t-t') = \langle\varphi(t)\tilde{\varphi}(t')\rangle - \langle\tilde{\varphi}(t')\varphi(t)\rangle \underset{(5.15)}{=} -\frac{\partial}{\partial t}\langle\varphi(t)\varphi(t')\rangle = -\frac{\partial}{\partial t} G_{\phi\phi}(t-t') \ , \tag{5.32}$$

and thereby (5.33) in the frequency/momentum representation. Similarly we may derive equivalent relations for the remaining two-point functions.

- In the case where the coupling is nonvanishing, i.e. $\bar{\gamma} \neq 0$, the propagators assume a more complicated form. In the ϕ-sector we must distinguish the propagator for the radial and massless modes:

$$G_{\phi\tilde{\phi}}(q,\omega) = \begin{cases} \left(-i\Omega^{-1}\omega + Zq^2 + R_\phi(q,\omega) + \bar{M}_R^2 - \frac{q^2\left(\partial^2 U/(\partial\phi\partial\mathcal{E})\right)^2}{-i\Omega_\mathcal{E}^{-1}\omega + Z_\mathcal{E} q^2 + R_\mathcal{E}(q,\omega)} \right)^{-1} & \text{(radial)} \ , \\ \left(-i\Omega^{-1}\omega + Zq^2 + R_\phi(q,\omega) + \bar{M}_0^2 \right)^{-1} & \text{(massless)} \ . \end{cases} \tag{5.35}$$

In the $\mathcal{E}$-sector, we have

$$G_{\mathcal{E}\tilde{\mathcal{E}}}(q,\omega) = \left(-i\Omega_\mathcal{E}^{-1}\omega + Z_\mathcal{E} q^2 + R_\mathcal{E}(q,\omega) - \frac{q^2\left(\partial^2 U/(\partial\phi\partial\mathcal{E})\right)^2}{-i\Omega^{-1}\omega + Zq^2 + R_\phi(q,\omega) + \bar{M}_R^2} \right)^{-1} . \tag{5.36}$$

Furthermore, the presence of the nonzero coupling leads to the mixed propagators:

$$\begin{aligned} G_{\mathcal{E}\tilde{\phi}}(q,\omega) &= \frac{\bar{\gamma} q^2 \phi(0)}{\Omega} \Big[\left(-i\Omega^{-1}\omega + Zq^2 + R_\phi(q,\omega) + \bar{M}_R^2 \right) \left(-i\Omega_\mathcal{E}^{-1}\omega + Z_\mathcal{E} q^2 + R_\mathcal{E}(q,\omega) \right) \\ &\quad - q^2 \left(\partial^2 U/(\partial\phi\partial\mathcal{E}) \right)^2 \Big]^{-1} , \end{aligned} \tag{5.37}$$

and

$$\begin{aligned} G_{\phi\tilde{\mathcal{E}}}(q,\omega) &= \frac{\bar{\gamma} q^2 \phi(0)}{\Omega_\mathcal{E}} \Big[\left(-i\Omega^{-1}\omega + Zq^2 + R_\phi(q,\omega) + \bar{M}_R^2 \right) \left(-i\Omega_\mathcal{E}^{-1}\omega + Z_\mathcal{E} q^2 + R_\mathcal{E}(q,\omega) \right) \\ &\quad - q^2 \left(\partial^2 U/(\partial\phi\partial\mathcal{E}) \right)^2 \Big]^{-1} . \end{aligned} \tag{5.38}$$

The remaining nonvanishing propagators can be expressed in terms of the retarded and advanced propagators by virtue of the fluctuation dissipation theorem. This yields the statistical correlation functions:

$$G_{\phi\phi}(q,\omega) = \frac{2}{\omega} \operatorname{Im} G_{\phi\tilde{\phi}}(q,\omega) \ , \tag{5.39}$$

$$G_{\mathcal{E}\mathcal{E}}(q,\omega) = \frac{2}{\omega} q^2 \operatorname{Im} G_{\mathcal{E}\tilde{\mathcal{E}}}(q,\omega) \ , \tag{5.40}$$

$$G_{\phi\mathcal{E}}(q,\omega) = \frac{2}{\omega} \operatorname{Im} G_{\phi\tilde{\mathcal{E}}}(q,\omega) \ , \tag{5.41}$$

$$G_{\mathcal{E}\phi}(q,\omega) = \frac{2}{\omega} q^2 \operatorname{Im} G_{\mathcal{E}\tilde{\phi}}(q,\omega) \ . \tag{5.42}$$

Let us point out, that the propagators in the $\mathcal{E}$-sector, or the mixed propagators only couple to the radial part of the ϕ-sector. This is evident from the structure factors where, e.g., the mixed propagators have only a nonvanishing component in the 1-direction.

We use the following diagrammatic rules for the retarded and statistical propagators:

$G_{\phi\phi}(q,\omega) =$ 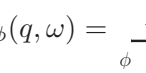

$G_{\phi\tilde{\phi}}(q,\omega) =$ 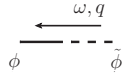

etc. (5.43)

and similarly for the propagators in the $\mathcal{E}$-sector, as well as the mixed propagators. The advanced propagators are written in terms of the same diagrammatic expression however, with

both the frequency and momentum reversed, since $G_{\tilde{\phi}\phi}(q,\omega) = \big(G_{\phi\tilde{\phi}}(q,\omega)\big)^* = G_{\phi\tilde{\phi}}(-q,-\omega)$, assuming that the effective action is real. The statistical correlation function is defined as the imaginary part of the retarded propagator and is therefore real by construction, i.e., $G_{\phi\phi}(q,\omega) = G_{\phi\phi}(-q,-\omega)$.

The nonvanishing three-vertices $\Gamma^{(3)}$ take the following form:

$$\Gamma^{(3)}_{\phi\phi\tilde{\mathcal{E}}}(q',\omega';q,\omega) \;=\;$$

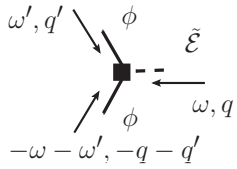

$$\;=\; q^2\,\frac{\partial^3 U}{\partial^2\phi\partial\mathcal{E}}\;, \tag{5.44}$$

$$\Gamma^{(3)}_{\mathcal{E}\phi\tilde{\phi}}(q',\omega';q,\omega) \;=\;$$

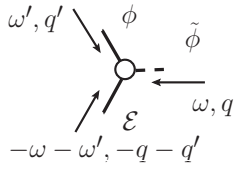

$$\;=\; \frac{\partial^3 U}{\partial^2\phi\partial\mathcal{E}}\;, \tag{5.45}$$

$$\Gamma^{(3)}_{\phi\phi\tilde{\phi}}(q',\omega';q,\omega) \;=\;$$

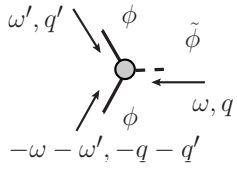

$$\;=\; \frac{\partial^3 U}{\partial\phi^3}\;. \tag{5.46}$$

Of course, within our truncation (5.28) we may evaluate the derivatives with respect to the fields and obtain, i.e., $\partial^3 U/(\partial\phi_a\partial\phi_b\partial\mathcal{E}) = \bar{\gamma}\delta_{ab}$ and the known structure factor from the $O(N)$ theory $\partial^3 U/(\partial\phi_a\partial\phi_b\partial\phi_c) = \bar{\lambda}\,(\phi_c\delta_{ab} + \phi_a\delta_{bc} + \phi_b\delta_{ca})$.

We will use these expressions in the next session to illustrate the contributions that are obtained for the RG flow equations of static and dynamic correlation functions.

5.4. RG flow equations

From the propagators and the given higher n-point functions, we derive the renormalization group equations from the exact flow equation for the scale-dependent effective action Γ. It is given by

$$\frac{\partial\Gamma}{\partial s} = \frac{1}{2}\,\mathrm{Tr}\int\frac{d^dq}{(2\pi)^d}\frac{d\omega}{2\pi}\,\frac{\partial R(q,\omega)}{\partial s}\,\Big(\Gamma^{(2)}(q,\omega) + R(q,\omega)\Big)^{-1}\;, \tag{5.47}$$

where we denote the logarithmic scale derivative by $s = \ln(k/\Lambda)$ in contrast to the previous sections, to distinguish the RG scale from the physical time. The classical action (5.11) is imposed at the high-momentum reference scale Λ. The trace in (5.47) denotes a summation over fields and internal indices – in particular, it includes a summation over both the physical fields as well as their response fields. The second functional derivative of the scale-dependent effective action were given in (5.21) – (5.26). Here, we use a mass-like regulator R that takes a block nondiagonal structure in the retarded/advanced basis, where it regulates the retarded and advanced components in the same way (see (5.30) – (5.38)). Furthermore, the regulator is chosen such that it acts only in the ϕ-sector of our model, i.e., $R_{\mathcal{E}} = 0$. This choice is sufficient

to regulate all contributions that appear in the evaluation of the renormalization group flow equations. We will drop the ϕ-index in the following, and write $R(q,\omega) = R_\phi(q,\omega)$.

Here, we regulate only the spatial momenta leaving the frequencies untouched, where $R(q) = Z(k^2 - q^2)\theta(k^2 - q^2)$, its shape being motivated by optimization criteria [58]. This provides a convenient choice, since that way the frequency integration can be performed analytically on the level of the flow equations. In fact, we will see shortly, that this greatly simplifies the discussion on the behavior of the RG flow.

With the regularized propagators defined in the previous section, Sec. 5.3, we evaluate the trace and obtain the flow equation

$$\begin{aligned}\frac{\partial\Gamma}{\partial s} &= \mathrm{Re}\int\frac{d^dq}{(2\pi)^d}\frac{d\omega}{2\pi}\frac{\partial R(q)}{\partial s}\left[\frac{N-1}{-i\Omega^{-1}\omega + Zq^2 + R(q) + \bar{M}_0^2}\right.\\ &\left. + \frac{-i\Omega_{\mathcal{E}}^{-1}\omega + Z_{\mathcal{E}}q^2}{\left(-i\Omega^{-1}\omega + Zq^2 + R(q) + \bar{M}_R^2\right)\left(-i\Omega_{\mathcal{E}}^{-1}\omega + Z_{\mathcal{E}}q^2\right) - q^2\left(\partial^2U/(\partial\phi\partial\mathcal{E})\right)^2}\right],\end{aligned} \tag{5.48}$$

that sums up both the two retarded and advanced contributions to the flow equations since we consider the real part of the diagrams. It is important to point out, that (5.48) provides only a formal definition of the flow equation for the scale-dependent effective action. The diagrams correspond to the closed one-loop retarded and advanced propagators with a single vertex insertion. Following the discussion in Sec. 5.1 these contributions are exactly zero. However, taking derivatives with respect to the fields, and afterwards setting them to their minimum values, we generate a hierarchy of flow equations for the higher n-point functions $\Gamma^{(n)}$. The diagrams for the RG flow of these quantities will in general be nonvanishing.

Of course, the dynamic properties of the theory are captured in the frequency-dependence of the propagators. Thus, to extract the dynamic behavior we should perform derivatives with respect to fields with a nonvanishing frequency-dependence. Then we may ask for the frequency-dependent contributions to $\partial\Gamma^{(n)}(\cdots;p,\omega)/\partial s$. Only after performing derivatives, is the frequency integration carried out. However, for the static properties of the theory it is irrelevant in which order we evaluate the frequency integral. In fact, performing the frequency integration first greatly simplifies the structure of the diagrams that contribute to the RG flow of static correlation functions. Furthermore, this illustrates that static couplings and scaling properties are in fact independent from the dynamics. Let us therefore consider first the static properties of the theory (5.19). Performing the frequency integration, we obtain the generating functional for static correlation functions

$$\frac{\partial\Gamma}{\partial s} = \frac{1}{2}\int\frac{d^dq}{(2\pi)^d}\frac{\partial R(q)}{\partial s}\left[\frac{N-1}{Zq^2 + R(q) + \bar{M}_0^2} + \frac{1}{Zq^2 + R(q) + \bar{M}_R^2 - \left(\partial^2U/(\partial\phi\partial\mathcal{E})\right)^2/Z_{\mathcal{E}}}\right], \tag{5.49}$$

fully resembling the flow equations of the $O(N)$ symmetric models. However, there are important differences. The first is the presence of the explicit $\mathcal{E}$-field dependence in the mass eigenvalues. On the other hand, the frequency integration induces as shift of the quartic

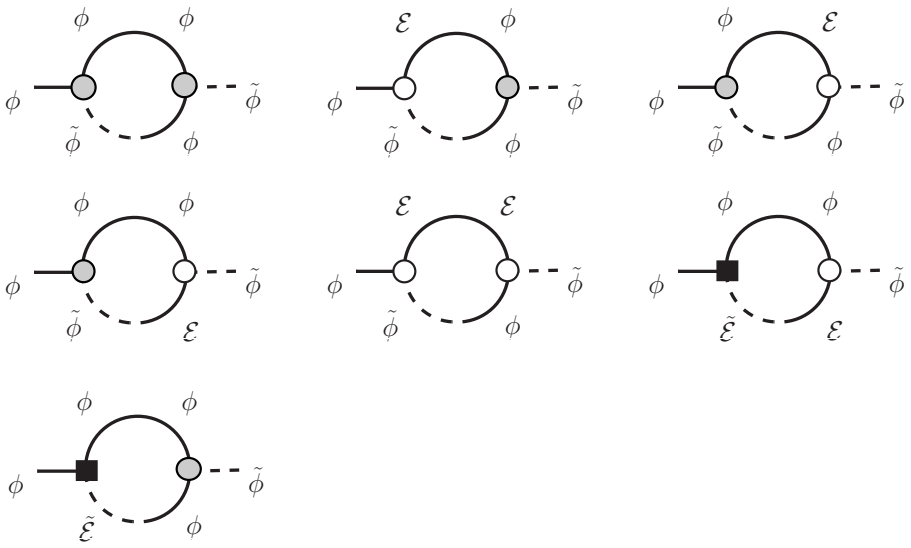

Figure 5.3.: Subset of diagrams that contribute to the frequency and momentum-dependent part of the two-point function $\Gamma^{(2)}_{\tilde{\phi}\phi}(p,\omega)$. These diagrams are evaluated to obtain the RG flow of the renormalization factor Z and the dynamic coefficient Ω^{-1}, and their respective scaling contributions η and η_Ω. We evaluate only the contributions from the Goldstone modes which typically yields a good approximation close to the critical point where the massless modes dominate the dynamics.

coupling given by the mixing $\partial^2 U/(\partial\phi\partial\mathcal{E})$ between the two sectors. If we evaluate the masses at the potential minimum, we obtain: $\bar{M}_0^2 = \bar{m}_0^2 = 0$, $\bar{M}_R^2 = \bar{m}_R^2 = 2\bar{\rho}_0(\bar{\lambda} - \bar{\gamma}^2/Z_\mathcal{E})$.[3] The renormalization factor $Z_\mathcal{E}$ for the conserved density yields the partially renormalized coupling $\bar{\gamma}^2/Z_\mathcal{E}$ that renormalizes in the same way as the quartic coupling $\bar{\lambda}$ in the ϕ-sector. Indeed, we may use this relation to redefine the quartic coupling in the following way, i.e., $\bar{\lambda} \to \bar{\lambda} - \bar{\gamma}^2/Z_\mathcal{E}$. After this identification, we see that the RG flow equations for frequency-independent n-point functions $\partial\Gamma^{(n)}/\partial s$ take the same form as the flow equations that we know from the $O(N)$ model. That is, the ϕ-sector is completely independent of the dynamics in the $\mathcal{E}$-sector, and we may use the results from the previous chapter.

From the flow equation (5.49) we may furthermore derive the scaling contribution to the renormalization factor. We evaluate the flow equations for the renormalization factor Z from the Goldstone modes only, neglecting the radial part. This usually provides a good approximation close to the critical point, where the massless modes give the dominant contribution. We obtain

$$-\frac{1}{Z}\frac{\partial Z}{\partial s} = \bar{\rho}_0\bar{\lambda}^2 \lim_{p\to 0}\frac{\partial}{\partial p^2}\int\frac{d^dq}{(2\pi)^d}\widehat{\frac{\partial}{\partial s}}\left[\frac{1}{Zq^2+R(q)}\frac{1}{Z(q+p)^2+R(q+p)+2\left(\bar{\lambda}-(\bar{\gamma}^2/Z_\mathcal{E})\right)\bar{\rho}_0}\right], \tag{5.50}$$

by projection onto the corresponding diagram, where the derivative $\widehat{\partial/\partial s}$ is defined in the usual way (see chapter 3). Only after the identification $\bar{\lambda} \to \bar{\lambda} - \bar{\gamma}^2/Z_\mathcal{E}$ do we restore the

[3] The additional field-dependence drops out at the physical point, where $\langle\varepsilon\rangle = 0$.

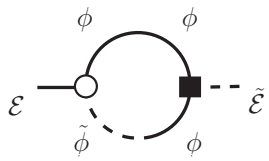

Figure 5.4.: Single diagram contributing to the flow equation of the two-point function $\Gamma^{(2)}_{\tilde{\mathcal{E}}\mathcal{E}}(p,\omega)$. This diagram gives the only contribution to the anomalous dimension $\eta_{\mathcal{E}}$ and includes propagators only from the ϕ-sector. Apart from the vertex insertions the same loop-integral contributes also to the potential flow.

known result from the $O(N)$ model.

Let us now comment on the dynamic properties of the model. Although the flow equation for the effective action (5.48) takes a rather simple form, functional derivatives with respect to frequency and momentum-dependent fields yield a large number of diagrams that may contribute in the flow. The diagrams that are evaluated to obtain the frequency dependence of the two-point functions $\Gamma^{(2)}$ are shown in Fig. 5.3. These are evaluated in the symmetry broken phase, where the order parameter assumes a nonvanishing expectation value. While the expression for each single diagram can be quite complicated, there is a considerable simplification if all diagrams are combined. We give the complete result for the flow equation after carrying out the momentum and frequency integration in the following section Sec. 5.5.

For the corresponding parameters in the $\mathcal{E}$-sector, i.e., $Z_{\mathcal{E}}$ and $\Omega_{\mathcal{E}}^{-1}$, there is only one single diagram that we have to evaluate, which is shown in Fig. 5.4. In fact, we may immediately infer from the structure of the diagram that the dynamic coefficient $\Omega_{\mathcal{E}}^{-1}$ does not evolve with the RG flow. This is due to the momentum-dependent vertex $\Gamma^{(3)}_{\phi\phi\tilde{\mathcal{E}}}(\cdots;p,\omega) = p^2\partial^3 U/(\partial\phi^2\partial\mathcal{E})$ (see (5.44)), which projects out the only contribution to $\partial\Omega_{\mathcal{E}}^{-1}/\partial s$:

$$\frac{\partial\Omega_{\mathcal{E}}^{-1}}{\partial s} \sim \mathrm{Im}\left[\lim_{\omega,p\to 0}\frac{\partial}{\partial\omega}\right.$$
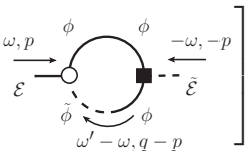

$$\left.\right] = 0\ , \tag{5.51}$$

In fact, this behavior fits our expectation that only the ratio of the two kinetic parameters should be physically relevant. One of the two frequencies Ω or $\Omega_{\mathcal{E}}$ is chosen to set the time-scale, while the other one measures the relative importance of the competing dynamics. The fact, that the diffusion rate is not renormalized is used to fix $\Omega_{\mathcal{E}} = 1$ and to measure the relaxation rate Ω with respect to this quantity.

Let us point out, that the momentum-structure of the three-vertex $\Gamma^{(3)}_{\phi\phi\tilde{\mathcal{E}}}$ also implies that no momentum-independent couplings are generated in the $\mathcal{E}$-sector. This is consistent with the initial requirement, that $\mathcal{E}$ should be a nonordering field. The contributions to the RG flow in the coupled $\mathcal{E}$-sector therefore turn out to be very simple, as far as this particular truncation is concerned. We only need to determine the scale-dependence of the renormalization factor $Z_{\mathcal{E}}$ in terms of the anomalous dimension $\eta_{\mathcal{E}} = -\partial \ln Z_{\mathcal{E}}/\partial s$ at the fixed point. Similarly to

the derivation of the flow equation for renormalization factor Z, we may directly carry out the frequency integration of the corresponding diagram. At the physical point, we obtain:

$$-\frac{1}{Z_{\mathcal{E}}}\frac{\partial Z_{\mathcal{E}}}{\partial s}=\left(\bar{\gamma}^2/Z_{\mathcal{E}}\right)\int\frac{d^dq}{(2\pi)^d}\widehat{\frac{\partial}{\partial s}}\left[\frac{N-1}{\left(Zq^2+R(q)\right)^2}+\frac{1}{\left(Zq^2+R(q)+2\left(\bar{\lambda}-\left(\bar{\gamma}^2/Z_{\mathcal{E}}\right)\right)\bar{\rho}_0\right)^2}\right]. \tag{5.52}$$

Here, we have summarized the contributions to the RG flow equations for Model C. In the following section these flow equations are given in their scale-invariant form, where we ask for possible fixed points solutions of the flow.

5.5. Scaling form of flow equations

To investigate the critical properties, we write the flow equations in a form such that the scale derivatives vanish at a fixed point. For that purpose, we introduce the dimensionless renormalized field squared $\rho=k^{2-d}Z\,\phi^2/2$ and potential $u(\rho,\mathcal{E})=k^{-d}U(\rho,\mathcal{E})$. The dimensionless renormalized coupling between the sectors is given by $\gamma=k^{d/2-2}Z^{-1}Z_{\mathcal{E}}^{-1/2}\bar{\gamma}$. To characterize the behavior of the ratio of renormalized kinetic coefficients $\Omega^{-1}Z^{-1}Z_{\mathcal{E}}$ (recall that we have set $\Omega_{\mathcal{E}}=1$), it is convenient to introduce the kinetic parameter $\kappa=1/(1+\Omega^{-1}Z^{-1}Z_{\mathcal{E}})$ which varies in the range $0\leq\kappa\leq1$ and captures the asymptotic scenarios, i.e., where the relaxation rate $\Omega\to0$ and $\Omega\to\infty$ (compared to the diffusion time-scale).

In the scaling regime we need the flow equations for the case of a nonvanishing rescaled field expectation value or potential minimum, $\rho_0\neq0$, defined by $u'(\rho_0)=0$ with $u'\equiv\partial u/\partial\rho$. At a fixed point, ρ_0 is constant and $\lim_{k\to0}k^{d-2}\rho_0/Z$ denotes the order parameter [19]. Within the 4th order local potential approximation (LPA) truncation around ρ_0, we obtain the flow equations for ρ_0 and the redefined effective coupling $\lambda\to u^{(2,0)}(\rho_0,0)-\gamma^2$:

$$\frac{\partial\rho_0}{\partial s}=(2-d-\eta)\rho_0+2v_d\left\{(N-1)l_1\left(0;\eta\right)+3l_1\left(2\rho_0\lambda;\eta\right)\right\}, \tag{5.53}$$

$$\frac{\partial\lambda}{\partial s}=(d-4+2\eta)\lambda+2v_d\lambda^2\left\{(N-1)l_2\left(0;\eta\right)+9l_2\left(2\rho_0\lambda;\eta\right)\right\}. \tag{5.54}$$

Here $v_d=\left(2^{d+1}\pi^{d/2}\Gamma\left(d/2\right)\right)^{-1}$ and the anomalous dimension is defined as $\eta=-\partial\ln Z/\partial s$. We encounter the same threshold functions as in the previous sections, given by $l_n(w;\eta)=(2n/d)\left(1-\eta/(2+d)\right)(1+w)^{-n-1}$ that parametrize the integral appearing from (5.47) and describe the net decoupling of heavy modes [19]. The flow equation for the coupling γ reads

$$\frac{\partial\gamma}{\partial s}=\left(d/2-2+\eta+\eta_{\mathcal{E}}/2\right)\gamma+2v_d\gamma(\lambda+\gamma^2)\left\{(N-1)l_2\left(0;\eta\right)+3l_2\left(2\rho_0\lambda;\eta\right)\right\}, \tag{5.55}$$

which has an explicit dependence on the anomalous dimension $\eta_{\mathcal{E}}=-\partial\ln Z_{\mathcal{E}}/\partial s$. The scale-dependence of the kinetic parameter takes the form

$$\frac{\partial\kappa}{\partial s}=\kappa(1-\kappa)\left\{\eta_\Omega(\kappa)-\eta+\eta_{\mathcal{E}}\right\}, \tag{5.56}$$

which depends also on the scaling contribution to the kinetic coefficient, $\eta_\Omega = -\partial \ln \Omega^{-1}/\partial s$. The anomalous dimensions are given by

$$\eta = 16\frac{v_d}{d}\rho_0\lambda^2 m_{2,2}\left(0, 2\rho_0\lambda; \eta\right) \ , \tag{5.57}$$

$$\eta_\mathcal{E} = -2v_d\gamma^2\left\{(N-1)l_2\left(0;\eta\right) + l_2\left(2\rho_0\lambda;\eta\right)\right\} \ , \tag{5.58}$$

where $m_{2,2}(w_1, w_2; \eta) = (1+w_1)^{-2}(1+w_2)^{-2}$ is η-independent in our case, and the scaling contribution to the kinetic coefficient reads

$$\eta_\Omega = \frac{1}{\rho_0}2v_d\Big\{l_1(0;\eta) + l_1(2\rho_0\lambda;\eta) - 2\,h_1\big(\rho_0(\lambda+\gamma^2), \gamma^2\rho_0(1-\kappa)/\kappa, (1-\kappa)/\kappa; \eta\big)\Big\} \ . \tag{5.59}$$

The function h_1 parametrizes the contributions to the kinetic coefficient and is a threshold function of similar type as l_1 in the family of l_n threshold functions. It is given by

$$\begin{aligned}
h_1(w_1, w_2, w_3; \eta) = \ & \frac{1}{(1+w_1)^2}\Bigg\{\frac{(1+w_1)\left(w_2 + (1+w_3)^2\right)}{1 + w_1 - w_2 + w_3 + w_1 w_3} \\
& + \left(\frac{2}{d} - 1\right)\,{}_2F_1\left(1, \frac{d}{2}; \frac{d+2}{2}; \frac{w_2}{w_1+1} - w_3\right) \\
& - \frac{d}{d+2}(w_2 + 2w_3)\,{}_2F_1\left(1, \frac{d+2}{2}; \frac{d+4}{2}; \frac{w_2}{w_1+1} - w_3\right) \\
& - \frac{d+2}{d+4}w_3^2\,{}_2F_1\left(1, \frac{d+4}{2}; \frac{d+6}{2}; \frac{w_2}{w_1+1} - w_3\right) \\
& - \frac{\eta}{2}\Bigg[\left(\frac{2}{d} - 1\right)\,{}_2F_1\left(1, \frac{d}{2}; \frac{d+2}{2}; \frac{w_2}{w_1+1} - w_3\right) \\
& - \frac{d}{d+2}(w_2 + 2w_3 - 1)\,{}_2F_1\left(1, \frac{d+2}{2}; \frac{d+4}{2}; \frac{w_2}{w_1+1} - w_3\right)\Bigg) \\
& - \frac{d+2}{d+4}\left(w_3^2 - w_2 - 2w_3\right)\,{}_2F_1\left(1, \frac{d+4}{2}; \frac{d+6}{2}; \frac{w_2}{w_1+1} - w_3\right) \\
& + \frac{d+4}{d+6}w_3^2\,{}_2F_1\left(1, \frac{d+6}{2}; \frac{d+8}{2}; \frac{w_2}{w_1+1} - w_3\right)\Bigg]\Bigg\} \ .
\end{aligned} \tag{5.60}$$

It is important to emphasize that (5.59) and in particular the form of the scaling function (5.60) are essentially the new results obtained within this work. They capture the complete information about the dynamics close to criticality. While the β-function (5.56) already suggests a set of fixed point solutions (namely $\kappa = 0$ and $\kappa = 1$) their existence and stability properties are determined by the function h_1. Therefore, before we go on to consider possible scaling solutions to the RG flow equations let us ask about the limiting properties of this function. In particular, we inquire about the two limits where $\kappa \to 0$ and $\kappa \to 1$.

- Let us start by examining the $\kappa \to 1$ case. In this limit, we may expand the hypergeometric function ${}_2F_1\left(1, a; a+1; z\right)$ and obtain

$$ {}_2F_1\left(1, a; a+1; z\right) = 1 + \frac{a}{1+a}z + \mathcal{O}(z^2) \ , \tag{5.61}$$

  where in this case $z = -1/\left(1 + \gamma^2\rho_0/(1+\lambda\rho_0)\right)(1-\kappa)/\kappa$ and the coefficient $a = d/2 + n$ is determined by the spatial dimension d plus some integer value of n. We see that $z \to 0$

in the $\kappa \to 1$ limit and the hypergeometric functions in (5.60) all evaluate to one. Thus, we get

$$h_1(w, 0, 0; \eta) = (2/d)(1 - \eta/(2 + d))(1 + w)^{-2} = l_1(w; \eta) \tag{5.62}$$

and the scaling contribution to the dynamic coefficient Ω^{-1} drastically simplifies:

$$\eta_\Omega = \frac{1}{\rho_0} 2v_d \left\{ l_1(0; \eta) + l_1(2\rho_0\lambda; \eta) - 2l_1\big(\rho_0(\lambda + \gamma^2); \eta\big) \right\} \ . \tag{5.63}$$

It can be expressed solely in terms of l_1 threshold functions. This limit captures the region where relaxation rate diverges and the system is characterized by a diffusive process in the presence of a homogeneous background field (see the following section for the physical interpretation of the scaling solutions).

- On the other hand, the opposite limit $\kappa \to 0$ is a bit more tricky. An expansion of the hypergeometric functions gives:

$${}_2F_1\left(1, a; a + 1; -1/z\right) = \Gamma(1 + a) \left\{ z^a \Gamma(1 - a) + z \left(1 - \frac{1 - a}{2 - a} z + \mathcal{O}(z^2) \right) \frac{\Gamma(a - 1)}{\Gamma(a)^2} \right\} \ , \tag{5.64}$$

where in this case $z = \big(1 + \gamma^2\rho_0/(1 + \lambda\rho_0)\big)\, \kappa/(1 - \kappa)$ and the property that $z > 0$ is assumed in the expansion (5.64). In the $z \to 0$ limit ($\kappa \to 0$) the hypergeometric functions do not reduce to a simple form. However, it is possible to show that the threshold function h_1 reduces to the following form:

$$\lim_{y \to \infty} h_1(w_1, w_2 y, y; \eta) = (2/d)(1 - \eta/(2 + d))(1 + w_1 - w_2)^{-2} = l_1(w_1 - w_2; \eta) \ . \tag{5.65}$$

For the scaling contribution η_Ω this yields the same expression in the $\kappa \to 1$ limit, albeit without the γ-dependence:

$$\eta_\Omega = \frac{1}{\rho_0} 2v_d \left\{ l_1(0; \eta) + l_1(2\rho_0\lambda; \eta) - 2l_1(\rho_0\lambda; \eta) \right\} \ . \tag{5.66}$$

In fact, this is just the known result for Model A (assuming that the derivation takes into account only the contributions from the Goldstone modes). Apparently, in the regime where the kinetic parameter $\kappa \to 0$ the scaling contribution to Ω^{-1} decouples from the conserved density – the γ-dependence drops out – yielding an RG flow which resembles that of the purely relaxational model. We will see shortly that this is indeed what happens.

This concludes our discussion of the flow equations and we now proceed to discuss their scaling solutions. Eqs. (5.53) – (5.59) constitute the full set of flow equations for this model, whose fixed point solutions are computed numerically.

5.6. Dynamical scaling regions

At a fixed point the coefficients $Z \sim k^{-\eta}$, $Z_\mathcal{E} \sim k^{-\eta_\mathcal{E}}$, and $\Omega^{-1} \sim k^{-\eta_\Omega}$ assume their scaling form while the anomalous dimensions η, $\eta_\mathcal{E}$, and η_Ω take on their scale-independent critical

values. The dynamic critical exponents are derived by examining the scaling behavior of the spectral function which is defined in terms of the imaginary part of the retarded propagator. At the critical point $-i\,\mathrm{Im}\,G_{\phi\tilde{\phi}} \sim k^{-2+\eta}$, where it is assumed that $q \sim k$ and $\omega \sim k^z$. The scaling assumption requires

$$\Omega^{-1} Z^{-1} k^{z-2} \sim k^{z-2+\eta-\eta_\Omega} = \text{const.}\,, \tag{5.67}$$

and we obtain $z = 2 - \eta + \eta_\Omega$. Similarly, from the scaling properties of the spectral function $-i\,\mathrm{Im}\,G_{\mathcal{E}\tilde{\mathcal{E}}}$ we derive the dynamic critical exponent $z_\mathcal{E} = 2 - \eta_\mathcal{E}$, keeping in mind that the scaling contribution to the kinetic coefficient $\Omega_\mathcal{E}$ is exactly zero.

The static critical behavior is encoded in the flow equations (5.53) and (5.54) characterizing the potential flow with the anomalous dimension (5.57). They form a closed set of equations and only depend on N and d for the $O(N)$ symmetric potential, which reflects the fact that the static universality class does not depend on the dynamic properties. In addition to the static properties, the dynamic universality class is further characterized in terms of the fixed point values of γ_* and κ_* along with the scaling exponents z and $z_\mathcal{E}$. From the form of the flow equations (5.55) and (5.56) we may already infer the possible scaling solutions. Of course, the existence and stability of these solutions is yet to be determined. We find the following possibilities:

- *Weak scaling region*: For $\kappa_* = 0$ and $\gamma_* \neq 0$ at the fixed point (region I), we obtain two independent dynamic scaling exponents z and $z_\mathcal{E}$, where $z > z_\mathcal{E}$. Since the kinetic parameter vanishes, the ratio of the renormalized relaxation rate of the order parameter and the diffusion rate is zero. Therefore, the order parameter relaxes only asymptotically compared to the diffusion time-scale in this regime, i.e., $\Omega/\Omega_\mathcal{E} = 0$.

- *Strong scaling region*: For $0 < \kappa_* < 1$ and $\gamma_* \neq 0$, we find from (5.56) with $\partial\kappa/\partial s = 0$ at the fixed point that $\eta_\Omega - \eta + \eta_\mathcal{E} = 0$ (region II). This leads to a locking of the dynamic critical exponents in both sectors, with $z = 2 - \eta_\mathcal{E} = z_\mathcal{E}$. This strong scaling holds when the fluctuations of the conserved density dictate the dynamic critical scaling for the order parameter. The kinetic parameter κ_* is in the intermediate range and the relaxation and diffusion process compete on equal terms. It is this region that is commonly referred to as Model C.

- *Anomalous diffusion region*: For critical $\kappa_* = 1$ and $\gamma_* \neq 0$ (region III), we find another weak scaling solution with independent values for the scaling exponents, i.e. $z < z_\mathcal{E}$, in contrast to region I. This corresponds to different fixed point values for $\eta_\mathcal{E}$ and η_Ω in these regimes, since they depend on γ_* and κ_* according to (5.58) – (5.59). Because the kinetic parameter is unity, the ratio of the renormalized diffusion rate and the relaxation rate must vanish. Since we have fixed $\Omega_\mathcal{E} = 1$, the ϕ-field must relax on extremely short time-scales. Thus, this scaling region describes the peculiar situation of a purely diffusive process in the presence of a practically homogeneous order-parameter field.

- *Decoupled scaling region*: If the two sectors decouple, i.e. $\gamma_* = 0$, then $\eta_\mathcal{E} = 0$ according

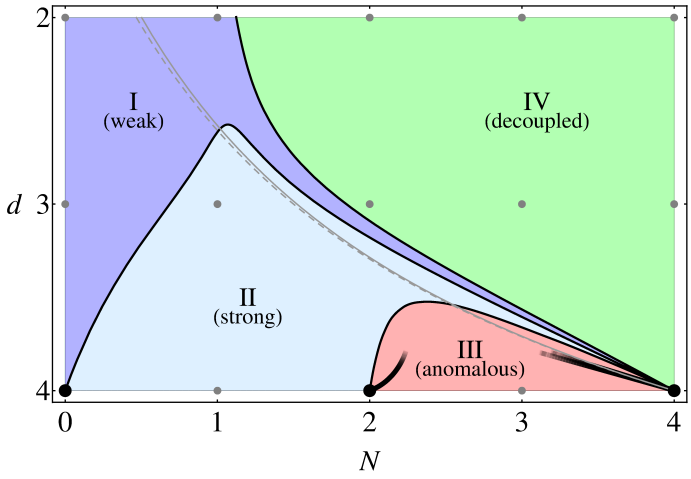

Figure 5.5.: Phase diagram for Model C as a function of dimension d and the number of field components N from the functional RG. For comparison to the ϵ-expansion, thick lines near $d = 4$ denote $\mathcal{O}(\epsilon)$ results [221]; thin/dashed lines denote the $\mathcal{O}(\epsilon^2)$ results according to [43, 231].

to (5.58) (region IV). In this case, the conserved density displays dimensional scaling with $z_{\mathcal{E}} = 2$. In this region, the physical field shows a dynamic critical scaling with leading exponent z in the Model A universality class. However, there can be nontrivial subleading corrections to the dynamic scaling even if the mode-coupling is zero [221]. The kinetic coefficient assumes the fixed point value $\kappa_* = 0$ which, similar to the weak scaling region I, describes a scenario where the order parameter relaxes asymptotically compared to the diffusion process.

Depending on the number of field-components N and the dimensionality d of the system the dynamic scaling properties of respective theory at the critical point can be characterized by either one of the above solutions (based on the assumption that there is always a stable fixed point). Our results, obtained within the 4th order LPA truncation, are shown in Fig. 5.5 where the different scaling regions (I – IV) are clearly visible. At their boundaries the corresponding fixed points exchange their stability properties, determined by the number of relevant eigendirections.

Therefore, let us examine the eigenvalues of the linearized RG flow around the fixed point values. This will give us the critical indices and the corresponding eigendirections that essentially define the stability of the above fixed point solutions. To derive the stability matrix, $\partial\beta_{i,j}/\partial g_{m,n}$, we write the $\beta_{i,j}$-functions in terms of the generalized couplings $g_{m,n} \in \{\lambda, \gamma, \ldots\}$ with $\beta_\lambda \equiv \partial\lambda/\partial s$ etc. After computing the solutions of the fixed point condition, where the β-functions vanish $\beta_\lambda(g_*) = \beta_\gamma(g_*) = 0$ etc. we determine the critical indices at the fixed

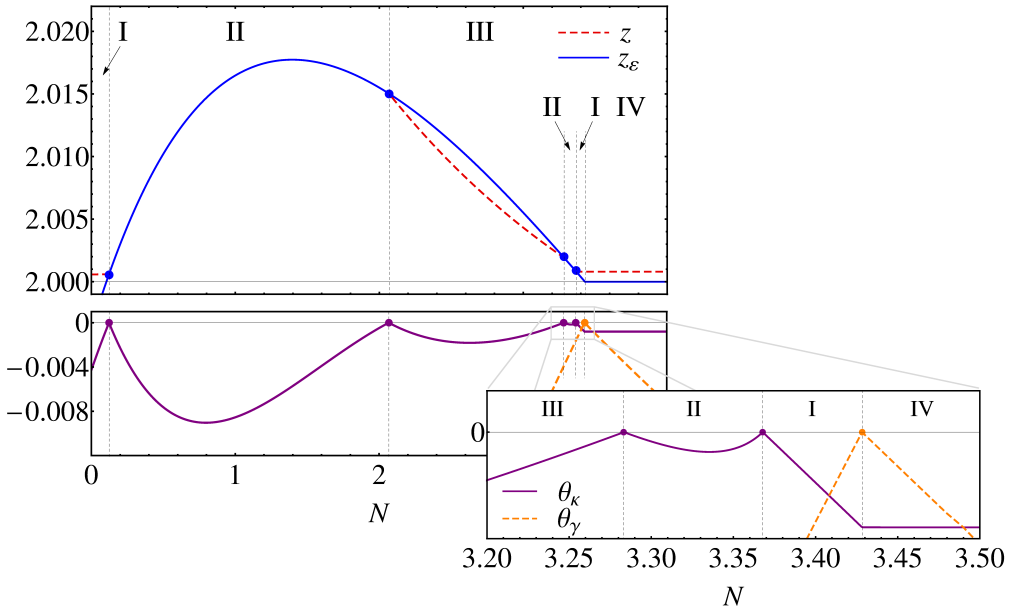

Figure 5.6.: (**Top**) Dynamic critical exponents z (red, dashed) and $z_\mathcal{E}$ (blue, continuous) as a function of N at fixed dimension $d = 3.75$. The different regions I – IV are clearly visible, along with the locking phenomenon ($z = z_\mathcal{E}$) in region II and the distinct values in the independent scaling regimes I and III. (**Bottom**) The subleading exponents θ_γ (orange, dashed) and θ_κ (purple, continuous) indicate the stability of the fixed point solutions. θ_γ controls the decoupling transition between regions I and IV, while θ_κ characterizes the kinetic properties of the respective phases where the fixed point coupling $\gamma_* \neq 0$. This is illustrated in the inset which shows an enlarged version the transition region around $N \simeq 3.35$ ($d = 3.75$).

points.[4] For a given fixed point determined by the couplings $g_{m,n\,*} \in g_*$, we have

$$\beta_{i,j} = \sum_{m,n} \frac{\partial \beta_{i,j}}{\partial g_{m,n}} \left(g_{m,n} - g_{m,n\,*}\right) + \mathcal{O}(g^2) \ , \tag{5.68}$$

where the expansion

$$g_{m,n} = g_{m,n\,*} + \sum_I c_I \, v^I_{m,n} (k/\Lambda)^{-\theta_I} \ , \tag{5.69}$$

is given in terms of the eigenvalues $-\theta_I$ and eigendirections v^I of the stability matrix at the fixed point, i.e.,

$$\frac{\partial \beta(g_*)}{\partial g} \, v^I = -\theta_I v^I \ . \tag{5.70}$$

If Re $\theta_I > 0$ the corresponding eigendirection v^I defines a relevant perturbation in the IR limit $k \to 0$, while in the case Re $\theta_I < 0$ the perturbation is irrelevant. As usual, for the discussion of the stability properties only the real part of θ_I is important, and we will denote by θ_I the real parts only. In the 4th order LPA truncation, apart from the leading order exponent $\theta_1 = 1/\nu$ being positive for all values of N and the subleading Wegner exponent

[4]Note, that g and g_* are defined to include the complete set of generalized couplings $g_{m,n}$.

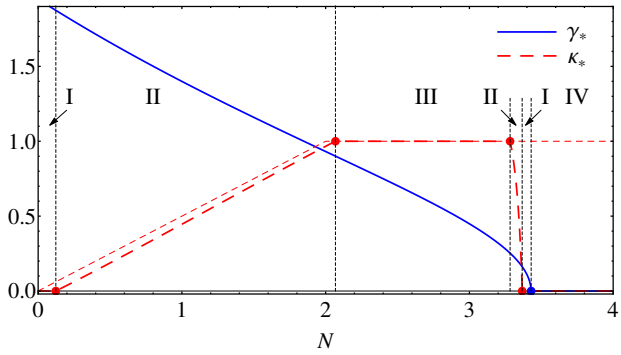

Figure 5.7.: Fixed point values for the mode coupling γ_* (blue, continuous) and kinetic parameter κ_* (red, dashed) as a function N at $d = 3.75$. The asymptotic result for κ_* in the limit $d \to 4^-$ is shown for comparison (thin, dashed line) where the region III extends over the range $2 < N < 4$.

$\theta_2 = -\omega$ which is always negative, we obtain two further exponents that relate to the scaling properties of the coupling γ and the kinetic parameter κ. We will denote them by θ_γ and θ_κ to mark their origin. In fact, these critical indices are determined exactly by the derivatives $\theta_\gamma = \partial\beta_\gamma/\partial\gamma$ and $\theta_\kappa = \partial\beta_\kappa/\partial\kappa$ at the fixed point – there is no mixing contributions from derivatives $\partial\beta_\lambda/\partial\lambda$ etc., from the static sector (and *vice versa*). Thus, these critical indices define a genuine extension of the known static universality class.

Our results for the correlation length exponent ν and for the anomalous dimension η (see Tab. 5.1) agree with those documented for functional renormalization group studies on the static universality class at this truncation level [19]. The characteristic behavior of the eigenvalues θ_γ and θ_κ is exemplified in Fig. 5.6 for fixed dimension $d = 3.75$ as a function of field components N. The eigenvalues are negative except at the boundaries between the phases (regions I to IV), where different fixed point solutions exchange their stability. The stable fixed point is characterized by only one relevant eigendirection, $\theta_1 = 1/\nu > 0$, while $\theta_2 < 0$, etc. In Fig. 5.7 also the corresponding fixed point values of γ_* and κ_* are shown that define the scaling regions I – IV. This provides additional information on properties of the fixed points as N is varied. In fact, from Fig. 5.7 it can be seen that the fixed point solutions with $\gamma_* \neq 0$ not only loose their stability but cease to exist beyond some value of N where the two sectors decouple, e.g., given by $N \simeq 3.4$ ($d = 3.75$).

5.7. Constraints on scaling behavior

Model C is special compared to other models for critical dynamics, as the dynamic critical scaling properties are directly related to the static close to criticality. In particular, there exists an exact scaling relation [40, 220, 221]

$$\eta_{\mathcal{E}} = -\alpha/\nu \ , \tag{5.71}$$

which relates the anomalous dimension $\eta_{\mathcal{E}}$ to the specific heat and correlation length exponents, α and ν, respectively. It applies only when the specific heat diverges $\alpha > 0$, while it is absent for $\alpha < 0$. Eq. (5.71) is derived from the observation that the operator ε corresponds to the relevant scaling part of the energy density $\varepsilon \sim \varphi^2$ (see, e.g., [9]) where the RG scaling dimension of the composite operator φ^2 is given by $(1-\alpha)/\nu$. Thus, at the critical point the two-point correlation function assumes a scaling form

$$\left\langle \varphi^2(k)\varphi^2(-k)\right\rangle \;\sim\; k^{2(1-\alpha)/\nu-d}\;, \tag{5.72}$$

where, using the scaling relation $2-\alpha = \nu d$ and from the knowledge that the two-point function satisfies $\langle \varepsilon(k)\varepsilon(-k)\rangle \sim k^{\eta_\varepsilon}$, we deduce (5.71). The anomalous dimension $\eta_{\mathcal{E}}$ enters the dynamic scaling exponent of the conserved density $z_{\mathcal{E}} = 2-\eta_{\mathcal{E}}$ and furthermore determines the dynamic critical exponent of the order parameter in the strong scaling regime (III). In this region, the dynamic critical scaling behavior of the order parameter is completely fixed by the static critical behavior, i.e. $z = 2 + \alpha/\nu$. We point out that such a relation does not hold, e.g., in the purely relaxational Model A [39].

From the scaling relation (5.71), we may infer certain properties of the (N, d) phase diagram solely from the static equilibrium properties of the $O(N)$ vector model. Here, we observe that our result for the phase diagram (Fig. 5.5) is compatible with known data for both critical dynamics and statics. In particular, the boundary between the scaling regions I and IV, which is characterized by the requirement that the coupling γ_* vanishes, and therefore $\eta_{\mathcal{E}} = 0$, can be derived from the $\alpha = 0$ line. For the two-dimensional Ising model, where $\alpha = 0$ is known exactly from the Onsager solution, our result for the phase boundary in Fig. 5.5 still occurs remarkably close to the exact result in comparison to the ϵ-expansion, considering the expected quality of our truncation. For the three-dimensional XY model the specific heat exponent is known to be negative $\alpha = -0.01056(38)$ [243], while $\alpha = 0.110(2)$ in the three-dimensional Ising universality class [244] (see in particular the compilation of critical exponents in Ref. [8]). This implies that at $d = 3$ the decoupling transition (I – IV) should lie between $1 < N < 2$. Our 4th order LPA results are consistent with this observation. Finally, close to the upper critical dimension $d \to 4^-$, α is known to vanish at $N = 4$ which holds exactly within our truncation.

In the strong scaling region, we may directly compare our results for the dynamic critical exponent to the value obtained from the corresponding scaling relation $z = 2 + \alpha/\nu$. Using most accurate high-temperature expansion data for $N = 1$ in $d = 3$ from Ref. [8], we obtain from this relation $z = 2.176(3)$. Our result $z = 2.059$ in comparison (see Tab. 5.1 for a summary of results) is reasonable considering the expected quality of a lowest-order derivative expansion in the presence of sizable anomalous dimensions. Note, that the Ising model in three dimensions is the only model with integer values of N and d that lies within the strong scaling region. In fact, it is the only case where the coupling to the conserved density is relevant (excluding the $N \to 0$ limit). For large values of N the conserved charge effectively decouples which yields Model A dynamic critical scaling.

N	ν	η	z	$z_{\mathcal{E}}$
1	0.523	0.055	2.059	2.059
2	0.604	0.059	2.027	2
3	0.685	0.054	2.025	2
4	0.747	0.047	2.021	2
∞	*1*	*0*	*2*	*2*

Table 5.1.: Critical exponents ($d = 3$) calculated from the functional RG to 4th order in the local potential approximation. The dynamic critical exponents z and $z_{\mathcal{E}}$ are in the Model C universality class in the strong scaling region ($N = 1$), while the leading dynamic critical scaling for $d = 3$ and $N > 1$ is in the Model A universality class.

In the weak and decoupled scaling regions (I and IV), where $\kappa_* = 0$, the leading dynamic scaling behavior of the physical field features a dynamic exponent in the universality class of Model A. We compare the contributions to $z - 2 = \eta_\Omega - \eta$ directly to the flow equations for Model A derived in Ref. [21] to $\mathcal{O}(\nabla^2)$ in the derivative expansion. We find that $\eta_\Omega - \eta = c\eta$ is satisfied exactly on the level of the RG flow equations in this region using the standard notation [39]. Furthermore, knowledge about the values of $c\eta$ allows us to deduce the shape of the transition line between the weak and strong scaling regions (I and II), which is characterized by the locking of dynamic critical exponents $z = z_{\mathcal{E}}$. In particular, the boundary is defined by the relation $\alpha/\nu = c\eta$. Using available data on the quantity $c\eta$ from the critical dynamics of Model A [214, 215, 245] and the static critical exponents α and ν [8] we find that $c\eta > 0$ ($d = 2$) and $c\eta - \alpha/\nu < 0$ ($d = 3$). Thus, we conclude that the phase boundary for $N = 1$ should pass between between $2 < d < 3$, which is in very good agreement with our results.

Let us comment on the limit $N \to 0$ since here the situation is less clear. In this limit, the $O(N)$ model is known to describe the statistical properties of linear polymers in dilute solutions and in the good-solvent regime [246]. In particular, this allows for a mapping of certain self-avoiding walk (SAW) models to this case (see, e.g., [8] for a review) where the scaling behavior of static correlation functions has been explored extensively. It is in this limit, that we observe an interesting behavior, where the boundary between regions I and II bends down for small values of N and finally runs into the point at $N = 0$ in $d = 4$ dimensions (see Fig. 5.5). Data from SAW models [247] for the case $N = 0$ and field-theoretic results [8] indicate that α/ν is positive between the upper and lower critical dimension $1 < d < 4$. However, we find a small negative contribution to the dynamic critical exponent of the conserved density, i.e. $z_{\mathcal{E}} - 2 < 0$ (as seen also in Fig. 5.6), while the dynamic critical exponent z receives a positive contribution in this regime and is compatible with a lower bound derived for the relaxational models [248]. We expect that this behavior is an artifact of the truncation and will disappear if higher order operators are included in the truncated series expansion for the effective potential. On that note, let us emphasize that the phase boundaries are determined by the stability transition between fixed points and

rely on an accurate computation of subleading scaling exponents. As we have seen at the example of the two-coupled scalar models in the previous chapter, these phase boundaries may shift substantially when the truncation is extended both to higher orders in the gradient expansion (including the field-dependence in the renormalization factors) as well as to higher orders in the fields for the series expansion of the effective potential. Thus, to obtain a better quantitative control over the phase structure of this model it is mandatory to consider more elaborate truncations.

5.8. Extended truncations

To improve the quality of our results and to check the convergence of critical indices it is necessary to go to higher orders in the derivative expansion and to use an extended basis of field operators for the truncated series expansion of the effective potential. In fact, we considered extended truncations of the type where higher order operators are included only in the ϕ and $\tilde{\phi}$-dependent part of the effective action:

$$\Gamma \sim \int d^d x\, dt\, \left\{ \tilde{\phi}_a \left(-i\Omega^{-1}\omega - Z\nabla^2 \right) \phi_a + \tilde{\phi}_a \mathcal{O}_a(\phi) + \ldots \right\} , \tag{5.73}$$

while the $\mathcal{E}$-dependent part and in particular, the coupling between the two sectors is kept fixed. This corresponds to a partial improvement on the truncation of the effective potential, which enters Eq. (5.19) via the derivatives $\partial U/\partial\phi$ and $\partial U/\partial\mathcal{E}$. While such an extended *ansatz* yields better results close to the upper critical dimension $d = 4$ near $N \simeq 4$, that are consistent with previous results obtained with the ϵ-expansion [40, 42, 43, 46, 220, 221, 231], around $d = 3$ an expansion of this form fails to reproduce the known behavior of the phase boundary between region I and IV. In particular, using an extended truncation (5.73) in $d = 3$ to 8th order in the fields shifts this phase boundary to larger values around $N \simeq 2.7$, while the static equilibrium properties indicate that the stability transition should lie between $1 < N < 2$. It is clear why such a truncation must fail – it does not define a consistent expansion, as one would expect that the corresponding field operators included in the extended *ansatz* for $\partial U/\partial\phi$ couple also to the $\mathcal{E}$-sector via the interaction term $\sim \tilde{\mathcal{E}}\nabla^2\partial U/\partial\mathcal{E}$. Any truncation that extends upon our 4th order LPA results should therefore simultaneously include higher order operators $\mathcal{O}_n(\phi)$ in both sectors, improving both on the potential in the ϕ-sector and the momentum-dependent coupling between the sectors.

Let us also point out that the diffusive dynamics (5.2) strongly constrains possible extensions of the truncation where higher order operators $\mathcal{O}_n(\mathcal{E})$ are included. The assumption of a *linear* diffusion process requires that the operators $\mathcal{E}$ and $\tilde{\mathcal{E}}$ should enter the scale-dependent effective action only in a bilinear form. Ignoring this constraint might yield a low-energy effective model that is in a different dynamic universality class, other than Model C. Also, different types of stochastic diffusion equations may require a different choice for the discretization of the dynamics. In that case, additional diagrams may contribute to the flow equations.

5.9. Summary and outlook

Here, we have studied a simple system with relaxational dynamics for the order parameter field in the presence of a diffusive mode in the framework of the functional RG, using a 4th order LPA truncation. We find that the dynamic critical properties are strongly constrained by the scaling properties of static correlation functions. However, interactions lead to a complex structure with a variety of possible phases with different dynamic scaling properties and nontrivial subleading scaling corrections. While the existence of the anomalous diffusion region and its associated dynamic critical scaling behavior was for a long time unclear [39, 40, 42, 42, 46, 220, 221] we unambiguously establish its existence and scaling properties. This is in contrast to the $\mathcal{O}(\epsilon^2)$ results presented in [43, 231] which seemed to indicate that this region is an artifact of the ϵ-expansion. Our results, do not rely on such an expansion and therefore might lead to a different conclusion on the phase structure of Model C in this region.

Of course, given the expected quality of the 4th order LPA truncation it would be desirable to obtain a better quantitative control over the phase diagram. This requires a reliable determination of subleading critical indices and thus requires us to consider extended truncations going to higher order in the derivative expansion. This was shown to yield accurate results at the example of the static scaling exponents in the three-dimensional Ising model [66, 67]. Possible extensions in this direction are left for future work.

It would be striking if one could establish the scaling properties of region III experimentally. In this region, the dynamics describes a diffusion process in the presence of a homogeneous scalar field configuration. Nevertheless, fluctuations of the order parameter are important and the nonzero coupling $\gamma_* \neq 0$ strongly affects the scaling properties of the conserved density, i.e. $z_\mathcal{E} = 2 - \eta_\mathcal{E} > 2$ which leads to sub-diffusion. It would be interesting to see if this region of the phase diagram is accessible with Monte Carlo simulations for fractal dimensions $3 < d < 4$ if the real-time dynamic critical behavior is identified with the dynamic properties of the Monte Carlo sampling process [249–252].

6. Universality and anomalous scaling far from equilibrium

In the previous chapter we considered the extensions of static universality classes by considering the long-time dynamics following a small perturbation in the critical equilibrium state. Our analysis relied on the assumption of linear response where at sufficiently long times the system always reaches thermodynamic equilibrium. However, the time evolution starting from a generic state certainly is much more complex and we may wonder if steady states exist also far from equilibrium. Such states are characterized by time translation invariance and might feature similar scaling properties as thermodynamic systems close to criticality. Practically such a state might be hard to reach from some initial state requiring a delicate tuning of parameters. Stochastic driven systems allow for a much more robust way to reach nonequilibrium, where typically some injection process leads to a strong occupation of modes which are removed by dissipation. If the injection scale sufficiently far away from the dissipation scale nonlinear interactions will transfer the excitations that were put into the system through an intermediate range of scales. In such a case one will observe a nonvanishing flux in the so-called inertial range. There the dynamics is effectively independent of the driving and dissipation mechanisms and one may expect universal scaling behavior characterized by the presence of dynamically conserved quantities.

A prominent example where such a nonequilibrium scaling behavior has been discussed is in hydrodynamic turbulence [49], as described by the incompressible Navier-Stokes equations

$$\frac{\partial u_a}{\partial t} + u_b \nabla_b u_a - \nu_0 \nabla^2 u_a = -\nabla_a p + f_a(x,t) \ . \tag{6.1}$$

Here, u_a is the velocity field, ν_0 is the kinematic viscosity, and p is the thermodynamic pressure. The incompressibility constraint $\nabla_a u_a = 0$ is enforced by projecting out the longitudinal modes via the projection operator $P_{ab}(\nabla) = \left(1 - (\nabla_a \nabla_b)\nabla^{-2}\right)$. This introduces an advective nonlinearity $\sim P_{ab}(\nabla) u_c \nabla_c u_b$ in (6.1) which essentially yields the strong nonlocal interactions characteristic of turbulent hydrodynamic flow. Of course, eq. (6.1) should be supplemented by some initial state and appropriate boundary conditions. The stochastic random force $f_a(x,t)$ is chosen to be Gaussian and white-in-time, i.e.,

$$\langle f_a(x,t) f_b(x',t') \rangle = 2 P_{ab}(\nabla) D(x-x') \delta(t-t') \ . \tag{6.2}$$

where the angular brackets denote an averaging with respect to the stochastic noise, while its spectrum of the driving force is completely characterized by the function $D(x-x')$. For

turbulent flow stirred at large scales and far from the boundaries one expects a universal scaling for the small-scale fluctuations. Indeed, experiment gives strong indications for such universal behavior in Navier-Stokes turbulence [253–257]. However, the exact values of the scaling exponents are still under debate.

Theoretically, the similarity of the problem to the theory of critical phenomena [258, 259] has led to many attempts to apply renormalization group methods [260–266], also in the context of the functional renormalization group [267, 268]. However, the nature of the fixed points and the competing scales of the system make the problem very hard to tackle, and until now there is no consensus on the relevance of fixed point solutions for hydrodynamic turbulence (see, e.g., Ref. [265, 269, 270] for an overview of the subject).

In such a situation it is useful to have a model system at hand that shares some essential properties with the original problem and allows for a clear physical understanding. One example that has featured prominently in this respect, is the Kraichnan model of linear passive advection [271]. Since the problem is linear, it is possible to close the equations of motion for n-point correlation functions and determine their scaling behavior exactly. This has lead to the understanding of a basic mechanism that might explain the anomalous scaling in hydrodynamic turbulence [272–275]. In fact, in this model anomalous scaling is related to the presence of zero modes while the nonanomalous part stems from the dimensional scaling contribution of the random forcing mechanism. Thus, in general, one may suspect a subtle interplay between the different scaling contributions. Although, the problem has little resemblance to the strong nonlocal interactions present in the Navier-Stokes equation, it nevertheless provides a first explanation for the observed universality of scaling behavior in hydrodynamic systems far from equilibrium. Of course, one must ask if these ideas can be extended to the case where strong nonlinear interactions dominate the dynamics.

Another model that has featured prominently over the years is the random-force-driven Burgers' equation [47, 48]. It displays the same type of advective nonlinearity that is present in the Navier-Stokes equation however, without the strong nonlocal interactions that are induced by incompressibility. Similar to the Kraichnan model it has led to an increased understanding of intermittency and anomalous scaling based on applications of field-theory techniques, e.g., where it was shown that the breaking of Galilei invariance by the forcing mechanism is responsible for intermittency [276, 277]. On the other hand instanton calculations [278–282] showed that certain field-force configurations give the dominant contribution to the asymptotic tails of the velocity distribution functions. Efficient numerical techniques [283] have also contributed strongly to determine the scaling spectrum of correlation functions [284, 285]. Nevertheless, the interpretation of the data is still somewhat unclear as the measured scaling behavior might be strongly influenced by different scaling contributions [286].

Here, we employ lattice Monte Carlo methods (see [55, 56] for an introduction) based on the functional integral formulation for classical dynamics [44–46, 234, 287] to determine the scaling

properties in the case where the system is driven to a nonequilibrium steady state. These techniques define a Markov process that leads to an optimal sampling of the functional integral. Since they rely only on the definition of a fundamental microscopic action, Monte Carlo simulations are directly transferable to other systems of interest and are free of any modeling assumptions. Though not directly competitive with conventional time-advancing methods as, e.g. pseudo-spectral or finite-difference methods, Monte Carlo simulations may provide a unique perspective on such important problems as, e.g. intermittency in fully developed turbulence [281]. In view of the well-established anomalous scaling behavior of Burgers' turbulence [48, 286] and the physical picture of the underlying mechanisms for intermittency [277, 279, 281], this provides an ideal setting to test these methods and understand possible systematic effects.

6.1. Random-force-driven Burgers' equation

The random-force-driven Burgers' equation

$$\frac{\partial u}{\partial t} + u\nabla u - \nu_0 \nabla^2 u = f(x,t) \ , \tag{6.3}$$

was originally conceived as a one-dimensional model for compressible hydrodynamic turbulence [288] and provides a useful benchmark setting to test new analytical and numerical methods for real-world turbulence [47, 48]. We will consider the special case where the system is driven by a self-similar Gaussian forcing that is white in time. The two-point correlation function of the stochastic forcing in Fourier space is given by

$$\langle f(k,t) f(k',t') \rangle = 2D_0 |k|^{3-y} \delta(k+k') \delta(t-t') \ , \tag{6.4}$$

where the parameter y determines the relative importance of the stirring mechanism at different scales, and the dimensionful constant D_0 measures its strength. Note, that the definition of the exponent y is chosen in accordance with the literature [260, 261, 265]. While large values of y lead to a forcing that acts predominantly in the infrared (IR), in the opposite case the system is strongly driven in the ultraviolet (UV). Independent of the forcing mechanism, kinematic viscosity ν_0 provides a dissipation scale η and for $\nu_0 \to 0$ the two characteristic scales η, and the finite system size L separate. In that case, the stochastic forcing drives the system into a nonequilibrium steady state, where in the range $\eta \ll k^{-1} \ll L$ the energy flux through wavenumber k behaves as $\Pi_\varepsilon(k) \sim k^{4-y}$. Thus, the parameter y serves to control the type of scaling behavior. Of course, depending on the value of this parameter the character of excitations in the system will be very different. While the large-scale dominated forcing leads to the appearance of coherent shocks (see Fig. 6.1) the short-range correlated regime is characterized by the the absence of such structures.

A particularly interesting scenario was first considered in [289, 290] where it was found that the special choice $y = 4$ for the stirring mechanism induces a constant flux of energy

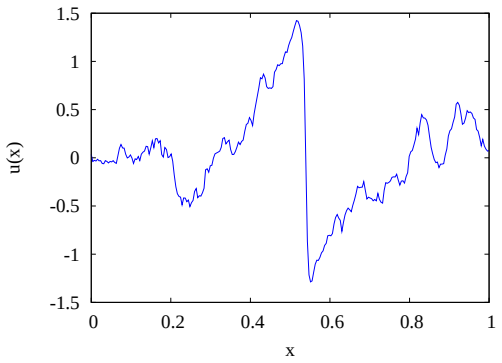

Figure 6.1.: Typical velocity profile $u(x)$ from a simulation on a 254×1024 (space $\times$ time) lattice, where x is taken in units of the spatial lattice size L. The system is forced with equal strength on all scales corresponding to the tuning parameter $y = 4$, where the flux $\Pi_\varepsilon(k) \sim k^{4-y} = \text{const.}$, yielding a Kolmogorov energy spectrum.

$\Pi_\varepsilon \sim$ const. (up to logarithmic corrections) where the interplay of the stochastic forcing and advective term leads to a Kolmogorov energy spectrum $E(k) \sim k^{-5/3}$. The physical picture behind this scenario is the appearance of shocks with a finite dissipative width (see, e.g., Fig. 6.1). The large fluctuations associated with the negative gradient of the front give the dominant contribution to the anomalous scaling of velocity differences $\delta_r u = u(x+r) - u(x)$, where $\langle |\delta_r u|^n \rangle \sim r^{\zeta_n}$, and the scaling exponents $\zeta_n = 1$ for $n \geq 3$ strongly deviate from the Kolmogorov scaling prediction $\zeta_n = n/3$ that follows from a naive dimensional analysis [47, 48]. These rare fluctuations are strongly non-Gaussian and lead to the known asymptotic left tail of the probability distribution function (PDF) for velocity differences $\mathcal{P}(\delta_r u)$ [281].

6.2. Field-theoretic approach

Here, we consider the problem of hydrodynamic turbulence from the functional integral point of view [45, 234, 287]. The functional integral gives a nonperturbative definition of the field theory and thus, it is ideally suited to study the strong and rare fluctuations present in fully developed turbulence that give the main contribution to the high-order moments of velocity differences.

The classical field-theoretic action for the random-force-driven Burgers' equation is obtained via the Martin-Siggia-Rose formalism [44–46, 234, 287]. The construction of the classical action follows the discussion in the previous chapter 5. That is, introducing the auxiliary response field $\tilde{u}$, we obtain the partition function

$$Z \sim \int [d\tilde{u}][du]\; e^{-S} \;, \tag{6.5}$$

with the classical action

$$S = \int_{[t_0,\infty]} dt\, dx \left\{ \tilde{u} \left(\frac{\partial u}{\partial t} + u\nabla u - \nu_0 \nabla^2 u \right) - D_0\, \tilde{u} (-\nabla^2)^{(3-y)/2} \tilde{u} \right\} \;, \tag{6.6}$$

where the quadratic noise term $\sim \tilde{u}|\nabla|^{3-y}\tilde{u}$ models the fluctuations that are put into the system by the stochastic forcing (6.4). One might notice the similarity of (6.6) to the field-theoretical action that we derived for Model C. However, here, the noise term yields a fluctuation dissipation relation only in the special case, where $y = 1$. For generic values of $y > 0$, fluctuations are equally important on all scales leading to strong correlations in the system. There is another important difference that distinguishes the dynamics from the case of the relaxational models that we considered in the previous chapter. It is related to the presence of a continuous symmetry. In particular, the action (6.6) is invariant under Galilean boosts, where under an infinitesimal Galilean transformation δ_{G} the fields transform as

$$\delta_{\mathrm{G}} u = \delta v\big(1 - t\nabla u\big) \ , \quad \delta_{\mathrm{G}}\tilde{u} = -\delta v\, t\nabla u \ , \tag{6.7}$$

with the corresponding real infinitesimal parameter δv. It is this symmetry that essentially determines the phenomenology of the system and leads to the complex scaling behavior [265, 277]. Note, that the functional integral is defined for the Wick-rotated field $\tilde{u} \to i\tilde{u}$ which yields an action that is bounded from below.

The classical action (6.6) is well-suited for analytic calculations where the auxiliary field is introduced to compute real-time correlation functions, e.g., response functions to some external perturbation. However, in the form (6.6) the action is hard to handle via lattice Monte Carlo techniques, where the additional phase factor $\sim i\tilde{u}(\partial u/\partial t + \cdots)$ leads to a poor importance sampling. Instead, we may integrate out the auxiliary field which yields the modified action

$$S = \frac{1}{4D_0}\int_{[t_0,\infty]} dt\, dx\, \left(\frac{\partial u}{\partial t} + u\nabla u - \nu_0\nabla^2 u\right)(-\nabla^2)^{-(3-y)/2}\left(\frac{\partial u}{\partial t} + u\nabla u - \nu_0\nabla^2 u\right) \ , \tag{6.8}$$

depending only on the physical field u. It defines a positive definite probability distribution functional, which may by sampled via Monte Carlo methods. We emphasize that we keep the initial time t_0 dependence in the following. This is of course necessary for practical reasons, since any numerical simulation must be carried out on a finite size system. In that case, it is an important question if the class of initial states that one is studying lies in the domain of attraction of the nonequilibrium steady state, since for generic initial conditions the system will typically relax to equilibrium after a short amount of time. The stochastic forcing mechanism is provided exactly for this reason – independent of the initial conditions it should always drive the system to the steady state. We will comment on the effect of the initial conditions in later sections when we consider the scaling behavior of correlation functions.

6.3. Scaling regimes

The classical action (6.6) depends on a single dimensionless coupling constant

$$g_0^2 = \frac{D_0}{\nu_0^3\Lambda^y} \ , \tag{6.9}$$

defined at the ultraviolet scale Λ, which is given in terms of the dimensionful force amplitude D_0 and the kinematic viscosity ν_0. It naturally appears in a perturbative treatment of the problem (see, e.g., [260]), where one typically considers the following rescaling of the fields

$$t \to \nu_0 t \ , \quad u \to (\nu_0/D_0)^{1/2} u \ , \quad \tilde{u} \to (D_0/\nu_0)^{1/2} \tilde{u} \ , \tag{6.10}$$

to endow the nonlinear interaction term $\sim \tilde{u}(u\nabla u)$ in (6.6) with the coupling g_0. Apart from the coupling constant g_0^2, the ratio between the lattice scale Λ and the infrared cutoff $1/L$ defined by the inverse lattice size provides for a second dimensionless quantity that we may control. Eventually, we will be interested in the scaling behavior of correlation functions in the range between $1/L \ll k \ll \Lambda$, where both limits $\Lambda \to \infty$ and $L \to \infty$ are taken at the end. Depending on the values of the renormalized coupling in the limit where both cutoffs are removed one might expect different fixed point solution that lead to a universal scaling behavior. Here, we give an overview on the dimensional scaling predictions:

Let us consider the simplest scenario first, where $g_0^2 = 0$. In particular, we may identify this limit with the situation where the dimensionful force amplitude vanishes. The only dimensionful parameter left is the kinematic viscosity which is assumed to take a nonvanishing finite value, $\nu_0 \neq 0$. From dimensional analysis we infer the possible infrared scaling behavior

$$\langle \delta_r u \rangle \sim \nu_0 r^{-1} \ , \tag{6.11}$$

for the first-order moment of field differences $\delta_r u = u(x+r) - u(x)$. At small-scales the effect of a finite viscosity leads to nonuniversal behavior where the properties of fluctuations strongly depend on the dissipative mechanism.

Keeping $g_0^2 = 0$ we inquire about the limit $\nu_0 \to 0$ where the viscous scale is removed. Here, we leave the infrared cutoff L finite and consider $L \to \infty$ only in the end. The situation is very different from the naive expectation – the presence of a dissipative anomaly [277] implies that removing the viscosity from the system still produces a finite effect. Thus, the mean dissipation rate $\varepsilon \sim \langle u^2 \rangle^{3/2}/L$ is nonzero in the $\nu_0 \to 0$ limit and defines a characteristic ultraviolet scale $\eta = (\nu_0^3/\varepsilon)^{1/4} \to 0^+$. Together with the infrared scale L this defines an intermediate region $\eta \ll k^{-1} \ll L$ where the assumption of scaling by dimensional analysis then leads to following behavior for velocity differences:

$$\langle \delta_r u \rangle \sim (\varepsilon r)^{1/3} \ . \tag{6.12}$$

This is simply the Kolmogorov scaling assumption that was used to derive the scaling spectrum of higher order moments for incompressible Navier-Stokes turbulence, i.e., $\langle (\delta_r u)^n \rangle \sim r^{\zeta_n}$, $\zeta_n = n/3$. From the second-order moment we obtain Kolmogorov's prediction for the energy spectrum

$$E(k) \sim k^{-5/3} \ , \tag{6.13}$$

in the scaling region $\eta \ll k^{-1} \ll L$. If we assume that this scaling solution indeed corresponds to a fixed point of the RG, then it must be characterized by stationarity. Since the dissipative

anomaly leads to a finite dissipation in the UV the scale-invariant solution describes a flux state, where one observes a constant flux of energy $\sim \varepsilon$ from the infrared to the ultraviolet.

If the coupling g_0^2 is nonzero, the forcing essentially controls the scaling properties of the fluid and we obtain

$$\langle \delta_r u \rangle \sim D_0^{1/3} r^{-1+y/3} \ , \tag{6.14}$$

from power counting. It is important to emphasize, that this result implies that the viscous scale is removed $\nu_0 \to 0$, to leave the single dimensionful parameter D_0. Let us consider the associated energy spectrum for this particular scaling solution. From the Fourier transform of the second moment, we obtain

$$E(k) \sim D_0^{2/3} k^{1-2y/3} \ , \tag{6.15}$$

which depends on the continuous parameter y. In particular, in Ref. [261] it was observed that (6.15) yields a Kolmogorov energy spectrum if $y = 4$. While this result has been motivated by perturbative renormalization group calculations, the existence of such a scaling solution has been put to doubt [265]. The essential problem concerns the role of infrared divergences that have to be controlled when the limit $L \to \infty$ is taken.

Of course, the given scaling scenarios simply follows from dimensional analysis and one must assume that the scaling is modified by anomalous dimensions of the corresponding operators. This applies in particular to the high order moments $\langle (\delta_r u)^n \rangle$ where both experiments and numerical simulations indicate strong intermittency effects. Also, the presence of a finite regulator in the IR may manifest itself in additional L-dependent scaling corrections. In fact, it is these scaling corrections, and the subtle interplay between the different scaling regions that makes it in practice quite difficult to extract scaling exponents under realistic conditions.

6.4. Lattice theory

The theory is defined on the sites of a regular space-time lattice. This way, we impose an ultraviolet cutoff that eliminates the details of those processes occurring deep in the dissipative regime. The measure in the functional integral (6.5) is then given by $[du] \to \prod du_{x,t}$, where $u_{x,t}$ define the site variables, and the action in (6.8) needs to be discretized appropriately. For that purpose, we replace the dynamics with a finite-difference equation using the backward-time discretization

$$\frac{\partial u}{\partial t} + u\nabla u - \nu_0 \nabla^2 \ \to \ \frac{1}{a_t}\left(u_{x,t} - u_{x,t-1}\right) + u_{x,t-1}\hat{\nabla} u_{x,t-1} - \nu_0 \hat{\nabla}^2 u_{x,t-1} \ , \tag{6.16}$$

where a_t denotes the lattice spacing in the time-direction and $\hat{\nabla}$ defines the lattice derivative operator. Eq. (6.16) corresponds to a causal propagation forward in time according to the Itō prescription. With this choice, it is safe to ignore the functional determinant that arises in the derivation of the classical-statistical action (6.6) (see the related discussion in Sec. 5 of

the previous chapter). The discretized action takes the form

$$\begin{aligned} S &= a_t \sum_t a_x^2 \sum_{x,x'} \left(\frac{1}{a_t} \left(u_{x,t} - u_{x,t-1} \right) + u_{x,t-1} \hat{\nabla} u_{x,t-1} - \nu_0 \hat{\nabla}^2 u_{x,t-1} \right) \\ &\quad \times D^{-1}_{x,x'} \left(\frac{1}{a_t} \left(u_{x',t} - u_{x',t-1} \right) + u_{x',t-1} \hat{\nabla} u_{x',t-1} - \nu_0 \hat{\nabla}^2 u_{x',t-1} \right) \ , \end{aligned} \tag{6.17}$$

given in units of the system size, where D^{-1} defines the inverse force spectrum (and includes the force amplitude D_0). So far, we have not specified the discretization for the spatial derivative. Here, we will consider the following choice

$$\hat{\nabla} u_{x,t} = \frac{1}{2a_x} \left(u_{x+1,t} - u_{x-1,t} \right) \ . \tag{6.18}$$

It is necessary to map the discretized theory to its continuum counterpart and one has to ensure that the parameters are well-defined in the continuum limit. For that purpose the kinematic viscosity is identified with $\nu_0 = \hat{\nu}_0 \, a_x^2 / a_t$ where $\hat{\nu}_0$ is the bare viscosity in lattice units, and the Reynolds number scales as $\mathrm{Re} \sim \nu_0^{-1}$. Furthermore, we have to ensure that the relevant scales of the system are resolved. In particular, we have to ensure that the dissipation scale fits on the lattice, i.e. $\eta = \mathrm{Re}^{-3/4} L \gtrsim a_x$ where L is the IR scale present in our system as a consequence of the finite lattice size. One may immediately recognize that this imposes a hard constraint on the realization of lattice simulations – fully developed turbulence, in the limit $\mathrm{Re} \to \infty$ requires a large computational effort where the number of lattice sites in the intermediate scaling regime increases as $L/\eta \sim \mathrm{Re}^{3/4}$, for given L. In practice, we are therefore bound to work at nonzero viscosity ν_0.

Let us point out, that the choice of discretization is a subtle issue for real-time dynamics. While an appropriate discretization in time is important for the cancellation of the functional determinant, it also controls the character of physical solutions to the dynamics. In fact, this is well-known from the direct numerical solution of first order partial differential equations, where certain discretization schemes simply do not yields globally regular solutions. The most prominent example for such a behavior is the forward-time centered-space discretization (FTCS) scheme for the linear advective equation (see, e.g., [291]). On the other hand, other discretizations may provide a dynamics that is conditionally stable, depending on the choice of the parameters in the problem. These observations are typically based on a linear stability analysis of the equations of motion and cannot be applied to nonlinear systems. However, we find that a similar constraint applies for our choice of discretization. In particular, the dynamics is only conditionally stable which relates to the value of the lattice viscosity. If the lattice viscosity is chosen to be larger than $\hat{\nu}_0 \simeq 1/2$ the dynamics will always feature instabilities. In fact, this particular bound is well understood from a similar discretization of the diffusion equation [291]. This immediately poses the question if these problems may be overcome by using implicit time-differencing schemes as one usually applies for direct numerical solvers of partial differential equations (see, e.g., [292]). In what sense such discretizations are optimal and may lead to unconditionally stable dynamics is left for future work.

6.5. Lattice Monte Carlo methods for classical-statistical dynamics

In this work two different types of algorithms are employed, an improved overrelaxation algorithm [293, 294] and a variant of the Hybrid Monte Carlo algorithm [295]. While both have been discussed at length in the literature in the context of equilibrium systems, we explain necessary adaptions and their application for simulations of classical-statistical dynamics in the presence of a stochastic driving term.

6.5.1. Overrelaxation algorithm

Depending on the specific discretization of the classical action or the type of real-time dynamics that one considers different lattice Monte Carlo algorithms may be applicable. In particular, it is possible to apply a local overrelaxation algorithm in the case where the discretized action assumes a multiquadratic form [293, 294, 296] for which specific improvements have been shown to reduce relaxation times significantly [297–299].

For the case of the discretized action for Burgers' equation (6.17) it is possible to define the single-site action in the following form

$$S_{\text{single-site}} = \beta(u_{x,t} - \mu)^2 + c \ , \tag{6.19}$$

where the coefficients β, μ, and c are in general complicated functions of the field variables, excluding the field value on the updated lattice site, e.g., $\mu = \mu\big(\{u_{x',t'}\}_{(x',t')\neq(x,t)}\big)$. This relies on the particular discretization, where the advective term is defined as

$$u_{x,t}\hat{\nabla}u_{x,t} = u_{x,t}\frac{u_{x+1,t} - u_{x-1,t}}{2a_x} \ . \tag{6.20}$$

Any other choice, where $u_{x,t}\hat{\nabla}u_{x,t}$ contains contributions that are quadratic in the fields $\sim u_{x,t}^2$ will lead to a more complicated action and cannot be treated by this procedure.

Writing the classical action in the form (6.19) the functional integral is sampled by applying a heatbath with effective temperature $\sim \beta^{-1}$ locally to each single-site variable $u_{x,t}$. Thus, we obtain the transition probability $P(u'_{x,t}|\{u_{x',t'}\})$ for $u_{x,t} \mapsto u'_{x,t}$ while keeping the other field values fixed. The newly updated field value is given by

$$u'_{x,t} = \mu + \sqrt{2\beta^{-1}}\,\xi \ , \tag{6.21}$$

where ξ implements the unit variance Gaussian noise. A single Markov step is composed of a complete update of all lattice sites.

The overrelaxation algorithm defines a particular improvement of the heatbath procedure, where the introduction of an additional relaxational parameter ω yields the transition probability $P_\omega\big(u'_{x,t}\,|\,\{u_{x',t'}\}\big)$, with the suggested field value

$$u'_{x,t} = \omega\mu + (1-\omega)u_{x,t} + \sqrt{2\beta^{-1}}\,\xi \ . \tag{6.22}$$

Here, the parameters μ and β are determined from the single-site action (6.19), while the parameter ω can be chosen freely in the range $0 < \omega < 2$. Of course, choosing $\omega = 1$ simply corresponds to the heatbath algorithm (6.21). However, setting the relaxational parameter $\omega \simeq 2$ has been shown to significantly reduce relaxation and autocorrelation times [297–299]. This corresponds to an "overshooting" of the naively expected optimal value μ, which defines the minimum of the single-site action (6.19).

Here, we have implemented a variant of this algorithm where the parameter ω is adapted iteratively during the Markov process, corresponding to the so-called Chebyshev acceleration [300], i.e.,

$$\omega_{n+1} = \begin{cases} 1 \;, & n = 0 \;, \\ \left(1 - (\rho^2/2)\,\omega_n\right)^{-1} \;, & n = 1 \;, \\ \left(1 - (\rho^2/4)\,\omega_n\right)^{-1} \;, & n \geq 2 \;. \end{cases} \tag{6.23}$$

$n \geq 0$ is a discrete index and labels the number of Markov steps, while the tuning parameter is fixed to some value in the range $0 \leq \rho^2 < 1$. In our simulations, we have set $\rho^2 \simeq 0.9999$. Note, that one might achieve better performance if the relaxation parameter is adapted only after a certain number $n_{\text{Chebyshev}}$ of Markov steps, while keeping its value fixed in between. We have found $n_{\text{Chebyshev}} \simeq 50$ to be an optimal choice.

6.5.2. Improved Hybrid Monte Carlo algorithm

While the overrelaxation algorithm decreases the characteristic relaxation time of the Markov process, it might not be the best choice for an efficient sampling of configurations if the action is nonlocal. In such a case, it might take a large number of Monte Carlo steps to produce a new statistically independent field configuration. This applies in particular to the case of hydrodynamic turbulence where the forcing mechanism strongly couples the degrees of freedom on all scales. Furthermore, since the range of applicability of the overrelaxation algorithm was strongly constrained by the discretization prescription, it might be useful to consider alternative methods that are generally applicable. What we want is an algorithm that updates field configurations globally and takes large steps through configurations space, while it should both feature short relaxation times and decrease the autocorrelation of measured observables.

An algorithm that was developed exactly for this purpose is the Hybrid Monte Carlo (HMC) [295, 301]. It was originally introduced for computations in lattice QCD involving dynamical fermions where the nonlocality arises from the inclusion of the fermion determinant (see, e.g., [302]). It is particularly well-suited as it allows for specific improvements to control the performance of the algorithm, e.g., mass preconditioning [303, 304], multiple time-scale integration [305], and preconditioning techniques [306, 307].

The HMC algorithm is based on the idea that the fields on the lattice should be updated

according to fictitious Hamiltonian

$$H_{\text{eff}} = \frac{1}{2}\sum_{x,t} \pi_{x,t}^2 + S(u) \ , \tag{6.24}$$

where the set of conjugate momenta $\pi_{x,t}$ are introduced. The effective Hamiltonian H_{eff} defines the generator for the fictitious time-evolution on an extended phase space $(u, \pi) \in \Xi$ and can be used to efficiently suggest new field configurations via a Molecular Dynamics (MD) update that integrates Hamilton's equations of motion:

$$\frac{\partial u}{\partial \tau} = \frac{\partial H_{\text{eff}}}{\partial \pi} = \pi \ , \qquad \frac{\partial \pi}{\partial \tau} = -\frac{\partial H_{\text{eff}}}{\partial u} = -\frac{\partial S}{\partial u} \ . \tag{6.25}$$

That is, starting from a given initial state (u, π) at initial time $\tau = 0$, eq. (6.25) defines a trajectory on the constant energy surface $H_{\text{eff}} = \text{const.}$ to (u', π') at final time τ. The MD time evolution of this system preserves the measure and is exactly reversible. It therefore satisfies the basic criteria for a Markov chain Monte Carlo update [55, 302]. In practice, any integration routine will proceed by evaluating the MD time evolution on a finite number of time steps $\tau_n = n\Delta\tau$, $n = 0, \ldots, n_{\text{steps}} - 1$, $\Delta\tau = \tau / n_{\text{steps}}$, thereby introducing a systematic error that is important to control. To avoid a necessary extrapolation to smaller stepsizes, thereby ruling out any systematic errors in the calculated observables, the newly suggested configuration is subjected to a final Metropolis acceptance step. This gives a penalty to those configurations that lead to a strong violation of energy conservation, i.e., $\delta H_{\text{eff}} = H_{\text{eff}}(u', \pi') - H_{\text{eff}}(u, \pi)$, such that on the average $\langle e^{-\delta H_{\text{eff}}} \rangle = 1$.

While the Molecular Dynamics procedure certainly provides for candidate configurations that are far from the starting point, it is not ergodic since the dynamics takes place only on the $H_{\text{eff}} = \text{const.}$ hypersurface. It updates the system according to the microcanonical ensemble, while we want to sample the canonical distribution $\sim e^{-H_{\text{eff}}}$. Of course, this restriction is easy to circumvent – we simply update the conjugate momenta regularly, after performing an MD update. This defines a fully ergodic algorithm with the desired fixed point distribution.

The HMC is built out of the following steps:

- A *momentum update* where the conjugate momenta are drawn from a Gaussian distribution with unit variance, i.e., $P(\pi) \sim e^{-\sum \pi_{x,t}^2/2}$.
- *Molecular Dynamics (MD) update* according to an approximate integrator

  $$T(\tau) : (u, \pi) \mapsto (u', \pi') \ , \tag{6.26}$$

  that should be area-preserving

  $$\det \frac{\partial(u', \pi')}{\partial(u, \pi)} = 1 \ , \tag{6.27}$$

  and satisfy reversibility, $R \circ T(\tau) \circ R \circ T(\tau) = 1$, where $R : (u, \pi) \mapsto (u, -\pi)$ describes a reversal of the conjugate momenta.

- *Metropolis accept/reject step* given by the conditional acceptance probability

$$P_{\rm acc}(u',\pi'|u,\pi) = \min\left(1, e^{-\delta H_{\rm eff}}\right) . \tag{6.28}$$

  This final step makes the Hybrid Monte Carlo an exact algorithm free of systematic stepsize errors.

Thus, a single HMC update is given by

$$\left(u',\pi'\right) = \Big(R\circ T(\tau)\,\theta(e^{-\delta H_{\rm eff}} - r) + \mathbb{1}\,\theta(r - e^{-\delta H_{\rm eff}})\Big)\,(u,\pi) \ , \tag{6.29}$$

where r is a random number drawn uniformly in the region $r \in [0,1]$, and the θ-functions implement the Metropolis accept/reject step. Note, that the final reversal of the momenta applies only in the case if the suggested configuration is accepted.

Any practical implementation of this algorithm will have to provide an integration scheme $T(\tau)$ that solves for the MD trajectory. A large class of integrators that preserve the measure and satisfy reversibility are the symmetric symplectic integrators [308]. These integrators are built on the observation that from the decomposition $H_{\rm eff} = H_1 + H_2$ of the effective Hamiltonian (6.24), where $H_1 = H_1(\pi)$ and $H_2 = H_2(u)$ denote the momentum and field-dependent part, one may construct a single update by a symmetric combination of operators

$$T_1(\Delta\tau) : (u,\pi) \mapsto \left(u + \Delta\tau\frac{\partial H_1}{\partial \pi}, \pi - \Delta\tau\frac{\partial H_1}{\partial u}\right) = \left(u + \Delta\tau\pi, \pi\right) , \tag{6.30}$$

$$T_2(\Delta\tau) : (u,\pi) \mapsto \left(u + \Delta\tau\frac{\partial H_2}{\partial \pi}, \pi - \Delta\tau\frac{\partial H_2}{\partial u}\right) = \left(u, \pi - \Delta\tau\frac{\partial S}{\partial u}\right) . \tag{6.31}$$

A simple example for such an integrator is the single-level Strömer-Verlet (leapfrog) method [291], where a symmetric integration

$$T(\tau) = \left[T_1(\Delta\tau/2)T_2(\Delta\tau)T_1(\Delta\tau/2)\right]^{n_{\rm steps}} , \tag{6.32}$$

is performed. This scheme preserves the energy to order $\mathcal{O}(\Delta\tau^2)$ in the stepsize, and improves on the naive application of $T(\tau)$ without such a decomposition, which yields an $\mathcal{O}(\Delta\tau)$ stepsize error. Higher-order integrators $\mathcal{O}(\Delta\tau^n)$ apply multiple steps and quickly increase in complexity. If the computations required to determine $\partial S/\partial u$ are very expensive it might be better to use a lower level integrator. Here, we adopt the two-level Omelyan integrator

$$T(\tau) = \left[T_1(\lambda\Delta\tau)T_2(\Delta\tau/2)T_1\big((1-2\lambda)\Delta\tau\big)T_2(\Delta\tau/2)T_1(\lambda\Delta\tau)\right]^{n_{\rm steps}} , \tag{6.33}$$

which reduces the coefficient of the $\mathcal{O}(\Delta^2)$ stepsize errors observed with the leapfrog integrator by an appropriate tuning of the parameter λ, where the standard value based on optimization criteria is $\lambda \simeq 0.1932$ [309]. A standard check for the numerics is to see if reversibility is satisfied. Furthermore, energy conservation should hold on average, i.e., $\langle e^{-\delta H_{\rm eff}}\rangle = 1$. Both these criteria are met by our implementation of the algorithm.

With the basic HMC algorithm introduced, let us ask about its properties when applied to classical-statistical systems with a stochastic forcing acting on all scales. A useful quantity

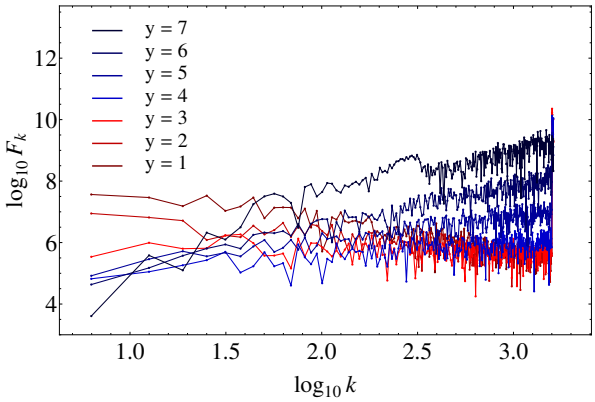

Figure 6.2.: Molecular Dynamics (MD) force spectrum $|F_{k,t}| = |\partial S/\partial u_{k,t}|$ computed in the stationary regime of the Markov chain Monte Carlo. The force spectrum is measured on a 512×1024 lattice (space $\times$ time) as a function of lattice momentum k for different choices of the power-law spectrum (6.4) given by the exponent y. The time-averaged forces scale as $\overline{|F_{k,t}|} \sim k^{(y-3)/2}$.

that one may employ to monitor the performance of the algorithm is the contribution $F = -\partial S/\partial u$ to the equations of motion (6.25). Typically, the system will strongly emphasize certain modes, while others are slowed down in comparison. This is illustrated in Fig. 6.2 where we show a typical sample of single-time measured MD forces $|F_{k,t}|$ in the Fourier representation for a fixed value of the physical time t in a single configuration. Clearly, the power-law forcing induces strong variations in the MD spectrum, where $\overline{|F_k|} \sim k^{(y-3)/2}$ on average, for $y = 1, \ldots, 7$. What is even more striking are the strong fluctuations induced by the real-time dynamics which cover a range of roughly two orders of magnitude. This makes the numerical solution quite demanding as the integrator has to tackle the different scales and avoid possible instabilities [310] triggered by a large values of the stepsize $\Delta\tau$. In fact, a naive application of the HMC will not work unless the stepsizes are chosen extremely small, which might stabilize the integrator but slows down the dynamics considerably.

Fortunately, there is a well-known technique that addresses this problem which is known as Fourier acceleration [311, 312]. It suggests an alternative MD update adapted to the situation where certain modes are strongly emphasized by the dynamics, which is based on the modified effective Hamiltonian

$$H_{\text{eff}}^{\text{FACC}} = \frac{1}{2} \sum_{x,x';t} \pi_{x,t} \Omega_{x,x'} \pi_{x',t} + S(u) \ . \tag{6.34}$$

This choice yields an improved sampling of the conjugate momenta, and adapts the stepsizes in the Molecular Dynamics to the force strength for a given mode. This is best illustrated by writing the equations of motion in this case

$$\frac{\partial u_k}{\partial \tau} = \Omega_k \pi_k \ , \qquad \frac{\partial \pi_k}{\partial \tau} = -\frac{\partial S}{\partial u_k} \ , \tag{6.35}$$

and performing the rescaling $\pi_k \to \Omega_k^{1/2} \pi_k$ and $\tau \to \Omega_k^{1/2} \tau$, which yields a trajectory length

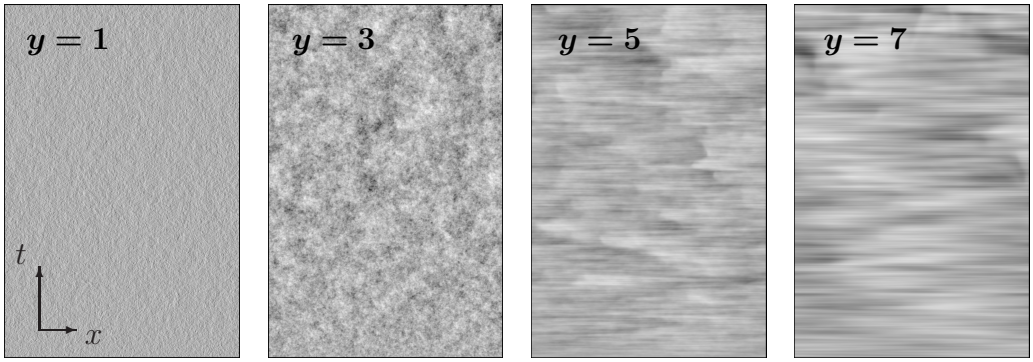

Figure 6.3.: Typical configurations (512×1024 lattice) generated for different values of the tuning parameter y chosen between the ultraviolet ($y \simeq 1$) and infrared dominated regime ($y \simeq 7$), with increasing values from left to right. A transition in the qualitative behavior of the configurations is clearly visible.

that is effectively momentum-dependent. In practice, Ω_k should be chosen such that it compensates for the strong fluctuations that are put into the physical field u by the stochastic forcing mechanism. In particular, we might choose $\Omega_k \sim \overline{|F_k|}^{-1/2}$ which accounts for the overall scale-dependence. However, we still have to deal with the strong fluctuations that are due to the real-time evolution of the system and may trigger an instability for the integrator. We therefore adapt Ω_k after each Markov step iteratively, where $\Omega_{k,t} = |F_{k,t}|^{-1/2}$ up to some proportionality factor that is related to the overall trajectory length. This stabilizes the HMC and enables simulations for any choice of stochastic forcing. We should point out, that a field-dependent Ω adapted at each step in the Markov process might alter the convergence properties of this HMC algorithm. In practice, one must certainly check if the right fixed point distribution is sampled.

With these observations we have chosen to implement an adaption of the HMC which is local in time but global in spatial dimension with a field-dependent sampling of the conjugate momenta. This requires a even-odd type update for the fields in the physical time direction. Such a quasi-local HMC enables us to monitor the behavior of the algorithm and check its performance for real-time dynamics of classical-statistical systems. The presented adaptions at the example of the overrelaxation algorithm and the HMC have proven to be sufficient to yield a stable algorithm for stochastic driven system. However, it is worth noting that it is not clear if a quasi-local algorithm (in time) is a necessary requirement to efficiently sample configurations for these systems. Also, while the suggested Fourier acceleration is absolutely mandatory for the stability of the HMC there is no such constraints for the overrelaxation algorithm. In fact, it has been shown that the overrelaxation algorithm is competitive with a stochastic optimal Fourier accelerated Langevin-type algorithm [294]. This might explain why the overrelaxation method performed so well without any significant amount of tuning necessary.

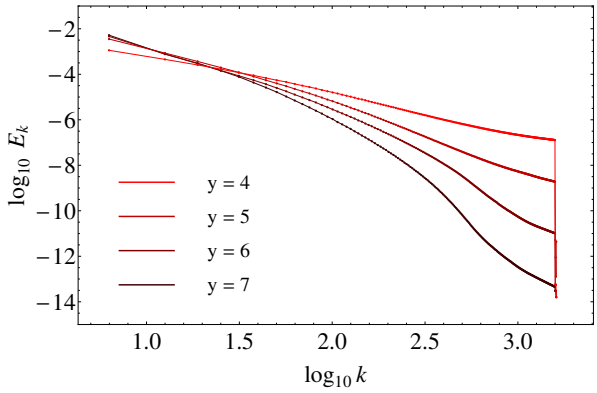

Figure 6.4.: Log-log plot of the energy spectrum $\langle E_k \rangle = \langle |u_k|^2 \rangle$ for different values of the tuning parameter y with the stochastic forcing acting on all scales. Around $y_c \simeq 6$ we observe a transition, where the ultraviolet scaling behavior is not dominated by the power-law forcing. The spectra were measured on a lattice size of 512×1024 (space $\times$ time).

6.6. Scaling behavior far from equilibrium

Here, we comment on the results obtained with the above introduced Monte Carlo techniques. Results obtained with the local overrelaxation algorithm focused on the special case where the power-law forcing leads to a Kolmogorov-type energy spectrum. These simulations have produced a significant amount of data, with a sample size, consisting of roughly $\mathcal{O}(10^6)$ configurations. Such a data set is sufficient to capture the rare fluctuations that give the dominant contribution to high order moments, $\langle (\delta_r u)^n \rangle$ up to 5th order. The HMC in contrast has so far been tested mainly for its stability and algorithmic improvements and has produced only a relatively small sample of $\mathcal{O}(10^4)$ configurations. Nevertheless, even on such a small sample size we may draw conclusions based on the energy spectrum and a possible transition to universal scaling behavior. With these simulations we have explored the complete region from the IR to the UV dominated regime, and we can in particular ask about the mechanism underlying the transition to the universal scaling behavior of small-scale fluctuations.

6.6.1. Transition to the large-scale forcing dominated regime

Forcing the system at equal strength over a wide range of scales will strongly affect the scaling properties of correlation functions measured in the intermediate range of scales $1/L \ll k \ll \Lambda$. This can already be seen at the example of typical configurations generated by the Markov chain Monte Carlo, where the characteristics of the stochastic forcing are changed by tuning the value of the exponent y, see Fig. 6.3. The system shows vastly different behavior going from the regime where only thermal noise is present ($y = 1$) to the IR dominated regime where coherent large-scale excitations dominate the flow.

Tuning the spectral characteristics of the forcing mechanism one might expect that beyond some finite value y_c the high-momentum modes will not be affected too much, while the IR behavior is still dominated by the Gaussian forcing. Here, for the case of the one-dimensional Burgers' equation, we see an indication for such a behavior when we examine the energy spectrum of the system for different values of y, Fig. 6.4. Beyond the value of $y_c \simeq 6$ the overall energy drops exponentially in the UV and the functional form is no longer determined by the power-law behavior of the stochastic forcing mechanism. In fact, this has an important consequence for the UV scaling properties of the fluid. In such region the scaling properties of small-scale fluctuations might exhibit universality. In fact, such a behavior was demonstrated in the case of the three-dimensional incompressible Navier-Stokes equation [313, 314], where a similar transition was observed also on the level of the scaling exponents ζ_n for moments of velocity differences.

6.6.2. Kolmogorov scaling in Burgers' equation

Here, we want to focus on the special case where the forcing spectrum is chosen to produce the Kolmogorov-type scaling (corresponding to the exponent $y = 4$ for the stochastic power-law forcing). We evaluate moments of velocity differences $\langle|\delta_r u|^n\rangle$ over an ensemble of configurations generated by the Markov chain Monte Carlo procedure. This analysis relies on the Monte Carlo data generated by the overrelaxation algorithm, where a sufficiently large sample of 5×10^5 statistically independent field configurations was gathered. For every configuration we measure velocity differences from a randomly chosen starting point. This dramatically reduces autocorrelations for our sample. In Fig. 6.5 we show, as an example, the 5th order structure function calculated for an ensemble from a 254×1024 lattice simulation. To determine the scaling range *a priori* is difficult, and a well-known problem in the literature (see, e.g., [49]). Here, we employ a working definition where it is defined as the range of scales that minimizes the χ^2 of a linear least-squares (LLS) fit to the fifth order structure function in the log-log plot. The corresponding region is indicated in Fig. 6.5. For comparison we have included the values of the local slope (evaluated over three consecutive space points) in the inset. We identify a plateau where the local exponents are nearly constant – this defines the value of the scaling exponent for the given moment $\langle|\delta_r u|^5\rangle$. We obtain the scaling spectrum (Fig. 6.5) where the error bars given are those of the LLS fit in the scaling range. Clearly, the $n = 5$ data point in Fig. 6.5 has minimal error which follows simply from our definition of the scaling range. We see that the scaling exponents are close to the bifractal scaling prediction [47, 48], and within error bars agrees with the results of [286], obtained at high spectral resolution.

We should point out that in general, with this method, we cannot rule out subleading terms or possible logarithmic corrections that may influence the scaling behavior [286, 313, 314]. In fact, such a situation is very likely and can lead to the appearance of multiscaling, corresponding to a continuous set of independent scaling exponents ζ_n [286] While in principle

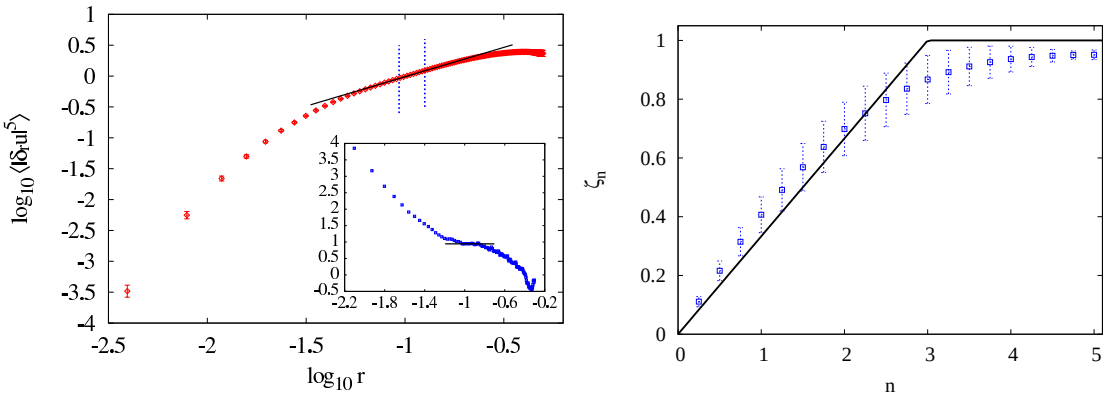

Figure 6.5.: (**Left**) Log-log plot of 5th order moment $\langle|\delta_r u|^5\rangle$ with a linear scaling function plotted for comparison ($y = 4$). The vertical bars indicate the region for the extraction of scaling exponents, while the inset shows the local slopes versus r. (**Right**) Scaling exponents ζ_n for nth order moment $\langle|\delta_r u|^n\rangle$ versus n. The black curve indicates the bifractal scaling prediction [48, 48].

these contributions should be taken into account for the accurate determination of the scaling behavior, in practice it is difficult to distinguish different types of scaling contributions without any further assumptions. Since we are dealing with a finite system both in space and time one may also expect finite size effects. In our simulations we have chosen periodic boundary conditions in space and a zero initial state with a free boundary at final time. For a space-time lattice of infinite extent the probability measure defines a stationary process at sufficiently late times, i.e., correlation functions will only depend on time differences. We have checked this property explicitly in our analysis – sufficiently far from the initial state the system is approximately in a stationary state.

We also check the statistics for velocity differences directly on the level of the probability distribution functions $\mathcal{P}(\delta_r u)$. This gives valuable qualitative information on the physical behavior in our simulations of Burgers' turbulence. In Fig. 6.6 we show the PDF of velocity differences for a set of values of the separation r, where we use the dimensionless variable $\phi = \delta_r u/\langle(\delta_r u)^2\rangle^{1/2}$ to quantify the fluctuations. At large scales, far from the inertial range we clearly recognize the effects of the random Gaussian forcing (red). In the dissipative region the left tail of the PDF is especially pronounced and captures the strong fluctuations described by the shocks (orange). For separations $\eta \ll r \ll L$ in the inertial range we see that the PDF $\mathcal{P}(\delta_r u)$, plotted for three different values of r, nicely collapse onto each other (blue). In particular, in the regime where the fluctuations are much smaller than the root-mean-square velocity $|\delta_r u| \ll u_{\mathrm{rms}}$ (generated by the stochastic forcing mechanism), the PDF of velocity differences has a universal scaling form

$$\mathcal{P}(\delta_r u) = r^{-z} f(\delta_r u/r^z) \ , \tag{6.36}$$

where z is the dynamic exponent and $f(u/r^z)$ is a scaling function for the PDF. In the asymptotic region $-\delta_r u/r^z \gg 1$ where $\delta_r u < 0$ we expect the algebraic scaling $\mathcal{P}(\delta_r u) \sim$

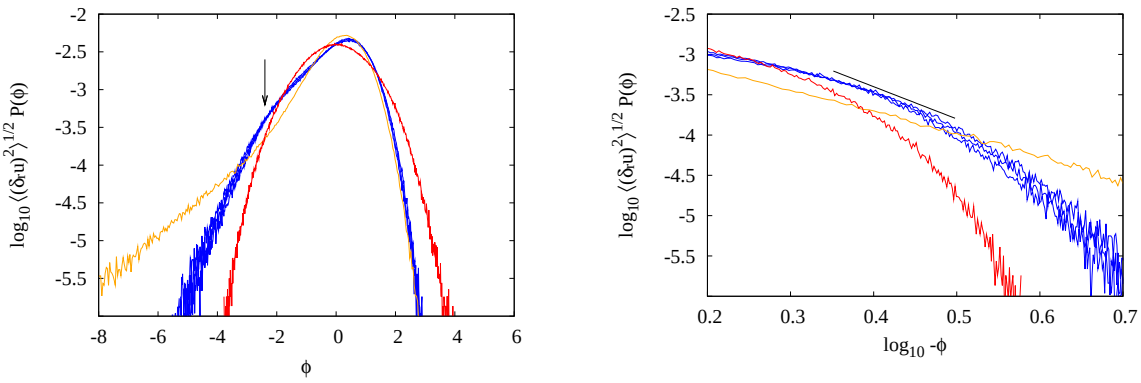

Figure 6.6.: Probability distribution functions $\mathcal{P}(\delta_r u)$ as a function of the dimensionless variable $\phi = \delta_r u / \langle (\delta_r u)^2 \rangle^{1/2}$ plotted for different values of r ($y = 4$). (**Left**) Collapse of the PDF in the universal regime (blue). In the energy-containing range (red) the fluctuations become Gaussian – the random forcing dominates – whereas in the dissipative regime (orange) fluctuations are strongly enhanced. (**Right**) Scaling region for the left tail of the PDF. The black line indicates the scaling prediction with exponent $\gamma = -4$.

$(\delta_r u)^\gamma$ with exponent $\gamma = -4$ [315]. The relevant region is shown in Fig. 6.6 (indicated by the arrow). The corresponding scaling prediction with exponent $\gamma = -4$ is plotted for comparison as the black slope in Fig. 6.6. Though our statistics are not sufficient to give a tight prediction on the scaling exponent, indications for the conjectured scaling behavior can be inferred from Fig. 6.6.

Finally, let us point out that the presence of the continuous Galilei symmetry in principle requires a gauge fixing to avoid an over counting of physically equivalent field configurations. These additional modes may be eliminated by a Faddeev-Popov procedure [9]. While gauge fixing is unavoidable for generic correlators [316, 317] this is not so for velocity differences $\delta_r u$, as solely considered in this work which are manifestly invariant under Galilean transformations.

6.7. Outlook

Also, we want to give a short remark on some issues that arise when turning to incompressible three-dimensional Navier-Stokes turbulence. It is well-known, that the inclusion of the pressure term is one of the main obstacles in simulations of turbulence, as the requirement of incompressibility introduces strong nonlocal correlations. In the functional integral formulation this leads to a nonvanishing Faddeev-Popov determinant that can be treated by standard procedures (see, e.g., [55]).

Let us finally comment on the possible applications of lattice Monte Carlo methods beyond the results presented in this work. In contrast to direct solvers, Monte Carlo techniques allow

for the simple inclusion of additional constraints in the microscopic action. Applying the importance sampling to such "improved actions" with additional constraints on the dynamics might lead to an efficient sampling of field configurations that contribute significantly to a specific class of observables. This is especially interesting since it was suggested that instanton configurations might play an important role to explain the asymptotic behavior of probability distribution functions and the scaling behavior of high-order moments [278, 280, 281]. A recent direct numerical simulation of the stochastic Burgers' equation [318] applying filtering techniques showed that such instantons might play an important role to describe the large fluctuations in this system. Of course, it remains an interesting questions for future work if it is possible to access such a regime directly via Monte Carlo methods.

6.8. Summary

Here, we have presented a first attempt to access the classical-statistical dynamics described by classical action (6.8) via lattice Monte Carlo methods. We have shown that lattice Monte Carlo simulations of driven nonequilibrium states are possible but require a careful set up. In particular, we have discussed the issue of proper discretization as well as the possible regulation of the dynamics in the context of numerical methods. In that respect, the Burgers' equation provides an ideal setting to test new numerical approaches. We have demonstrated that our simulations are able to reproduce the well-known anomalous scaling for large order moments of velocity differences, where the forcing acts over a wide range of scales and leads to a Kolmogorov energy spectrum. It is important to remark that this is possible without exploiting the integrability property of the Burgers' equation, as was done, e.g., with a fast Legendre transform algorithm in [283, 286]. Thus, Monte Carlo simulations are directly applicable to other physical systems of interest where it is important to have alternative methods at hand to establish nonequilibrium scaling behavior.

An important point, isolated from the numerical efficiency, concerns the role of subleading scaling corrections and their impact on the determination of the scaling spectrum [286, 313, 314]. The dynamics of the Burgers' equation with a power-law forcing induces scaling corrections that lead to a subtle interplay of different types of scaling behavior. A detailed analysis of the data, and the necessary extrapolation to the limits $\Lambda \to \infty$ and $L \to \infty$, certainly requires a thorough understanding of possible scaling contributions aided by, e.g., renormalization group studies.

7. Conclusions

In this thesis we have applied different nonperturbative techniques to determine the scaling behavior of strongly correlated systems near and far from equilibrium. We have shown that the functional renormalization group allows to access important nonperturbative information, from the static scaling behavior near the quantum phase transition of graphene-like systems to real-time scaling properties near thermal equilibrium. We have also established Monte Carlo simulations as a new approach to determine the anomalous scaling behavior of high-order moments in stationary states far from equilibrium.

At zero temperature the ground state properties of many-body systems are essentially determined by strong short-range interactions. Their presence may drive the system to a strongly-correlated state where fluctuations play a dominant role. In this work, we considered a system of spinless fermions on the honeycomb lattice which can be seen as a simple model for suspended graphene. For the low-energy degrees of freedom we found that the theory is adequately described by a $U(2)$ symmetric matrix-Yukawa model, and we discussed the physical relevance of possible order parameters. In particular, we noticed the possibility of two phase transitions – a transition to a nontrivial topological insulator state, as well as a chiral phase transition between the semimetal and charge density wave (CDW)/Kekulé ordered phase. We discussed the critical properties specifically at the chiral phase transition which is effectively described by an NJL-type instability and is characterized by large values of the anomalous dimensions, $\eta_B \simeq 1$ for the order parameter and $\eta_F \simeq 0.25$ for the fermions, indicating the dominance of strong fluctuations. This has been corroborated by an extensive functional renormalization group study of a dynamically bosonized $U(N)$ symmetric Thirring model [319] where for small values of the flavor number a similar behavior was found. Let us comment on possible extensions of this work. It is important to include the unscreened long-range Coulomb interactions that are present at the charge-neutral point and control the presence of the phase transition in suspended graphene. Current experiments do not seem to indicate the transition to a gapped phase, however show that the strong Coulomb interaction leads to a renormalization of the Fermi velocity [36]. It would be interesting to see if the functional renormalization group can capture this behavior. Also, it is important to explore the relation of our results to lattice Monte Carlo simulations of the three-dimensional Thirring model [320, 320, 321] and models including the Coulomb interaction [31–33, 322, 323].

In the second chapter, we analysed the nature of possible multicritical behavior in a $O(N_1) \oplus O(N_2)$ symmetric model without fermions. Here, we determined the fixed points that relate to

multicritical behavior and analysed their corresponding stability regions. The largest critical exponents compare nicely with high-order field theoretic expansions at fixed dimension $d = 3$, or in $\epsilon = 4 - d$, as well as Monte Carlo data [163, 171, 184, 188–193, 206]. However, to capture the subleading scaling behavior requires more sophisticated truncations where we expect in particular a change in the stability regions of the respective fixed point solutions in the (N_1, N_2) phase diagram. It is important to see, if taking into account the field-dependence of the renormalization factors, or going to higher orders in the derivative expansion will provide a clear picture for the nature of the multicritical point of the $N = 3$ model where conflicting results have been published indicating either a bicritical [170, 202, 203] or tetracritical point for the phase diagram [163, 171, 193, 206]. Here, the functional renormalization group may provide a different perspective on the problem. A particularly interesting line of inquiry is the inclusion of fermions. In fact, two competing order parameters naturally occur in the $U(2)$ symmetric matrix-Yukawa model relating to the topological and chiral phase transition. Here, it is interesting to see if the interplay between bosonic and fermionic fluctuations might lead to a different conclusion on the low-temperature regime of the phase diagram, where the two critical lines of the toplogical and chiral transition meet [88].

The presence of conservation laws strongly affects the dynamic scaling behavior, where we have investigated a system consisting of a $O(N)$ symmetric order parameter coupled to an additional conserved density. For the long-time relaxation dynamics near equilibrium we established a new scaling region that describes the anomalous diffusion of a conserved density in the presence of a homogeneous order parameter. Previous studies of this model in the context of the ϵ-expansion produced ambiguous results [40, 42, 220, 221], while more recent work even excluded the existence of such a phase based on the observation of an essential singularity that previous applications of the ϵ-expansion could not resolve [43, 231]. In contrast, we give a clear statement on the existence of this phase using the nonperturbative functional renormalization group that does not rely on such an expansion. This clearly illustrates the importance of nonperturbative functional techniques that take into account the strong correlations in the system. Let us mention that this also allows for a direct approach to theories of fundamental interactions, independent of any assumption concerning their low-energy effective behavior, with possible applications to the dynamic scaling properties at the QCD critical point [229, 324].

In the final chapter, we introduced a new numerical approach to the problem of hydrodynamic turbulence via Monte Carlo simulations. Monte Carlo methods are generally applicable and provide a direct link to other field-theoretical approaches, e.g., based on the functional renormalization group [22, 23, 325]. We have demonstrated that such simulations are possible and lead to the well-known scaling behavior of small-scale fluctuations in the one-dimensional random-force-driven Burgers' equation [286]. This provides an important check of Monte Carlo techniques and furthermore allows a direct and controlled investigation of possible subleading scaling contributions. It is important to separate these systematic effects before considering more complicated models. Although this approach is not the method of choice

for general-purpose studies, it is unique for studying rare and intense structures associated to instantons [278, 280, 281] that dominate the distribution of rare events on the attractor. A recent work based on filtering techniques applied to direct numerical simulations gives a clear indication for the importance these configurations for realistic hydrodynamic flow [318]. For future work, it will be interesting to see if it is possible to introduce an importance sampling to highlight – in a fully non-perturbative way – those configurations that contribute to the tails of the probability distribution functions.

Appendix A.

Definition of propagators

In our calculations we frequently need the full regularized propagator G evaluated in a constant background field. For the inverse regularized propagator we have

$$G^{-1}(q) = \begin{pmatrix} Z_B(1+r_B)q^2 + \bar{M}_B^2 & 0 & 0 \\ 0 & 0 & Z_{F,k}(1+r_F)\not{q}^T - i\bar{M}_F \\ 0 & Z_F(1+r_F)\not{q} + i\bar{M}_F & 0 \end{pmatrix} , \quad \text{(A.1)}$$

where $\bar{M}_B^2$ and $\bar{M}_F$ define the scale-dependent mass matrices that depend on the particular background field configuration. The regulator shape functions are provided in Appendix B.

The background field propagator takes the form

$$G(q) \equiv \begin{pmatrix} G_B(q) & 0 & 0 \\ 0 & 0 & G_F^{(+)}(q) \\ 0 & G_F^{(-)\,T}(q) & 0 \end{pmatrix} , \quad \text{(A.2)}$$

where the boson propagator is given by

$$G_B(q) = \left(Z_B(1+r_B)q^2 + \bar{M}_B^2\right)^{-1} , \quad \text{(A.3)}$$

and the fermion propagator

$$G_F^{(\pm)}(q) = \widetilde{G}_F(\bar{M}_F)\left(Z_F(1+r_F)\not{q} \mp i\bar{M}_F\right) , \quad \text{(A.4)}$$

with

$$\widetilde{G}_F(q) = \left(Z_F^2(1+r_F)^2q^2 + \bar{M}_F^2\right)^{-1} . \quad \text{(A.5)}$$

Since the propagators are functions of the mass matrices $\bar{M}_B$ and $\bar{M}_F$, they do not necessarily have to be diagonal in flavor space. While it is easy to evaluate the flow equation for the effective potential in the diagonal basis, it is useful to keep the propagators in their nondiagonal form for the computation of flow equations for the anomalous dimensions and Yukawa coupling.

Appendix B.

Threshold functions

For generic regulators the threshold functions are defined by

$$l_n^{(B)}(w;\eta_B) = \frac{\delta_{n,0}+n}{2}\int_0^\infty dy\, y^{\frac{d}{2}-1}\frac{1}{Z_B}\frac{\partial R_B}{\partial t}\left[Z_B G_B\left(Z_B w\right)\right]^{n+1} \tag{B.1}$$

$$l_n^{(F)}(w;\eta_F) = \left(\delta_{n,0}+n\right)\int_0^\infty dy\, y^{\frac{d}{2}} Z_F\left(1+r_F\right)\frac{\partial}{\partial t}\left(Z_F r_F\right)\left[Z_F^2\widetilde{G}_F\left(Z_F^2 w\right)\right]^{n+1} \tag{B.2}$$

$$l_{n_1,n_2}^{(FB)}(w_1,w_2;\eta_F,\eta_B) = -\frac{1}{2}\int_0^\infty dy\, y^{\frac{d}{2}-1}\widehat{\frac{\partial}{\partial t}}\left\{\left[Z_F^2\widetilde{G}_F\left(Z_F^2 w_1\right)\right]^{n_1}\left[Z_B G_B\left(Z_B w_2\right)\right]^{n_2}\right\} \tag{B.3}$$

$$m_2^{(F)}(w;\eta_F) = -\frac{1}{2}\int_0^\infty dy\, y^{\frac{d}{2}-1}\widehat{\frac{\partial}{\partial t}}\left\{\left[Z_F^2\widetilde{G}_F\left(Z_F^2 w\right)\right]^2\frac{\partial}{\partial y}\left[Z_F^2\widetilde{G}_F\left(Z_F^2 w\right)\right]\right\}^2 \tag{B.4}$$

$$m_4^{(F)}(w;\eta_F) = -\frac{1}{2}\int_0^\infty dy\, y^{\frac{d}{2}+1}\widehat{\frac{\partial}{\partial t}}\left\{\frac{\partial}{\partial y}\left[\left(1+r_F\right)Z_F^2\widetilde{G}_F\left(Z_F^2 w\right)\right]\right\}^2 \tag{B.5}$$

$$m_{n_1,n_2}^{(B)}(w_1,w_2;\eta_B) = \frac{1}{2}\int_0^\infty dy\, y^{\frac{d}{2}}\widehat{\frac{\partial}{\partial t}}\Big\{\left[Z_B G_B\left(Z_B w_1\right)\right]^{n_1}\frac{\partial}{\partial y}\left[Z_B G_B\left(Z_B w_1\right)\right] \times\left[Z_B G_B\left(Z_B w_2\right)\right]^{n_2}\frac{\partial}{\partial y}\left[Z_B G_B\left(Z_B w_2\right)\right]\Big\} \tag{B.6}$$

$$m_{n_1,n_2}^{(FB)}(w_1,w_2;\eta_F,\eta_B) = -\frac{1}{2}\int_0^\infty dy\, y^{\frac{d}{2}}\widehat{\frac{\partial}{\partial t}}\Big\{\left(1+r_F\right)\left[Z_F^2\widetilde{G}_F\left(Z_F^2 w_1\right)\right]^{n_1} \times\left[Z_B G_B\left(Z_B w_2\right)\right]^{n_2}\frac{\partial}{\partial y}\left[Z_B G_B\left(Z_B w_2\right)\right]\Big\} \tag{B.7}$$

where we have defined the dimensionless quantity $y = q^2/k^2$. Here, it is understood that the regulators and propagators are taken as functions of y, i. e. $R_B(y) \equiv R_B(q^2)/k^2$, $G_B(y) \equiv k^2 G_B(q^2)$, etc. and the parameters w, w_1, and w_2 denote dimensionless renormalized quantities. Furthermore we use the formal scale derivative

$$\widehat{\frac{\partial}{\partial t}} \equiv \frac{\partial_t R_B}{\partial t}\frac{\partial}{\partial\left(G_B^{-1}\right)} + \frac{2}{Z_F}\frac{\widetilde{G}_F^{-1}(0)}{1+r_F}\frac{\partial}{\partial t}\left(Z_F r_F\right)\frac{\partial}{\partial\left(\widetilde{G}_F^{-1}\right)}\,, \tag{B.8}$$

that includes the scale-dependence of the regulator functions.

Optimized regulator and threshold functions

For the optimized regulator [58, 59] the shape functions are given by

$$r_B(y) = \left(\frac{1}{y} - 1\right)\theta(1-y)\ , \tag{B.9}$$

$$r_F(y) = \left(\frac{1}{\sqrt{y}} - 1\right)\theta(1-y)\ , \tag{B.10}$$

and the threshold functions can be calculated analytically. They take the following form:

$$l_n^{(B)}(w;\eta_B) = \frac{2(\delta_{n,0}+n)}{d}\left(1-\frac{\eta_B}{d+2}\right)\frac{1}{(1+w)^{n+1}} \tag{B.11}$$

$$l_n^{(F)}(w;\eta_F) = \frac{2(\delta_{n,0}+n)}{d}\left(1-\frac{\eta_F}{d+1}\right)\frac{1}{(1+w)^{n+1}} \tag{B.12}$$

$$\begin{aligned} l_{n_1,n_2}^{(FB)}(w_1,w_2;\eta_F,\eta_B) = {} & \frac{2}{d}\frac{1}{(1+w_1)^{n_1}(1+w_2)^{n_2}}\left\{\frac{n_1}{1+w_1}\left(1-\frac{\eta_F}{d+1}\right)\right. \\ & \left. + \frac{n_2}{1+w_2}\left(1-\frac{\eta_B}{d+2}\right)\right\} \end{aligned} \tag{B.13}$$

$$m_2^{(F)}(w;\eta_F) = \frac{1}{(1+w)^4} \tag{B.14}$$

$$\begin{aligned} m_4^{(F)}(w;\eta_F) = {} & \frac{1}{(1+w)^4} + \frac{1-\eta_F}{d-2}\frac{1}{(1+w)^3} \\ & - \left(\frac{1-\eta_F}{2d-4}+\frac{1}{4}\right)\frac{1}{(1+w)^2} \end{aligned} \tag{B.15}$$

$$m_{n_1,n_2}^{(B)}(w_1,w_2;\eta_B) = \frac{1}{(1+w_1)^{n_1}(1+w_2)^{n_2}} \tag{B.16}$$

$$m_{n_1,n_2}^{(FB)}(w_1,w_2;\eta_F,\eta_B) = \left(1-\frac{\eta_B}{d+1}\right)\frac{1}{(1+w_1)^{n_1}(1+w_2)^{n_2}} \tag{B.17}$$

Bibliography

[1] C. Domb, *The critical point: A historical introduction to the modern theory of critical phenomena*. Taylor & Francis London, 1996.

[2] H. E. Stanley, *Introduction to Phase Transitions and Critical Phenomena*. Oxford University Press, 1987.

[3] M. A. Stephanov, "QCD phase diagram and the critical point," *Prog. Theor. Phys. Suppl.* **153** (2004) 139–156, `arXiv:hep-ph/0402115 [hep-ph]`.

[4] S. Schweber, *QED and the men who made it: Dyson, Feynman, Schwinger, and Tomonaga*. Princeton University Press, 1994.

[5] T. Kinoshita, *Quantum Electrodynamics*, vol. 7. World Scientific, 1990.

[6] K. G. Wilson, "Renormalization group and critical phenomena. 1. Renormalization group and the Kadanoff scaling picture," *Phys. Rev.* **B4** (1971) 3174–3183.

[7] K. G. Wilson, "Renormalization group and critical phenomena. 2. Phase space cell analysis of critical behavior," *Phys. Rev.* **B4** (1971) 3184–3205.

[8] A. Pelissetto and E. Vicari, "Critical phenomena and renormalization group theory," *Phys. Rep.* **368** (2002) 549–727, `arXiv:cond-mat/0012164 [cond-mat]`.

[9] J. Zinn-Justin, *Quantum field theory and critical phenomena*, vol. 113 of *Int. Ser. Monogr. Phys.* Oxford University Press, 2002.

[10] G. Parisi, "Field theoretic approach to second-order phase transitions in two-dimensional and three-dimensional systems," *J. Stat. Phys.* **23** (1980) 49–82.

[11] K. G. Wilson and M. E. Fisher, "Critical exponents in 3.99 dimensions," *Phys. Rev. Lett.* **28** (1972) 240–243.

[12] K. Wilson and J. B. Kogut, "The Renormalization group and the ϵ expansion," *Phys. Rep.* **12** (1974) 75–200.

[13] G. Parisi, "The Theory of Nonrenormalizable Interactions. 1. The Large N Expansion," *Nucl. Phys.* **B100** (1975) 368.

[14] C. Wetterich, "Exact evolution equation for the effective potential," *Phys. Lett.* **B301** (1993) 90–94.

[15] C. Wetterich, "The Average action for scalar fields near phase transitions," *Z. Phys.* **C57** (1993) 451–470.

[16] C. Bagnuls and C. Bervillier, "Exact renormalization group equations. An Introductory review," *Phys. Rep.* **348** (2001) 91, arXiv:hep-th/0002034 [hep-th].

[17] B. Delamotte, "An Introduction to the nonperturbative renormalization group," arXiv:cond-mat/0702365 [cond-mat].

[18] H. Gies, "Introduction to the functional RG and applications to gauge theories," arXiv:hep-ph/0611146 [hep-ph].

[19] J. Berges, N. Tetradis, and C. Wetterich, "Nonperturbative renormalization flow in quantum field theory and statistical physics," *Phys. Rep.* **363** (2002) 223–386, arXiv:hep-ph/0005122 [hep-ph].

[20] J. M. Pawlowski, "Aspects of the functional renormalisation group," *Ann. Phys.* **322** (2007) 2831–2915, arXiv:hep-th/0512261 [hep-th].

[21] L. Canét and H. Chaté, "Non-perturbative Approach to Critical Dynamics," *J. Phys.* **40** (2007) 1937–1950, arXiv:cond-mat/0610468 [cond-mat.stat-mech].

[22] L. Canét, H. Chaté, B. Delamotte, and N. Wschebor, "Non-perturbative renormalization group for the Kardar-Parisi-Zhang equation," *Phys. Rev. Lett.* **104** (2010) 150601, arXiv:0905.1025 [cond-mat.stat-mech].

[23] L. Canét, H. Chaté, and B. Delamotte, "General framework of the non-perturbative renormalization group for non-equilibrium steady states," *J. Phys.* **A44** (2011) 495001, arXiv:1106.4129 [cond-mat.stat-mech].

[24] L. M. Sieberer, S. D. Huber, E. Altman, and S. Diehl, "Dynamical Critical Phenomena in Driven-Dissipative Systems," *Phys. Rev. Lett.* **110** (2013) 195301.

[25] J. Berges and G. Hoffmeister, "Nonthermal fixed points and the functional renormalization group," *Nucl. Phys.* **B813** (2009) 383–407, arXiv:0809.5208 [hep-th].

[26] J. Berges and D. Mesterházy, "Introduction to the nonequilibrium functional renormalization group," *Nucl. Phys. Proc. Suppl.* **228** (2012) 37–60, arXiv:1204.1489 [hep-ph].

[27] K. Novoselov, A. Geim, S. Morozov, D. Jiang, M. Katsnelson, *et al.*, "Two-dimensional gas of massless Dirac fermions in graphene," *Nature* **438** (2005) 197, arXiv:cond-mat/0509330 [cond-mat.mes-hall].

[28] A. K. Geim and K. S. Novoselov, "The rise of graphene," *Nature Mater.* **6** (2007) 183–191.

[29] D. Son, "Quantum critical point in graphene approached in the limit of infinitely strong Coulomb interaction," arXiv:cond-mat/0701501 [cond-mat.str-el].

[30] V. P. Gusynin, S. G. Sharapov, and J. P. Carbotte, "AC Conductivity of Graphene: From Tight-Binding Model to $2+1$-Dimensional Quantum Electrodynamics," *Int. J. Mod. Phys.* **B21** (2007) 4611–4658, arXiv:0706.3016.

[31] J. E. Drut and T. A. Lähde, "Is graphene in vacuum an insulator?," *Phys. Rev. Lett.* **102** (2009) 026802, arXiv:0807.0834 [cond-mat.str-el].

[32] J. E. Drut and T. A. Lähde, "Critical exponents of the semimetal-insulator transition in graphene: A Monte Carlo study," *Phys. Rev.* **B79** (2009) 241405, arXiv:0905.1320 [cond-mat.str-el].

[33] W. Armour, S. Hands, and C. Strouthos, "Monte Carlo Simulation of the Semimetal-Insulator Phase Transition in Monolayer Graphene," *Phys. Rev.* **B81** (2010) 125105, arXiv:0910.5646 [cond-mat.str-el].

[34] O. V. Gamayun, E. V. Gorbar, and V. P. Gusynin, "Gap generation and semimetal-insulator phase transition in graphene," *Phys. Rev.* **B81** (2010) 075429, arXiv:0911.4878 [cond-mat.str-el].

[35] G. W. Semenoff, "Chiral symmetry breaking in graphene," *Phys. Scripta* **T146** (2012) 014016, arXiv:1108.2945 [hep-th].

[36] D. C. Elias, R. V. Gorbachev, A. S. Mayorov, S. V. Morozov, A. A. Zhukov, P. Blake, L. A. Ponomarenko, I. V. Grigorieva, K. S. Novoselov, F. Guinea, and A. K. Geim, "Dirac cones reshaped by interaction effects in suspended graphene," *Nature Phys.* **7** (2011) 701–704, arXiv:1104.1396 [cond-mat.mes-hall].

[37] D. E. Sheehy and J. Schmalian, "Quantum Critical Scaling in Graphene," *Phys. Rev. Lett.* **99** (2007) 226803, arXiv:0707.2945 [cond-mat.mes-hall].

[38] E. Vicari, "Critical phenomena and renormalization-group flow of multi-parameter Φ^4 field theories," *PoS* **LAT2007** (2007) 023, arXiv:0709.1014 [hep-lat].

[39] P. C. Hohenberg and B. I. Halperin, "Theory of Dynamic Critical Phenomena," *Rev. Mod. Phys.* **49** (1977) 435–479.

[40] B. I. Halperin, P. C. Hohenberg, and S.-k. Ma, "Renormalization-group methods for critical dynamics: 1. Recursion relations and effects of energy conservation," *Phys. Rev.* **B10** (1974) 139–153.

[41] C. De Dominicis, E. Brézin, and J. Zinn-Justin, "Field Theoretic Techniques and Critical Dynamics. 1. Ginzburg-Landau Stochastic Models Without Energy Conservation," *Phys. Rev.* **B12** (1975) 4945.

[42] K. K. Murata, "Dynamics of a coupled-mode system: Explicit analysis at order ϵ^2," *Phys. Rev.* **B13** (1976) 2028–2043.

[43] R. Folk and G. Moser, "Critical Dynamics of Model C Resolved," *Phys. Rev. Lett.* **91** (2003) 030601.

[44] P. C. Martin, E. D. Siggia, and H. A. Rose, "Statistical Dynamics of Classical Systems," *Phys. Rev.* **A8** (1973) 423–437.

[45] H.-K. Janssen, "On a Lagrangean for classical field dynamics and renormalization group calculations of dynamical critical properties," *Z. Phys.* **B23** (1976) 377–380.

[46] C. De Dominicis and L. Peliti, "Field Theory Renormalization and Critical Dynamics Above T_c: Helium, Antiferromagnets and Liquid Gas Systems," *Phys. Rev.* **B18** (1978) 353–376.

[47] U. Frisch and J. Bec, "Burgulence," `arXiv:nlin/0012033`.

[48] J. Bec and K. Khanin, "Burgers turbulence," *Phys. Rep.* **447** (2007) 1–66, `arXiv:0704.1611 [nlin.CD]`.

[49] U. Frisch, *Turbulence. The legacy of A. N. Kolmogorov.* Cambridge University Press, 1995.

[50] K. Aoki, "Introduction to the nonperturbative renormalization group and its recent applications," *Int. J. Mod. Phys.* **B14** (2000) 1249–1326.

[51] J. Polónyi, "Lectures on the functional renormalization group method," *Cent. Eur. J. Phys.* **1** (2003) 1–71, `arXiv:hep-th/0110026 [hep-th]`.

[52] O. J. Rosten, "Fundamentals of the Exact Renormalization Group," *Phys. Rep.* **511** (2012) 177–272, `arXiv:1003.1366 [hep-th]`.

[53] P. Kopietz, L. Bartosch, and F. Schutz, "Introduction to the functional renormalization group," *Lect. Notes Phys.* **798** (2010) 1–380.

[54] W. Metzner, M. Salmhofer, C. Honerkamp, V. Meden, and K. Schonhammer, "Functional renormalization group approach to correlated fermion systems," *Rev. Mod. Phys.* **84** (2012) 299, `arXiv:1105.5289 [cond-mat.str-el]`.

[55] H. Rothe, "Lattice gauge theories: An Introduction," *World Sci. Lect. Notes Phys.* **43** (1992) 1–381.

[56] I. Montvay and G. Münster, *Quantum fields on a lattice.* Cambridge University Press, 1994.

[57] C. Itzykson and J. Zuber, *Quantum Field Theory.* Dover, 2006.

[58] D. F. Litim, "Optimization of the exact renormalization group," *Phys. Lett.* **B486** (2000) 92–99, arXiv:hep-th/0005245 [hep-th].

[59] D. F. Litim, "Optimized renormalization group flows," *Phys. Rev.* **D64** (2001) 105007, arXiv:hep-th/0103195 [hep-th].

[60] C. Wetterich, "Spinors in euclidean field theory, complex structures and discrete symmetries," *Nucl. Phys.* **B852** (2011) 174–234, arXiv:1002.3556 [hep-th].

[61] S. Floerchinger, "Analytic Continuation of Functional Renormalization Group Equations," *JHEP* **1205** (2012) 021, arXiv:1112.4374 [hep-th].

[62] T. R. Morris, "Derivative expansion of the exact renormalization group," *Phys. Lett.* **B329** (1994) 241–248, arXiv:hep-ph/9403340 [hep-ph].

[63] T. R. Morris, "On truncations of the exact renormalization group," *Phys. Lett.* **B334** (1994) 355–362, arXiv:hep-th/9405190 [hep-th].

[64] T. R. Morris, "Properties of derivative expansion approximations to the renormalization group," *Int. J. Mod. Phys.* **B12** (1998) 1343–1354, arXiv:hep-th/9610012 [hep-th].

[65] T. R. Morris and M. D. Turner, "Derivative expansion of the renormalization group in $O(N)$ scalar field theory," *Nucl. Phys.* **B509** (1998) 637–661, arXiv:hep-th/9704202 [hep-th].

[66] L. Canét, B. Delamotte, D. Mouhanna, and J. Vidal, "Optimization of the derivative expansion in the nonperturbative renormalization group," *Phys. Rev.* **D67** (2003) 065004, arXiv:hep-th/0211055 [hep-th].

[67] L. Canét, B. Delamotte, D. Mouhanna, and J. Vidal, "Nonperturbative renormalization group approach to the Ising model: A Derivative expansion at order ∂^4," *Phys. Rev.* **B68** (2003) 064421, arXiv:hep-th/0302227 [hep-th].

[68] D. F. Litim, "Critical exponents from optimized renormalization group flows," *Nucl. Phys.* **B631** (2002) 128–158, arXiv:hep-th/0203006 [hep-th].

[69] D. F. Litim and L. Vergara, "Subleading critical exponents from the renormalization group," *Phys. Lett.* **B581** (2004) 263–269, arXiv:hep-th/0310101 [hep-th].

[70] D. F. Litim and D. Zappala, "Ising exponents from the functional renormalisation group," *Phys. Rev.* **D83** (2011) 085009, arXiv:1009.1948 [hep-th].

[71] N. Tetradis, "Renormalization group study of weakly first order phase transitions," *Phys. Lett.* **B431** (1998) 380–386, arXiv:hep-th/9706088 [hep-th].

[72] N. Tetradis, "The Exact renormalization group and first order phase transitions," *Int. J. Mod. Phys.* **A16** (2001) 1927–1940, arXiv:hep-th/0012107 [hep-th].

[73] A. K. Geim, "Graphene: Status and Prospects," *Science* **324** (2009) 1530, arXiv:0906.3799 [cond-mat.mes-hall].

[74] A. Castro Neto, F. Guinea, N. Peres, K. Novoselov, and A. Geim, "The electronic properties of graphene," *Rev. Mod. Phys.* **81** (2009) 109–162.

[75] Y. Zhang, Y.-W. Tan, H. L. Stormer, and P. Kim, "Experimental observation of the quantum Hall effect and Berry's phase in graphene," *Nature* **438** (2005) 201–204, arXiv:cond-mat/0509355.

[76] M. I. Katsnelson, K. S. Novoselov, and A. K. Geim, "Chiral tunnelling and the Klein paradox in graphene," *Nature Phys.* **2** (2006) 620–625, arXiv:cond-mat/0604323.

[77] C. W. J. Beenakker, "*Colloquium*: Andreev reflection and Klein tunneling in graphene," *Rev. Mod. Phys.* **80** (2008) 1337–1354.

[78] M. I. Katsnelson, "Zitterbewegung, chirality, and minimal conductivity in graphene," *Eur. Phys. J.* **B51** (2006) 157–160, arXiv:cond-mat/0512337.

[79] J. C. Meyer, A. K. Geim, M. I. Katsnelson, K. S. Novoselov, T. J. Booth, and S. Roth, "The structure of suspended graphene sheets," *Nature* **446** (2007) 60–63, arXiv:cond-mat/0701379.

[80] K. I. Bolotin, K. J. Sikes, Z. Jiang, M. Klima, G. Fudenberg, J. Hone, P. Kim, and H. L. Stormer, "Ultrahigh electron mobility in suspended graphene," *Solid State Commun.* **146** (2008) 351–355, arXiv:0802.2389 [cond-mat.mes-hall].

[81] X. Du, I. Skachko, A. Barker, and E. Y. Andrei, "Approaching ballistic transport in suspended graphene," *Nat. Nanotechnol.* **3** (2008) 491–495, arXiv:0802.2933.

[82] V. N. Kotov, B. Uchoa, V. M. Pereira, F. Guinea, and A. H. Castro Neto, "Electron-Electron Interactions in Graphene: Current Status and Perspectives," *Rev. Mod. Phys.* **84** (2012) 1067–1125, arXiv:1012.3484 [cond-mat.str-el].

[83] J. Braun, "Fermion Interactions and Universal Behavior in Strongly Interacting Theories," *J. Phys.* **G39** (2012) 033001, arXiv:1108.4449 [hep-ph].

[84] S. Sachdev, *Quantum Phase Transitions*. Cambridge University Press, 2001.

[85] J. E. Drut and D. T. Son, "Renormalization group flow of quartic perturbations in graphene: Strong coupling and large-N limits," *Phys. Rev.* **B77** (2008) 075115, arXiv:0710.1315 [cond-mat.str-el].

[86] V. Juričić, I. F. Herbut, and G. W. Semenoff, "Coulomb interaction at the metal-insulator critical point in graphene," *Phys. Rev.* **B80** (2009) 081405, arXiv:0906.3513 [cond-mat.str-el].

[87] I. F. Herbut, V. Juričić, and O. Vafek, "Relativistic Mott criticality in graphene," *Phys. Rev.* **B80** (2009) 075432, arXiv:0904.1019 [cond-mat.str-el].

[88] S. Raghu, X.-L. Qi, C. Honerkamp, and S.-C. Zhang, "Topological Mott Insulators," *Phys. Rev. Lett.* **100** (2008) 156401.

[89] E. V. Gorbar, V. P. Gusynin, V. A. Miransky, and I. A. Shovkovy, "Magnetic field driven metal insulator phase transition in planar systems," *Phys. Rev.* **B66** (2002) 045108, arXiv:cond-mat/0202422 [cond-mat].

[90] I. F. Herbut, "Interactions and phase transitions on graphene's honeycomb lattice," *Phys. Rev. Lett.* **97** (2006) 146401, arXiv:cond-mat/0606195 [cond-mat].

[91] I. F. Herbut, V. Juričić, and B. Roy, "Theory of interacting electrons on the honeycomb lattice," *Phys. Rev.* **B79** (2009) 085116, arXiv:0811.0610 [cond-mat.str-el].

[92] G. W. Semenoff, "Condensed matter simulation of a three-dimensional anomaly," *Phys. Rev. Lett.* **53** (1984) 2449.

[93] F. D. M. Haldane and S. Raghu, "Possible Realization of Directional Optical Waveguides in Photonic Crystals with Broken Time-Reversal Symmetry," *Phys. Rev. Lett.* **100** (2008) 013904.

[94] S. Raghu and F. D. M. Haldane, "Analogs of quantum-Hall-effect edge states in photonic crystals," *Phys. Rev.* **A78** (2008) 033834.

[95] R. A. Sepkhanov, Y. B. Bazaliy, and C. W. J. Beenakker, "Extremal transmission at the Dirac point of a photonic band structure," *Phys. Rev.* **A75** (2007) 063813.

[96] R. A. Sepkhanov, J. Nilsson, and C. W. J. Beenakker, "Proposed method for detection of the pseudospin-$\frac{1}{2}$ Berry phase in a photonic crystal with a Dirac spectrum," *Phys. Rev.* **B78** (2008) 045122.

[97] S. Bittner, B. Dietz, M. Miski-Oglu, P. Oria Iriarte, A. Richter, and F. Schäfer, "Observation of a Dirac point in microwave experiments with a photonic crystal modeling graphene," *Phys. Rev.* **B82** (2010) 014301, arXiv:1005.4506 [cond-mat.mes-hall].

[98] S. Bittner, B. Dietz, M. Miski-Oglu, and A. Richter, "Extremal transmission through a microwave photonic crystal and the observation of edge states in a rectangular Dirac billiard," *Phys. Rev.* **B85** (2012) 064301, arXiv:1110.3263 [cond-mat.other].

[99] B. Roy, "Multi-critical behavior of $Z_2 \times O(2)$ Gross-Neveu-Yukawa theory in graphene," *Phys. Rev.* **84** (2011) 113404, arXiv:1106.1419 [cond-mat.str-el].

[100] K. Osterwalder and R. Schrader, "Axioms for Euclidean Green's functions," *Commun. Math. Phys.* **31** (1973) 83–112.

[101] M. Gomes, R. S. Mendes, R. F. Ribeiro, and A. J. da Silva, "Gauge structure, anomalies and mass generation in a three-dimensional Thirring model," *Phys. Rev.* **D43** (1991) 3516–3523.

[102] H. Gies and L. Janssen, "UV fixed-point structure of the three-dimensional Thirring model," *Phys. Rev.* **D82** (2010) 085018, arXiv:1006.3747 [hep-th].

[103] R. Jackiw and S. Templeton, "How Superrenormalizable Interactions Cure their Infrared Divergences," *Phys. Rev.* **D23** (1981) 2291.

[104] J. Kogut, M. A. Stephanov, and D. Toublan, "On two color QCD with baryon chemical potential," *Phys. Lett.* **B464** (1999) 183–191, arXiv:hep-ph/9906346 [hep-ph].

[105] J. Kogut, M. A. Stephanov, D. Toublan, J. Verbaarschot, and A. Zhitnitsky, "QCD-like theories at finite baryon density," *Nucl. Phys.* **B582** (2000) 477–513, arXiv:hep-ph/0001171 [hep-ph].

[106] L. von Smekal, "Universal Aspects of QCD-like Theories," *Nucl. Phys. B Proc. Suppl.* **228** (2012) 179–220, arXiv:1205.4205 [hep-ph].

[107] P. Heinzner, A. Huckleberry, and M. Zirnbauer, "Symmetry classes of disordered fermions," *Commun. Math. Phys.* **257** (2005) 725–771, arXiv:math-ph/0411040 [math-ph].

[108] A. Altland, "Low-Energy Theory of Disordered Graphene," *Phys. Rev. Lett.* **97** (2006) 236802, arXiv:cond-mat/0607247.

[109] E. McCann, K. Kechedzhi, V. I. Falko, H. Suzuura, T. Ando, and B. L. Altshuler, "Weak-Localization Magnetoresistance and Valley Symmetry in Graphene," *Phys. Rev. Lett.* **97** (2006) 146805, arXiv:cond-mat/0604015.

[110] P. M. Ostrovsky, I. V. Gornyi, and A. D. Mirlin, "Quantum Criticality and Minimal Conductivity in Graphene with Long-Range Disorder," *Phys. Rev. Lett.* **98** (2007) 256801, arXiv:cond-mat/0702115.

[111] S. Das Sarma, S. Adam, E. H. Hwang, and E. Rossi, "Electronic transport in two-dimensional graphene," *Rev. Mod. Phys.* **83** (2011) 407–470, arXiv:1003.4731 [cond-mat.mes-hall].

[112] J. Verbaarschot and I. Zahed, "Spectral density of the QCD Dirac operator near zero virtuality," *Phys. Rev. Lett.* **70** (1993) 3852–3855, arXiv:hep-th/9303012 [hep-th].

[113] J. J. M. Verbaarschot, "The Spectrum of the QCD Dirac operator and chiral random matrix theory: The Threefold way," *Phys. Rev. Lett.* **72** (1994) 2531–2533, arXiv:hep-th/9401059 [hep-th].

[114] J. Verbaarschot and T. Wettig, "Random matrix theory and chiral symmetry in QCD," *Ann. Rev. Nucl. Part. Sci.* **50** (2000) 343–410, arXiv:hep-ph/0003017 [hep-ph].

[115] M. R. Zirnbauer, "Riemannian symmetric superspaces and their origin in random-matrix theory," *J. Math. Phys.* **37** (1996) 4986–5018.

[116] M. R. Zirnbauer, "Symmetry Classes," arXiv:1001.0722 [math-ph].

[117] J. Gonzalez, F. Guinea, and M. Vozmediano, "Non-Fermi liquid behavior of electrons in the half filled honeycomb lattice (A Renormalization group approach)," *Nucl. Phys.* **B424** (1994) 595–618, arXiv:hep-th/9311105 [hep-th].

[118] R. D. Pisarski, "Chiral Symmetry Breaking in Three-Dimension Electrodynamics," *Phys. Rev.* **D29** (1984) 2423.

[119] A. P. Polychronakos, "Symmetry breaking patterns in $(2+1)$-dimensional gauge theories," *Phys. Rev. Lett.* **60** (1988) 1920.

[120] G. V. Dunne and S. M. Nishigaki, "3-D two color QCD at finite temperature and baryon density," *Nucl. Phys.* **B670** (2003) 307–328, arXiv:hep-ph/0306220 [hep-ph].

[121] Y. Araki and G. Semenoff, "Spin versus charge-density-wave order in graphenelike systems," *Phys. Rev.* **B86** no. 121402, (2012) , arXiv:1204.4531 [cond-mat.str-el].

[122] C.-Y. Hou, C. Chamon, and C. Mudry, "Electron fractionalization in two-dimensional graphene-like structures," *Phys. Rev. Lett.* **98** (2007) 186809, arXiv:cond-mat/0609740 [cond-mat.mes-hall].

[123] F. D. M. Haldane, "Model for a Quantum Hall Effect without Landau Levels: Condensed-Matter Realization of the 'Parity Anomaly'," *Phys. Rev. Lett.* **61** (1988) 2015–2018.

[124] B. A. Bernevig and S.-C. Zhang, "Quantum Spin Hall Effect," *Phys. Rev. Lett.* **96** (2006) 106802.

[125] C. Chamon, C.-Y. Hou, R. Jackiw, C. Mudry, S.-Y. Pi, *et al.*, "Electron fractionalization for two-dimensional Dirac fermions," *Phys. Rev.* **B77** (2008) 235431, arXiv:0712.2439 [hep-th].

[126] S. Ryu, C. Mudry, C.-Y. Hou, and C. Chamon, "Masses in graphenelike two-dimensional electronic systems: Topological defects in order parameters and their fractional exchange statistics," *Phys. Rev.* **B80** (2009) 205319, arXiv:0908.3054 [cond-mat.str-el].

[127] J. I. Latorre and T. R. Morris, "Exact scheme independence," *JHEP* **0011** (2000) 004, arXiv:hep-th/0008123 [hep-th].

[128] J. Braun, H. Gies, and D. D. Scherer, "Asymptotic safety: a simple example," *Phys. Rev.* **D83** (2011) 085012, arXiv:1011.1456 [hep-th].

[129] N. Tetradis and C. Wetterich, "Critical exponents from effective average action," *Nucl. Phys.* **B422** (1994) 541–592, arXiv:hep-ph/9308214 [hep-ph].

[130] D. U. Jungnickel and C. Wetterich, "Effective action for the chiral quark-meson model," *Phys. Rev.* **D53** (1996) 5142–5175, arXiv:hep-ph/9505267 [hep-ph].

[131] J. Berges and C. Wetterich, "Equation of state and coarse grained free energy for matrix models," *Nucl. Phys.* **B487** (1997) 675–720, arXiv:hep-th/9609019 [hep-th].

[132] L. Rosa, P. Vitale, and C. Wetterich, "Critical exponents of the Gross-Neveu model from the effective average action," *Phys. Rev. Lett.* **86** (2001) 958–961, arXiv:hep-th/0007093 [hep-th].

[133] F. Höfling, C. Nowak, and C. Wetterich, "Phase transition and critical behavior of the $D = 3$ Gross-Neveu model," *Phys. Rev.* **B66** (2002) 205111, arXiv:cond-mat/0203588 [cond-mat].

[134] P. Strack, S. Takei, and W. Metzner, "Anomalous scaling of fermions and order parameter fluctuations at quantum criticality," *Phys. Rev.* **B81** (2010) 125103, arXiv:0905.3894 [cond-mat.str-el].

[135] B. Obert, S. Takei, and W. Metzner, "Anomalous criticality near semimetal-to-superfluid quantum phase transition in a two-dimensional Dirac cone model," *Ann. Phys.* **523** (2011) 621–628, arXiv:1104.2988 [cond-mat.str-el].

[136] I. F. Herbut and Z. Tesanovic, "Critical fluctuations in superconductors and the magnetic field penetration depth," *Phys. Rev. Lett.* **76** (1996) 4588, arXiv:cond-mat/9605185 [cond-mat].

[137] J. Hove and A. Sudbo, "Anomalous Scaling Dimensions and Stable Charged Fixed Point of Type-II Superconductors," *Phys. Rev. Lett.* **84** (2000) 3426–3429.

[138] I. Lawrie and S. Sarbach, "Theory of Tricritical Points," *Phase transitions and critical phenomena* **9** (1984) 2–155.

[139] R. B. Griffiths, "Thermodynamics Near the Two-Fluid Critical Mixing Point in ^{3}He-^{4}He," *Phys. Rev. Lett.* **24** (1970) 715–717.

[140] R. B. Griffiths, "Proposal for Notation at Tricritical Points," *Phys. Rev.* **B7** (1973) 545–551.

[141] E. K. Riedel and F. J. Wegner, "Tricritical Exponents and Scaling Fields," *Phys. Rev. Lett.* **29** (1972) 349–352.

[142] F. J. Wegner and E. K. Riedel, "Logarithmic Corrections to the Molecular-Field Behavior of Critical and Tricritical Systems," *Phys. Rev.* **B7** (1973) 248–256.

[143] E. K. Riedel and F. J. Wegner, "Effective critical and tricritical exponents," *Phys. Rev.* **B9** (1974) 294–315.

[144] M. Blume, V. Emery, and R. B. Griffiths, "Ising Model for the λ Transition and Phase Separation in ^{3}He-^{4}He Mixtures," *Phys. Rev.* **A4** (1971) 1071–1077.

[145] R. B. Griffiths and J. C. Wheeler, "Critical Points in Multicomponent Systems," *Phys. Rev.* **A2** (1970) 1047–1064.

[146] A. Hankey, T. Chang, and H. Stanley, "Tricritical points in multicomponent fluid mixtures: A geometric interpretation," *Phys. Rev.* **A9** (1974) 2573–2578.

[147] A. Barducci, R. Casalbuoni, S. De Curtis, R. Gatto, and G. Pettini, "Chiral symmetry breaking in QCD at finite temperature and density," *Phys. Lett.* **B231** (1989) 463.

[148] A. Barducci, R. Casalbuoni, G. Pettini, and R. Gatto, "Chiral phases of QCD at finite density and temperature," *Phys. Rev.* **D49** (1994) 426–436.

[149] M. A. Stephanov, K. Rajagopal, and E. V. Shuryak, "Signatures of the tricritical point in QCD," *Phys. Rev. Lett.* **81** (1998) 4816–4819, `arXiv:hep-ph/9806219 [hep-ph]`.

[150] A. M. Halász, A. Jackson, R. Shrock, M. A. Stephanov, and J. Verbaarschot, "On the phase diagram of QCD," *Phys. Rev.* **D58** (1998) 096007, `arXiv:hep-ph/9804290 [hep-ph]`.

[151] J. Berges and K. Rajagopal, "Color superconductivity and chiral symmetry restoration at nonzero baryon density and temperature," *Nucl. Phys.* **B538** (1999) 215–232, `arXiv:hep-ph/9804233 [hep-ph]`.

[152] D. R. Nelson, J. M. Kosterlitz, and M. E. Fisher, "Renormalization-Group Analysis of Bicritical and Tetracritical Points," *Phys. Rev. Lett.* **33** (1974) 813–817.

[153] M. E. Fisher and D. R. Nelson, "Spin Flop, Supersolids, and Bicritical and Tetracritical Points," *Phys. Rev. Lett.* **32** (1974) 1350–1353.

[154] J. Kosterlitz, D. R. Nelson, and M. E. Fisher, "Bicritical and tetracritical points in anisotropic antiferromagnetic systems," *Phys. Rev.* **B13** (1976) 412–432.

[155] A. Aharony, "Old and new results on multicritical points," *J. Stat. Phys.* **110** (2003) 659–669, `arXiv:cond-mat/0201576`.

[156] A. Pelissetto and E. Vicari, "Multicritical behavior of two-dimensional anisotropic antiferromagnets in a magnetic field," *Phys. Rev.* **B76** (2007) 024436, `arXiv:cond-mat/0702273`.

[157] S.-C. Zhang, "A Unified Theory Based on $SO(5)$ Symmetry of Superconductivity and Antiferromagnetism," *Science* **275** (1997) 1089–1096.

[158] X. Hu, "Bicritical and Tetracritical Phenomena and Scaling Properties of the $SO(5)$ Theory," *Phys. Rev. Lett.* **87** (2001) 057004.

[159] E. Demler, S. Sachdev, and Y. Zhang, "Spin-Ordering Quantum Transitions of Superconductors in a Magnetic Field," *Phys. Rev. Lett.* **87** (2001) 067202.

[160] Y. Zhang, E. Demler, and S. Sachdev, "Competing orders in a magnetic field: Spin and charge order in the cuprate superconductors," *Phys. Rev.* **B66** (2002) 094501.

[161] M. Hasenbusch, A. Pelissetto, and E. Vicari, "Instability of the $O(5)$ multicritical behavior in the $SO(5)$ theory of high-T_c superconductors," *Phys. Rev.* **B72** (2005) 014532, arXiv:cond-mat/0502327 [cond-mat].

[162] K.-S. Liu and M. E. Fisher, "Quantum lattice gas and the existence of a supersolid," *J. Low Temp. Phys.* **10** (1973) 655–683.

[163] P. Calabrese, A. Pelissetto, and E. Vicari, "Multicritical phenomena in $O(N_1) \oplus O(N_2)$ symmetric theories," *Phys. Rev.* **B67** (2003) 054505, arXiv:cond-mat/0209580 [cond-mat].

[164] E. Domany, D. Mukamel, and M. E. Fisher, "Destruction of first-order transitions by symmetry-breaking fields," *Phys. Rev.* **B15** (1977) 5432–5441.

[165] A. D. Bruce and A. Aharony, "Coupled order parameters, symmetry-breaking irrelevant scaling fields, and tetracritical points," *Phys. Rev.* **B11** (1975) 478–499.

[166] E. Domany and M. E. Fisher, "Equations of state for bicritical points. III. Cubic anisotropy and tetracriticality," *Phys. Rev.* **B15** (1977) 3510–3521.

[167] R. Folk, Y. Holovatch, and G. Moser, "Field theory of bicritical and tetracritical points. I. Statics," *Phys. Rev.* **E78** (2008) 041124.

[168] R. Folk, Y. Holovatch, and G. Moser, "Field Theoretical Approach to Bicritical and Tetracritical Behavior: Static and Dynamics," *J. Phys. Stud.* **13** (2009) 4003–4003, arXiv:0906.3624 [cond-mat.stat-mech].

[169] M. Caselle, M. Hasenbusch, A. Pelissetto, and E. Vicari, "The critical equation of state of the two-dimensional Ising model," *J. Phys.* **A34** (2001) 2923–2948, arXiv:cond-mat/0011305.

[170] W. Selke, "Multicritical points in the three-dimensional XXZ antiferromagnet with single-ion anisotropy," *Phys. Rev.* **E87** (2013) 014101, arXiv:1211.1052 [cond-mat.stat-mech].

[171] M. Hasenbusch and E. Vicari, "Anisotropic perturbations in three-dimensional $O(N)$-symmetric vector models," *Phys. Rev.* **B84** (2011) 125136.

[172] B. Delamotte and L. Canet, "What can be learnt from the nonperturbative renormalization group?," *Condens. Matter Phys.* **8** (2005) 163–179, arXiv:cond-mat/0412205 [cond-mat].

[173] B. Delamotte, M. Dudka, Y. Holovatch, and D. Mouhanna, "Analysis of the $3d$ massive renormalization group perturbative expansions: a delicate case," arXiv:1012.3739 [cond-mat.stat-mech].

[174] B. Delamotte, M. Dudka, Y. Holovatch, and D. Mouhanna, "About the relevance of the fixed dimension perturbative approach to frustrated magnets in two and three dimensions," *Phys. Rev.* **B82** (2010) 104432, arXiv:1009.1492 [cond-mat.stat-mech].

[175] D. Mesterházy, J. Berges, and L. von Smekal, "Effect of short-range interactions on the quantum critical behavior of spinless fermions on the honeycomb lattice," *Phys. Rev.* **B86** (2012) 245431, arXiv:1207.4054 [cond-mat.str-el].

[176] S. Bornholdt, N. Tetradis, and C. Wetterich, "Coleman-Weinberg phase transition in two scalar models," *Phys. Lett.* **B348** (1995) 89–99, arXiv:hep-th/9408132 [hep-th].

[177] S. Bornholdt, N. Tetradis, and C. Wetterich, "High temperature phase transition in two scalar theories," *Phys. Rev.* **D53** (1996) 4552–4569, arXiv:hep-ph/9503282 [hep-ph].

[178] J. A. Adams, J. Berges, S. Bornholdt, F. Freire, N. Tetradis, *et al.*, "Solving nonperturbative flow equations," *Mod. Phys. Lett.* **A10** (1995) 2367–2380, arXiv:hep-th/9507093 [hep-th].

[179] J. Berges, N. Tetradis, and C. Wetterich, "Coarse graining and first order phase transitions," *Phys. Lett.* **B393** (1997) 387–394, arXiv:hep-ph/9610354 [hep-ph].

[180] K.-I. Aoki, K.-i. Morikawa, W. Souma, J.-i. Sumi, and H. Terao, "The Effectiveness of the local potential approximation in the Wegner-Houghton renormalization group," *Prog. Theor. Phys.* **95** (1996) 409–420, arXiv:hep-ph/9612458 [hep-ph].

[181] K.-I. Aoki, K. Morikawa, W. Souma, J.-I. Sumi, and H. Terao, "Rapidly converging truncation scheme of the exact renormalization group," *Prog. Theor. Phys.* **99** (1998) 451–466, arXiv:hep-th/9803056 [hep-th].

[182] R. D. Pisarski and F. Wilczek, "Remarks on the Chiral Phase Transition in Chromodynamics," *Phys. Rev.* **D29** (1984) 338–341.

[183] J. Berges, D. Jungnickel, and C. Wetterich, "Two flavor chiral phase transition from nonperturbative flow equations," *Phys. Rev.* **D59** (1999) 034010, arXiv:hep-ph/9705474 [hep-ph].

[184] J. M. Carmona, A. Pelissetto, and E. Vicari, "The N component Ginzburg-Landau Hamiltonian with cubic anisotropy: A Six loop study," *Phys. Rev.* **B61** (2000) 15136–15151, arXiv:cond-mat/9912115 [cond-mat].

[185] R. Guida and J. Zinn-Justin, "Critical exponents of the N-vector model," *J. Phys.* **A31** (1998) 8103.

[186] D. J. Amit and L. Peliti, "On dangerous irrelevant operators," *Ann. Phys.* **140** (1982) 207.

[187] M. Tissier, D. Mouhanna, J. Vidal, and B. Delamotte, "Randomly dilute Ising model: A nonperturbative approach," *Phys. Rev.* **B65** (2002) 140402.

[188] B. N. Shalaev, S. A. Antonenko, and A. I. Sokolov, "Five-loop $\sqrt{\epsilon}$-expansions for random Ising model and marginal spin dimensionality for cubic systems," *Phys. Lett.* **A230** (1997) 105–110, arXiv:cond-mat/9803388.

[189] H. Kleinert and V. Schulte-Frohlinde, "Exact five loop renormalization group functions of ϕ^4 theory with $O(N)$ symmetric and cubic interactions: Critical exponents up to ϵ^5," *Phys. Lett.* **B342** (1995) 284–296, arXiv:cond-mat/9503038 [cond-mat].

[190] H. Kleinert and S. Thoms, "Large order behavior of two coupling constant ϕ^4 theory with cubic anisotropy," *Phys. Rev.* **D52** (1995) 5926–5943, arXiv:hep-th/9508172 [hep-th].

[191] H. Kleinert, S. Thoms, and V. Schulte-Frohlinde, "Stability of 3-D cubic fixed point in two coupling constant ϕ^4 theory," *Phys. Rev.* **B56** (1997) 14428, arXiv:quant-ph/9611050 [quant-ph].

[192] K. Varnashev, "Stability of a cubic fixed point in three-dimensions: Critical exponents for generic N," *Phys. Rev.* **B61** (2000) 14660, arXiv:cond-mat/9909087 [cond-mat].

[193] K. B. Varnashev, "The stability of a cubic fixed point in three dimensions from the renormalization group," *J. Phys.* **A33** (2000) 3121–3135, arXiv:cond-mat/0005087.

[194] R. Folk, Y. Holovatch, and T. Yavors'kii, "Pseudo-ϵ expansion of six-loop renormalization-group functions of an anisotropic cubic model," *Phys. Rev.* **B62** (2000) 12195–12200.

[195] P. H. Ginsparg, "Applied Conformal Field Theory," arXiv:hep-th/9108028 [hep-th].

[196] A. Aharony, "Dependence of Universal Critical Behavior on Symmetry and Range of Interaction," *Phase transitions and critical phenomena* **6** (1976) 357–424.

[197] G. Grinstein and J. Toner, "Dislocation-Loop Theory of the Nematic-Smectic *A*-Smectic *C* Multicritical Point," *Phys. Rev. Lett.* **51** (1983) 2386–2389.

[198] A. Aharony, "Comment on 'Bicritical and Tetracritical Phenomena and Scaling Properties of the $SO(5)$ Theory'," *Phys. Rev. Lett.* **88** (2002) 059703.

[199] M. Hasenbusch, "Finite size scaling study of lattice models in the three-dimensional Ising universality class," *Phys. Rev.* **B82** (2010) 174433.

[200] M. Campostrini, M. Hasenbusch, A. Pelissetto, and E. Vicari, "The Critical exponents of the superfluid transition in He-4," *Phys. Rev.* **B74** (2006) 144506, arXiv:cond-mat/0605083 [cond-mat].

[201] M. Campostrini, M. Hasenbusch, A. Pelissetto, P. Rossi, and E. Vicari, "Critical exponents and equation of state of the three-dimensional Heisenberg universality class," *Phys. Rev.* **B65** (2002) 144520, arXiv:cond-mat/0110336 [cond-mat].

[202] H. Rohrer and C. Gerber, "Bicritical and Tetracritical Behavior of $GdAlO_3$," *Phys. Rev. Lett.* **38** (1977) 909–912.

[203] A. R. King and H. Rohrer, "Spin-flop bicritical point in MnF_2," *Phys. Rev.* **B19** (1979) 5864–5876.

[204] S. Friederich, H. C. Krahl, and C. Wetterich, "Functional renormalization for spontaneous symmetry breaking in the Hubbard model," *Phys. Rev.* **B83** (2011) 115125, arXiv:1012.5436 [cond-mat.str-el].

[205] A. Eichhorn, D. Mesterházy, and M. M. Scherer, "Multicritical behavior in models with two competing order parameters," arXiv:1306.2952 [cond-mat.stat-mech].

[206] P. Calabrese, A. Pelissetto, and E. Vicari, "Critical structure factors of bilinear fields in $O(N)$ vector models," *Phys. Rev.* **E65** (2002) 046115.

[207] M. Grahl and D. H. Rischke, "Functional renormalization group study of the two-flavor linear sigma model in the presence of the axial anomaly," arXiv:1307.2184 [hep-th].

[208] T. Senthil, A. Vishwanath, L. Balents, S. Sachdev, and M. P. A. Fisher, "Deconfined Quantum Critical Points," *Science* **303** (2004) 1490–1494, arXiv:cond-mat/0311326.

[209] T. Senthil, L. Balents, S. Sachdev, A. Vishwanath, and M. P. A. Fisher, "Quantum criticality beyond the Landau-Ginzburg-Wilson paradigm," *Phys. Rev.* **B70** (2004) 144407, arXiv:cond-mat/0312617.

[210] B. I. Halperin, P. C. Hohenberg, and S.-k. Ma, "Calculation of Dynamic Critical Properties Using Wilson's Expansion Methods," *Phys. Rev. Lett.* **29** (1972) 1548–1551.

[211] A. Krinitsyn, V. Prudnikov, and P. Prudnikov, "Calculations of the dynamical critical exponent using the asymptotic series summation method," *Theor. Math. Phys.* **147** (2006) 561–575.

[212] I. M. Khalatnikov, "Absorption and Dispersion of Sound in a Superfluid Liquid near the λ Point," *JETP Lett.* **30** (1969) 268.

[213] D. P. Bélanger, B. Farago, V. Jaccarino, A. R. King, C. Lartigue, and F. Mezei, "Random exchange Ising model dynamics: $Fe_{0.46}Zn_{0.54}F_2$," *J. Phys. Colloques* **49** (1988) C8–1229–1230.

[214] R. Bausch, V. Dohm, H. K. Janssen, and R. K. P. Zia, "Critical Dynamics of an Interface in $1 + \epsilon$ Dimensions," *Phys. Rev. Lett.* **47** (1981) 1837–1840.

[215] R. Folk and H.-G. Moser, "Critical dynamics: a field-theoretical approach," *J. Phys.* **A39** (2006) R207–R313.

[216] K. Kawasaki, "Dynamics of Critical Fluctuations. III: A Study of the Dynamical Scaling Law," *Prog. Theor. Phys.* **40** (1968) 706–733.

[217] L. P. Kadanoff and J. Swift, "Transport Coefficients near the Liquid-Gas Critical Point," *Phys. Rev.* **166** (1968) 89–101.

[218] P. Calabrese and A. Gambassi, "Aging at criticality in model C dynamics," *Phys. Rev.* **E67** (2003) 036111.

[219] P. Calabrese and A. Gambassi, "Ageing properties of critical systems," *J. Phys.* **A38** (2005) R133, `arXiv:cond-mat/0410357 [cond-mat]`.

[220] B. I. Halperin, P. C. Hohenberg, and S.-k. Ma, "Renormalization-group methods for critical dynamics: 2. Detailed analysis of the relaxational models," *Phys. Rev.* **B13** (1976) 4119–4131.

[221] E. Brézin and C. De Dominicis, "Field Theoretic Techniques and Critical Dynamics. 2. Ginzburg-Landau Stochastic Models with Energy Conservation," *Phys. Rev.* **B12** (1975) 4945.

[222] C. Hohenemser, L. Chow, and R. M. Suter, "Dynamical critical behavior of isotropic ferromagnets," *Phys. Rev.* **B26** (1982) 5056–5073.

[223] U. Krey, "On the critical dynamics of a disordered system," *Phys. Lett.* **A57** (1976) 215 – 216.

[224] G. Grinstein, S.-k. Ma, and G. F. Mazenko, "Dynamics of spins interacting with quenched random impurities," *Phys. Rev.* **B15** (1977) 258–272.

[225] B. I. Halperin and C. M. Varma, "Defects and the central peak near structural phase transitions," *Phys. Rev.* **B14** (1976) 4030–4044.

[226] R. Bausch and B. I. Halperin, "Renormalization-group analysis of the critical dynamics of a Hamiltonian model with a scalar displacive transition," *Phys. Rev.* **B18** (1978) 190–205.

[227] P. Prelovšek and I. Sega, "Mode-coupling theory for the central peak in the Ising model in a transverse field," *Ferroelectrics* **26** (1980) 729–732.

[228] B. Berdnikov and K. Rajagopal, "Slowing out-of-equilibrium near the QCD critical point," *Phys. Rev.* **D61** (2000) 105017, `arXiv:hep-ph/9912274 [hep-ph]`.

[229] D. T. Son and M. A. Stephanov, "Dynamic universality class of the QCD critical point," *Phys. Rev.* **D70** (2004) 056001, `arXiv:hep-ph/0401052 [hep-ph]`.

[230] V. K. Akkineni and U. C. Täuber, "Nonequilibrium critical dynamics of the relaxational models C and D," *Phys. Rev.* **E69** (2004) 036113.

[231] R. Folk and G. Moser, "Critical dynamics of stochastic models with energy conservation (model C)," *Phys. Rev.* **E69** (2004) 036101.

[232] J. Berges, S. Schlichting, and D. Sexty, "Dynamic critical phenomena from spectral functions on the lattice," *Nucl. Phys.* **B832** (2010) 228–240, `arXiv:0912.3135 [hep-lat]`.

[233] R. Bausch, H. K. Janssen, and H. Wagner, "Renormalized field theory of critical dynamics," *Z. Phys.* **B24** (1976) 113–127.

[234] R. V. Jensen, "Functional integral approach to classical statistical dynamics," *J. Stat. Phys.* **25** (1981) 183–210.

[235] F. Langouche, D. Roekaerts, and E. Tirapegui, "Functional Integral Methods for Stochastic Fields," *Physica* **A95** (1979) 252–274.

[236] H. Leschke and M. Schmutz, "Operator orderings and functional formulations of quantum and stochastic dynamics," *Z. Phys.* **B27** (1977) 85–94.

[237] J. Honkonen, "Ito and Stratonovich calculuses in stochastic field theory," `arXiv:1102.1581 [cond-mat.stat-mech]`.

[238] N. G. van Kämpen, "Itô versus Stratonovich," *J. Stat. Phys.* **24** (1981) 175–187.

[239] A. Andreanov, G. Biroli, and A. Lefèvre, "Dynamical field theory for glass-forming liquids, self-consistent resummations and time-reversal symmetry," *J. Stat. Mech.* **7** (2006) 8, `arXiv:cond-mat/0510669`.

[240] H. K. Janssen, B. Schaub, and B. Schmittmann, "New universal short-time scaling behaviour of critical relaxation processes," *Z. Phys.* **B73** (1989) 539–549.

[241] R. Folk, Y. Holovatch, and G. Moser, "Field theory of bi- and tetracritical points: Relaxational dynamics," *Phys. Rev.* **E78** (2008) 041125, arXiv:0809.3146 [cond-mat.stat-mech].

[242] R. Folk, Y. Holovatch, and G. Moser, "Biconical critical dynamics," *Europhys. Lett.* **91** (2010) 46002, arXiv:1006.1766 [cond-mat.stat-mech].

[243] J. Lipa, D. Swanson, J. Nissen, T. Chui, and U. Israelsson, "Heat Capacity and Thermal Relaxation of Bulk Helium very near the Lambda Point," *Phys. Rev. Lett.* **76** (1996) 944–947.

[244] M. Campostrini, A. Pelissetto, P. Rossi, and E. Vicari, "25th order high temperature expansion results for three-dimensional Ising like systems on the simple cubic lattice," *Phys. Rev.* **E65** (2002) 066127, arXiv:cond-mat/0201180 [cond-mat].

[245] E. V. Albano, M. A. Bab, G. Baglietto, R. A. Borzi, T. S. Grigera, E. S. Loscar, D. E. Rodriguez, M. L. Rubio Puzzo, and G. P. Saracco, "Study of phase transitions from short-time non-equilibrium behaviour," *Rep. Prog. Phys.* **74** (2011) 026501.

[246] P. G. de Gennes, *Scaling concepts in polymer physics*. Cornell University Press, 1979.

[247] S. Havlin and D. Ben-Avraham, "New approach to self-avoiding walks as a critical phenomenon," *J. Phys.* **A15** (1982) L321–L328.

[248] E. Katzav and M. Schwartz, "Exponent Inequalities in Dynamical Systems," *Phys. Rev. Lett.* **107** (2011) 125701.

[249] H. Müller-Krumbhaar and K. Binder, "Dynamic properties of the Monte Carlo method in statistical mechanics," *J. Stat. Phys.* **8** (1973) 1–24.

[250] K. Binder, *Monte Carlo methods in statistical physics*. Springer Series in Solid-State Sciences (Book 80). Springer, 1986.

[251] A. D. Sokal, *Monte Carlo methods in statistical mechanics: Foundations and New Algorithms*. Cours de Troisieme Cycle en Suisse Romande. 1989.

[252] Z. B. Li, L. Schulke, and B. Zheng, "Dynamic Monte Carlo measurement of critical exponents," *Phys. Rev. Lett.* **74** (1995) 3396–3398, arXiv:hep-th/9410234 [hep-th].

[253] K. R. Sreenivasan and R. A. Antonia, "The Phenomenology of Small-Scale Turbulence," *Annu. Rev. Fluid Mech.* **29** (1997) 435–472.

[254] T. Gotoh, D. Fukayama, and T. Nakano, "Velocity field statistics in homogeneous steady turbulence obtained using a high-resolution direct numerical simulation," *Phys. Fluids* **14** (2002) 1065–1081.

[255] R. Benzi, L. Biferale, R. T. Fisher, L. P. Kadanoff, D. Q. Lamb, and F. Toschi, "Intermittency and Universality in Fully Developed Inviscid and Weakly Compressible Turbulent Flows," *Phys. Rev. Lett.* **100** (2008) 234503, arXiv:0709.3073 [nlin.CD].

[256] T. Ishihara, T. Gotoh, and Y. Kaneda, "Study of High-Reynolds Number Isotropic Turbulence by Direct Numerical Simulation," *Annu. Rev. Fluid Mech.* **41** (2009) 165–180.

[257] R. Benzi, L. Biferale, R. Fisher, D. Q. Lamb, and F. Toschi, "Inertial range Eulerian and Lagrangian statistics from numerical simulations of isotropic turbulence," *J. Fluid Mech.* **653** (2010) 221–244.

[258] M. Nelkin, "Turbulence, critical fluctuations, and intermittency," *Phys. Rev.* **A9** (1974) 388–395.

[259] G. Eyink and N. Goldenfeld, "Analogies between scaling in turbulence, field theory and critical phenomena," *Phys. Rev.* **E50** (1994) 4679–4683, arXiv:cond-mat/9407021.

[260] D. Forster, D. R. Nelson, and M. J. Stephen, "Large-distance and long-time properties of a randomly stirred fluid," *Phys. Rev.* **A16** (1977) 732–749.

[261] C. De Dominicis and P. C. Martin, "Energy spectra of certain randomly-stirred fluids," *Phys. Rev.* **19** (1979) 419–422.

[262] V. Yakhot and S. A. Orszag, "Renormalization-group analysis of turbulence," *Phys. Rev. Lett.* **57** (1986) 1722–1724.

[263] V. Yakhot and S. A. Orszag, "Renormalization group analysis of turbulence. I - Basic theory," *J. Sci. Comp.* **1** (1986) 3–51.

[264] E. V. Teodorovich, "Using the renormalization-group method to describe turbulence (Review)," *Izv. Acad. Sci. USSR Atmos. Oceanic Phys.* **29** (1993) 149–163.

[265] G. L. Eyink, "The renormalization group method in statistical hydrodynamics," *Phys. Fluids* **6** (1994) 3063–3078.

[266] L. T. Adzhemyan, N. V. Antonov, M. V. Kompaniets, and A. N. Vasil'ev, "Renormalization-Group Approach to the Stochastic Navier-Stokes Equation," *Int. J. Mod. Phys.* **B17** (2003) 2137–2170, arXiv:nlin/0207007.

[267] P. Tomassini, "An exact renormalization group analysis of 3D well developed turbulence," *Phys. Lett.* **B411** (1997) 117–126, arXiv:hep-th/9709185.

[268] A. A. Fedorenko, P. Le Doussal, and K. J. Wiese, "Functional renormalization-group approach to decaying turbulence," *J. Stat. Mech.* **1304** (2013) P04014, arXiv:1212.2117 [nlin.CD].

[269] L. T. Adzhemyan, N. V. Antonov, and A. N. Vasil'ev, "Quantum field renormalization group in the theory of fully developed turbulence," *Phys. Usp.* **39** no. 12, (1996) 1193.

[270] L. T. Adzhemyan, N. V. Antonov, and A. N. Vasil'ev, *The field theoretic renormalization group in fully developed turbulence*. CRC Press, 1999.

[271] R. H. Kraichnan, "Anomalous scaling of a randomly advected passive scalar," *Phys. Rev. Lett.* **72** (1994) 1016–1019.

[272] K. Gawedzki and A. Kupiainen, "Anomalous Scaling of the Passive Scalar," *Phys. Rev. Lett.* **75** (1995) 3834–3837.

[273] M. Chertkov, G. Falkovich, I. Kolokolov, and V. Lebedev, "Normal and anomalous scaling of the fourth-order correlation function of a randomly advected passive scalar," *Phys. Rev.* **52** (1995) 4924–4941.

[274] D. Bernard, K. Gawedzki, and A. Kupiainen, "Anomalous scaling in the N-point functions of a passive scalar," *Phys. Rev.* **E54** (1996) 2564–2572.

[275] G. Falkovich, K. Gawedzki, and M. Vergassola, "Particles and fields in fluid turbulence," *Rev. Mod. Phys.* **73** (2001) 913–975.

[276] A. M. Polyakov, "The Theory of turbulence in two-dimensions," *Nucl. Phys.* **B396** (1993) 367–385, `arXiv:hep-th/9212145 [hep-th]`.

[277] A. M. Polyakov, "Turbulence without pressure," *Phys. Rev.* **E52** (1995) 6183–6188, `arXiv:hep-th/9506189`.

[278] G. Falkovich, I. Kolokolov, V. Lebedev, and A. A. Migdal, "Instantons and intermittency," *Phys. Rev.* **E54** (1996) 4896–4907, `arXiv:chao-dyn/9512006 [chao-dyn]`.

[279] V. Gurarie and A. Migdal, "Instantons in the Burgers equation," *Phys. Rev.* **E54** (1996) 4908–4914, `arXiv:hep-th/9512128`.

[280] E. Balkovsky, G. Falkovich, I. Kolokolov, and V. Lebedev, "Viscous instanton for Burgers' turbulence," `arXiv:chao-dyn/9603015 [chao-dyn]`.

[281] E. Balkovsky, G. Falkovich, I. Kolokolov, and V. Lebedev, "Intermittency of Burgers' Turbulence," *Phys. Rev. Lett.* **78** (1997) 1452–1455.

[282] A. I. Chernykh and M. G. Stepanov, "Large negative velocity gradients in Burgers turbulence," *Phys. Rev.* **E64** (2001) 026306, `arXiv:nlin/0001023`.

[283] A. Noullez and M. Vergassola, "A fast Legendre transform algorithm and applications to the adhesion model," *J. Sci. Comp.* **9** (1994) 259–281.

[284] F. Hayot and C. Jayaprakash, "Multifractality in the stochastic Burgers equation," *Phys. Rev.* **E54** (1996) 4681–4684.

[285] F. Hayot and C. Jayaprakash, "From scaling to multiscaling in the stochastic Burgers equation," *Phys. Rev.* **E56** (1997) 4259–4262.

[286] D. Mitra, J. Bec, R. Pandit, and U. Frisch, "Is Multiscaling an Artifact in the Stochastically Forced Burgers Equation?," *Phys. Rev. Lett.* **94** (2005) 194501, `arXiv:nlin/0406049`.

[287] R. Phythian, "The functional formalism of classical statistical dynamics," *J. Phys.* **A10** (1977) 777–789.

[288] J. M. Burgers, *The nonlinear diffusion equation: asymptotic solutions and statistical problems.* D. Reidel Pub. Co., 1973.

[289] A. Chekhlov and V. Yakhot, "Kolmogorov turbulence in a random-force-driven Burgers equation," *Phys. Rev.* **E51** (1995) R2739–R2742.

[290] A. Chekhlov and V. Yakhot, "Kolmogorov turbulence in a random-force-driven Burgers equation: Anomalous scaling and probability density functions," *Phys. Rev.* **E52** (1995) 5681–5684.

[291] W. H. Press, S. A. Teukolsky, W. T. Vetterling, and B. P. Flannery, *Numerical Recipes: The Art of Scientific Computing.* Cambridge University Press, 2007.

[292] W. F. Ames, *Nonlinear partial differential equations.* Academic Press, 1992.

[293] S. L. Adler, "An overrelaxation method for the Monte Carlo evaluation of the partition function for multiquadratic actions," *Phys. Rev.* **D23** (1981) 2901.

[294] S. L. Adler, "Overrelaxation algorithms for lattice field theories," *Phys. Rev.* **D37** (1988) 458.

[295] S. Duane, A. Kennedy, B. Pendleton, and D. Roweth, "Hybrid Monte Carlo," *Phys. Lett.* **B195** (1987) 216–222.

[296] C. Whitmer, "Overrelaxation methods for Monte Carlo simulations of quadratic and multiquadratic actions," *Phys. Rev.* **D29** (1984) 306–311.

[297] F. R. Brown and T. J. Woch, "Overrelaxed Heat Bath and Metropolis Algorithms for Accelerating Pure Gauge Monte Carlo Calculations," *Phys. Rev. Lett.* **58** (1987) 2394.

[298] M. Creutz, "Overrelaxation and Monte Carlo Simulation," *Phys. Rev.* **D36** (1987) 515.

[299] S. L. Adler, "Metropolis overrelaxation for lattice gauge theory for general relaxation parameter omega," *Phys. Rev.* **D38** (1988) 1349.

[300] R. S. Varga, *Matrix iterative analysis*. Prentice Hall, 1962.

[301] M. Lüscher, "Computational Strategies in Lattice QCD," arXiv:1002.4232 [hep-lat].

[302] A. Kennedy, "Algorithms for dynamical fermions," arXiv:hep-lat/0607038 [hep-lat].

[303] M. Hasenbusch, "Speeding up the hybrid Monte Carlo algorithm for dynamical fermions," *Phys. Lett.* **B519** (2001) 177–182, arXiv:hep-lat/0107019 [hep-lat].

[304] M. Lüscher, "Schwarz-preconditioned HMC algorithm for two-flavour lattice QCD," *Comput. Phys. Commun.* **165** (2005) 199–220, arXiv:hep-lat/0409106 [hep-lat].

[305] C. Urbach, K. Jansen, A. Shindler, and U. Wenger, "HMC algorithm with multiple time scale integration and mass preconditioning," *Comput. Phys. Commun.* **174** (2006) 87–98, arXiv:hep-lat/0506011 [hep-lat].

[306] M. Clark and A. Kennedy, "Accelerating dynamical fermion computations using the rational hybrid Monte Carlo (RHMC) algorithm with multiple pseudofermion fields," *Phys. Rev. Lett.* **98** (2007) 051601, arXiv:hep-lat/0608015 [hep-lat].

[307] R. Frezzotti and K. Jansen, "A Polynomial hybrid Monte Carlo algorithm," *Phys. Lett.* **B402** (1997) 328–334, arXiv:hep-lat/9702016 [hep-lat].

[308] J. Sexton and D. Weingarten, "Hamiltonian evolution for the hybrid Monte Carlo algorithm," *Nucl. Phys.* **B380** (1992) 665–678.

[309] I. P. Omelyan, I. M. Mryglod, and R. Folk, "Optimized Verlet-like algorithms for molecular dynamics simulations," *Phys. Rev.* **E65** (2002) 056706, arXiv:cond-mat/0110438.

[310] R. Edwards, I. Horvath, and A. Kennedy, "Instabilities and nonreversibility of molecular dynamics trajectories," *Nucl. Phys.* **B484** (1997) 375–402, arXiv:hep-lat/9606004 [hep-lat].

[311] C. Davies, G. Batrouni, G. Katz, A. S. Kronfeld, G. Lepage, *et al.*, "Fourier acceleration in lattice gauge theories. 1. Landau gauge fixing," *Phys. Rev.* **D37** (1988) 1581.

[312] G. Katz, G. Batrouni, C. Davies, A. S. Kronfeld, P. Lepage, *et al.*, "Fourier acceleration. 2. Matrix inversion and the quark propagator," *Phys. Rev.* **D37** (1988) 1589.

[313] L. Biferale, M. Cencini, A. S. Lanotte, M. Sbragaglia, and F. Toschi, "Anomalous scaling and universality in hydrodynamic systems with power-law forcing," *New J. Phys.* **6** (2004) 37, arXiv:nlin/0401020.

[314] L. Biferale, A. S. Lanotte, and F. Toschi, "Effects of Forcing in Three-Dimensional Turbulent Flows," *Phys. Rev. Lett.* **92** (2004) 094503, arXiv:nlin/0310022.

[315] V. Yakhot and A. Chekhlov, "Algebraic Tails of Probability Density Functions in the Random-Force-Driven Burgers Turbulence," *Phys. Rev. Lett.* **77** (1996) 3118–3121.

[316] A. Berera and D. Hochberg, "Gauge symmetry and Slavnov-Taylor identities for randomly stirred fluids," *Phys. Rev. Lett.* **99** (2007) 254501, arXiv:0711.0825 [hep-th].

[317] A. Berera and D. Hochberg, "Gauge fixing, BRS invariance and Ward identities for randomly stirred flows," *Nucl. Phys.* **B814** (2009) 522–548, arXiv:0902.1611 [hep-th].

[318] T. Grafke, R. Grauer, and T. Schäfer, "Instanton filtering for the stochastic Burgers equation," *J. Phys.* **A46** (2013) 062002, arXiv:1209.0905 [physics.flu-dyn].

[319] L. Janssen and H. Gies, "Critical behavior of the $(2+1)$-dimensional Thirring model," arXiv:1208.3327 [hep-th].

[320] **UKQCD Collaboration** Collaboration, L. Del Debbio, S. Hands, and J. Mehegan, "The Three-dimensional Thirring model for small N(f)," *Nucl. Phys.* **B502** (1997) 269–308, arXiv:hep-lat/9701016 [hep-lat].

[321] S. Christofi, S. Hands, and C. Strouthos, "Critical flavor number in the three dimensional Thirring model," *Phys. Rev.* **D75** (2007) 101701, arXiv:hep-lat/0701016 [hep-lat].

[322] S. Hands and C. Strouthos, "Quantum Critical Behaviour in a Graphene-like Model," *Phys. Rev.* **B78** (2008) 165423, arXiv:0806.4877 [cond-mat.str-el].

[323] W. Armour, J. B. Kogut, and C. Strouthos, "Chiral symmetry breaking and monopole dynamics in non-compact QED3 coupled to a four-fermi interaction," *Phys. Rev.* **D82** (2010) 014503, arXiv:1004.3053 [hep-lat].

[324] K. Rajagopal and F. Wilczek, "Static and dynamic critical phenomena at a second order QCD phase transition," *Nucl. Phys.* **B399** (1993) 395–425, arXiv:hep-ph/9210253 [hep-ph].

[325] L. Canét, H. Chaté, B. Delamotte, and N. Wschebor, "Non-perturbative renormalisation group for the Kardar-Parisi-Zhang equation: general framework and first applications," *Phys. Rev.* **E84** (2011) 061128, arXiv:1107.2289 [cond-mat.stat-mech].